ERRATA

P iii, para 2, 6th line: "are reported" for "reported"

P vii, 15th line: "Conclusions" for "Conclusion"

P x, 19th line: "Conclusions" for "Conclution"

P xx, line 22: "model" for "mode"

P 1.3, 2nd line: "MPa" for "Mpa"

P 1.4, para 2, line 7: "occurrence" for "occurrance"

P 2.1, para 1, line 7: "prediction" for "predication"

P 2.4, para 1, 5th line: "uncertainty" for "uncertainly"

P 2.30, para1 and 2, 3rd line: "hollow" for "hallow"

Figures 3.1, 3.14, and 4.1: "Compressive" for "Compresive"

P 3.5, para 1, line 7: "stress of" for "stress"

P 3.8, para 2, line 11, P. 3.12 line 2, and Table 3.5: "kN" for "KN"

P 3.25, para 1, beginning of line 9: delete "base of the"

P 3.30, para 2, first line: "Roeder" for "Reoder"

P 3.33, line 13: "Conclusions" for "Conclusion"

P 3.34, para 4, line 3: "piles" for "pile"

P 4.4, last para, line 3: "ensure" for "insure"

P 4.7, para 2, line 3: "cyclic" for "cycling"

P 5.3, para 4, line 3: "±250 kN" for "±250"

P 6.9, first line: "relationship" for "relation"

BOND STRENGTH OF CONCRETE

PLUGS EMBEDDED IN TUBULAR

STEEL PILES

By

Abolghasem Nezamian

B.Sc(Hons), CPEng, MIIStructE, MIISeismicE

A thesis submitted in fulfilment of the

requirements for the degree of

Doctor of Philosophy in Civil Engineering

Monash University

August 2003

STATEMENT OF ORIGINALITY

This thesis contains no material, which has been accepted for the award of any Degree or Diploma in any university. To the best my knowledge and belief the thesis contains no material previously published or written by another person except where due to reference is made in the text.

Abolghasem Nezamian

August 2003

SUMMARY

This thesis develops a bond strength formulation, based upon experimental research and the finite element analysis, to predict ultimate bond strength, slip and bond stress distribution in concrete plugs embedded in tubular steel piles. The effect of shrinkage of the concrete on the behavior of concrete plug in steel tube subjected to pull-out and push out loadings is identified in the experimental testing and included in analytical model.

Pull-out and push out test results are presented and discussed. Test results are examined against the current code provisions and recommendations. Mathematical expressions are adopted to calculate the bond strength of concrete plugs in steel tubular piles. The failure mechanisms and models are discussed. Experimental tests on fifteen concrete plug specimens subjected to cyclic loading reported. The purpose of these tests was to investigate the behavior of the concrete plug in the steel tube under repeated loading

The loss of composite action can be attributed to an accumulation of damage (ie slip growth) in the pile/plug interface under repeated loading. Based upon the results from the cyclic loading tests, empirical relationships were developed for the rate of slip growth of the concrete plug as a function of the load and the number of cycles.

The ultimate capacity and load slip response of specimens under cyclic loading can be reasonably approximated from the static ultimate strength and load slip of the specimen by reducing the ultimate strength values of the static test by a cyclic reduction factor. The cyclic reduction factor is defined as the factor by which the cyclic strength of the specimen may be obtained from the static strength for a given displacement. Based upon the test results from the cyclic tests, an average cyclic reduction was obtained.

A non linear finite element solution scheme with axi-symmetric elements was developed. It included a time dependant shrinkage model based on European Code MC1990, and a linear tension-softening model for concrete and Coulomb friction model for the interface. The model is used to predict the ultimate strength, load-slip response and longitudinal and hoop strains along the outer surface of the steel tube. The numerical values agreed well with the measured values from the tests. This tool is suitable for the investigation of parameter variations on the ultimate strength of a concrete plug in a steel tube specimen subjected to a static pull-out and push-out force.

The investigation ultimately proposes bond strength formulations to predict the bond strength between a concrete plug and internal surface of the steel tube to transfer applied loads from concrete pile caps to steel piles under axial static pull-out, push-out.

ACKNOWLEDGEMENTS

CONTENTS

8.   BOND STRENGTH FORMULATION

9.   CONCLUTION AND FURTHER WORK

R   REFERENCES

A1   STRAIN GAUGE ARRANGMENTS

LIST OF FIGURES

LIST OF TABLES

1 INTRODUCTION

1.1 General

This research project is concerned with the bond strength of reinforced concrete plugs embedded in tubular steel piles subjected to pull-out, push-out and cyclic loadings.

The investigation ultimately proposes a model to describe the behavior of a reinforced concrete plug into a tubular steel pipe under axial static pull-out, push-out and cyclic loadings. The model will be used to predict the bond strength between a concrete plug and internal surface of the steel tube to transfer applied loads from concrete pile caps to steel piles. Based upon the test results of experimental work in this stage and previous tests, a model of partially reinforced concrete filled circular hollow steel sections is developed as a finite element model and bond strength and slip growth formulations, are developed to calculate,

- Ultimate Bond Strength
- Slip
- Load slip response
- Bond stress distribution
- Incremental Slip

In calculating the bond strength, slip, bond stress distribution and incremental slip due to repeated loading, the model can also take into account the effect of the shrinkage of the concrete plug. This contribution to the body of knowledge of the behavior of reinforced concrete plugs embedded into steel pipes will lead to a greater confidence in the prediction of bond strength in applications such as the substructure of offshore facilities.

1.2 Background

The legs of platforms of many offshore and coastal structures are usually founded on tubular steel piles through reinforced concrete pile caps. Wave, wind and earthquake loads tend to induce compressive and uplift forces in the legs, that in turn, subject the piles to compression and tension. This transfer of forces takes place through a concrete "plug" embedded in the top of the pile. The resistance of the embedded concrete plug is made up of the steel-concrete bond strength through the plug length, (see Figure 1).
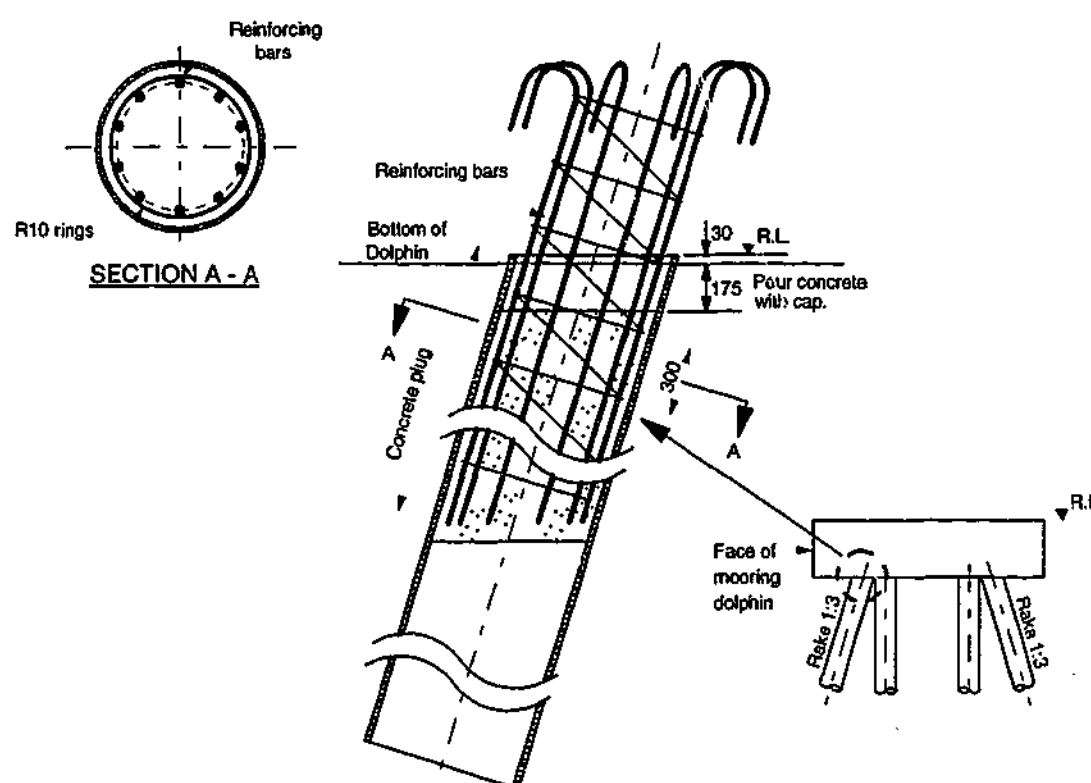
Figure 1.1 A typical connection between steel pile and concrete pile cap

The composite action in such a system is due to the chemical adhesions between the concrete and the internal surface of steel pile and mechanical interlock. Investigations have shown that these mechanisms depend on the surface roughness of the steel tube and the variation of shape of the cross section of the

steel tube. Values of bond strength for non reinforced concrete plugs in compression reported in the literature, varied from 0.4 to 1.0 Mpa.

Due to lack of reliable allowable bond strength for design purposes, the investigation of pull out bond strength within concrete filled circular steel sections was initiated in 1997 in the Civil Engineering Department of Monash University. The investigation continued through 1998 and 1999 to evaluate the bond strength of push out and cyclic loading conditions. Dr. Riadh Al- Mahaidi and Professor Paul Grundy have supervised students to accomplish experimental investigations.

1.2.1 Behavior under push out loading

The investigations at Monash University indicated that the bond strength between concrete and steel is lower in compression than tension. The bond strength of the reinforced concrete plug embedded in steel tube in compression is a function of both chemical adhesion of the steel – concrete interface and mechanical interlocking between the concrete core and steel surface.

The micro adhesion of the interface relates to the surface roughness of the steel section and the mechanical interlocking of the concrete plug in the steel tube during push out is attributed mainly to the dilation through Poisson's ratio effect of the concrete within the steel tube, causing an increase in contact stresses, which results in an increase in friction. Load transfer through bond in the vicinity of the load source is higher than that near the base of the concrete plug due to the same Poisson effect. At the top of the typical specimen, there is very little vertical load transfer to the steel tube. The concrete, which is subject to very high compression stresses, expands laterally, so that top of the steel section is forced to grip the concrete plug. In the vicinity of the base of the plug, the steel tube carries most of the longitudinal load. This causes the tube to expand, while the expansion of the concrete plug is very small due to the low level of compressive stress in the concrete core. This leads to separation between the steel and concrete at the bottom.

Push-out Force — High contact pressure / Due to the Poisson's effect

High compressive stress on concrete

Low compressive stress in the steel tube

High compressive stress in the steel tube
Low compressive stress on concrete

Separation
Due to the Poisson's effect

Steel Tube
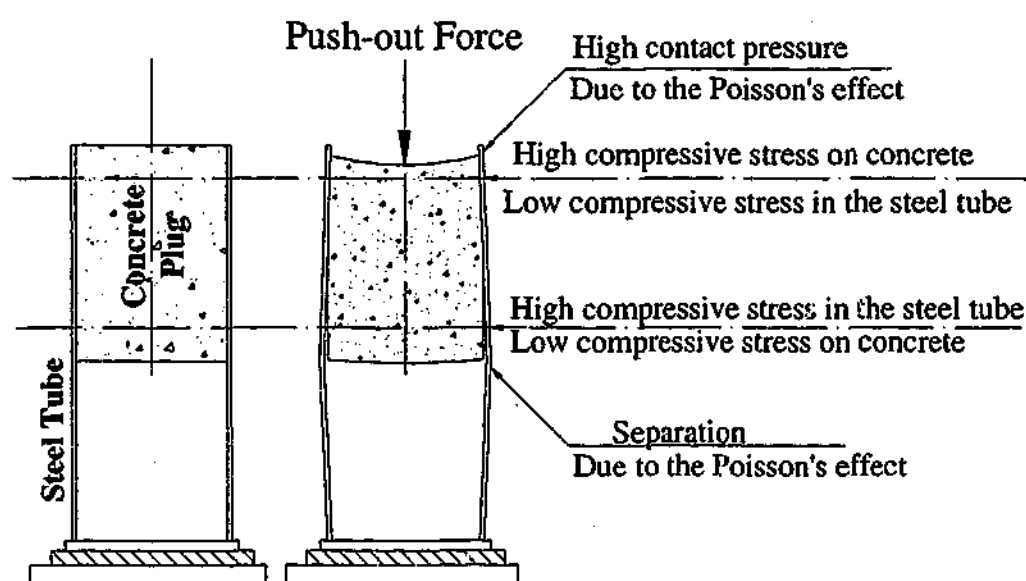
Concrete Plug

Figure 1.2 Bond strength mechanisms in push out

1.2.2   Behavior under pull out loading

In the tension (pull out) case, the reverse is expected to occur. That is, near the base of the concrete plug, the steel tube contraction is much higher than that of the concrete core, causing it to grip the concrete plug. Near the top part of the plug, the tension force is transferred to the concrete through the reinforcing bars embedded in the concrete plug and in the pile cap. The tensile stresses that develop in the concrete core result in the contraction of the concrete, while the steel tube contraction is relatively very small. This should result in the occurance of separation between the steel tube and the concrete.

The main mechanism that is believed to contribute to the high bond strength in pull out tests was the dilation of concrete due to the wedging action exerted by the deformed steel bars against the concrete layer between the steel bars and the steel tube.

Pull-out Force

Separation
Due to the Poisson's effect

High tensile stress on concrete
Low tensile stress in the steel tube

High tensile stress in the steel tube
Low tensile stress on concrete

High contact pressure
Due to the Poisson's effect

Concrete Plug

Steel Tube
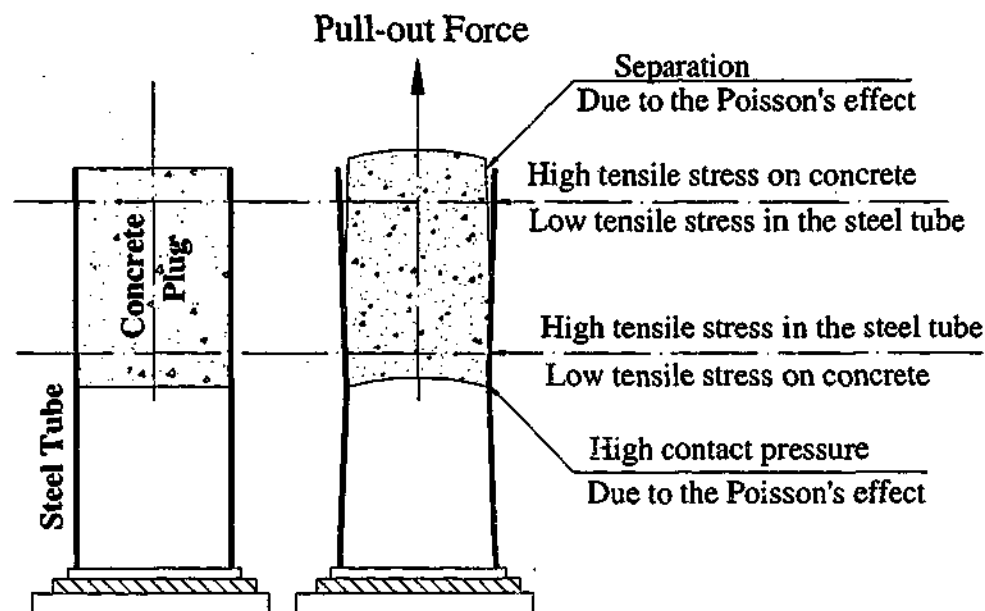
Figure 1.3 Bond strength mechanisms in pull-out

1.2.3 Cyclic loading

Generally, the cyclic loading reduced the ultimate capacity of specimens. The cyclic loading was shown to reduce the stiffness of the system consistently with each and every cycle. Variations between the degradation of the stiffness of the specimens of the different depths were minimal, when subjected to similar stresses.

1.3 Report Organization

Areas of the literature that were particularly important to the conduct of this research are reviewed in Chapter 2 of the report. These areas are the behavior of concrete plugs embedded in steel tubes under tension, compression and cyclic loading, the effective parameters on bond strength and finite element analysis.

In Chapter 3 the previous static pull-out and push-out tests are presented and explained. In Chapter 4, the experimental program that was undertaken on the combination of pull – out, push – out and cyclic loading tests in stages 1 and 2 of

the experimental set are described. The results of that testing program are presented and discussed in Chapter 5. The objective of the implementation of Non linear finite element analysis (NLFEA), the physical model, its geometry and simplification are presented in Chapter 6.

In Chapter 7 the results from the NLFEA models are compared with the data from the experimental tests on concrete plug specimens under axial static loading.

The final formulation of bond strength is performed in Chapter 8 and Chapter 9 gives the conclusions from this work, together with suggestions for further work.

2 LITERATURE REVIEW

2.1 Introduction

This chapter is intended to give the reader an insight into previous research on the behavior and strength of concrete filled circular steel tubes. As outlined in Chapter 1, the particular focus of this research is the bond strength of concrete plug steel tubular piles and significant attention is given to previous investigations that have included the bond between concrete plug and steel tube interface. Experimental investigations that have been undertaken as well as recommendations, analytical models and formulation of bond strength predication are discussed.

The basis of these recommendations is discussed in this section and the ability that these methods have in prediction of bond strength and therefore the ultimate strength of this type of structure is assessed.

2.2 Composite Columns

Concrete filled steel tubular columns are a composite column made by filling steel tubes with plain or reinforced concrete. This gives the advantage of combining the properties of steel hollow sections with the confined concrete. Concrete filled steel tubular (CFST) columns offer a number of advantages in both design and construction.

The steel tube

- Acts as permanent formwork for the plastic concrete
- Provides well-distributed steel as reinforcement in the most efficient position to resist applied bending moments

- Confines the hardened concrete, which increases its strain capacity and strength
- Protects the surface of the concrete from damage and deleterious environmental effects, such as carbonation

In turn, the concrete increases the critical buckling stress of the (imperfect) steel tube by changing its buckling mode, particularly for noncircular sections.

Overall, this kind of composite column

- Improves the speed of construction
- Reduces the cross sectional dimensions of the column for a given column strength, thereby making more floor area available
- Offers higher impact resistance and considerable toughness
- Improves overall member ductility and energy absorption

Some disadvantages include a reduced fire resistance, and connections between the steel floor beams and tubular columns sometimes being limited to simple joints because of the difficulty to achieve full moment continuity.

Nonetheless, in many situations, the advantages offered by CFST columns outweigh their disadvantages. Consequently, this form of construction has enjoyed an increase in popularity in recent years and has been used primarily as columns supporting platforms or as a pile-platform connection in offshore structures, roofs of oil storage tanks, columns for large industrial workshops and open-air overhead cranes, as well as piles and piers for bridges and viaducts. Their use as columns in multistory buildings has increased in recent years as the benefit of increased load-carrying capacity for a reduced cross section, resulting an increased in net floor space, has been realized. Because of their excellent ductility, CFST columns have also been used in earthquake resistant structures, particularly in Japan.

In recent years, many investigations have proposed analysis and design rules for concrete filled steel columns based on experimental models of steel tubes filled with concrete and tested in compression.

One of the concerns associated with composite columns is the influence of bond strength between inside of the steel tube and infill concrete upon the behavior under different loadings. Most of past experimental investigations in behavior of CFST columns assumed full bond and a complete continuity of strains between steel and concrete.

In fact, the composite action in CFST columns is due to the chemical bond strength and mechanical interlock. Investigations have shown that the ultimate capacity of the column and the bond strength effective mechanisms depend on the following parameters.

- Variation of shape of the cross – section of the steel tube
- Roughness of the steel tube internal surface.
- Imperfection of the interior of the tube
- Tube diameter to wall thickness ratio (D/t)
- Length-to-plug diameter ratio (L/D)
- Confinement of the concrete core
- Shrinkage and compressive strength of the concrete

Each of these research areas will be considered in this chapter.

2.3 Bond Strength of Concrete Filled Steel Tubes

The bond between the concrete core and the steel tube is an important characteristic of the response of composite CFST columns. It is believed that the bond strength has a significant effect on the behavior of composite members. However, careful examination of previous test results indicates that there is still uncertainly about the effect of bond strength on the response of CFSTs.

The bond stress demand varies for different structural systems and different locations in a structure. Demand was always greatest in regions of geometric discontinuously such as connections and foundation supports. Far less bond stress demand is required in connections where elements penetrate concrete filled or concrete fill the tube partially.

The earliest experimental study of bond strength of concrete filled steel tubes was carried out by Virdi and Dowling (1975). A number of parameters were varied to study their effects on the bond strength between concrete and steel. It was concluded that the resistance to the push out test in filled tubes derives primarily from the interlocking of concrete in two types of imperfections in steel. The first relates to the surface roughness of the steel and the second relates to variation in the shape of the cross section, away from the ideal cylindrical surface. The interlocking of concrete in the surface roughness of steel, that is micro locking, contributes a useful component of the ultimate bond strength related to the initially stiff region of the load deflection characteristics. This bond is broken when the concrete interface attains a local strain of 0.0035 associated with the compressive crushing of concrete. This component of bond resistance is distinguished from the resistance obtained due to the interlocking of the concrete in the undulating surface of the steel tube. This latter type of interlocking, termed macro locking is, related to the later stage of the load-deflection characteristics associated with the primarily frictional movement. The remarkable parallel nature of the characteristics in this region tends to confirm this relationship. It was also noted by Virdi and Dowling, that by better compaction both micro locking and macro locking could be enhanced, resulting in a higher value of ultimate bond

strength. It was suggested that ultimate bond strength is not influenced to any appreciable degree by factors such as the length of concrete and steel interface, steel tube diameters or thickness, or the concrete strength. Virdi and Dowling proposed the bond strength of 1 MPa for design.

Morishita et al (1979) conducted tests based on measuring the strain in the steel rather than a relative movement of concrete to the steel. The reason for this was to more accurately mirror conditions in composite construction. The aim of this experimental study was to investigate the relationship between concrete strength and bond. The results showed that, contrary to the Virdi and Dowling (1975) study, there was a relationship between strength and bond. The quoted bond strength was 0.2 to 0.4 MPa. This is considerably lower than that found by Virdi and Dowling. The second study by Morishita et al (1980) was aimed at increasing the bond strength between steel and concrete. This was achieved by using expansive concrete and checker plate steel tubes. Both these measures enhance the micro locking described by Virdi and Dowling (1975). The conclusion of this study was that both methods improved initial bond. When only expansive concrete was used, the resistance dropped to levels that normal concrete attained after the initiation of slipping. It also showed that expansive concrete bond increased with concrete strength.

Okamato and Maeno (1988) investigated the effect of bond strength between the steel tube and concrete core on the behavior of C;T columns filled with high strength concrete. The objective of this study was to investigate the effects of aspect ratio, level of axial force and bond strength on the bending capacity of the columns. Tests were conducted on nine square columns filled with high strength concrete (f_c' =98.1 MPa). In order to control the bond strength, a mortar layer with a thickness of 10 mm was placed between the steel tube and the concrete core. According to the test results, it was concluded that; (1) the bond strength has no significant effect on the flextural capacity of CFT columns, (2) the flextural capacity considerably increased by increasing axial load, (3) the steel tube has a significant effect on improving the compressive strength of concrete and

preventing the brittle failure that is normally associated with unconfined high strength concrete. The range of variables used in Okamoto's study was limited. Moreover, for each test the two main variables (level of axial force and mortar strength) were changed at the same time. In this situation, a solid conclusion is difficult to be made.

Contrary to Okamato and Maeno (1988), the experimental studies carried by Matumara and Matai (1992) indicated that the bending moment capacity would increase by improving the bond between steel tube and concrete core. To improve bond strength, steel tubes with inner ribs were used. The tests were carried out on eight cantilever square columns. In this research the effects of inner ribs and the level of axial force were investigated. Voids were provided at the top of columns to clarify the effect of the inner ribs. Each column was subjected to constant axial load and cyclic lateral load. Columns with inner ribs showed larger energy dissipation and higher ductility.

An extensive investigation of the push out strength of concrete filled tubular members was undertaken by Shakir – Khalil (1991, 1993a, 1993b). The main parameters studied were the shape of the tube, interface length, interface condition and the use of mechanical connectors. The first test series were aimed at determining the difference between CHS (circular hollow sections) and RHS (rectangular hollow sections) in an oiled or non-oiled state. The result was that an oiled specimen had approximately half of the bond resistance compared to the normal specimen. It was also noted that, in agreement with Virdi and Dowling (1975), specimen length was not a significant factor on the bond strength. Further, it was shown that CHS had a superior load carrying capacity compared to the RHS. The resistance of the circular section is enhanced due to the much stiffer confinement of the concrete during slip as it rides over the asperities and irregularities of profile of the steel tube. A bond strength of 0.4 MPa was proposed for design purposes.

Roeder et al. (1999) tested 20 specimens in company with a finite element analysis to examine the bond stress capacity of circular CFT members. The

variables involved were the diameter of the concrete core, the wall thickness of the steel tube and the shrinkage of the concrete core. It was concluded that shrinkage can be very detrimental to bond stress capacity, and the importance of shrinkage depends upon the characteristics of the concrete, the diameter of the tube and the surface condition inside the tube. It also was noted that the bond capacity is smaller with large diameter tubes and large D/t ratios. The bond capacity is interrelated with slip at the steel concrete interface. An exponential distribution of bond stress prior to slip was expected, and more uniform distribution occurs after slip. Eventually a bond strength formulation was suggested that estimates the bond stress capacity and design recommendations at different performance levels.

Kilpatrick and Rangan (1999) undertook a series of tests to study the influence of the shear transfer by bond between the infill concrete and the inner surface of the circular steel tube. Three different case of bond were examined together with four different loading regimes and slenderness ratios. Companion tests on similar empty steel tubes were also undertaken to highlight the synergistic effect of the steel and concrete acting compositely together. It was concluded that the bond strength might be a consideration for stub columns because it appeared to influence both the strength of the column and its load-shortening response, as indicated by the discontinuities. It was also noted that the bond did not play a significant role in the behavior of beams and eccentrically loaded short and slender columns because the concrete was longitudinally confined.

2.4   The Influence of Shape and Aspect Ratio of the Steel Tube and Length to Depth of Concrete Core

Tests to investigate the axial strength of CFT columns have been performed on Varieties of cross sectional shapes, steel tube diameter to thickness (D/t) and plug length to diameter L/D ratios. Furlong (1967) investigated 13 specimens with D/t ratios ranging from 29 to 98. Results indicated that each component of the

composite column resisted load independent of each other, and consequently there was no bond between the steel tube and concrete and no increase in the load resisting capacity due to confinement of the concrete core. Knowels and Park (1969) studied 12 circular and seven square columns with D/t ratios of 15, 22, and 59, and L/D ratios ranging from 2 to 21. Results indicated that the tangent modulus method accurately predicted the capacity for columns with L/D ratios greater than11 but were slightly conservative for columns with small slenderness ratios. It was concluded that this larger than expected capacity for composite columns with L/D less than 11 was due to the increase of concrete strength resulting from triaxial confinement effects. It was observed that for certain values of longitudinal strain the concrete began to increase in volume due to micro cracking, which induced concrete confinement by the steel tube. This confinement increased the bond strength and the overall load resisting capacity of the CFT column. However this increase was noted for circular tubes only, not for square or rectangular shapes. Furthermore, it was determined that this increase occurred only in short columns. For columns with large L/D ratios the composite section failed by column buckling before reaching the strains necessary to cause an increase in concrete core volume.

Sakino et al. (1985) tested 18 circular specimens with D/t ratios ranging between 18 and 192. In this investigation, three otherwise identical specimens were subjected to different load conditions. Axial load was applied to the concrete and the steel tube simultaneously for the first specimen group. The load was applied exclusively to the concrete core in the second specimen group, and the load application was similar to this in the third group except that the inside tube wall was greased before casting the concrete. Results indicated that when the steel tube and the concrete core were loaded simultaneously, the tube provided no confinement and bond between the steel tube and the concrete core until post-yielding behavior. In the concrete loaded only specimens, some longitudinal stresses were noted in the steel tube even for the columns with the greased wall. Therefore, regardless of the loading condition, the wall of the steel tube appeared to be primarily in a biaxial stress state. The test results indicated that the bond strength is a function of mechanical interlocking between steel tube and the

concrete core. It can be suggested that the mechanical interlocking is attributed mainly to the dilation through Poisson's ratios effect on concrete within the steel tube, causing an increase between contact pressure and friction.

Although test results indicated that the axial stiffness of the concrete loaded only columns were about half that of the other CFTs tested, the concrete loaded only columns obtained a greater yield and ultimate axial load capacity.

The above research demonstrated that slender columns did not exhibit the beneficial effects of composite behavior, in which concrete strength increased over that of the cylinder strength due to confinement. Thus, it was concluded that the concrete core and the steel tube acted independently of each other. Short columns however, exhibited greater than predicted capacity, generally associated with the higher concrete strength due to the bond strength between the steel tube and the concrete core and also confinement offered by the steel tube.

Virdi and Dowling (1975) tested three specimens each of five different lengths to study the influence of contact length on bond strength. The contact length was varied from 149 to 445 mm corresponding to length to diameter ratios of 1.0, 1.5, 2.0, 2.5, and 3.0. Average bond strengths of 1.96, 1.76, 2.09, 2.3, and 2.63 MPa were respectively reported. Test results indicated that except for the shortest contact length the bond strength appeared to increase with contact length. However it was concluded that the contact length of the concrete core and steel tube interface does not have any appreciable influence on the bond strength. Eighteen specimens with D/t ratios of 17.7,26.5, 31.2, 34.3, 34.5 and 34 were tested. Test results suggested that the aspect ratio has no significant effect on average bond strength.

Contrary to Virdi and Dowling's conclusion, Shakir – Khalil's (1991, 1993a, 1993b) test results indicated that an effective wall width, which is dependent on the wall thickness of the steel tube, might be a feasible concept when dealing with the resistance of the concrete-filled rectangular hollow section to a push out force. It was also noted that, in agreement with Virdi and Dowling (1975), specimen

length was not a significant factor on the bond strength. Further, it was shown that circular sections are much more effective than rectangular sections in resisting push out forces. This was probably due to the fact that the resistance of the circular section to a push out force is greatly enhanced as a result of any longitudinal variation in the internal dimensions of the steel tube.

Roeder et. al.'s (1999) test results in an analytical study to examine the bond stress capacity of circular CFT members indicated that the maximum average bond stress capacity is somewhat smaller with longer column lengths and larger D/t ratios and diameters due to the lack of the stiffness to enforce the benefits of irregularity in the cross section.

Test results of the above references showed that the average bond stress for rectangular tubes was approximately 70% smaller than the average for circular tubes. It also indicated that the influences of the steel tube aspect ratio (D/t) and concrete core length to depth (L/D) on the bond strength are not completely understood.

In this thesis, circular steel tube with the steel tube aspect ratio (D/t) of 21 was used for all specimens in experiment and a parametric study of the steel tube aspect ratio (D/t) of 20 to 40 was then investigated using NLFEA solution scheme. The concrete core length to diameter (L/D) varied from 1 to 4 to investigate effect of (L/D) on bond strength of partially filled steel tube with reinforced concrete.

2.5 The Influence of Surface Roughness and Imperfection of the Steel Tube

The bond transfer between the steel tube and the concrete core depends on the radial displacements due to the pressure of the concrete on the shell and the shrinkage of the concrete core, together with the rugosity (or internal surface irregularities) of the interior surface of the tube.

Virdi and Dowling (1975) concluded from a large number of tests results that mechanical interlock of the concrete core increases with the irregularities in the steel tube. This mechanical keying could however, arise due to two different types of irregularities. The first type occurred due to the roughness of the steel surface. The rupture of this primary interlocking may then be related to local crushing of the concrete layer in contact with the steel tube. This lends substance to the adoption of the strain of 0.0035 as a critical value for the definition of ultimate bond strength. The second type of bond resistance occurred due to the imperfection of the steel tube. This type of interlocking contributed in essence to the frictional resistance associated with the later flat portion of the load-deflection response.

Shakir – Khalil (1993a) tested specimens with two types of interface conditions. The interface of half of the specimens in this series was covered with oil prior to the casting of the concrete core. The average bond strength result for each group indicated that the 'dry' specimens give average bond strengths that are about twice those of 'oiled' specimens for both rectangular and circular specimens. It was concluded that the push out resistance of concrete filled steel hollow sections is rather sensitive to the roughness and conditions of the steel-concrete interface and also to the irregularities in the internal dimensions of the steel hollow section. These factors respectively affected the micro- and macro-resistances of the section to the push out force. It was also noted that the 'oiled' specimens exhibited a longer transitional curve between the linear part of load-slip response and the point at which the maximum load was reached.

Roeder et al. (1999) concluded that the roughness and conditions of the steel-concrete interface and also the irregularities on the inside of the tube significantly increase the bond strength on specimens of small diameter (150 mm) and small d/t ratios. However, the evidence of the experiments suggested that tubes with larger d/t ratios and diameters lack the stiffness to enforce the benefits of irregularities in the cross section.

Kilpatrick and Rangan (1999) tested a series of stub CFST columns with three different concrete-steel interfaces. For the first specimens as a maximum bond condition, self-tapping screws were inserted through holes in the wall of the steel tube. For the second group as a partial bond condition, an intermediate level of shear transfer was achieved by a thorough degreasing of the inside of each specimen in the as received condition. Chemical adhesion between the concrete and the inner surface of the steel tube in the as received condition was minimized by heavily coating the surface with oil for third specimens as a minimum bond condition. The measured strengths of the stub columns (L/D=3.5) ranged from 990 kN for the minimum bond case to 1063 kN for the maximum bond case, which is a range of ±36.5kN, or 3.6%. The maximum forces sustained for short columns (L/D ≅10) varied between 440 kN for the minimum bond column and 450 for the partial-bond column. It was concluded that concrete-steel interface conditions, which was called bond conditions in this investigation, did not significantly influence the strength of the composite columns tested.

Results of the above references showed that the average bond stress improved with the increase of the roughness and irregularities of the internal surface of steel tube.

2.6   The Influence of the Concrete Strength, Age and Shrinkage

Virdi and Dowling (1975) tested three specimens each of six different design concrete strengths varying from 24 to 41 MPa. Test results indicated that the bond strength was not greatly influenced by the variation in the concrete compressive strength. It was also noted that higher strength concrete, due to its naturally higher shrinkage, will tend to diminish the mechanical interlocking, thereby reducing the influence of concrete strength on bond strength. In another series of tests specimens were tested at different ages of the concrete to study the influence of concrete age on the bond. It was concluded that the bond strength increased with age of concrete up to 21 days of age and decreased thereafter. The results showed

noticeably lower values of bond strength for the group of specimens tested at the age of 47-48 days.

Roeder et al. (1999) concluded that shrinkage could be very detrimental to the bond stress capacity. Care must he exercised about the shrinkage potential of the concrete mix when the use of bond stress is being relied upon in large diameter steel tubes. It was also noted that the bond strength was not related to the strength of concrete.

Kilpatrick and Rangan (1999) suggested that shrinkage could be a consideration for the large diameter columns. This is because, unless special precautions are taken to eliminate shrinkage of the concrete through the depth of the cross section, a significant gap, perhaps approximately a millimeter may develop between the inner face of the tube and the hardened concrete. This gap could only be subsequently closed by lateral expansion (Poisson's effect) of the concrete compressed in the longitudinal direction. If this was not achieved, the compressive concrete would therefore behave in the un-confined state, and the beneficial effect of composite action would be severely reduced or lost entirely.

Results of the above references show that the concrete compressive strength has no consistent effect on the bond strength. On the contrary, shrinkage of the concrete seemed to be very detrimental to bond stress capacity and CFTS behavior.

2.7   Confinement Effects on Concrete

Multi-axial stress states govern in many cases the load resistance of concrete structures. It is known that under multi-axial compression the load resistance and the deformation capacity of concrete are increased. There is a strong interaction of the non-linear deformation and the activation of confining stresses. Hence, a realistic description of the deformations of concrete in tri-axial compression is as important as the formulation of the strength envelope.

It has been observed that the ultimate axial capacity of CFT columns is larger than the sum of uncoupled steel and concrete failure loads. The confining of the steel tube on the concrete causes the increase in the failure load. The structural behavior of CFST columns is considerably affected by the difference between the Poisson's ratios of the steel tube and concrete. In the initial stage of loading, the Poisson's ratio for the concrete is lower than that of the steel tube. Thus the steel tube has no confinement effect on the concrete. As longitudinal strain increases, the lateral expansion of concrete gradually becomes greater than expansion of steel tube. At this stage the concrete becomes tri-axially stressed and the steel tube biaxially stressed.

Mei et al. (2001) conducted an experiment on the stress-strain characteristics of steel sleeve confined high-strength concrete (HSC). The axial load and strain of the concrete, and the axial and hoop strains of the confining steel sleeve were measured. From these measurements, accurate stress-strain relations of the concrete core were produced, along with confinement calculations based on von-Mises elastoplastic response of the steel sleeves. Confinements varied from 5 to 19 MPa were calculated. This confinement had a profound effect on the concrete, as much as tripling its unconfined strength of 70 MPa. The increase of ductility was found to develop more slowly for low amounts of confining steel due to a lagging development of confining pressure.

It was suggested that the ACI equation for estimating the secant modulus of elasticity $E_c = 0.043 w^{1.5} \sqrt{f_{cm}}$ predicts values as much as 20% too high for concrete with a compressive strength in the vicinity of 80 MPa. Furthermore, the ACI code current expression for the modulus of rupture $f_r = 0.4 \sqrt{f_c'}$ may be too conservative for HSC. The alternative expression $f_r = 0.1(f_c')^{2/3}$ appeared to be more representative of the test data.

It was proposed that the anticipated (theoretical) failure stress for each case be estimated using the Mohr-Coulomb failure criterion. Consider a tri-axial failure

state of stress with isotropic stresses in the horizontal orientation ($f_2' = f_3'$). The following formula was proposed to calculate confined compression strength f_{cc}' to the confining stress f_2'.

$$f_{cc}' = f_2' K_p + 2c\sqrt{K_p} \tag{2-1}$$

Where c is the cohesion intercept; $K_p = \tan^2(45+\phi/2)$; and ϕ is the angle of internal friction, often taken approximately equal to 48 degrees.

It was concluded by Mei et al. (2001) that HSC is pressure sensitive with an internal friction angle of 49.5 degrees base on Mohr-Coulomb failure envelope. It exhibited, however, a much smaller Poisson type of lateral expansion due to axial compression. As a result, interactive confinement is slow to develop unless larger than common amount of confining steel is used. When interactive confinement due to lateral reinforcement is developed, it results in significant gains in ductility, which for the experiments conducted in this investigation developed in a linear relation to the amount of confining reinforcement.

Mender et al. (1988) proposed a unified stress-strain approach to predict the pre-yield and post-yield behavior of confined concrete members subjected to axial compressive stresses. The model utilizes the equation given by Popovics in 1973, originally developed to represent the stress-strain response of unconfined concrete. This model is based on a constant confining pressure σ_R. The axial stress of the confined concrete f_{cc} for any given strain ε_{cc} is related to peak confined strength f_{cc}' as follows:

$$f_{cc} = \frac{f_{cc}' x r}{r - 1 + x^r} \tag{2-2}$$

$$x = \frac{\varepsilon_{cc}}{\varepsilon_{cc}'} \tag{2-3}$$

where ε'_{cc} is the strain at the peak strength f'_{cc}

$$r = \frac{E_{co}}{E_{co} - E_{sec}} \qquad\qquad (2\text{-}4)$$

where E_{co} is the tangent elastic modulus of unconfined concrete, and can be estimated as $5000\sqrt{f'_c}$ (MPa). E_{sec} is the secant modulus of confined strength and can be estimated as $f'_{cc} / \varepsilon'_{cc}$.

The peak confined strength f'_{cc} is a function of the unconfined strength f'_c and the constant lateral pressure σ_R as follows

$$f'_{cc} = f'_c \left(2.254\sqrt{1 + 7.94\frac{\sigma_R}{f'_c}} - 2\frac{\sigma_R}{f'_c} - 1.254 \right) \qquad\qquad (2\text{-}5)$$

The strain at peak-confined strength ε'_{cc} is given as a function of the strain at peak unconfined strength of concrete ε'_c by

$$\varepsilon'_{cc} = \varepsilon'_c \left[1 + 5\left(\frac{f'_{cc}}{f'_c} - 1 \right) \right] \qquad\qquad (2\text{-}6)$$

Given a value of the unconfined strength f'_c, and constant confining pressure σ_R, can be used to evaluate f'_{cc}. The corresponding strain ε'_{cc} can be estimated by Eq. (2-6). This model can predict the behavior under a constant confinement pressure.

In this thesis, a combination of Mohr-Coulomb failure envelope and Mender et al (1988) formulation was used in initial parametric study of NLFEA to consider effect of confinement on behavior of concrete plugs in tubular steel piles.

2.8   Cyclic Loading Effects

Dynamic tests are quite useful in the evaluation of the behavior of structural elements subjected to accidental or dynamic loading. This type of dynamic test, for which loading conditions differ significantly from those of conventional static loading, allows the degree of damage of the structural element to be measured under the effect of repeated cyclic loading.

During static loading it has been established that concrete confinement in a steel tube is more efficient than confinement by conventional reinforcement (Lahlou 1994). However, the potential role of the autogenous shrinkage of the concrete and the effect of the tube-concrete interface on the behavior of the composite element are still ignored by most researchers. This would not hold true in the case of load cycling, which may lead to localized failure that can increase the damage under repeated loading and unloading cycles.

Lahlou et al (1999) conducted an experimental study on the behavior of short concrete columns confined by steel tubes under cyclic compression loading. Eight 115 × 350 mm columns were subjected to rapid compression loading cycles. The test results were compared with those obtained with similar columns subjected to monotonic static compression loading. It was concluded that the envelope of the rapid loading cycle curves could be approximated from the static load-displacement curve by multiplying the ordinate values by a dynamic amplification factor. This factor depends on the rate of strain, the concrete compressive strength, and perhaps the confinement level. Once the first (and sometimes the second) cycle is completed, during which concrete is consolidated within the tube, the cyclic behavior of the concrete column confined inside the steel tube may be similar to that of elastoplastic material where the branches of unloading-reloading curves remain perfectly linear and parallel. Damage manifests itself only by a progressive plastic strain. Columns confined inside of

steel tube show a great capacity for absorbing and dissipating energy input from dynamic loading excitations.

The previous work on behavior of the CFT columns in cyclic loading was concluded that the key attributes of behavior include the following:

1. The stiffness of CFTs on load reversal is of the same order of magnitude as the stiffness of the virgin beam-column (i.e., they unload elastically). However, the elastic stiffness degrades somewhat after the first half-cycle of loading (i.e., after concrete begins to crush) before sustaining a relatively constant value (Sakino and Tomii, 1981).

2. The zone of approximate linear behavior, effectively the elastic zone, of a CFT shrinks with successive cycles of plasticity, although it never vanishes completely. As a CFT specimen is cycled, the concrete begins to crush, leading to a noticeable loss of elastic strength. The elastic strength loss propagates further as the steel undergoes cycles in which local bucking occurs (Sakino and Tomii, 1981).

3. The maximum strength of a CFT decreases as the specimen is cycled. The experiments of Sakino and Tomii (1981) indicated that CFTs initially exhibit an increase in capacity beyond their normal monotonic strength. This may be due either to cyclic strain hardening of the steel, or perhaps to the experiments having fixity conditions that offered more resistance than expected.

4. CFTS exhibit the "Bauschinger effect", a phenomenon commonly associated with the stress-space behavior of metals (Dafalias and Popov 1975). The Bauschinger effect exhibited at the stress level by the steel tube thus propagates to the stress-resultant level (Hilmy and Abel 1985).

5. CFT specimens exhibit a gradual softening behavior from the initiation of plasticity to the point at which they exhibit a gradual a bounding stiffness, as evidenced in each cycle (Dafalias and Popov 1975; Hilmy and Abel 1985).

To the best knowledge of the writer, there exists no data or experimental studies on the bond strength of CFT columns subjected to cyclic loading.

2.9 Nonlinear Finite Element Analysis

Researchers have suggested analytical models and design procedures for composite columns and design codes have been formulated. Large discrepancies between various design codes and experimental studies exist in terms of geometric and strength parameters, even when the same design philosophy is adopted. The disagreement between the results indicates that more accurate design guidelines are required.

Nonlinear finite element analysis intended to provide tools to predict the structural characteristics of CFT columns such as strength, stiffness, and ductility that will lead to efficient use of CFT columns in structural systems. In view of the advantages and opportunities for innovation that CFT columns provide for earthquake resistant systems, the detailed description of nonlinear response of CFTs under axial loading certainly advances the state-of-the-art in design.

The purpose of this section is to give a brief overview of the current state of the art models of non-linear finite element analysis to determine axial capacity available in literature. The models that are considered in this section are those that are capable of accounting for variation of the geometry and materials specifications of a cross section.

Hajjar et al. (1998) proposed a fiber-based distributed plasticity finite element formulation to perform three-dimensional monotonic analysis of square or rectangular concrete-filled steel tube (CFT) beam-columns. This stiffness-based beam-column element formulation accounted comprehensively for all significant geometric nonlinearity exhibited by CFT beam-columns as part of composite frame structures, and the steel and concrete constitutive models account for the significant inelastic phenomena, which are seen in CFT experiments. In addition, the finite element formulation accounted for slip between the steel and concrete components of the CFT by incorporation of a nonlinear slip interface. The formulation was able to capture behavior ranging from perfect bond to immediate

slip. The calibration and verification of the slip formulation were presented, and the finite element model was verified against experiments of CFT beam columns subjected to monotonic loading. The fiber element approach discretely models the CFT element end cross section into a grid of fibers, and the steel and concrete stress-strain behavior is tracked explicitly at each fiber. The calibrated parameters suggested that little slip is experienced in a CFT member before the bond strength of the slip interface is breached. In addition, the calibration value of bond strength used for analysis is higher than the value recommended by design codes, suggesting that the recommended design values may be conservative. However, regarding the previous studies, even for the more extreme conditions, slip is seen to have little effect on the global behavior of a composite CFT member subjected to flexure. Nevertheless, understanding the effect of slip more fully on the behavior of CFTs in composite structures warrants further compressive parametric studies.

Shams and Saadegvaziri (1999) developed a three-dimensional finite element model for CFT columns. The finite element model was calibrated against existing experimental results. Analyses of columns under axial loading indicated that the stress-strain properties of the confined concrete are highly affected by the geometrical configuration of the column as well as material properties of the concrete. A comprehensive parameter study was performed to identify the effect of different parameters such as width-wall thickness ratio (aspect ratio) and concrete uni-axial compressive stress. Based on this study the following conclusions were reached.

1. It was found that D/t, unconfined compressive strength of concrete, and cross-sectional shape have significant effect on the response of CFT columns, and then the relative effect is quantified. The confinement effect in circular columns is higher than that in square columns due to a more uniform stress distribution. Concrete with lower unconfined compressive strength exhibits higher confinement ratio than higher strength concrete.

2. The effect of composite action on important parameters of the stress-strain relationship for concrete, such as peak stress and strain at the maximum stress, are quantified. Based on the obtained results relating to confinement effect D/t, and between confined peak stress and unconfined compressive strength of concrete, analytical models were proposed to determine the maximum compressive stress and corresponding strain in concrete for both circular and square CFT columns.

Johansson and Akesson (2001) proposed a elasto-plastic model based on the Druker-Prager yield criterion having a confinement-sensitive sub-model. The model was calibrated against a series of laboratory experiments where a number of concrete cylinders were exposed to an active confinement pressure. Furthermore, the model was used in a FE study of concrete-filled steel tubes, in which the state of stress is more complex, and the confining stress is more complex and the confining stresses on the concrete core are induced by passive confinement provided by the steel tube. It was concluded that the confinement sensitivity affected both the strength and the hardening parameter and thereby also the plastic modulus. The confinement dependence is introduced by means of two adjustment functions, which derived either from tri-axial material tests or by the presented theoretical expressions. Since the shape of the descending branch of the concrete stress-strain relationship is not confinement-sensitive, the post-peak behavior of the composite columns was not captured adequately. It was also noted that for the columns with the load applied to the entire section, the bond strength did not affect the structural behavior. However, when the load was applied only to the concrete section, the load resistance increases and the stiffness decreases with lower bond strength.

Aval et al (2002) proposed a composite beam column element for large displacement nonlinear inelastic analysis of concrete filled steel tube (CFT) columns. The bond/slip formulation represented the interaction between concrete and steel over the entire contact surface between the two materials. Thus the modeling accounted for the two factors that caused the slippage between the steel shell and the concrete core. The first factor was the difference between axial

elongation of the steel shell and the concrete core, and the second was the difference between curvatures in the cross section for the concrete core and the steel shell. These effects are integrated over the perimeter and were added to the virtual work expression of the basic element. The model was used to analyse several CFT columns under constant concentric axial load and cyclic lateral load. The effect of semi- and perfect bond was investigated and compared with experiments. The results showed that the use of a studded or ribbed steel shell caused greater ultimate strength and higher dissipation of energy than the columns with non-studded steel shell. It was also noted that under the assumption of uni-axial state of stress-strain properties of the constituent materials are required to define the properties of any cross section.

2.9.1   Concrete material model

Hajjar et al. (1996 and 1998) used empirical uni-axial nonlinear stress-strain models to represent implicitly the multi-axial stress-strain behavior of the steel.
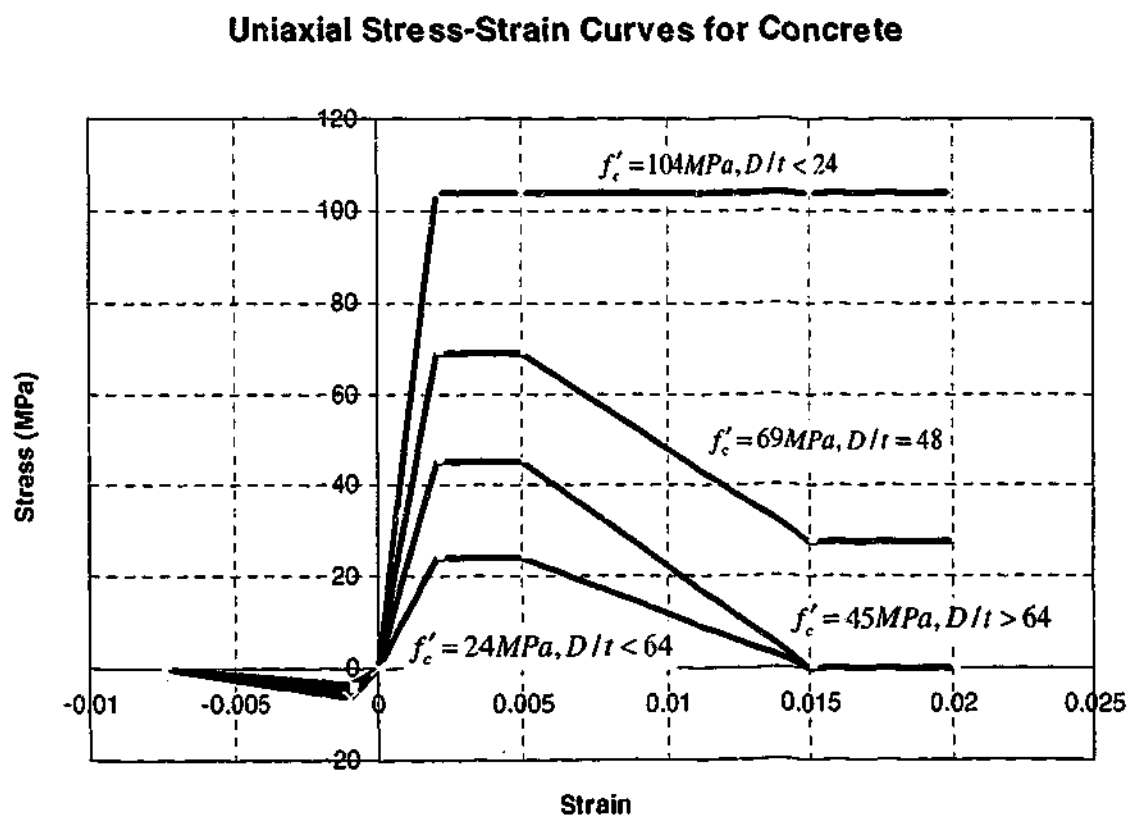
Figure 2.1 Uniaxial Stress-Strain Curves for Concrete

Figure 2.1 illustrates the basic form used to represent implicitly the multiaxial stress-stain curve for various combinations of concrete strength and D/t ratio. The rupture strength of the concrete, f_r, is given as $0.623\sqrt{f_c'}$, with all stress quantities in MPa.

Schneider (1998) modeled the concrete core using 20-node brick elements, with three translation degrees of freedom at each node. The three-dimensional concrete material model available in ABAQUS was developed to simulate conditions with uniaxial strain and relatively low confining pressure. Therefore, reasonable results were expected with confinement on the order of one fourth of the uniaxial compressive stress or less. Since the experimental results suggested that little confinement was observed for the concrete prior of the yield, this material model for the concrete was considered adequate. The unconfined uniaxial stress-strain curve for the concrete used in this analysis is shown in Fig. 2.2.

Concrete Material Model
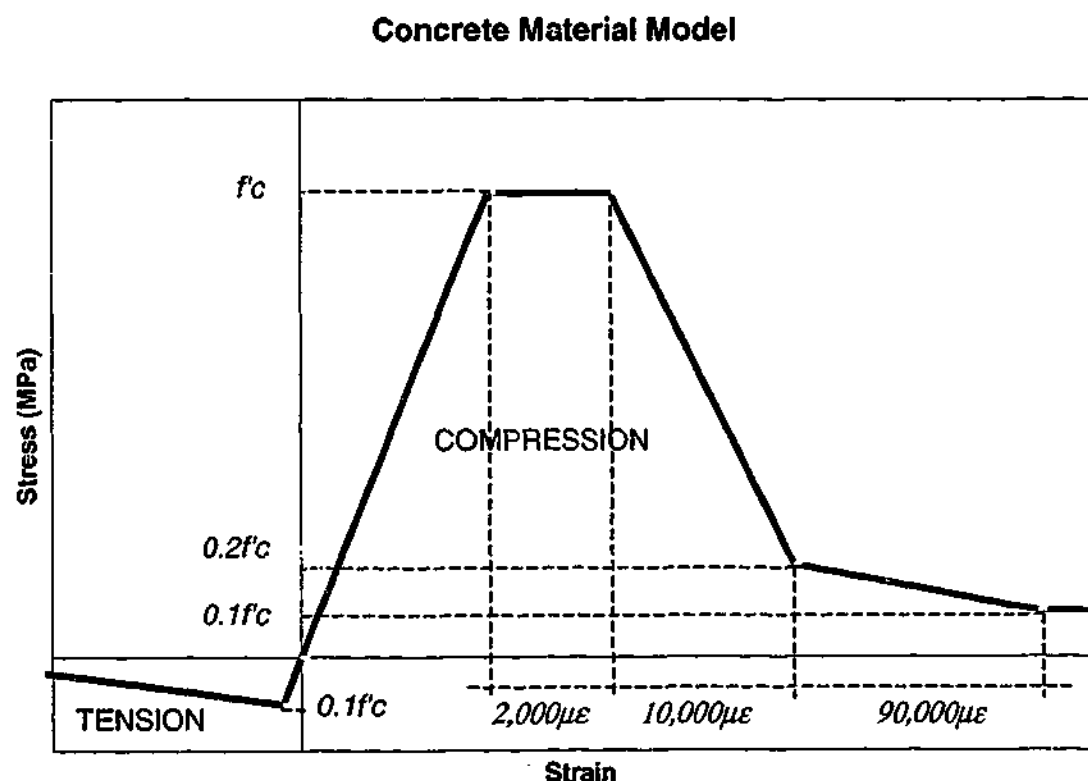
Figure 2.2 The Concrete Material Model

The stiffness beyond the ultimate strength of the concrete was indicative of the amount of confinement expected. This portion of the curve was adjusted according to experimental results.

Johansson and Akesson (2001) used a classical elasto-plastic model, but it is extended to include a confinement sensitive hardening behavior by means of two adjustment functions connected to the strength and the plastic modulus. The underlying model was chosen as the Drucker-Prager model with associative evolution laws. This was a choice guided by the aim of demonstrating a principle for introducing the confinement sensitivity into the constitutive formulation, but also guided by the fact that the main contributing factor for capturing the confinement sensitivity is given by the hardening rule. That is, the shape of the yield surface only comes into play at onset of yielding and its contribution to the response is not as dominant as the effect of the hardening rule.

To consider the increased concrete strength and strain due to confinement the following empirical formulation were used (Richard et al. 1928)

$$f_{cc} = f_{co} + k\sigma_{lat} \tag{2-7}$$

where f_{cc} is axial compressive strain of the concrete confined by the lateral stress σ_{lat}, f_{co} is uni-axial compressive strength of the concrete, and k is the so-called tri-axial factor and is found to be 4.1.

$$\varepsilon_{cc} = \varepsilon_{co}\beta_1\left[\left(1+\frac{k\sigma_{lat}}{f_{co}}\right) - \beta_2\right] \tag{2-8}$$

where ε_{cc} is axial compressive strength at peak stress, ε_{co} is axial compressive strain at peak uni-axial stress, $\beta_1 = 5$ and $\beta_2 = 0.8$.

The method chosen to introduce the confinement dependence into a hardening sub-model was by means of two adjustment functions f and g. These two functions are defined as polynomials of arbitrary power, i.e.

$$f(\sigma_{lat}) = \sum_{i=0}^{b} a_i . \sigma_{lat}^i \qquad (2\text{-}9a)$$

$$g(\sigma_{lat}) = \sum_{i=0}^{b} b_i . \sigma_{lat}^i \qquad (2\text{-}9b)$$

The first function scaled the strength K according to the current confinement while the second function scales the hardening parameter κ. In equations $(2\text{-}9a)$ and $(2\text{-}9b)$ the constants a_i and b_i were calibrated from pertinent test data.

The values for f_{cc} and ε_{cc} were calculated using equations $(2\text{-}7)$ and $(2\text{-}8)$ and corresponding values of K_{max} and κ_{max} according equations $(2\text{-}9a)$ and $(2\text{-}9b)$, respectively. The tri-axial factor k was set to 3.0 and the friction angle of 30°. Poisson's ratio for the concrete in the elastic part was approximately as $\nu_c = 0.2$.

Aval et al. (2002) and Shams and Saadegvaziri (1999) used a model based on the obtained results relating confinement ratio and D/t (aspect ratio), and between confinement ratio and uniaxial compressive strength. The following empirical formulations were used to consider the increased concrete strength and strain due to confinement.

$$f_{cc}' = f_c' \left(1 + \frac{A}{1 + \left(\dfrac{D/t}{B}\right)^\alpha} \right) \qquad (2\text{-}10)$$

where f_{cc}' is axial compressive strain of the concrete confined by the lateral stress f_c' is uni-axial compressive strength of the concrete, D/t is width to thickness of

steel tube, α is the shape factor and A and B are empirical parameters expressed in terms of f_c'.

$$\varepsilon_{cc} = \varepsilon_o \left(1 + \frac{3.51}{\left(\frac{D/t}{60}\right)^\alpha} \right) \qquad (2-11)$$

where ε_{cc} is axial compressive strength at peak stress, ε_o is axial compressive strain at peak uni-axial stress. For circular columns $\alpha = 1$ and the empirical equations A and B are as follows:

$$A = 1.83e^{-\left(\frac{f_c'}{3.55}\right)} \qquad (2-12)$$

$$B = -32.517 + \frac{510}{f_c'} \qquad (2-13)$$

The tensile behavior of the model takes into account tension stiffening and the degradation of the unloading and reloading stiffness for increasing values of the maximum tensile strain after initial cracking. A linear rate of tensile strength reduction is adopted in this model.

In this thesis, a combination of Mohr-Coulomb failure envelope and Mender et al (1988) formulation was initially used to consider effect of confinement on behavior of concrete plugs in tubular steel piles.

During the initial parametric study, it was found that the level of compressive stressing concrete is lower than the compressive strength of the concrete. Therefore, to minimize the numerical errors, it was decided to model the shrinkage of the concrete considering with only cracking criteria and non-linearity of the interface. It assumes that the compressive response of the concrete is elastic prior to cracking.

2.9.2   Steel tube material model

Hajjar et al. (1996 and 1998) assumed the compressive branch of the steel tube stress-strain curve to retain stress of f_y after yielding, but strain hardening neglected to account indirectly for the biaxial stress state in the steel due to confinement of the concrete.

Schneider (1998) and Johansson and Akesson (2001) modeled the steel tube using 8-node shell element with five degrees of freedom at each node. Inelastic material and geometric nonlinear behavior were used for this element. von Mises yield criteria defined yield surface, and the Prandtl-Reuss flow rule was used to determine inelastic deformations. No strain hardening characteristic were assumed for the steel tube.

Aval et al. (2002) and Shams and Saadegvaziri (1999) used the Von Mises elastic-plastic model with kinematic hardening for the steel tube.

In this thesis, the Von Mises elastic plastic material model and shell element were used for the steel tube.

2.9.3   The interface model

Hajjar et al. (1998) used a model based on the assumption that the steel and concrete are separated by a layer of springs, which determine the load transfer between the two materials based on nonlinear spring stiffness. Thus, to track the differential movement between these materials for a three-dimensional geometrically nonlinear CFT arbitrary oriented in space, and to allow for automated assembly of CFT elements into a global stiffness matrix of a composite frame during geometrically nonlinear analysis. The value of initial slip stiffness of k_{slip} of 10^4 MPa was chosen for the computation model.

Schneider (1998) used an interface gap element, which is available in ABAQUS, for the interface between the concrete and the steel components. The element has two faces, when the faces were in contact, normal forces developed between the two materials resulting in frictional forces. A coefficient of friction of 0.25 was used in the analytical models. On the other hand, if the gap element experienced tension, the element faces separate from each other, resulting no contact between the concrete and steel and consequently no bond developed.

Shams and Saadegvaziri (1999) modeled the interface between the concrete and steel tube using a gap contact elements. The gap contact elements is a special purpose contact elements that allow the nodes to be in contact or separate with respect to particular directions and separation condition. For this analysis, gap elements were placed between adjacent nodes of steel tube and the concrete with a fixed contact direction perpendicular to surface of the steel tube. The initial separation distance was specified as zero, in which case the gap initially closed (i.e. the concrete and steel tube are initially in contact with each other).

Johansson and Akesson (2001) used surface-based interaction with a contact pressure-over closure model in normal direction, and a coulomb friction model in the directions tangential to the surface to simulate the bond between the steel tube and concrete core. According to Baltay and Gjesvic (1990) the coefficient of friction, μ, between concrete and steel has a value between 0.2 and 0.6. In this study the best agreement was obtained when a coefficient of friction of 0.6 was used.

Aval et al. (2002) used a distributed bond interface element to represent relative slippage. The bond behavior were modeled by elastic-perfect plastic behavior with a yield point of 0.8 N/mm^2 and elastic stiffness of E_b = 1.6 N/mm^3 (See Figure 2.3.)
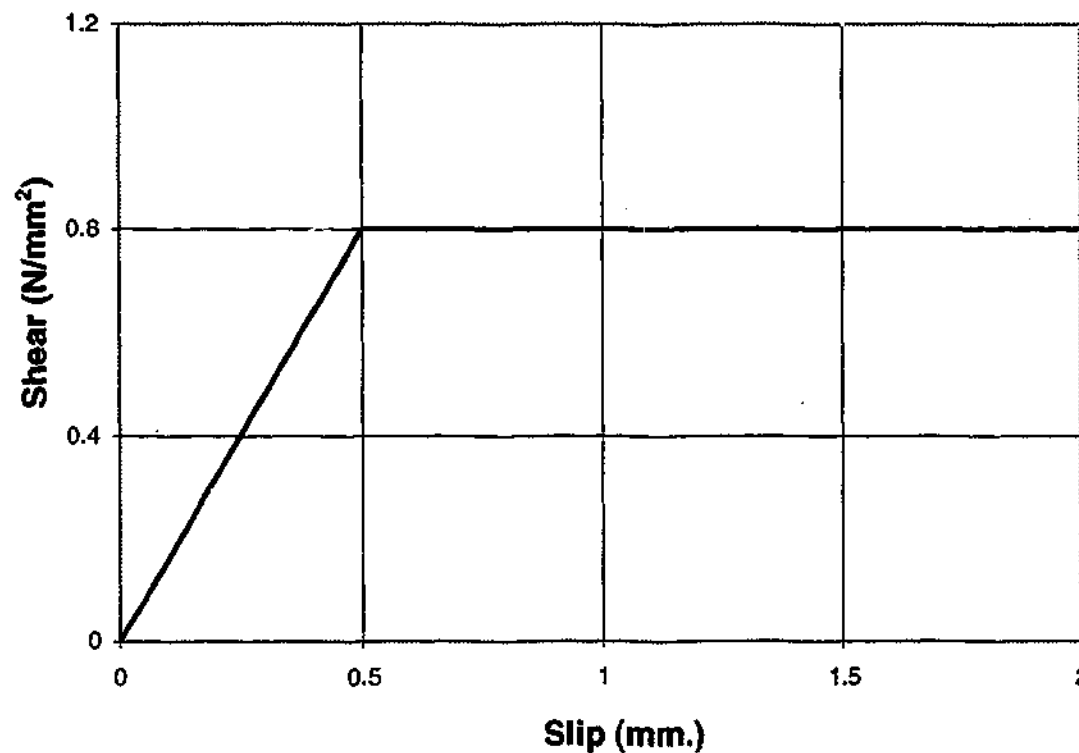
Figure 2.3 Description of interface bond element

In this thesis, the interface was modeled with the Coulomb friction material model
and gap element.

2.10 Current codes provisions, recommendations or assumptions on bond strength value

The codes provisions of British standard BS5400, Steel, concrete and composite
bridges (1979) were developed based on Shakir – Khalil's experimental work. It
is recommended that shear connectors should be provided where the shear
stresses at the steel / concrete interface, due to the design ultimate loads, would
otherwise exceed 0.4 N/mm^2 for concrete filled steel sections.

According to Eurocode 4 (Adopted European Prestandard EVN 1994-1-1:1992, European Committee for standardization), the design shear strength due to bond and friction for the concrete filled hallow section should be taken as 0.4 N/mm^2.

Both codes recommend the same value for bond/shear strength between concrete and steel regardless of concrete properties, length of concrete embedment, shapes of steel hallow section and roughness of steel hollow section internal surface.

Roeder et al. (1999) proposed a bond stress evaluation model for ultimate and serviceability design stages (see Figure 2.4.).
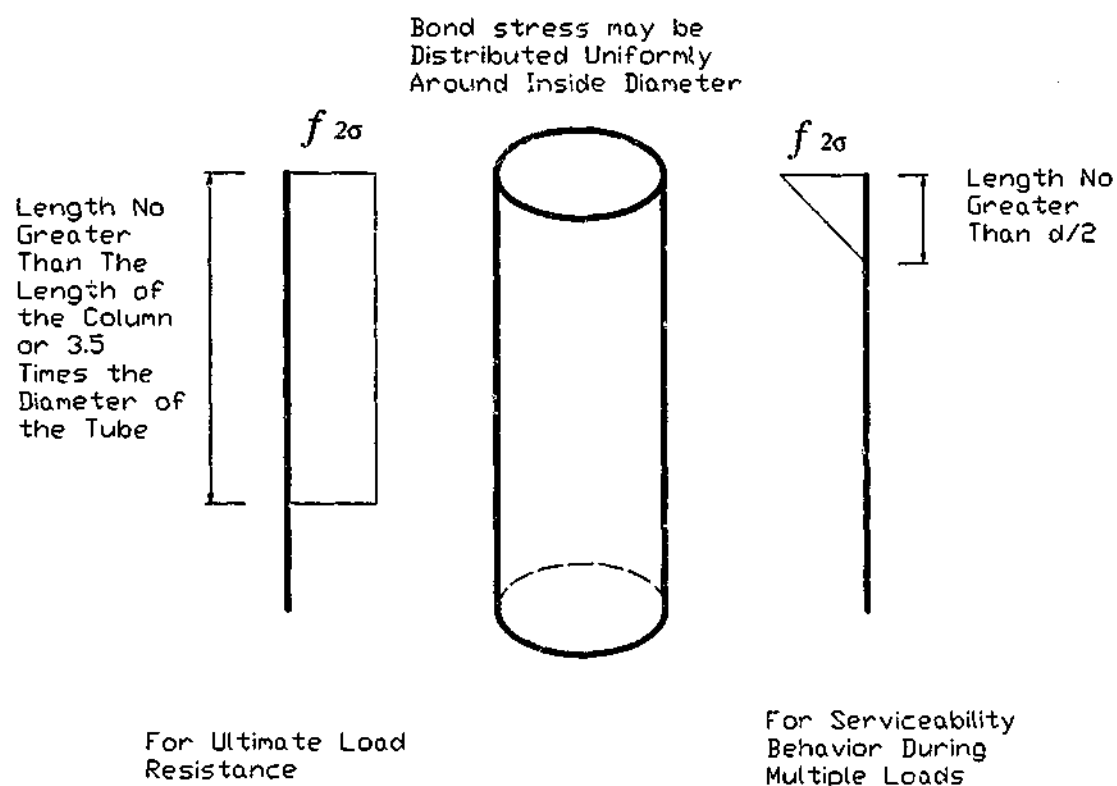
Figure 2.4. Proposed Bond Stress Evaluation Models

The following equation was suggested to calculate maximum average bond stress capacity as a function of aspect ratio.

$$f_{2\sigma} = 2.019 - 0.026(d/t)$$ (2-14)

where d, is the diameter of the steel tube and t, is thickness of steel tube. This equation suggested that no reliable bond could be achieved with d/t ratios greater than 80.

One of the applications of this research project is the connection of cast in steel shell (CISS) piles to the pile cap. The applied loads transfer thorough bond strength of the concrete plug embedded in the tubular steel pile. Silva and Seible (2001) conducted an experimental and analytical study to evaluate the seismic response of CISS piles and its connection to the pile cap. To develop the tensile forces present in the steel shell, average bond strength μ_{ave} of 2.07 MPa (300 psi) was assumed for analysis, which leads to development length $l_{d,shell}$ given by

$$l_{d,shell} = \frac{D_j^2 - D_i^2}{4\mu_{ave}D_i} f_{yj}$$ (2-15)

where D_j and D_i are the outside and inside diameter of the steel shell, respectively and f_{yj} is the steel shell yield strength.

Other researchers recommended the bond strength of concrete core into the steel tube values between 0.4 to 1.0 MPa, based on the push out tests.

2.10.1 Bond strength recommendation for pile sleeve connections

The connections between the piles and the pile skirt sleeves are generally made by grouting to provide load transfer between structure and piles. In pull out tests of reinforced concrete plugs embedded in tubular steel tube, the concrete layer between the reinforcement and the steel tube can be simulated as a grouted connection. The concrete layer mainly provides load transfer between the reinforcement and steel tube.

Offshore technical (OT) report (OTO 2001 016) recommended the following formulation for the characteristic bond strength of grouted connection, with or without mechanical shear connectors.

$$f_{buc} = KC_l \left(9C_s + 1100h/s\right)\left(f_{cu}\right)^{1/2} \qquad\qquad (2\text{-}16)$$

where:

f_{buc} is the characteristic bond strength (in N/mm^2)

f_{cu} is the characteristic grout compressive strength (in N/mm^2)

K is the stiffness factor defined below

C_l is the coefficient for grouted length to pile diameter ratio

C_s is the surface condition factor

h is the minimum shear connector outstand (in mm)

s is the nominal shear connector spacing (in mm)

$$K = \left[m(D/t)_g\right]^{-1} + \left[(D/t)_p + (D/t)_s\right]^{-1} \qquad\qquad (2\text{-}17)$$

where:

m is the modular ratio of steel to grout

D is the outside diameter

t is the wall thickness

and suffixes g, p and s related to grout, pile and sleeve respectively.

In the absence of other data the modular ratio m may conservatively be taken as 18 for the long term (i.e. 28 days or more).

The available data on the parameter C_l is limited. In the absence of data relating to a specific tubular and shear connector geometry, the following values of C_l should be assumed.

L/D_p	C_l
2	1.0
4	0.9
8	0.8
≥ 12	0.7

where L is the nominal grouted connection length.

Intermediate values for $L/D_p < 12$ should be calculated by linear interpolation.

The surface condition factor C_s should be taken accordingly to the following

i.   If shear connector are present and satisfy the requirements $h/s \geq 0.005$ then C_s may be taken as 1.0.

ii.   For plain pipe connections and for connections with shear connectors but with $h/s < 0.005$, then in the absence of the test data, Cs should be taken as 0.6.

The values in i. And ii. Above refer to shotblasted or lightly rusted surface conditions. Other conditions (e.g. painted surfaces) should receive special consideration.

In summary then, previous research has identified that the following factors may affect the bond strength of concrete plugs embedded in steel tubular piles:

- Concrete core compressive strength and elastic modulus
- Steel tube and concrete plug annulus geometries
- Outstand and spacing of reinforcement
- Concrete plug length to pile diameter ratio
- Inner surface condition of steel tube
- Long term concrete shrinkage or expansion

2.11   Objective of This Research

In light of the above comments relating to existing studies that have included the effective parameters on the bond strength of concrete plugs into the steel tubes, as well as current state of the art analytical methods that have capacity to predict the strength of CFT columns and bond strength, several outstanding issues are to be addressed in this research.

1) Produce or collect experimental results that specifically isolate the effect on bond strength of variation of concrete plug length, concrete strength, steel tube aspect ratio and presence of reinforcement in pull out, push out and cyclic loading tests.

2) Examine the failure mechanisms associated with the type of load arrangements.

3) Formulate an experimental method capable of estimating the magnitude, and distribution of bond stress along the interface between concrete core and the steel tube.

4) Use the above results to quantify the effectiveness of the concrete shrinkage in relation to the bond strength and structural behavior of concrete plug inside the steel tube.

5) Determine suitable FE modeling procedures that allow extrapolation of experimental results to evaluate the effect of subtle changes in the concrete strength and pile geometry on the ultimate bond strength.

6) Perform a study in which current state of the art general theories of calculation of bond strength capacity are examined for their performance against existing experimental work and the experimental work that will be produced as part of this study.

7) Discuss the contributions of the concrete and the steel tube to the bond strength

3   PULL-OUT AND PUSH-OUT TESTS

3.1   Introduction

This chapter presents the results of pull-out (Bean 1997) and push-out (O'Loughlin 1998) tests that were carried out in the Department of Civil Engineering of Monash University. Subsequent analysis of these results is also presented in this chapter. The primary focus of this discussion is to isolate the effect of concrete plug length on the ultimate strength and failure mechanisms of the specimens tested. The mechanisms, which contribute to bond strength, are discussed in this section.

Test results are examined against current code provisions and recommendations. Mathematical expressions are adopted to calculate the bond strength of concrete plugs in steel tubular piles.

3.2.   Pull-Out Tests

Previous investigations of bond strength within concrete filled steel tubes were limited to push-out tests of unreinforced plugs. The pull-out investigation aimed to evaluate the bond strength of reinforced concrete plugs in the steel tubular piles in pull-out loading.

3.2.1   Test specimens

Eleven specimens were initially constructed for pull-out tests, of which seven were prepared eventually for push-out tests after completion of the pull-out tests. The principal variable was the length of concrete plug, L. Only one circular steel tube size and concrete strength were used. The tubes had an average outside diameter D_i of 237 mm, with an average thickness of 11.5 mm (Section1). Two of the

supplied steel tubes had an average thickness of 10 mm with an out side diameter of 237mm (section 2). Internal diameter and thickness of all tubes were measured. The following is a summary of these measurements for section 1.

Measurements taken   = 28

Mean diameter   ≈ 214.1 mm

Standard of Deviation ≈ 0.7 mm

Mean thickness   ≈ 11.5 mm

Standard Deviation   ≈ 0.6 mm

In table 3.1 below, the letter S followed by a number designates the test specimen by the length of concrete plug. The pull-out test specimens were divided into three groups, with different tube and concrete plug lengths. The first group included three specimens with tube length of 500 mm and concrete plug length of 250 mm, the second group included three specimens with tube length of 750 mm and concrete plug length of 500 mm and the third group included two specimens with tube length of 1000 mm and concrete plug length of 750 mm.

Table 3.1 Specification of pull-out test specimens

Specimen ID	Tube Length	Concrete Plug Length (mm)	L/D_i	Strain gauging
S250-1	500	250	1.06	Gauged
S250-2	500	250	1.06	Gauged
S250-3	500	250	1.06	Not Gauged
S500-1	750	500	2.11	Gauged
S500-2[*]	750	500	2.11	Not Gauged
S500-3[*]	750	500	2.11	Not Gauged
S750-1	1000	750	3.16	Gauged
S750-2	1000	750	3.16	Gauged

[*] These specimens are those referred to as "section 2"

Excess rust slag within the steel tubes was removed with a wire brush. The average concrete compressive cylinder strength was 50 MPa and the slump of 75 mm was reported on delivery. The reinforcing bars in all specimens consisted of 6 Y 24 bars (24 mm diameter deformed bar with yield strength of 400 MPa). Based on the net area at the threaded end of bars, the steel ratio is 5.2 % of the gross area of the concrete plug. In pull-out tests, the tension was applied by an attachment to the threaded ends of the rebars.
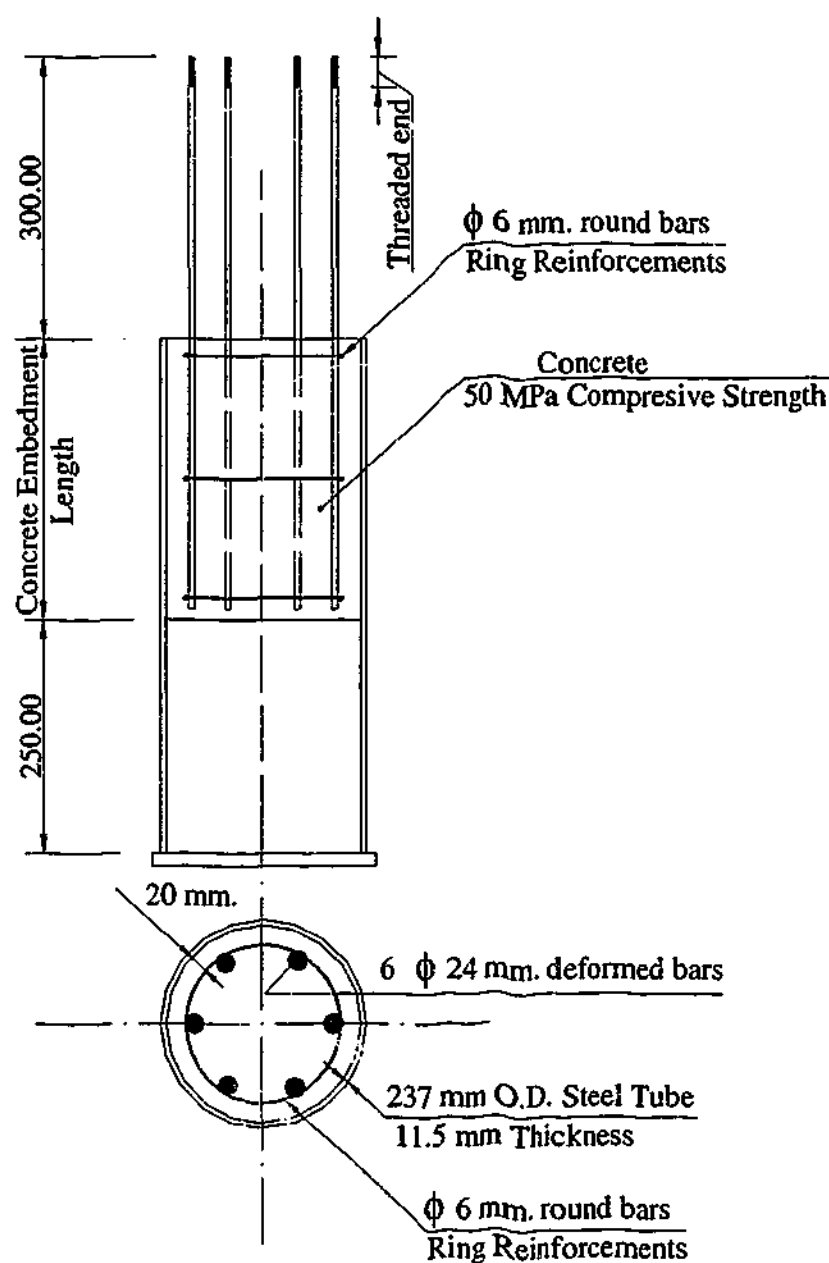
Figure 3.1 A typical pull-out test specimen

A string LVDT (linear variable deferential transducer) was located at the top of the concrete plug to measure the relative movement between the concrete core and the steel tube. Most specimens were strain gauged along the outer surface of steel tube within the length of concrete plug. Both longitudinal and hoop strain gauges were used. The purpose of these gauges was to determine the load transfer mechanism from the concrete plug to the steel tube. Additional strain gauges were used on the opposite side of the tubes in order to establish whether the loading arrangement introduced significant eccentricity in the specimen. As shown in Figure 3.2 below, the loads were applied through a thick disc plate bolted to the top of reinforcing bars.
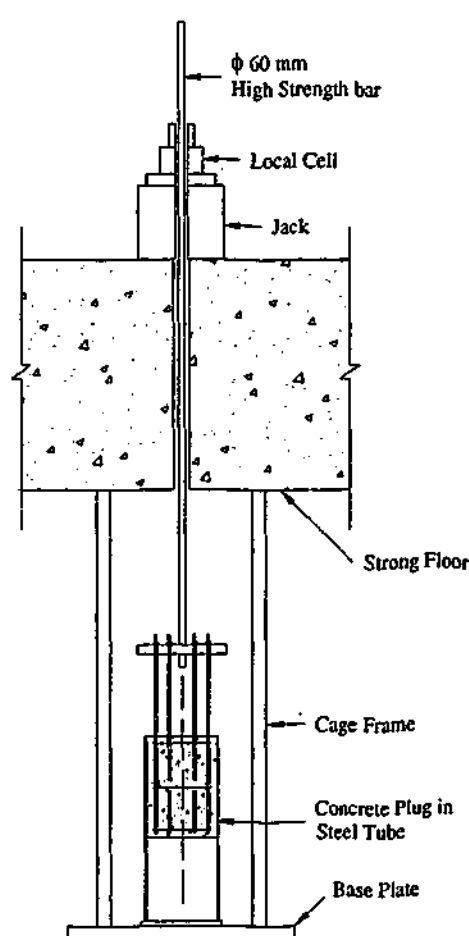
Figure 3.2 Pull-out test arrangement

3.2.2   Test results

Two specimens having a concrete plug embedment of 750 mm were tested. When the applied pull-out load reached 1222 kN, the threaded portions of the steel bars of specimen S750-1 failed explosively. No significant slip was recorded at this load level. Slip of the concrete core measured from the center of the specimen was observed to be linear with respect to load and the plot relating slip to applied load gave no indication of pull-out failure. The maximum slip at 1000 kN load level ranged from 0.44 to 0.57 mm, which corresponds to an average bond stress 2.42 MPa. To avoid the explosive failure of the steel bar, specimen S750-2 was loaded to 1000 kN only.

Three specimens having a concrete plug embedment of 500 mm were tested. These specimens were loaded to 1000 kN. At this load level, no signs of excessive slip were detected, and an indication of ultimate bond strength was not reached. The maximum slip at peak load ranged from 0.36 mm to 0.57 mm. This is comparable to the maximum slips in specimens S750-1 and S750-2. The average bond stress that corresponds to the 1000 kN level is 2.95 MPa.

Three specimens with 250 mm length of concrete plugs were the only specimens that achieved full bond failure. They carried maximum loads of 810, 720 and 1035 kN, with corresponding average bond strength of 5.1 MPa. Table 2 lists the values of peak loads achieved and the corresponding average bond strength. The slip values are also tabulated.

Table 3.2 Tests results of pull-out tests

Specimen ID	Concrete Plug Length	L/D$_i$	Peak Load (KN)	Failure Condition	Strain gauge Condition	Average Bond Strength (MPa)	Slip at Peak (mm.)
S750-1	750	3.16	1222	Bar failure	Gauged	2.42	0.57
S750-2	750	3.16	1000	No failure	Gauged	1.98	0.59
S500-1	500	2.11	1000	No failure	Gauged	2.95	0.38
S500-2	500	2.11	1000	No failure	Not Gauged	2.95	0.58
S500-3	500	2.11	1000	No failure	Not Gauged	2.95	0.43
S250-1	250	1.06	810	Failed	Gauged	4.8	0.7
S250-2	250	1.06	720	Failed	Gauged	4.3	0.9
S250-3	250	1.06	1035	Failed	Gauged	6.2	0.85

3.2.3   Bond strength mechanisms in pull-out tests

It should be noted that the bond resistance is a function of both the micro chemical adhesion and mechanical macro locking between the concrete core and the steel surface. The former depends on the surface roughness of the steel section, and the latter related to the frictional resistance to movement along the steel – concrete interface and dependent on the dilation/contraction due to Poisson's ratio effect of the concrete plug and steel tube.

The pull-out strength of the concrete plugs is attributed mainly to the dilation/contraction through the Poisson's ratio effect of the concrete and the steel tube, causing an increase in contact stresses, which results in an increase in friction. At the top of a typical specimen, the concrete, which is subject to very

high tension stresses contracts laterally, and this leads to separation between the steel and concrete. On the other hand, in the vicinity of the base of the plug, the steel tube carries most of the longitudinal load. This causes the tube to contract, while the expansion of the concrete plug is very small due to the low level of tension stress in the concrete core. This results in a gripping mechanism between the steel tube and the concrete plug at the bottom (see figure 3.3).
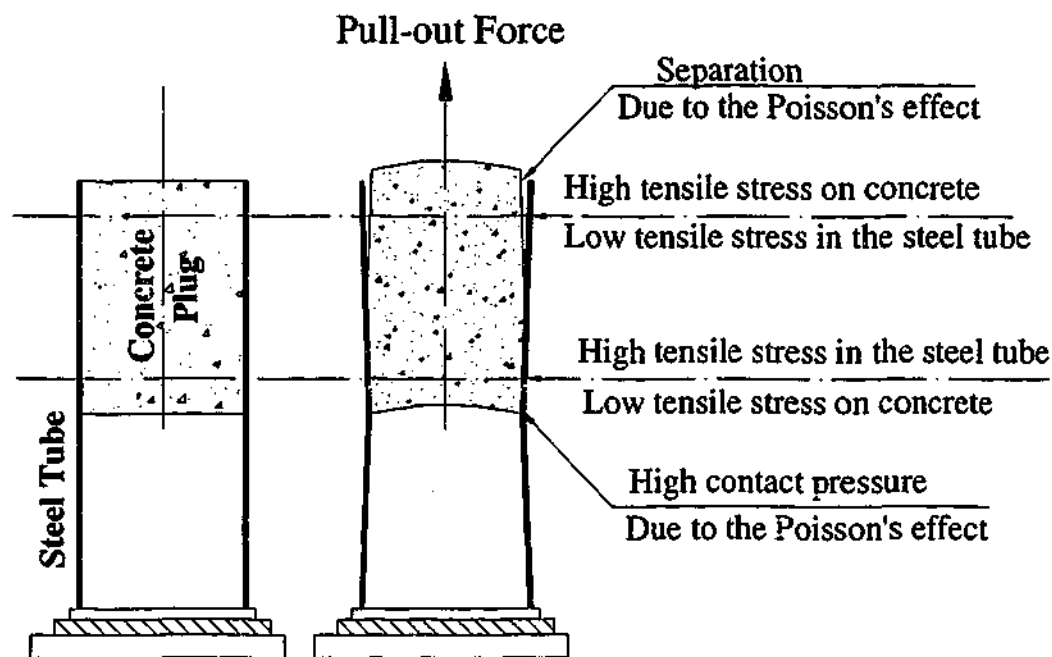
Figure 3.3 Bond strength mechanisms in pull-out tests

Considering the fact that deformed bars was used as reinforcement, the ribs on the bars tend to impart wedge pressure on the outer concrete layer, causing dilation of this layer. This dilation enhances the frictional stresses between the steel tube and the concrete.

When a small amount of slip occurs, friction resistance is enhanced by an increase in contact pressure through the concrete riding over the steel asperities.One of the main aims of the investigation was to study these mechanisms and to quantify the load transfer rate from the concrete plug to the steel tube due to contribution of above mechanisms.

3.2.4 Load slip response

After rising to a peak load, the load response of S250-1 was characterized by a gradual decrease in load transfer as slip increased. Specimens S250-2 and S250-3 exhibited a stick-slip mechanism of bond failure. Sudden slip occurred with sharp decrease in the load capacity followed by gradual increase in resistance. This process continued until the slip values exceeded 30 mm. The plugs for these two specimens were then pulled out to examine the concrete surface in contact with the steel tube. Inspection showed that voids up to 25 mm in size were present on the contact surface, and this might have contributed to the type of bond failure exhibited by these specimens. However the load – slip curves of the specimens of this group are seen to exhibit a nearly bilinear response prior to peak load (Figure 3.4). The position of the change of slope seems to indicate that bond resistance of the specimen changes from a non-slip mechanism action (chemical adhesion between the interface of concrete plug and steel tube) to the very small – slip mechanism action (mechanical macro locking between the concrete core and steel surface).

The slip response of specimens S500 also shows a nearly bilinear response. A permanent slip is evident upon unloading the specimens. The change of slope of the load – slip curves during loading is assumed to commence with the breaking of chemical adhesion and activation of the mechanical locking mechanism, which was also observed in S250 specimens (Figure 3.5). As can be seen from the figure, the load-slip response of specimens S750 shows a nearly linear relationship between load and slip, with a permanent small slip remaining on S750-2 after unloading. The linear slope of the load – slip curves suggests that the bond resistance of these specimens comes mostly from chemical adhesive (micro lock between concrete core and steel surface) for the limited applied load of 1000 KN (Figure 3.6).
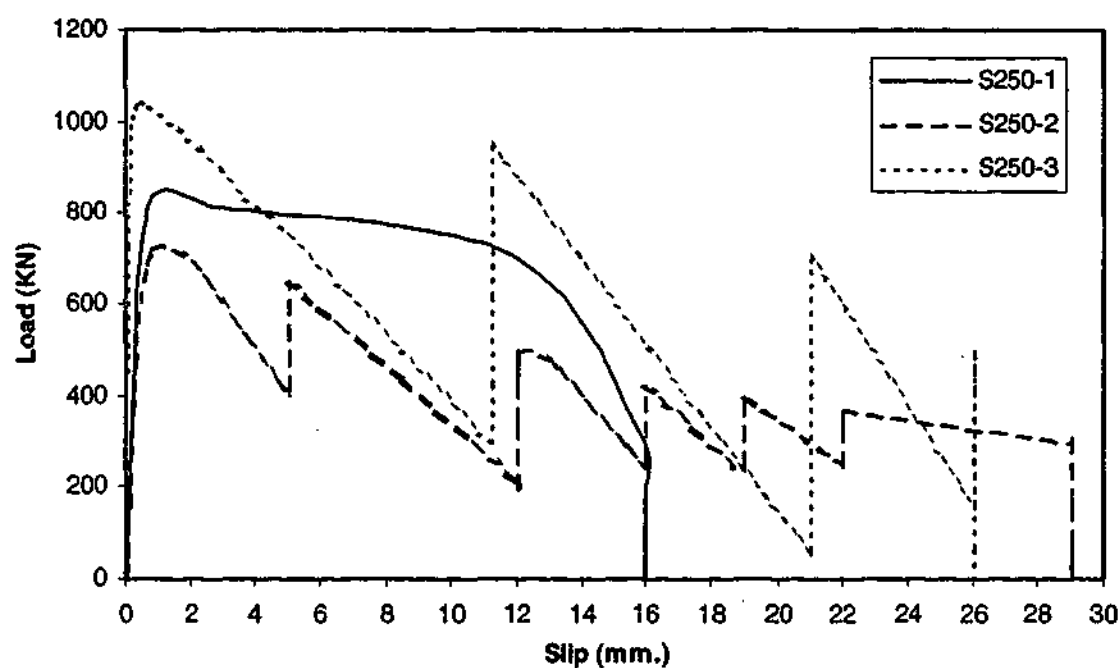
Figure 3.4 Load – slip relationship of specimens S250
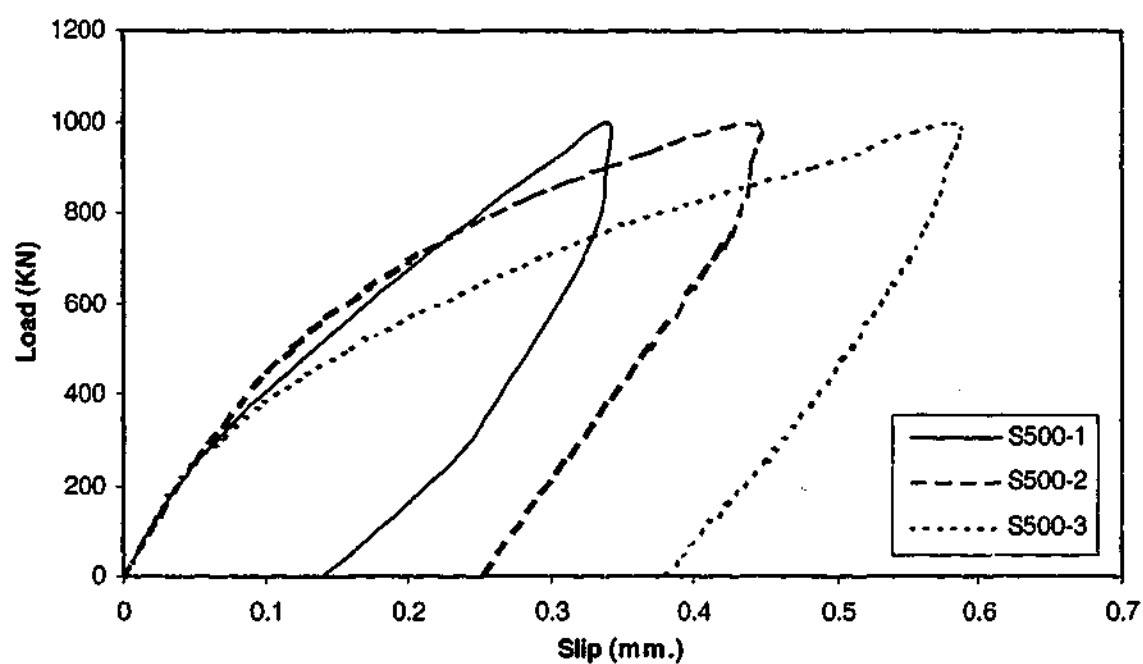
Figure 3.5 Load – slip relationship of specimens S500
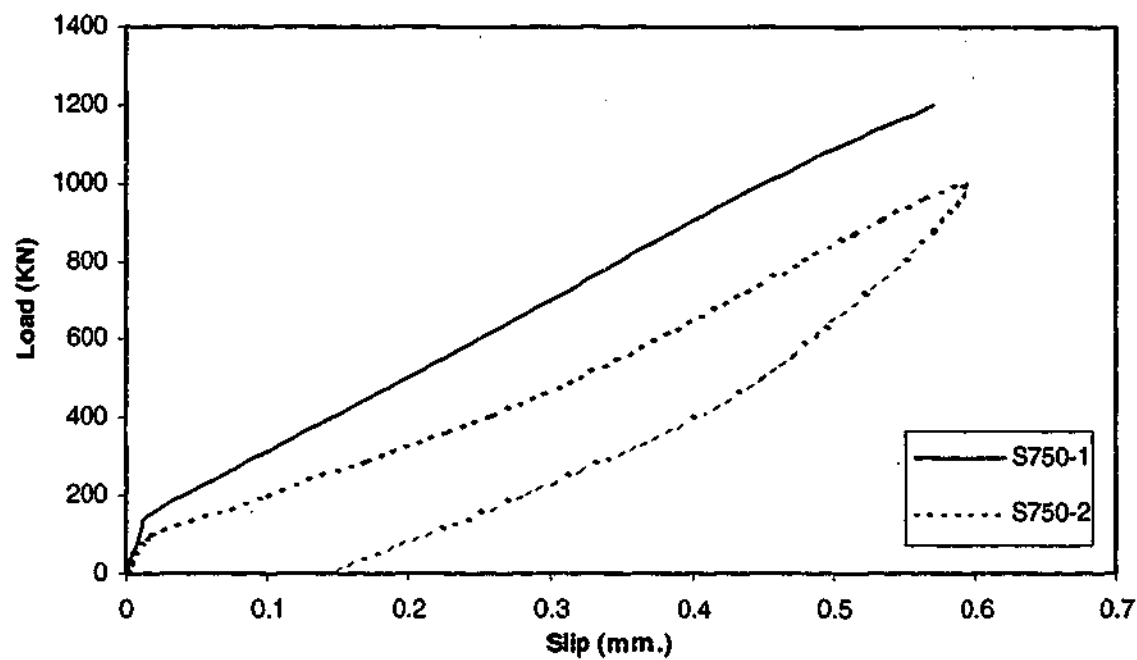
Figure 3.6 Load – slip relationship of specimens S750
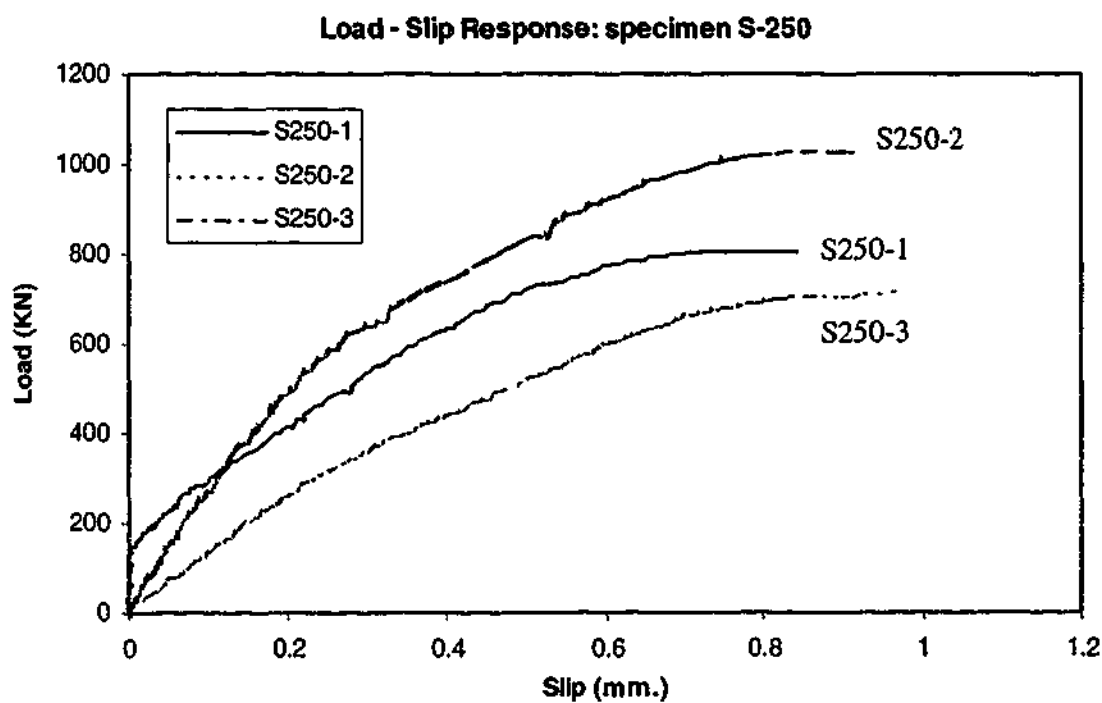
Figure 3.7 A close up of load – slip relationship of specimens S250

Figure 3.9 to Figure 3.11 show the load – longitudinal strain relationship of specimens S250-1, S250-2, and S500-1 along the length of the steel tube. The number that follows the follows the letter V indicates the distance of the strain gauge from bottom of concrete plug (see Figure 3.8).
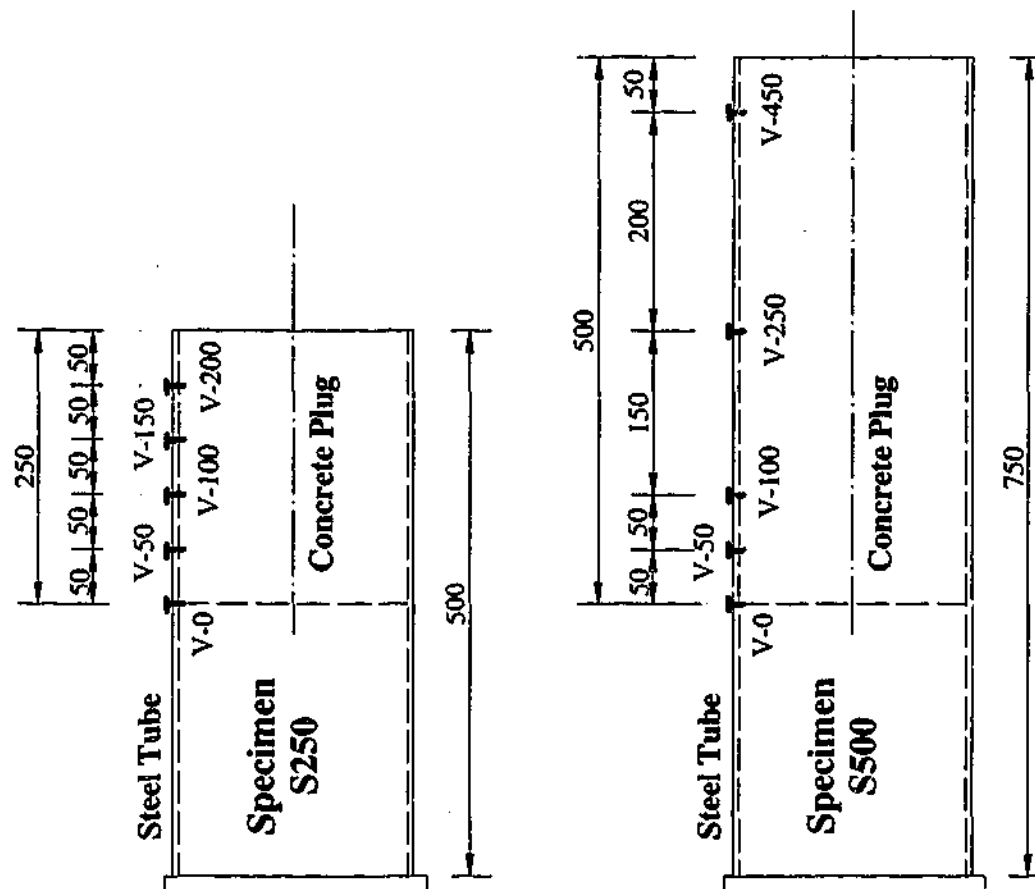
Figure 3.8 Arrangement of strain gauges

As can be seen form the figures, the load – longitudinal strain relationships exhibit two different stages of shear transfer stress distributions. At the first stage, all longitudinal strain gauges along the steel tube experienced a steady increase of longitudinal strain as the applied load increased, which indicates a nearly uniform shear/bond stress distributions along the interface surface. At the second stage, strains near the top and bottom of the concrete plug have risen sharply. This is attributed to dilation through the Poisson's ratio effect at the bottom and dilation of the concrete layer surrounding the steel bar cage caused by wedging effect of the ribs of the deformed bars. A sudden increase of shear/bond stress occurs at the

transition point of first and second stage, whereas the applied load reached around the load level of 230 KN for specimens S250 and 470 KN for specimen S500-1.

The two stages of load – longitudinal strain relationship indicated that initially the resistance of the specimens against pull-out comes from chemical adhesion between the concrete and the inner surface of the steel tube. As the applied load reaches a maximum capacity of bond strength due to the micro chemical adhesion, some of the microscopic connections on the interface surface break, leading to a mechanical locking mechanism. This causes the change of slope of the load – slip relationships. From the load – longitudinal strain and load – slip relationship, the average chemical adhesion bond strength of 1.36 MPa and 1.38 MPa were achieved for specimens S250 and S500, respectively.
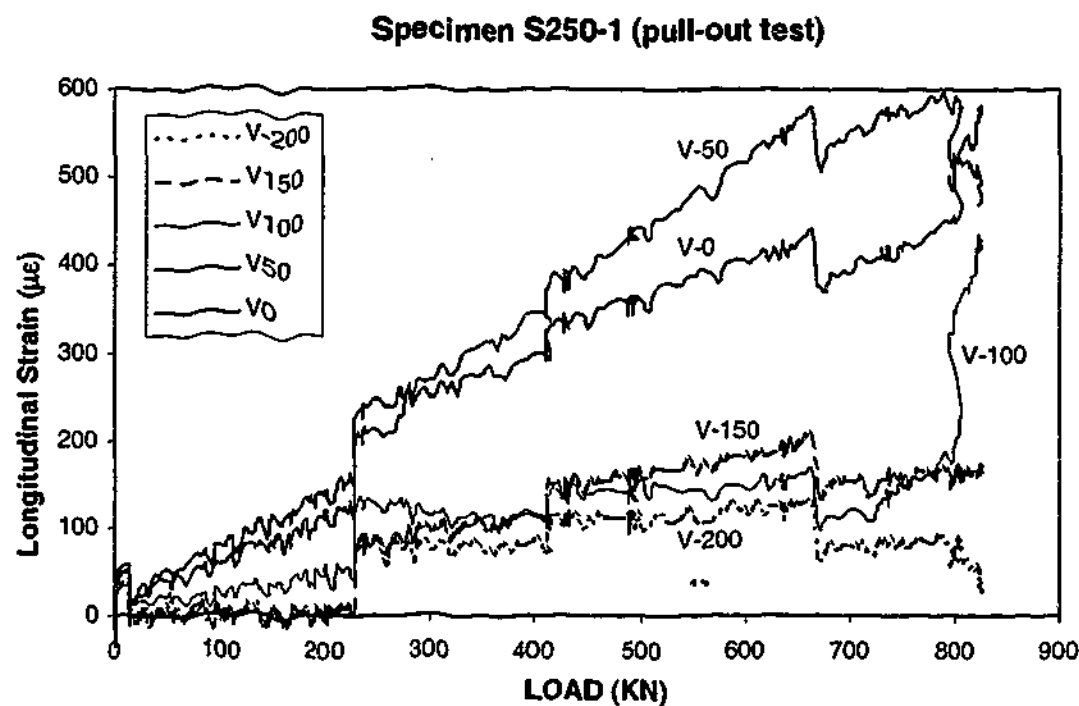
Figure 3.9: Measured load – longitudinal strains for specimens S250-1

Specimen S250-2 (pull-out test)
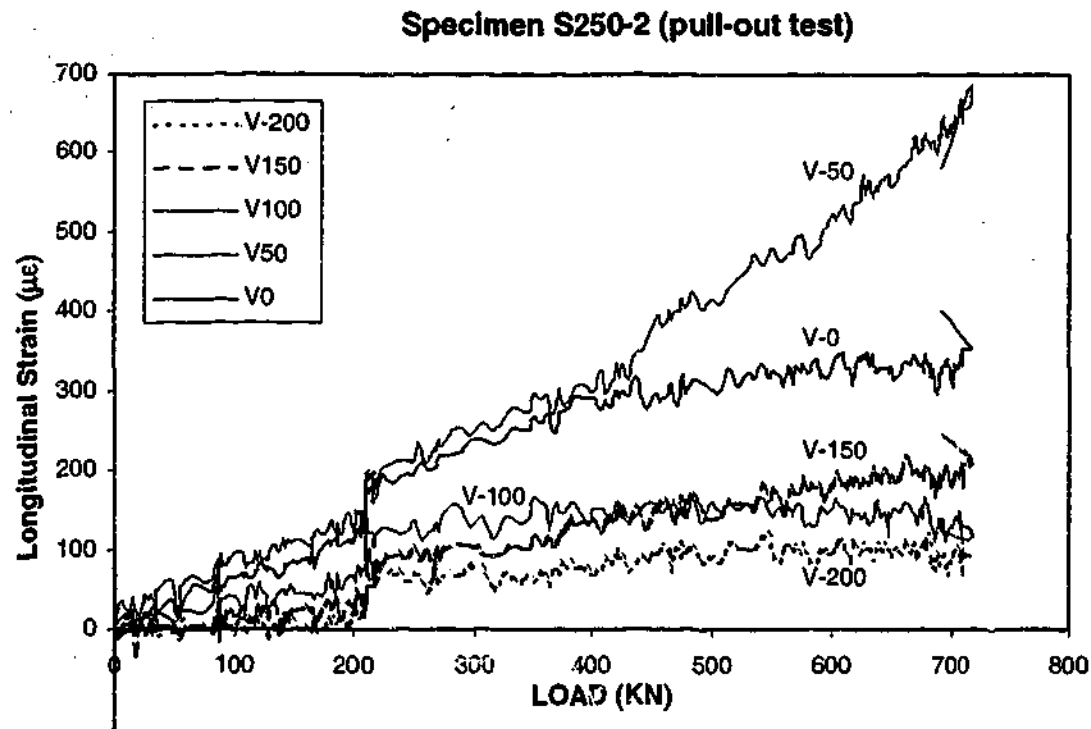
Figure 3.10: Measured load – longitudinal strains for specimens S250-2

Specimen S500-1 (pull-out test)
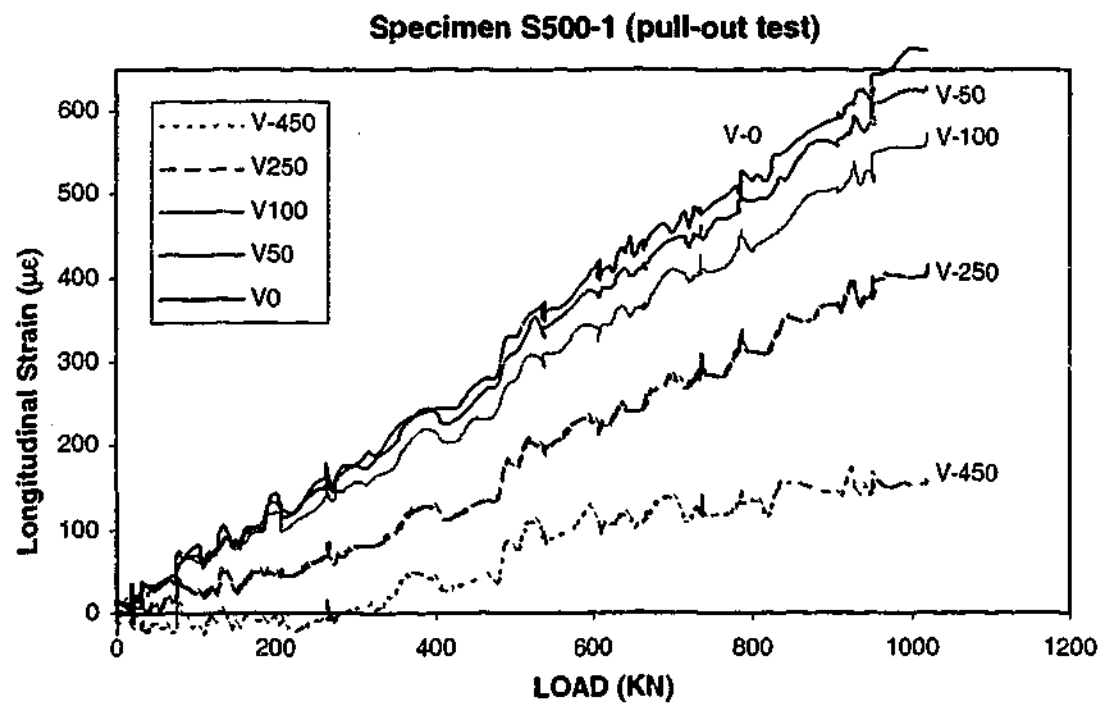
Figure 3.11: Measured load – longitudinal strains for specimens S500-1

3.2.5   Comparison of the recommendations and test results

The pull-out test results are presented in Figures 3.4 to 3.6 and Table 3.2. The measured mean ultimate strength of specimens S250 was 855 kN.

Using the recommendation for the ultimate bond strength of the CFT column given by equation *(2-24)* (Roeder et al. 1999), the minimum average bond stress, $f_{2\sigma}$, is determined as follows:

$$f_{2\sigma} = 2.019 - 0.026(d/t)$$

$$T_{ultimate} = \pi D_{cp} L f_{2\sigma} \tag{3-1}$$

Where d is steel tube diameter, t is steel tube thickness, $T_{ultimate}$ is ultimate pull-out strength, D_{cp} is diameter and L is length of the concrete plug. Table 3.3 shows calculated values for the bond stress and corresponding ultimate pull-out force based on Roeder's (1999) recommendation.

It is evident that Eq. (3-1) gives higher estimates of ultimate bond strength than the code (BS 5400) value of 0.4 MPa. However, Eq. (3-1) still underestimates the bond strength, when compared with the measured values. The estimated ultimate pull-out strength of specimens S250 is equal to 29% of the experimental average ultimate strength. The estimated ultimate pull-out strength of specimens S500 and S750 are also lower than the achieved level of average bond strength in the experiment.

The results indicate that Roeder's (1999) recommendation for the bond strength is very conservative for the case of reinforced concrete plugs embedded in steel tubular piles subjected to pull-out. The recommendation was made regardless of the concrete plug length, concrete material characteristics and internal surface

condition of the steel tube, which seem to influence the bond strength of the concrete plug.

Table 3.3 Roeder's (1999) recommendations against the pull-out test results

Specimen ID	Concrete Plug Length	D/t	Peak Load (KN)	Failure Condition	Average Bond Strength (MPa)	Calculated bond stress (Roeder)	Ultimate pull-out strength (Roeder)
S750-1	750	19.6	1222	Bar failure	2.42	1.51	762
S750-2	750	19.6	1000	No failure	1.98	1.51	762
S500-1	500	19.6	1000	No failure	2.95	1.51	508
S500-2*	500	22.7	1000	No failure	2.95	1.43	481
S500-3*	500	22.7	1000	No failure	2.95	1.43	481
S250-1	250	19.6	810	Failed	4.8	1.51	254
S250-2	250	19.6	720	Failed	4.3	1.51	254
S250-3	250	1.06	1035	Failed	6.2	1.51	254

Offshore technology (OT) report (OTO 2001-016) recommendation for the characteristic bond strength can be adopted and idealized for the concrete plug as follows:

$$f_{buc} = 9KC_t C_s (f_{cu})^{1/2}$$ (3-2)

where:

f_{bnc} is the characteristic bond strength (in N/mm^2)

f_{cu} is the characteristic concrete compressive strength (in N/mm^2)

K is the stiffness factor defined below

C_l is the coefficient for concrete plug length to pile diameter ratio

C_s is the surface condition factor

$$K = \left[m(D/t)_g\right]^{-1} + (D/t)_p^{-1}$$ (3-3)

Where:

m is the modular ratio of steel to plug

D_p is the pile diameter

t_p is the pile wall thickness

To adopt OTO's(2001) recommendations for this study, diameter to thickness of the concrete layer between steel bars and steel tube is taken as $(D / t)_g$. The modular ratio of m is also taken as $E_{steel} / E_{concrete} = 5.5$ (short term loading)

The available data on the parameter C_l are limited. In the absence of data relating to a specific tubular geometry, the following values of C_l should be assumed.

L/D_p	C_l
2	1.0
4	0.9
8	0.8
≥ 12	0.7

where L is the plug length.

For normal internal surface of the pile, in the absence of test data, Cs could be taken as 0.6.

Table 3.4 below shows calculated values for the bond stress and ultimate pull-out force based on the adopted OTO (2001) report recommendation.

Table 3.4 The OTO's (2001) recommendations against the pull-out test results

Specimen ID	Concrete Plug Length	D/t	Peak Load (KN)	Failure Condition	Average Bond Strength (MPa)	Calculated bond stress (OTO)	Ultimate pull-out strength (OTO)
S750-1	750	19.6	1222	Bar failure	2.42	3.67	1853
S750-2	750	19.6	1000	No failure	1.98	3.67	1853
S500-1	500	19.6	1000	No failure	2.95	4.06	1376
S500-2*	500	22.7	1000	No failure	2.95	3.80	1288
S500-3*	500	22.7	1000	No failure	2.95	3.80	1288
S250-1	250	19.6	810	Failed	4.8	4.06	685
S250-2	250	19.6	720	Failed	4.3	4.06	685
S250-3	250	1.06	1035	Failed	6.2	4.06	685

The estimated ultimate pull-out strength of specimens S250 is equal to 80% of the experimental average ultimate strength.

The estimated ultimate pull-out strength of specimens S500 and S750 are higher than the achieved level of the bond strength with a reasonable margin.

The results indicate that the OTO's (2001) recommendation for the bond strength is in agreement with the test results. Furthermore, the concrete plug length, concrete material characteristics and internal surface condition of the steel tube were considered in the recommendation.

3.3   Failure Mechanism in the Pull-out Test

Figure 3.12 shows a completely pulled out concrete plug from a steel tube after the specimen failed in a pull-out test.

Figure 3.12 Pulled out concrete plug

The failure mechanism displayed by the specimens was at the base of the concrete plug, where the steel tube contraction is much higher than that of the concrete core, causing it to grip the concrete plug. The diagonal tension crack that formed in the concrete layer between the longitudinal reinforcement and the steel tube extended to the end of the embedded longitudinal reinforcement where it began running in hoop direction. This crack appeared to correspond to a tension splitting

of the concrete plug at ultimate pull-out capacity of the specimen. This type of mechanism is shown in Figure 3.13 below.
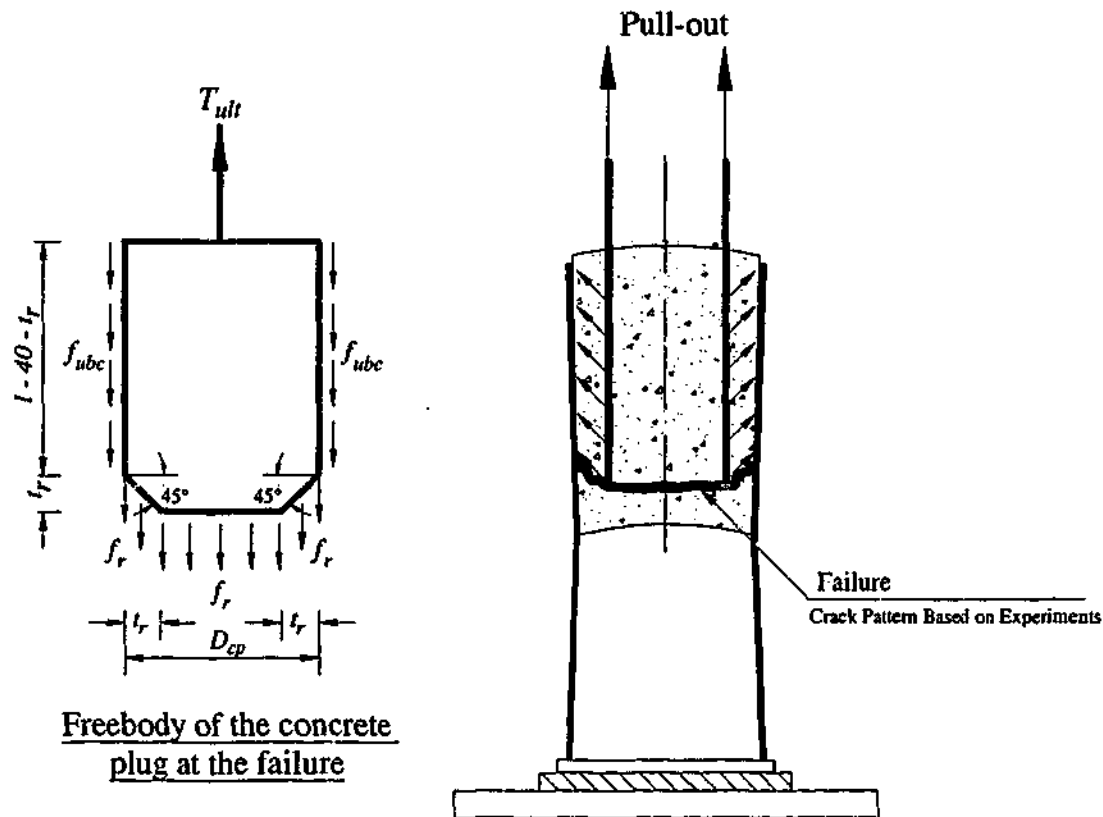
Figure 3.13 Failure of the concrete plug in the pull-out test

As a result of the failure of the concrete plug in the pull-out test, the following formulation is proposed based on free body diagram of the concrete plug at the failure.

$$T_{ult} = f_{buc}(l - 40 - t_r)\pi D_{cp} + f_r \pi (0.5 D_{cp} + .414 t_r)^2 \qquad (3-4)$$

Where T_{ult} is ultimate pull-out strength, f_{buc} is the bond stress, D_{cp} is concrete plug diameter, f_r is tensile strength of the concrete, l is length of concrete plug and t_r is thickness of concrete layer between the tube and reinforcement.

Table 3.5 below shows the ultimate pull-out capacity of the specimens using above formulation and bond stresses recommended by the adopted OTO (2001) method.

Table 3.5 Ultimate pull-out strength of the specimens based on the failure model

Specimen ID	Measured Peak Load (KN)	Average Bond Strength (MPa)	Calculated bond stress (OTO)	Ultimate Pull-out strength (OTO's recommendations)	Ultimate pull-out strength (proposed failure model)
S750-1	1222	2.42	3.67	1853	1930
S750-2	1000	1.98	3.67	1853	1930
S500-1	1000	2.95	4.06	1376	1419
S500-2*	1000	2.95	3.80	1288	1329
S500-3*	1000	2.95	3.80	1288	1329
S250-1	810	4.8	4.06	685	700
S250-2	720	4.3	4.06	685	700
S250-3	1035	6.2	4.06	685	700

The estimated ultimate pull-out strength from proposed failure model for specimens S250 is 700 kN, which is only 17% lower than the experimental results. The estimated ultimate pull-out strengths for specimens S500 and S750 are higher than achieved pull-out loads. However, it was not possible to evaluate the results from different estimation methods with ultimate pull-out force for specimens S500 and S750 due to the limited ultimate capacity of longitudinal reinforcement to apply the pull-out force.

However, the estimated values from the proposed failure model are slightly (%2) higher than values from OTO's (2001) recommendations. Therefore, it would be

adequately accurate to use OTO's (2001) recommendation and adopted formulation for estimation of the pull-out strength.

3.4   Push-out Tests

The ultimate strength of the specimens subjected to pull-out force was not reached, due to the higher than expected strength of the specimens and the limited ultimate capacity of longitudinal reinforcement to apply the pull-out force. Therefore, it was decided to test the remaining specimens to determine the push-out capacity of the specimens (O'Loughlin 1998).
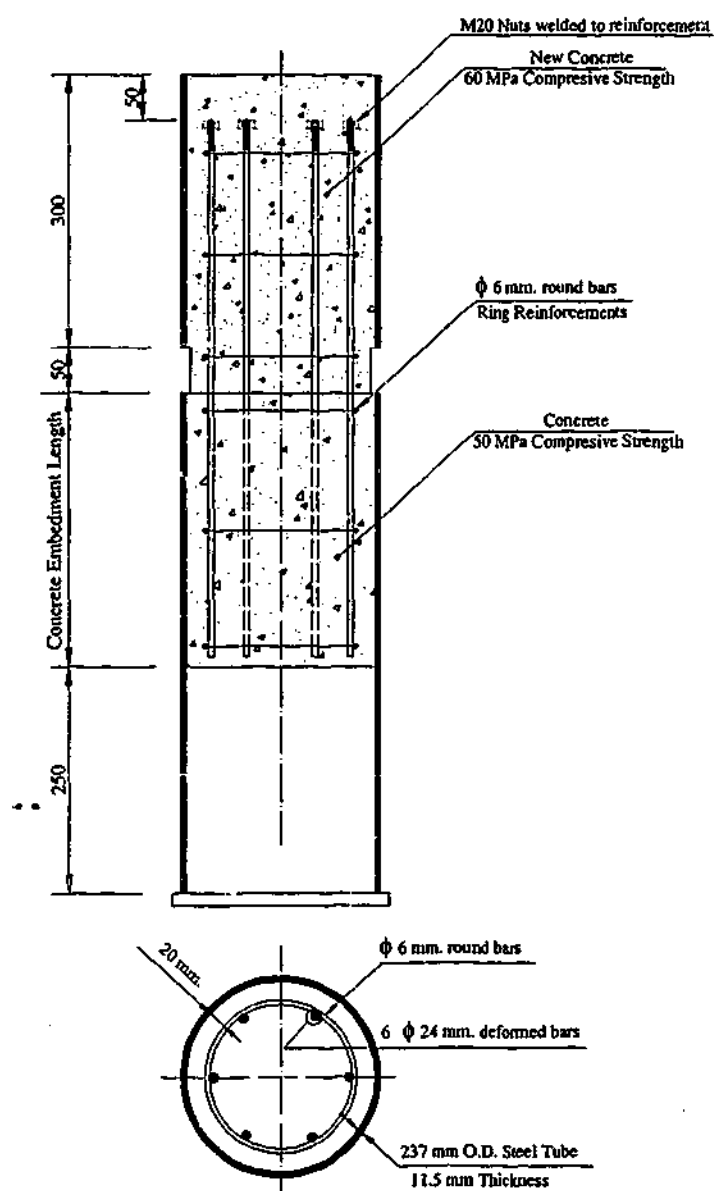
Figure 3.14 A typical push-out test specimen

3.4.1 Test specimens

Seven specimens were prepared for the push-out test, which initially were constructed for the pull-out tests. A typical test specimen for push-out testing is shown in Figure 3.14.

The pile head applied the push-out force on the concrete plug, which was cast on top of specimens after specimens were tested on the pull-out test. The average concrete compressive strength was 60 MPa for pile head concrete. The loads were increased through the pile head to ensure that the additional concrete would only be applying pressure on the embedded concrete (see Figure 3.15 below).
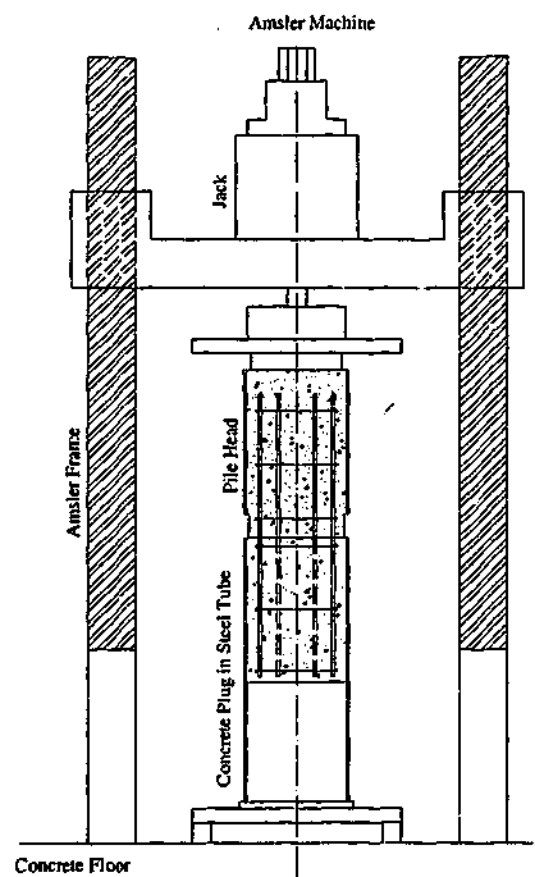
Figure 3.15 Push-out test arrangement

The test specimens had three different tube and concrete plug lengths. The first group included two specimens with tube lengths of 750 mm and concrete plug lengths of 500 mm. Both had already been tested for pull-out. The second group had three specimens with tube lengths of 1000 mm and concrete plug lengths of 750 mm, of which two had already been tested for pull-out. The third group had two specimens with tube lengths of 1250 mm and concrete plug lengths of 1000 mm. (See Table 3.6)

Table 3.6 Specification of push-out test specimen

Specimen ID	Tube Length	Concrete Plug Length (mm)	L/D$_i$	Strain gauging
S1000-1	1250	100C	4.22	Not Gauged
S1000-2	1250	1000	4.22	Not Gauged
S750-1	1000	750	3.16	Gauged
S750-2	1000	750	3.16	Gauged
S750-3	1000	750	3.16	Not Gauged
S500-1	750	500	2.11	Gauged
S500-2	750	500	2.11	Not Gauged

Two LVDTs were located on the steel tube to measure the relative movement between the pile head and the steel tube.

3.4.2   Test results

The two specimens having a concrete plug embedment of 1000 mm were not the subject of prior pull-out tests. They carried maximum loads of 1360 and 1350 kN, with a corresponding average ultimate shear/bond strength of 2.01 MPa.

Two of the three specimens having a concrete plug embedment of 750 mm had already been subjected to a pull-out force of 1000KN without failure or noticeable damage. They carried maximum loads of 3445, 3700 and 2503 kN, with a corresponding average ultimate shear/bond strength of 6.37 MPa.

The two specimens having a concrete plug embedment of 500 mm had already been subjected to a pull-out force of 1000KN. They carried maximum loads of 694 and 681 kN, with a corresponding average ultimate shear/bond strength of 2.04 MPa. Table 3.7 lists the values of peak loads achieved and the corresponding average bond strength. The slip values at peak load and previous pull-out test situations are also tabulated

Table 3.7 Push-out test results

Specimen ID	Peak Load (kN)	Previous pull-out test	Average Bond Stress (MPa)	Slip at Peak Load (mm.)
S1000-1	1360	Not tested	2.02	1.0
S1000-2	1350	Not tested	2.0	1.25
S750-1	3445	1000 kN	6.83	2.5
S750-2	3700	1222 kN	7.33	24
S750-3	2503	Not tested	4.96	11
S500-1	694	1000 kN	2.06	2
S500-2	681	1000 kN	2.02	1.5

3.4.3   Bond strength mechanisms in push-out

The push-out strength is attributed mainly to the dilation through the Poisson's ratio effect of the concrete within the steel tube, causing an increase in radial contact pressure, which enhances friction resistance. Load transfer through the bond in the vicinity of the load source is higher than that near the base of the concrete plug due to the same Poisson ratio effect. At the top of a typical specimen very little longitudinal load is transferred to the steel tube. The concrete, which is subject to very high compression stresses, expands laterally, so that the top of the steel section is forced to grip the concrete plug. In the vicinity of the base of the base of the plug, the steel tube carries most of the longitudinal load. This causes the tube to expand, while the expansion of the concrete plug is very small due to the low level of compressive stress in the concrete core. This leads to separation between the steel and concrete (see Figure 3.16).
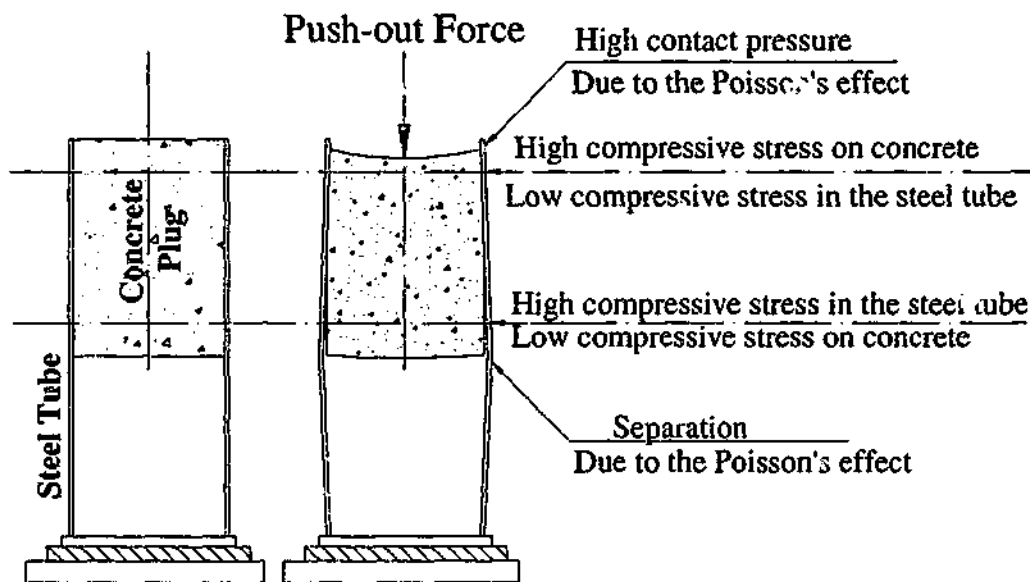
Figure 3.16 Bond strength mechanisms in push-out tests

3.4.4   Load slip response

Figures 3.17 to 3.19 show the load – slip relationships of all specimen groups with different plug and steel tube lengths. Figures 3.20 to 3.22 show the initial phase of the relationship in more detail.

The significantly different behavior associated with the three different lengths of embedment is amenable to only partial explanation.

The S1000 series exhibited a decaying shear/bond stress after peaking at a slip of 1.0-1.25 mm. This is the expected result associated with plugs in a properly circular straight pile. The fretting of the cemented matrix on the steel surface has a powdering effect removing the interlock with asperities on the steel surface, and lowering the effective coefficient of friction. The lower pull-out strength of specimens S1000 compared to S750 could be due to higher effect of shrinkage and initial pull-out test on specimens S750-1 and S750-2.

The S750 series did not exhibit the decay in shear/bond stress after an initial peak. A *possible* explanation is that the tubular member was not as straight or truly circular in cross-section as in the other two series. Macro interlock effects are then created when the slip becomes significant. These raise the contact stress between the pile and the concrete plug, which increases the frictional resistance. Although two of the three specimens in this series had been subjected to prior pull-out loads of 1000 kN, this was considered to be insufficient to generate permanent reverse slip and interface damage to affect the result.

The S500 series exhibited some slip at quite low initial load (less than 100 kN). This is attributed to reversal of permanent slip created by a prior pull-out load of 1000 kN which must have been close to peak capacity. These specimens had a push-out capacity 681 kN and 694 kN - significantly less than the pull-out capacity. The initial slip of 0.2 to 0.5 mm is believed to be the recovery of permanent pull-out slip. Finally in this series, the push-out load dipped after an

early peak at about 2 mm slip, but then recovered, indicating some macro effects previously discussed.

The ultimate shear/bond strength was approximately 2.0 MPa for the S1000 and S500 series, and 5.0-7.3 MPa for the S750 series. This apparently anomalous behavior is attributed to the mechanical model of shear transfer and the significant prior damage to the plug pile interface of the S500 series.

The mechanical model of shear transfer involves increased contact pressure between plug and pile due to the Poisson effect. In push-out loading the plug expands at the top, enhancing shear transfer at the top, until the plug and pile reach a state of uniform axial strain over most of the remaining length of plug, with little shear transfer. In pull-out loading, the pile contracts at the bottom of the plug, enhancing transfer there from the pile to the rebar. Above this point the concrete plug and pile have similar axial strain with little shear transfer.
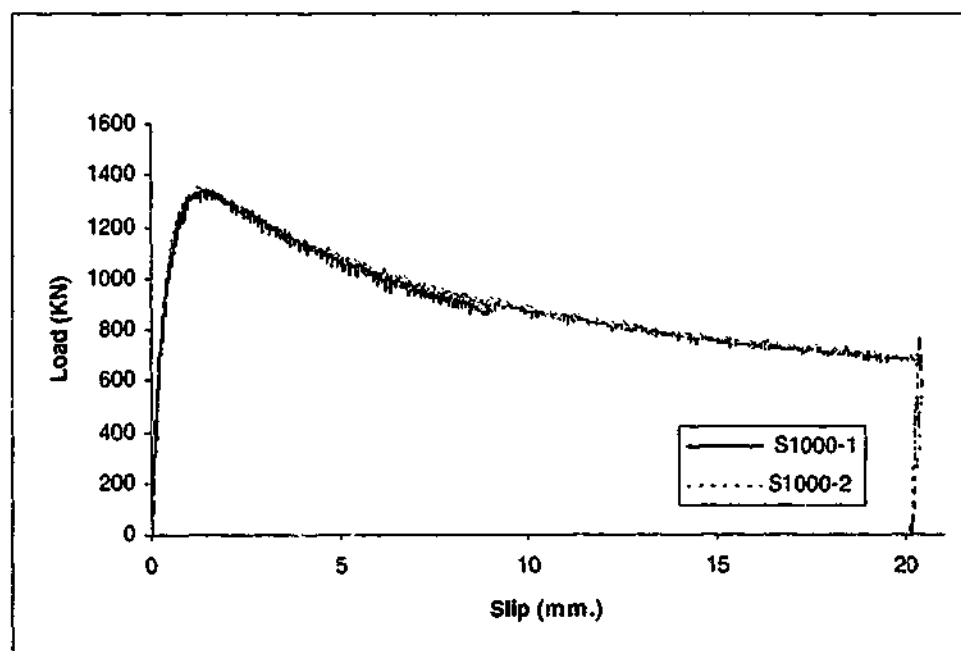
Figure 3.17. Load – slip relationship of specimens S1000
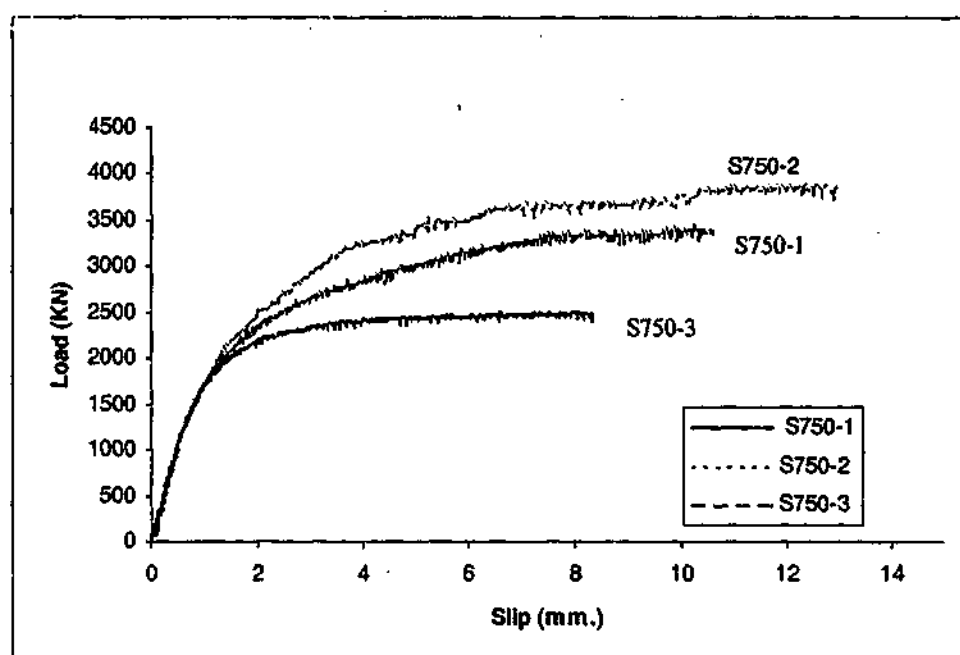
Figure 3.18 Load – slip relationship of specimens S750
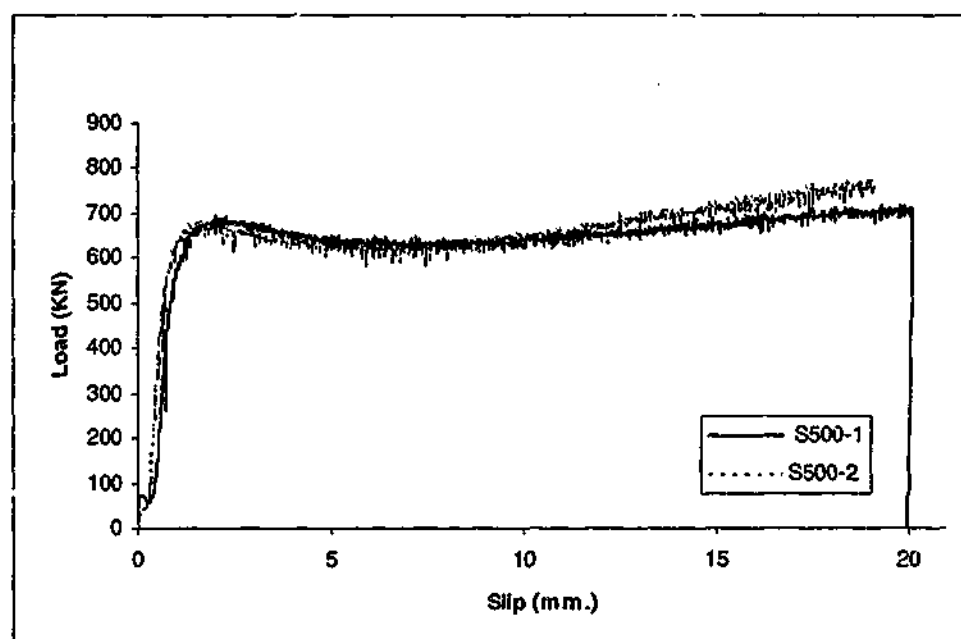
Figure 3.19 Load – slip relationship of specimens S500
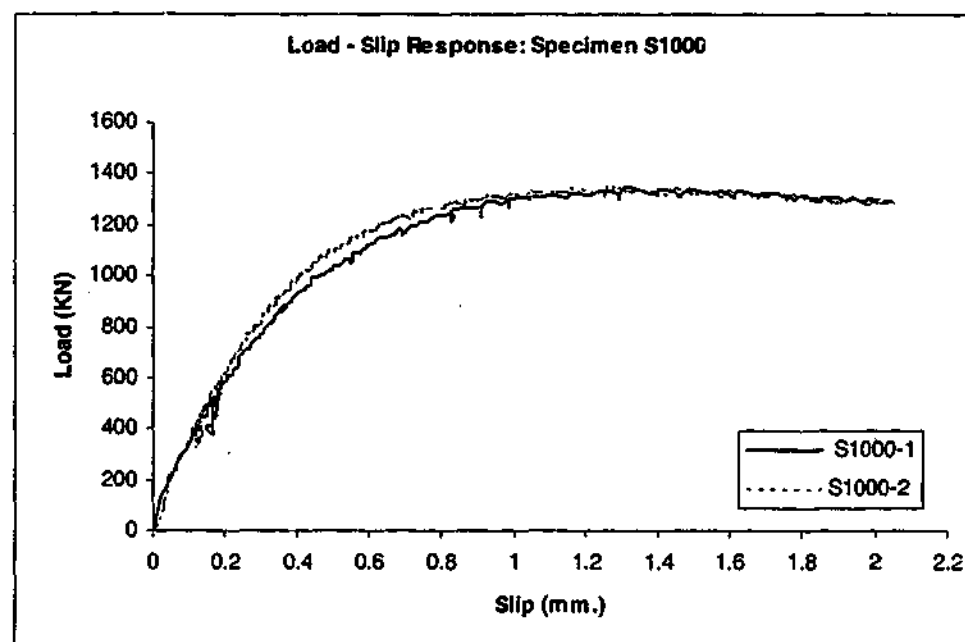
Figure 3.20 A close up of load – slip relationship of specimens S1000
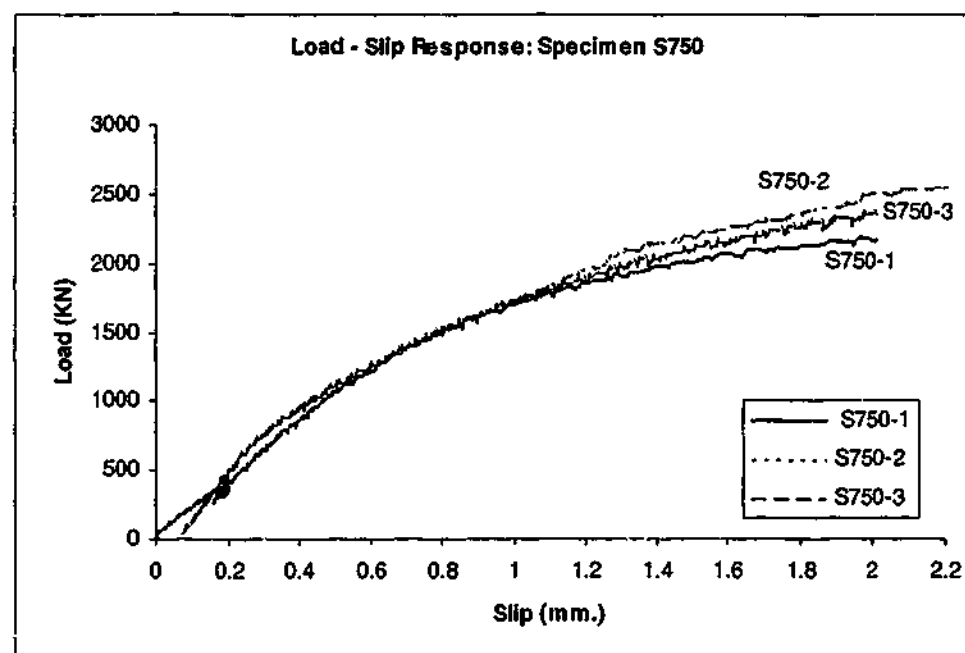
Figure 3.21 A close up of load – slip relationship of specimens S750
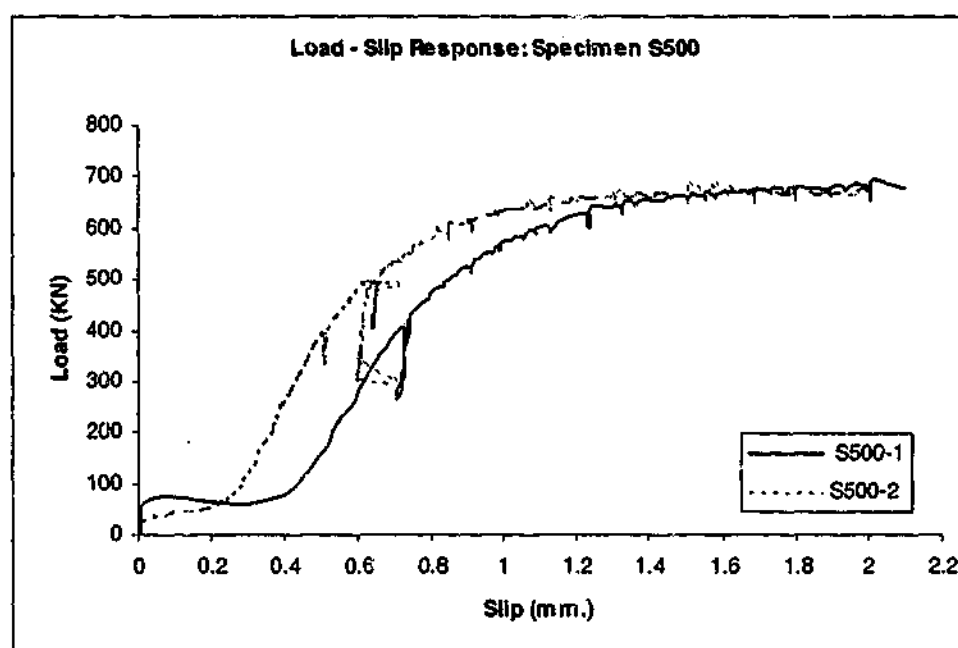
Figure 3.22 A close up of load – slip relationship of specimens S500

3.4.5 Comparison of the recommendations and test results

The push-out test results are presented in Figures 3.17 to 3.22 and Table 3.6. The measured mean ultimate strength of 1355 kN, 3216 kN and 687 kN were achieved for specimens S1000, S750 and S500 respectively.

Using the Reoder et al. (1999) recommendation for the ultimate bond strength of the CFT column given by equations *(2-24)* and *(3.1)*, the minimum average bond stress, $f_{2\sigma}$, and corresponding ultimate push-out strength $T_{ultimate}$, are calculated (see Table 3.8)

Table 3.8 Roeder's (1999) recommendations against the push-out test results

Specimen ID	D/t	Peak Load (KN)	Previous Pull-out test	Average Bond Strength (MPa)	Calculated bond stress (Roeder)	Ultimate pull-out strength (Roeder)
S1000-1	19.6	1360	Not tested	2.02	1.51	1017
S1000-2	19.6	1350	Not tested	2.0	1.51	1017
S750-1	19.6	3445	1000 kN	6.83	1.51	762
S750-2	19.6	3700	1222 kN	7.33	1.51	762
S750-3	19.6	2504	Not tested	4.96	1.51	762
S500-1	19.6	694	1000 kN	2.06	1.51	509
S500-2	22.7	681	1000 kN	2.02	1.46	492

It is evident that Eq. (3-1) gives higher estimates of ultimate bond strength than the code (BS 5400) value of 0.4 MPa. However, Eq. (3-1) still underestimates the bond strength, when compared with the measured values. The estimated ultimate push-out strengths from this recommendation are much lower than the experimental average ultimate strength.

The results indicated that the Roeder's (1999) recommendation for the bond strength is not accurate for the case of reinforced concrete plug embedded in steel tubular piles subjected to push-out. The recommendation was made regardless of the concrete plug length, concrete material characteristics and internal surface condition of the steel tube, which seem to influence on the bond strength of the concrete plug.

The adopted OT report (OTO-2001-016) recommendations for the characteristic bond strength can be used for the concrete plug in push-out.

Table 3.4 shows calculated values for the bond stress and corresponding ultimate push-out force based on the adopted OT report recommendations.

Table 3.9 The OTO's (2001) recommendations against the push-out test results

Specimen ID	D/t	Peak Load (KN)	Previous Pull-out test	Average Bond Strength (MPa)	Calculated bond stress (OTO)	Ultimate pull-out strength (OTO)
S1000-1	19.6	1360	Not tested	2.02	3.26	2194
S1000-2	19.6	1350	Not tested	2.0	3.26	2194
S750-1	19.6	3445	1000 kN	6.83	3.67	1851
S750-2	19.6	3700	1222 kN	7.33	3.67	1851
S750-3	19.6	2503	Not tested	4.96	3.67	1851
S500-1	19.6	694	1000 kN	2.06	4.06	1367
S500-2	22.7	681	1000 kN	2.02	3.8	1281

The experimental ultimate push-out strength of specimens S1000 is 1355 kN, which is 38% lower than the estimated average ultimate strength. This was due to shrinkage of the concrete, which decreased the stiffness of the interface and C_s, the surface condition factor by 38% to 0.37. The plug length to pile diameter ratio seemed also to influence the lower value than estimated for ultimate push-out capacity. On the other hand, the coefficients need to be calibrated for the application of concrete plugs embedded in steel tubular piles.

The estimated ultimate push-out strength of specimens S750 is 1851 kN and lower than experimental result of 3216 kN by 42 %. This was due to consolidation of the concrete from initial pull-out tests. The initial pull-out tests increased the radial pressure on the concrete and contact pressure between the concrete and the steel. This affected the macro resistance of the section in push-out tests.

The estimated ultimate push-out strengths of specimens S500 are higher than the achieved level of the bond strength in experiments due to initial pull-out tests. In this case, the initial pull-out tests damaged the interface as the specimen reached around the ultimate pull-out strength load.

The results indicated that the OTO's (2001) recommendation for the bond strength is more closely correlated with test results compared to the Roeder's(1999) recommendation and codes provisions.

3.5 Conclusion

This study of the bond resistance in reinforced concrete filled steel tubes indicates that a mechanical interlock mechanism, which is dependent on the length of the concrete plug, might be a feasible concept when dealing with the bond strength of reinforced concrete plugs embedded in steel tubular piles.

The pull-out bond strength tested in specimens having concrete plug embedment length to tube inner diameter L/D =1 ranged from 4.3 to 6.2 MPa and average of 5.1 MPa. It was not possible to determine the pull-out bond strength for specimens with L/D >1, due to yielding and rupture of the embedded steel bars preceding the development of full bond strength.

The push-out strength of reinforced concrete plugs embedded in tubular steel piles revealed capacities higher than reported by others, attributed in part to the presence of reinforcement in the plug. Bond strengths from 2.0 to 7.3 MPa and

average of 3.89 MPa were achieved. The possibility that the push-out strength of the S500 (short plug) series was affected by prior pull-out loading has been considered.

Bond strength is a function of both chemical adhesion of the steel-concrete interface and mechanical interlock between the concrete core and steel surface. To overcome mechanical interlock a small dilation of the tube occurs as it rides over the asperities of the interface, generating radial contact pressure, which enhances frictional resistance.

However, the main mechanism that is believed to contribute to the high bond strength in pull-out and push-out tests was the pronounced Poisson effect increasing radial contact stress at the base of the connection. A second factor was the presence of reinforcement in the plug.

The adopted bond strength formulation showed a good correlation with test results. The recommendation needs to be calibrated more accurately for an application of concrete plugs embedded in steel tubular pile.

In this chapter the previous pull-out and push-out test results have been presented and discussed. In the next chapter the experimental program for cyclic loading is outlined.

4 EXPERIMENTAL PROGRAM FOR CYCLIC TESTS

4.1 Scope and purpose of the tests

Achieving the objective of the research outlined in Section 2.11 required two stages of experimental work. The first stage of the experimental work focused on the determination of the effect of the initial cyclic loading on the ultimate pull out strength (Whitburn 1999). The second stage of the experimental work required detailed instrumentation of specimens to determine the shear transfer between the concrete plug and the steel tube. The determination of the effect of shrinkage on bond strength is also explored in this set of experiments. A total of fifteen specimens were tested for the purpose of investigating the effect of cyclic loading on the bond strength of concrete plugs embedded in tubular steel piles. The specimens were the subject of a combination of push out, pullout and cyclic loadings. The tests were carried out in accordance with the previous test results contained in Chapter 3, dealing with pull-out, push-out and cyclic loading tests.

A special purpose test rig was designed and constructed. This chapter describes the design and construction of the specimens and the test rig, together with a description of the experimental procedure. The selection of variable concrete plug length and fixed length of steel tubes, material properties, and loading arrangements, as well as instrumentation are considered in this section.

4.2 Material Properties of specimens

4.2.1 Concrete

Concrete was ordered from a local concrete distributor. The measured mean strength at 38 days was 39.7 MPa. The concrete had a slump value of 100 mm on arrival.

4.2.2   Steel tube

Austral Piling supplied the required circular steel tubes. Sections supplied can be classified into two categories, both with external diameters of approximately 232 mm. Three of the supplied sections were slightly thicker than the other sections. The first category "section 1" has an average internal diameter of 222.1 mm and average tube thickness of 11.0 mm. The second category "section 2" has an average internal diameter of 218 mm and average tube thickness of 13.0 mm. The steel tube was manufactured by cold-forming and high-frequency electric resistance welding to produce a strong pipe to tight dimensional tolerances, and confirmed with Australian Standards. It has minimum yield strength of 350 MPa and minimum ultimate strength of 450 MPa.

4.2.3   Reinforcement

The reinforcing bars in all specimens consisted of 6 Y 24 deformed bars with ultimate strength $F_u = 600$ MPa. Based on the gross area of the bars at the threaded end, the steel ratio is 5.2 % of the gross area of the concrete plug. This is considered to be at the high end of steel ratio in most codes of practice. The bars were secured with the use of 6 mm stirrups, which were located on the inside of the reinforcing bars.

In practice stirrups are usually wire tied to the reinforcement bars, but in order to maintain uniformity between specimens, the stirrups were tack welded to main bars.

4.2.4   Formwork

Formwork was made from plywood. The plywood sheeting was cut into circular discs that sat snugly in the steel tubes. Timber blocks were glued and screwed to the base of the ply forms to provide the necessary clearance at the end.

4.2.5   Base plate

The selected base plates were found in the laboratories, being 100 mm thick they were assumed to be rigid enough for application to testing. Six 22 mm holes were drilled on each base plate to connect the bottom of the specimens on the test rig during the pull out and cyclic loading tests using six M20.

4.3   Design and Construction of the Specimens

4.3.1   Introduction

As discussed before, the investigation procedures were designed with regard to previous investigations at Monash University. The fifteen specimens were constructed for the two stages of test procedures divided into two groups. It was decided that a cyclic loading test rig would be used to undertake the investigation of the effect of cyclic loading on the bond strength of concrete plugs embedded in steel tube.

As discussed, previous research has identified that the specimens subjected to pull out, push out or cyclic loading should meet certain requirements, and these are restated here.

- Use of six deformed bar size 24 as a longitudinal reinforcement, which provided a steel ratio of 5.2 % for all specimens.
- Concrete plug depth of 1.0 D to 2.0D
- Threaded projection at the end of longitudinal reinforcement
- Use of 6 mm stirrups inside longitudinal reinforcement
- Use of longitudinal and transverse strain gauges on steel tube

When these requirements are met, the longitudinal and transverse strain gauges should record the longitudinal and transverse strains on the steel tube, caused by longitudinal and hoop stresses when a specimen is subjected to pull-out, push-out or cyclic loading. Bond strength would be calculated based on the ultimate failure load in each loading case.

4.3.2   Ultimate pull-out force

The pull out load will apply on six Y 24 deformed bars, therefore the ultimate pull out force can be calculated as follows;

$$T_u = A_s \times F_u = 6 \times \pi \times 12^2 \times 600 = 1628 \text{ KN}$$

Effective area on threaded end of bars govern the ultimate Pull out force

$$1624 \times 20^2 / 24^2 = 1130 \text{ KN}$$

For safety purposes the ultimate pull out and push out test are limited to 1000 KN

4.3.3   Specimen construction

The steel tubes were cut to the length of 600 mm. The inner surfaces of the steel tubes were scrubbed with a wire brush to remove any excess rust, dirt or any other material.

The formwork was fabricated and placed at the bottom of the specimens considering the different depth of concrete plugs. The specified reinforcing cages were placed into the specimens and tack welded in position, to insure the cage would not move during the pouring of the concrete.

One cubic meter of 32 MPa concrete with slump of 80 – 100 mm, was ordered from CSR concrete to pour the concrete into each specimen. The result of the slump test on the concrete batch on arrival showed a slump of 100 mm and the cylinder compressive strength test results indicated 39.7 MPa at age of 38 days. The concrete was carefully placed and then vibrated into each specimen, to ensure satisfactory compaction of the concrete (the machinery used was a poker vibrator).

The specifications of the constructed specimens are shown in table 4.1.

Table 4.1 Constructed specimens' specifications

Specimen ID	Tube Length mm.	Tube Internal Diameter (mm)	Tube Wall Thickness (mm)	Concrete Plug Length (mm)	L/D_i
S1.0D-1	600	222.1	11	222	1.0
S1.0D-2	600	222.1	11	222	1.0
S1.0D-3	600	222.1	11	222	1.0
S1.25D-1	600	222.1	11	277.5	1.25
S1.25D-2	600	222.1	11	277.5	1.25
S1.25D-3	600	222.1	11	277.5	1.25
S1.5D-1	600	222.1	11	333	1.5
S1.5D-2	600	222.1	11	333	1.5
S1.5D-3	600	222.1	11	333	1.5
S1.75D-1	600	222.1	11	388.5	1.75
S1.75D-2	600	222.1	11	388.5	1.75
S1.75D-3	600	222.1	11	388.5	1.75
S2D-1	600	218	13	444	2
S2D-2	600	218	13	444	2
S2D-3	600	218	13	444	2

The top surface was plastered to provide a level surface, and to ensure even distribution of the compressive forces. The supporting timber formwork was removed, and the base plates were then welded to each sample. This process involved placing the samples into the test rig to ensure the reinforcement bars were correctly aligned with the testing rig. The base plate was then tack welded and removed from the rig and fully welded with three passes afterward.
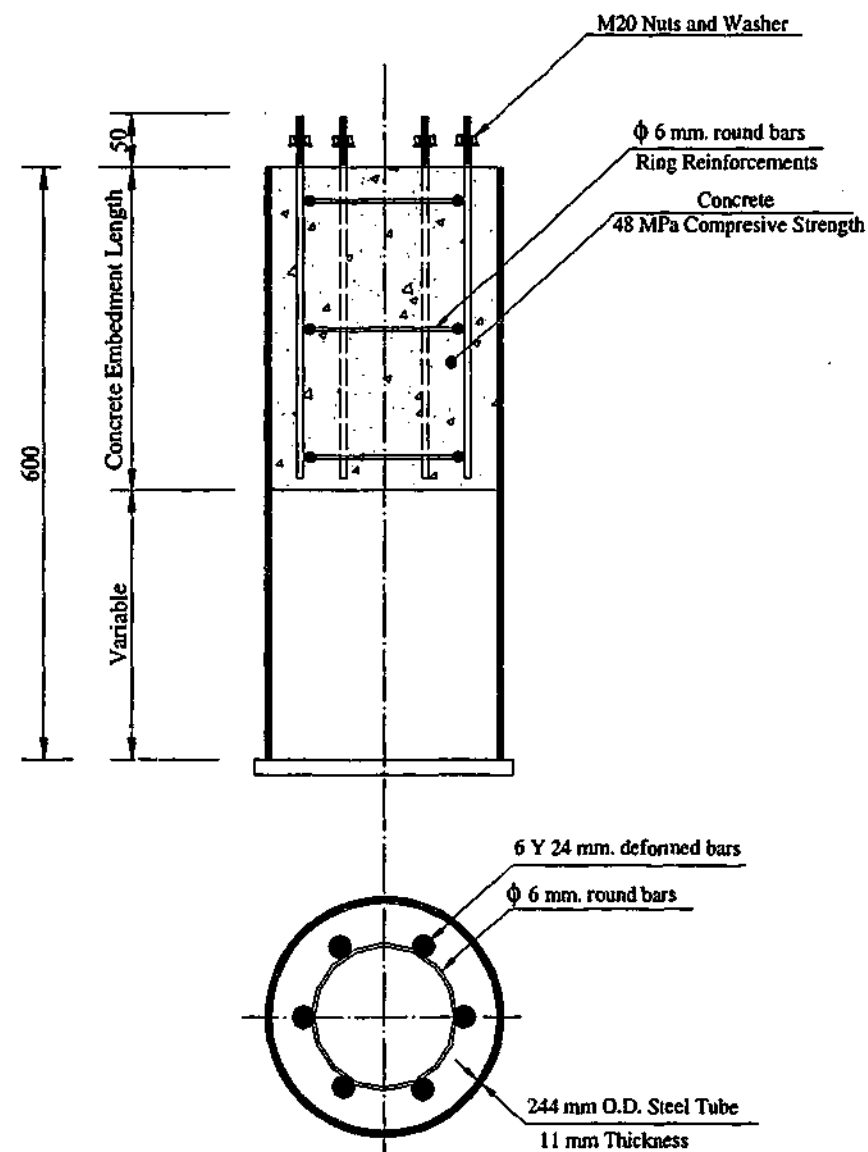
Figure 4.1 A typical test specimen for the cyclic test

4.4 Design and Construction of the test rig

4.4.1 Connection of the specimens to the test rig

The connection between the specimens and the test rig should transfer pull out, push out and cyclic loadings from actuator to the specimens. To achieve these requirements, six holes of 22 mm diameter were drilled in the base plate of each specimen, to be bolted to the test rig using six M20 high strength bolts after the specimen was lowered and placed into the testing apparatus. Six holes of 22 mm diameter were also drilled in the loading plate of the actuator with the same positioning of the threaded deformed bar of specimens. As a result, the loading plate can be placed on the top concrete surface of the specimens to apply compression on the concrete plugs. The threaded deformed bars are bolted to the loading plate to apply pull out force on the concrete plug.

4.4.2 Actuator and controller

An Instron servo controlled actuator, model 10077E, of 1000 kN dynamic and 1250 kN static capacity was used to load the specimens on pull out, push out and cycling loadings tests. This gave a comfortable margin of capacity over the anticipated ultimate pull out and push out forces of 1000 kN (Section 4.3.2). An Instron 8500 controller, which allowed load and displacement control, and had a programmable trapezoidal control waveforms, which were utilized for the cyclic loading tests, controlled the actuator. Displacement control was used for the pull out and push out tests, and load control (with displacement limit set) was used for all cyclic testing.

4.4.3 Support stand

The support stand was designed as a vertical 40 mm steel head plate (to connect to the bottom of specimens), welded and braced to a 20 mm steel base plate. The base plate was bolted to the strong floor using four bolts. Figures 4.2 to 4.6 show the placement and connection of a specimen to the test rig.
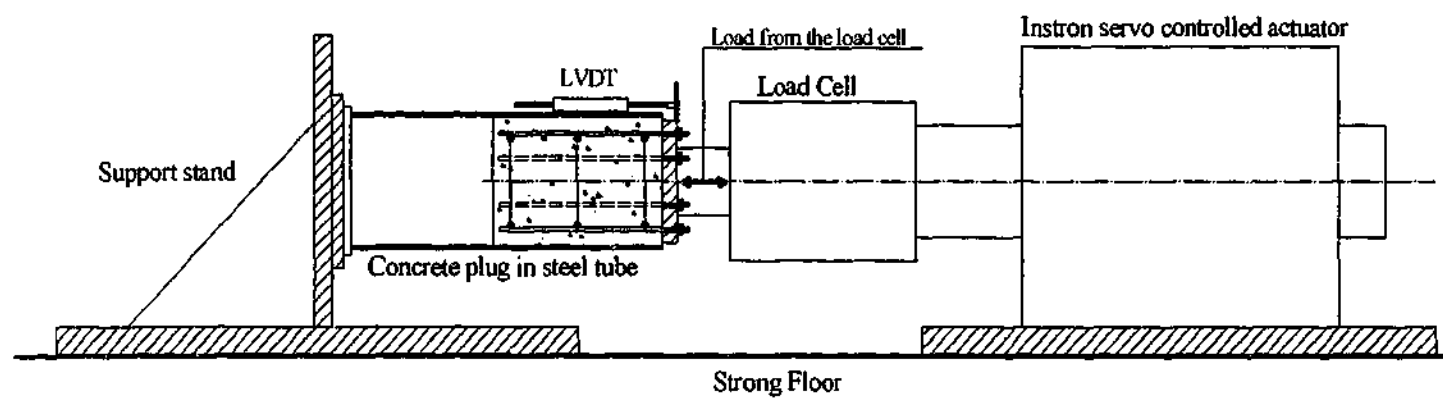
Figure 4.2 Cyclic loading test arrangements
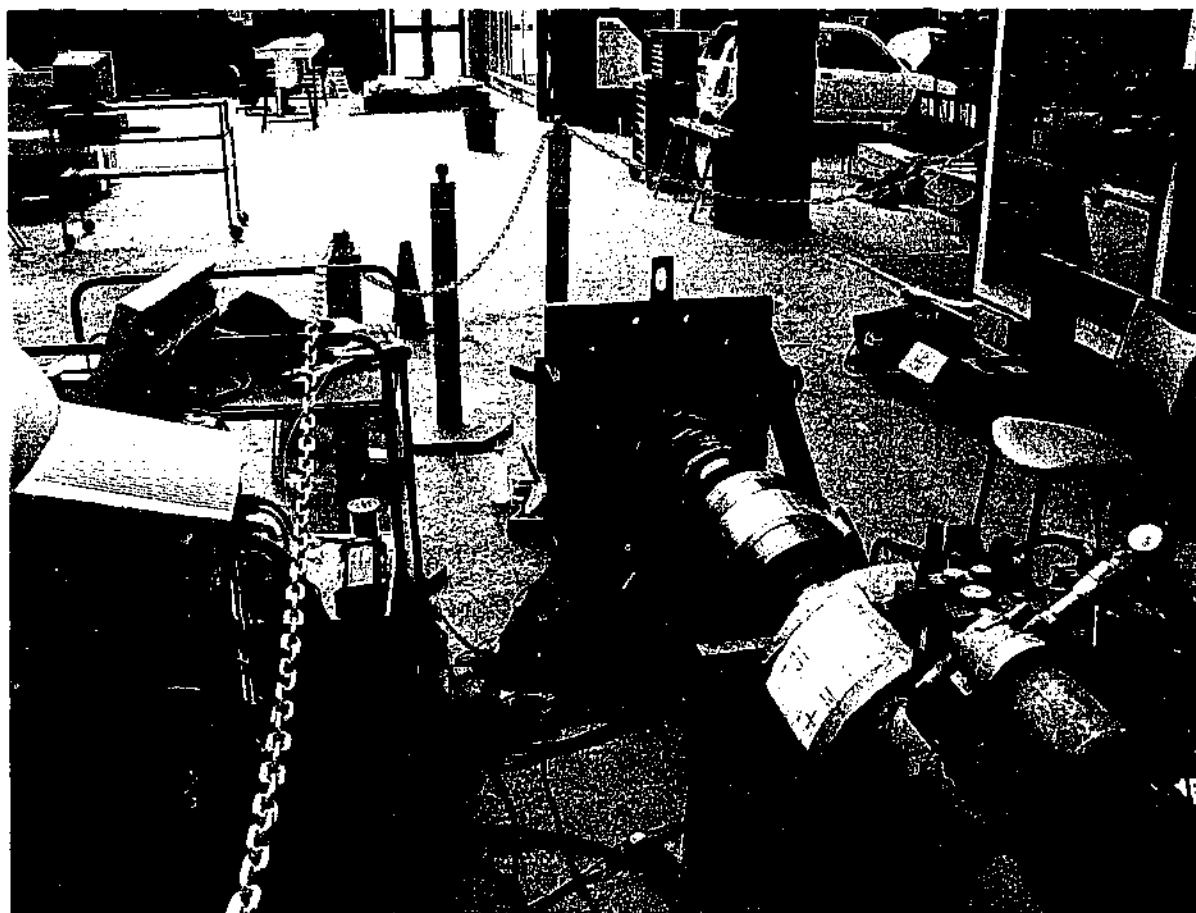
Figure 4.3 Support Stand
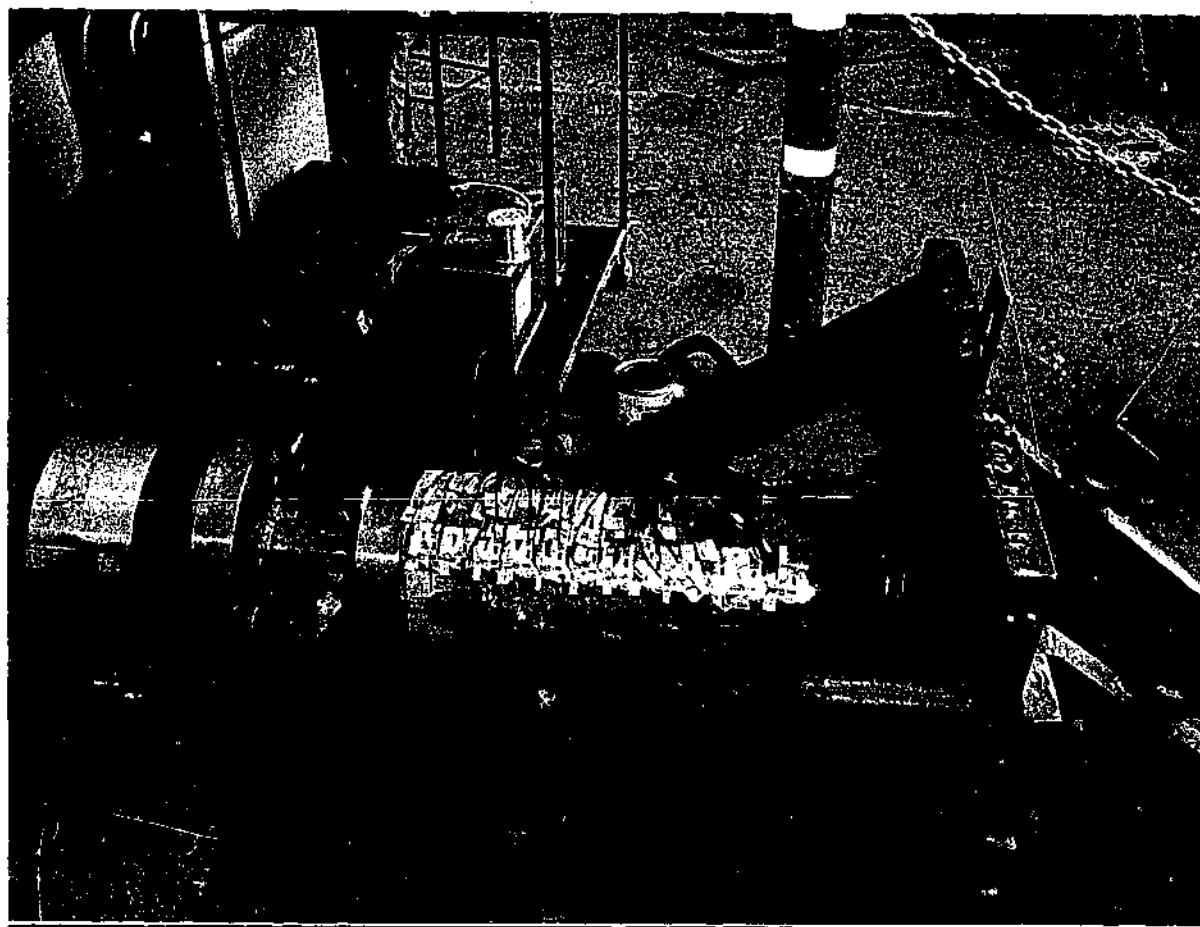
Figure 4.4 Placement of a specimen into the test rig
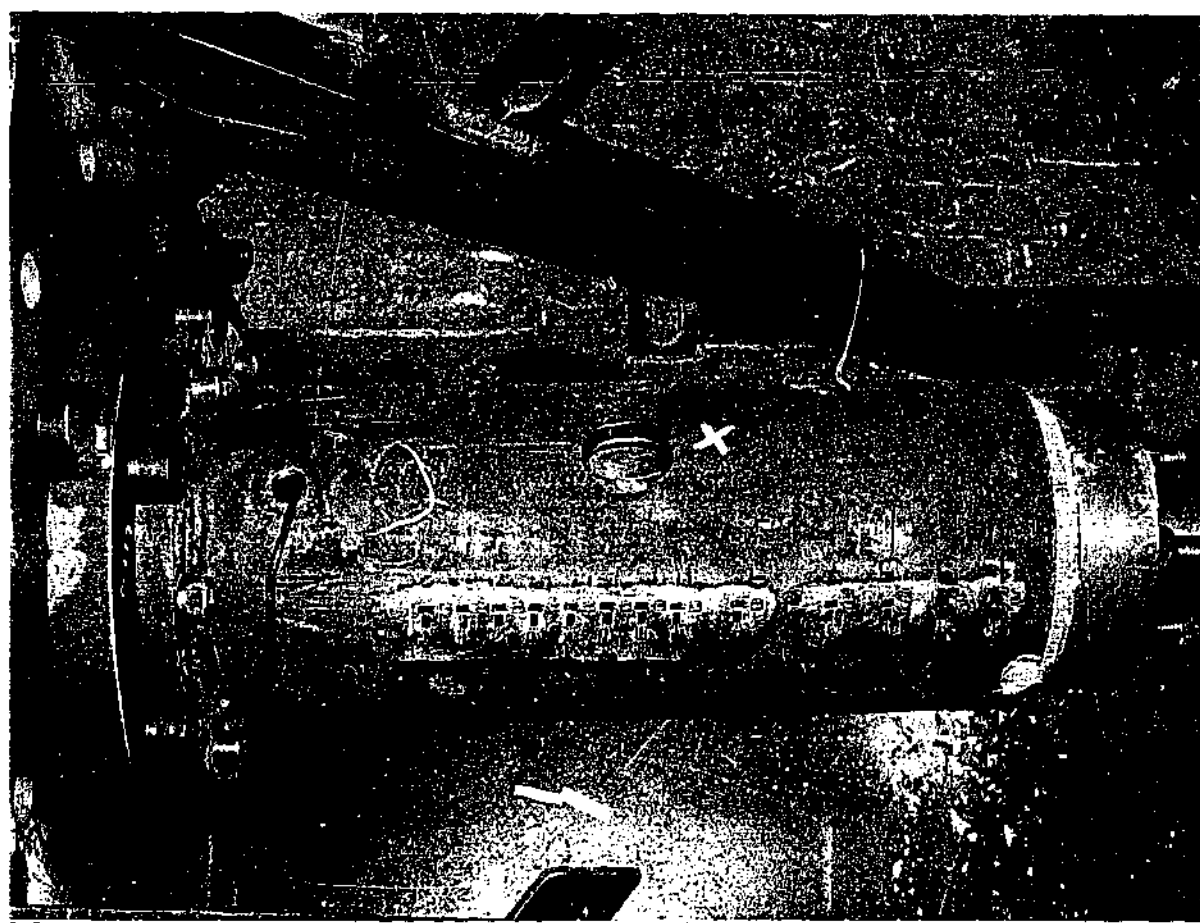
Figure 4.5 Specimen bolted on head plate of the support stand
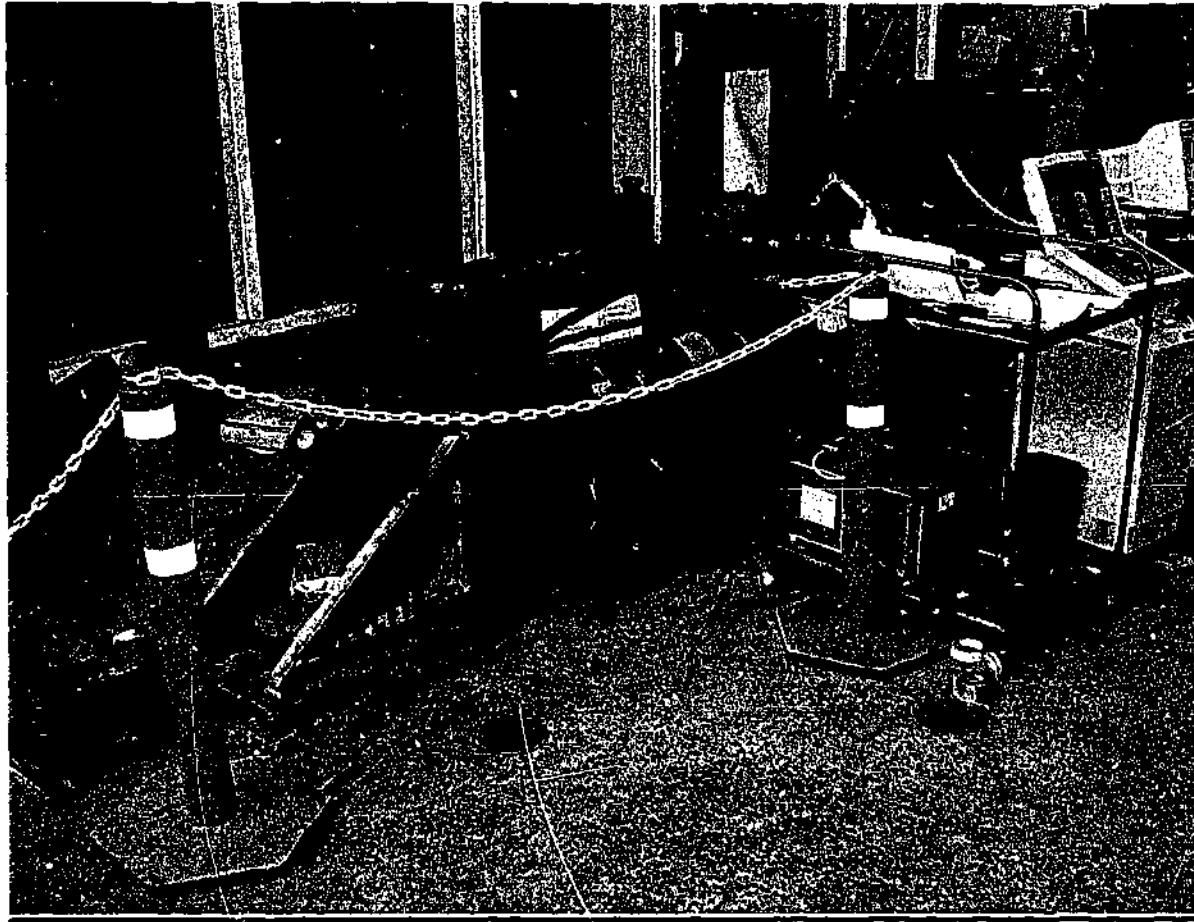
Figure 4.6 Support stand bolted to the strong floor

4.5   Experimental Procedure For Stage 1

4.5.1   Steps

The steps involved in performing a test on initial cyclic loading and pull-out tests in Stage one are listed below:

1.   Full weld the base plate to the steel tube at bottom of each constructed specimen.
2.   Prepare the specified locations for applying the strain gauges.
3.   Place strain gauges on the specified locations using super glue.
4.   Place the specimen into the test rig, bolting loosely.

5. Extend the actuator so that the loading plate is pushed against the concrete plug with a force of 5 kN, and bolted to the bars, to ensure the specimen is aligned and positioned properly.

6. Tighten the bolts that secure the specimen to the test rig.

7. Repeat the previous two steps

8. Fully retract the actuator, switch off the supply to the actuator, and fully tighten the bolts securing the specimen to the support stand and actuator.

9. Wire up all strain gauges

10. Connect the wires to the data acquisition box to record strain on steel tube.

11. Set up the linear differential transducer on top of concrete plug to measure slip directly between the steel tube and the concrete plug at top of concrete plug.

12. Connect the LVDT to the data acquisition system

13. Test all strain gauges

14. Set the actuator load to zero.

15. Run the data acquisition computer program to record the required data

16. Run the actuator control program to apply pull out and cyclic loading on specimen.

17. Stop the data acquisition program at the preset point of displacement.

18. Un tighten the bolts, cut off wires from the specimen

19. Remove the specimen from the test rig.

4.5.2   Rate of loading and number of cycles

The monotonic tests (pull out) were conducted at a displacement rate (as measured by the linear variable differential transducer inside the actuator) of 0.015 mm/sec. The time taken to reach the peak load was varied in the order of 5 to 40 minutes.

The cyclic tests were conducted with a symmetric cyclic loading. For every cyclic test, the loading was repeated for a predetermined number of cycles, with data being continuously recorded. The load range was then increased, and the new

loading was repeated, usually for the same number of cycles. Each initial cyclic loading included two load ranges.

For the cyclic tests the load versus time function was triangular. A typical function is shown in Figure 4.7 below. Each completed cyclic test had 10 cycles at each load range, with a cycle time of 4 minutes. The total elapsed time for a complete cyclic loading test for a load range was typically of the order of 20 minutes.

Type of tests on each specimen and the loading rates and number of cycles per load range in Stage one are summarized in Table 4.2.

Table 4.2 Summary of the conducted tests in stage 1

Specimen ID	Type of test	Maximum of Load	Max. of slip (mm)	Hold time (min)	Time for one cycle	No. of cycles per load range
S1.0D-1	1- Pull out	665kN	2.3 mm.	15 min	-	-
	2- Push out	525 kN	7.5 mm.	19 min	-	-
S1.0D-2	1- Cyclic loading	150 kN	0.6 mm.	40 min	4 min	10
	2- Cyclic loading	250 kN	1.0 mm.	40 min	4 min	10
	3- Pull out	711 kN	12.2 mm.	24 min	-	-
S1.0D-3	1- Cyclic loading	150 kN	0.2 mm.	40 min	4 min	10
	2- Cyclic loading	250 kN	0.7 mm.	40 min	4 min	10
	3- Pull out	410 kN	11.7 mm.	39 min	-	-
S1.5D-1	1- Pull out	1000kN	1.7mm.	17 min	-	-
	2- Push out	1000 kN	1.5mm.	18 min	-	-
S1.5D-2	1- Cyclic loading	230 kN	0.2 mm.	40 min	4 min	10
	2- Pull out	500 kN	1.8 mm.	8 min	-	-
	3- Push out	400 kN	6.8 mm.	24 min	-	-
S1.5D-3	1- Cyclic loading	230 kN	0.1 mm.	40 min	4 min	10
	2- Cyclic loading	400 kN	2.4 mm.	40 min	4 min	10
	3- Pull out	404 kN	9.2 mm.	39 min	-	-

Load vs. Time for Specimen S1.0D-2
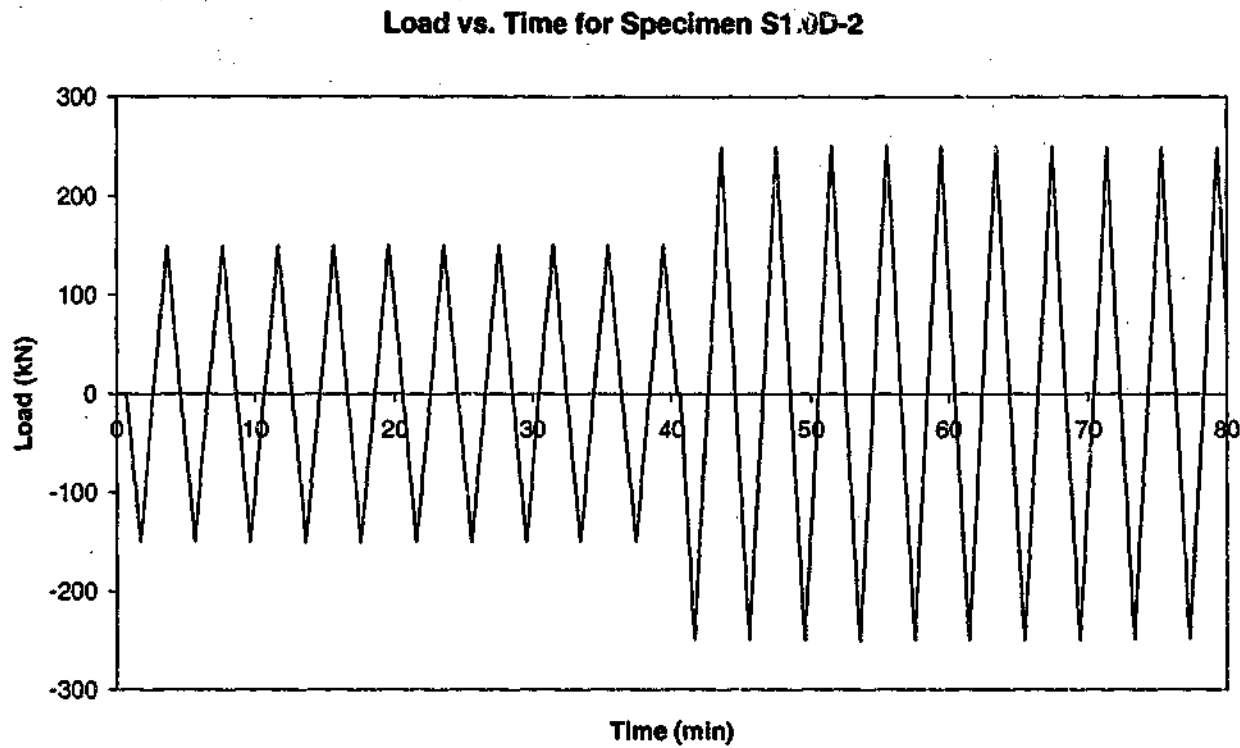
Figure 4.7: A typical load versus time function for Stage 1

4.5.3 Data acquisition

During a test the following data were acquired:

- Time
- Load from the actuator load cell
- Ram displacement from the built- in linear variable differential transducer in the actuator (this displacement included movement due to the compliance of the test rig, and was not used in any subsequent data analysis)
- Longitudinal displacement (slip) between the steel tube and the concrete plug, measured by monitoring a linear variable differential transducer directly on the top of the concrete plug

- Longitudinal and transverse strain along the steel tube, measured by monitoring the voltage differential through the strain gauges (refer to Figure 4.13). A data taker was essentially used to convert the analog voltage input into digital data that can be recorded on the computer (refer Figure 4.12).

A linear variable differential transducer's measuring slip were sampled at 20 Hz and a continuous moving average over twenty values was taken to return a slip value every second. The LVDT needed to be calibrated to obtain the slope factors between the voltage and the displacement of the LVDT. This simply involved using a micrometer and moving the LVDT between 0 and 24 mm at 2 mm intervals, and recording the milli volt reading at each point. The process was completed three times, and the average of the three trials was used to calculate the slip.

The data acquisition was controlled using the software " HP VEE" version 5.01. A typical acquisition set up is shown in Figure 4.11 below.

4.6 Experimental Procedure for Stage 2

4.6.1 Steps

The steps involved in performing a test on pull out, push out or cyclic loading are listed below:

1. Full weld the base plate to the steel tube at bottom of each constructed specimen.
2. Cut a hole on the base plate and a hole on bottom part of steel tube to locate one linear differential transducer at the bottom of concrete plug.
3. Prepare the specified locations for applying the strain gauges.
4. Place strain gauges on the specified locations using super glue.

5. Set up one linear differential transducer on bottom of concrete plug to measure slip directly between the steel tube and the concrete plug at bottom of concrete plug.

6. Place the specimen into the test rig, bolting loosely.

7. Extend the actuator so that the loading plate is pushed against the concrete plug with a force of 5 kN, and bolted to the bars, to ensure the specimen aligned and positioned properly.

8. Tighten the bolts that secure the specimen to the test rig.

9. Repeat the previous two steps

10. Fully retract the actuator, switch off the supply to the actuator, and fully tighten the bolts securing the specimen to the support stand and actuator.

11. Wire up all strain gauges

12. Connect the wires to the data acquisition box to record strain on steel tube.

13. Set up one linear differential transducer on top of concrete plug to measure slip directly between the steel tube and the concrete plug at top of concrete plug.

14. Connect Both LVDT to the data acquisition system

15. Test all strain gauges

16. Set the actuator load to zero.

17. Run the data acquisition computer program to record the required data

18. Run the actuator control program to apply push out, pull out and cyclic loading on specimen.

19. Stop the data acquisition program at the preset point of displacement.

20. Untighten the bolts, cut off wires from the specimen

21. Remove the specimen from the test rig.

4.6.2   Rate of loading and number of cycles

The monotonic tests (pull out and push out) were conducted at a displacement rate (as measured by the linear variable differential transducer inside the actuator) of 0.015 mm/sec. The time taken to reach the peak load was varied in the order of 5 to 40 minutes.

The cyclic tests were conducted with a symmetric cyclic loading. For every cyclic test, the loading was repeated for a predetermined number of cycles, with data being continuously recorded. The load range was then increased, and the new loading was repeated, usually for the same number of cycles. The number of load ranges in one test varied from 2 to a maximum of 9 depending on the failure of the specimen at the preset slip between the steel tube and the concrete plug, measured by the linear variable differential transducer on top of the concrete plug.

For the cyclic tests the load versus time function was triangular. A typical function is shown in Figure 4.8. Each completed cyclic test had 10 cycles at each load range, with a cycle time of 2 minutes. Some specimens were subjected to 10 cycles at each load range, with a cycle time of 4 minutes. The total elapsed time for a complete cyclic loading test for a load range was typically of the order of 20 minutes.

The type of tests on each specimen and the loading rates and number of cycles per load range are summarized in Table 4.3.

Table 4.3 Summary of the conducted tests in Stage 2

Specimen ID	Type of test	Maximum of Load	Max. of slip (mm.)	Hold time (min)	Time for one cycle	No. of cycles per load range
S1.25D-1	1- Push out	443 kN	2.75 mm.	51 min	-	-
	2- Pull out	460 kN	24.5 mm.	36 min	-	-
S1.25D-2	1- Cyclic loading	260 kN	1.05 mm.	20 min	2 min	10
	2- Cyclic loading	310 kN	7.95 mm.	20 min	4 min	5
	3- Pull out	439 kN	24.1 mm.	20 min	-	-
S1.25D-3	1- Cyclic loading	245 kN	8.02 mm.	7 min	4	1.75
	2- Pull out	540 kN	20.9 mm.	12 min	-	-
S1.75D-1	1- Push out	395 kN	7.48 mm.	7 min	-	-
	2- Pull out	330 kN	12 mm.	12 min.	-	-

| Specimen ID	Type of test	Maximum of Load	Max. of slip (mm.)	Hold time (min)	Time for one cycle	No. of cycles per load range
S1.75D-2	1- Cyclic loading	100 kN	0.12 mm.	20 min	4 min	5
	2- Cyclic loading	125 kN	0.17 mm.	20 min	4 min	5
	3- Cyclic loading	150 kN	0.23 mm.	20 min	4 min	5
	4- Cyclic loading	175 kN	0.30 mm.	20 min	4 min	5
	5- Cyclic loading	200 kN	0.37 mm.	20 min	4 min	5
	6- Cyclic loading	225 kN	0.56 mm.	20 min	4 min	5
	7- Cyclic loading	250 kN	0.84 mm.	20 min	4 min	5
	8- Cyclic loading	275 kN	1.67 mm.	20 min	4 min	5
	9- Cyclic loading	300 kN	14.8 mm.	16 min	4 min	4
S1.75D-3	1- Pull out	431 kN	1.37 mm.	9 min	-	-
	2- Cyclic loading	150 kN	0.03 mm.	20 min	4 min	5
	3- Cyclic loading	200 kN	2.16 mm.	20 min	4 min	5
	4- Cyclic loading	225 kN	7.72 mm.	20 min	4 min	5
	5- Cyclic loading	250 kN	18.6 mm.	14 min	4 min	3.5
S2D-1	1- Push out	1000 kN	1.89 mm.	60 min	-	-
	2- Pull out	1000 kN	1.24 mm.	40 min	-	-
	3- Cyclic loading	500 kN	4.75 mm.	44 min	4 min	11
	4- Cyclic loading	550 kN	2.95 mm.	40 min	4 min	7
	5- Cyclic loading	600 kN	2.97 mm.	5 min	4 min	1.25
	6- Cyclic loading	600 kN	3.25 mm.	5 min	4 min	1.25
	7- Cyclic loading	600 kN	16.0 mm.	30 min	4 min	7.25
S2D-2	1- Pull out	479 kN	16.7 mm.	2 min	-	-
S2D-3	1- Cyclic loading	200 kN	0.54 mm.	20 min	4 min	5
	2- Cyclic loading	250 kN	1.43 mm.	20 min	4 min	5
	3- Cyclic loading	300 kN	2.97 mm.	20 min	4 min	5
	4- Cyclic loading	350 kN	30.8 mm.	5 min	4 min	1

Load vs time for specimen S2D-1-C1
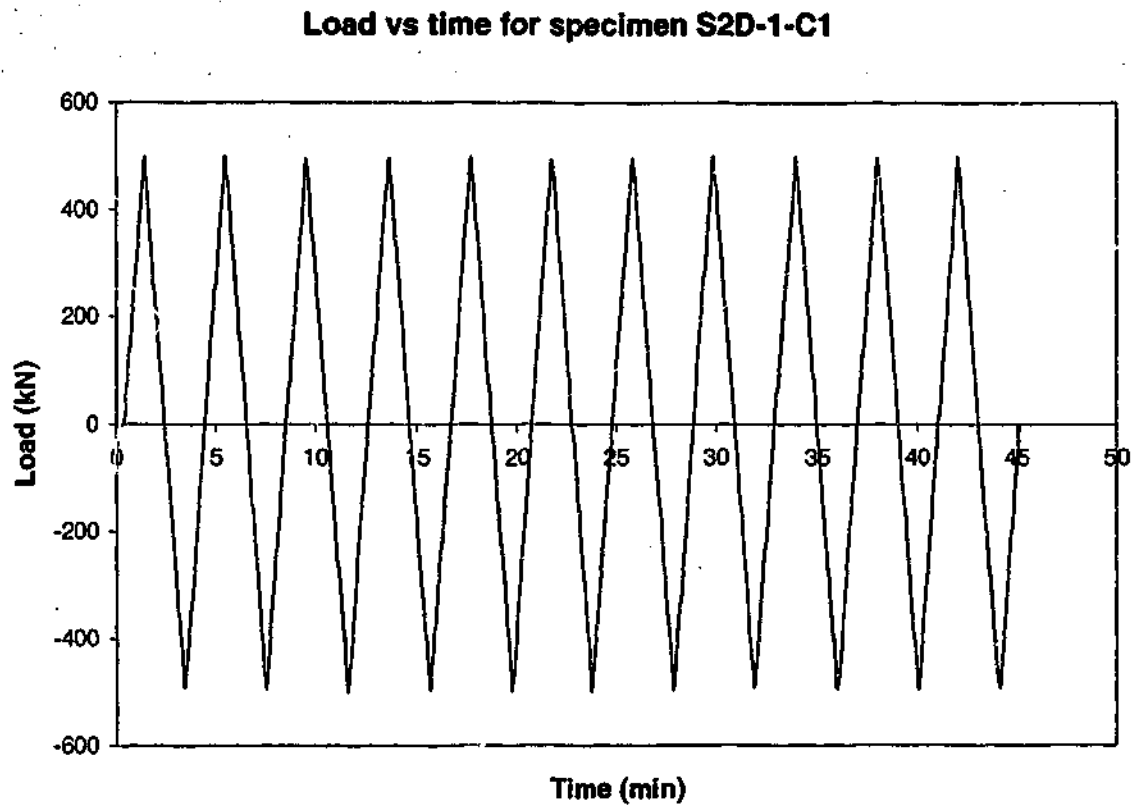
Figure 4.8 A typical load versus time function for Stage 2

4.6.3 Data acquisition

During a test the following data were acquired:

- Time
- Load from the actuator load cell
- Ram displacement from the built- in linear variable differential transducer in the actuator (this displacement included movement due to the compliance of the test rig, and was not used in any subsequent data analysis)

- Longitudinal displacement (slip) between the steel tube and the concrete plug, measured by monitoring a linear variable differential transducer directly onto top and bottom of the concrete plug (refer to Figures 4.9 and 4.10) (in this way the compliance of the test rig was excluded from the slip measurements)

- Longitudinal and transverse strain along the steel tube, measured by monitoring the voltage differential through the strain gauges (refer to Figure 4.13). A data taker essentially used to convert the analog voltage input into digital data that can be recorded on the computer (refer to Figure 4.12).

The two linear variable differential transducers' measuring slips were sampled at 20 Hz and a continuous moving average over twenty values was taken to return a slip value every two second. The LVDTs needed to be calibrated to obtain the slope factors between the voltage and the displacement of the LVDT. This simply involved using a micrometer and moving the LVDT between 0 and 24 mm at 2 mm intervals, and recording the milli volt reading at each point. The process was completed three times, and average of the three trials was used to calculate the slip.

The data acquisition was controlled using the software " HP VEE" version 5.01. A typical acquisition set up is shown in Figure 4.11 below.
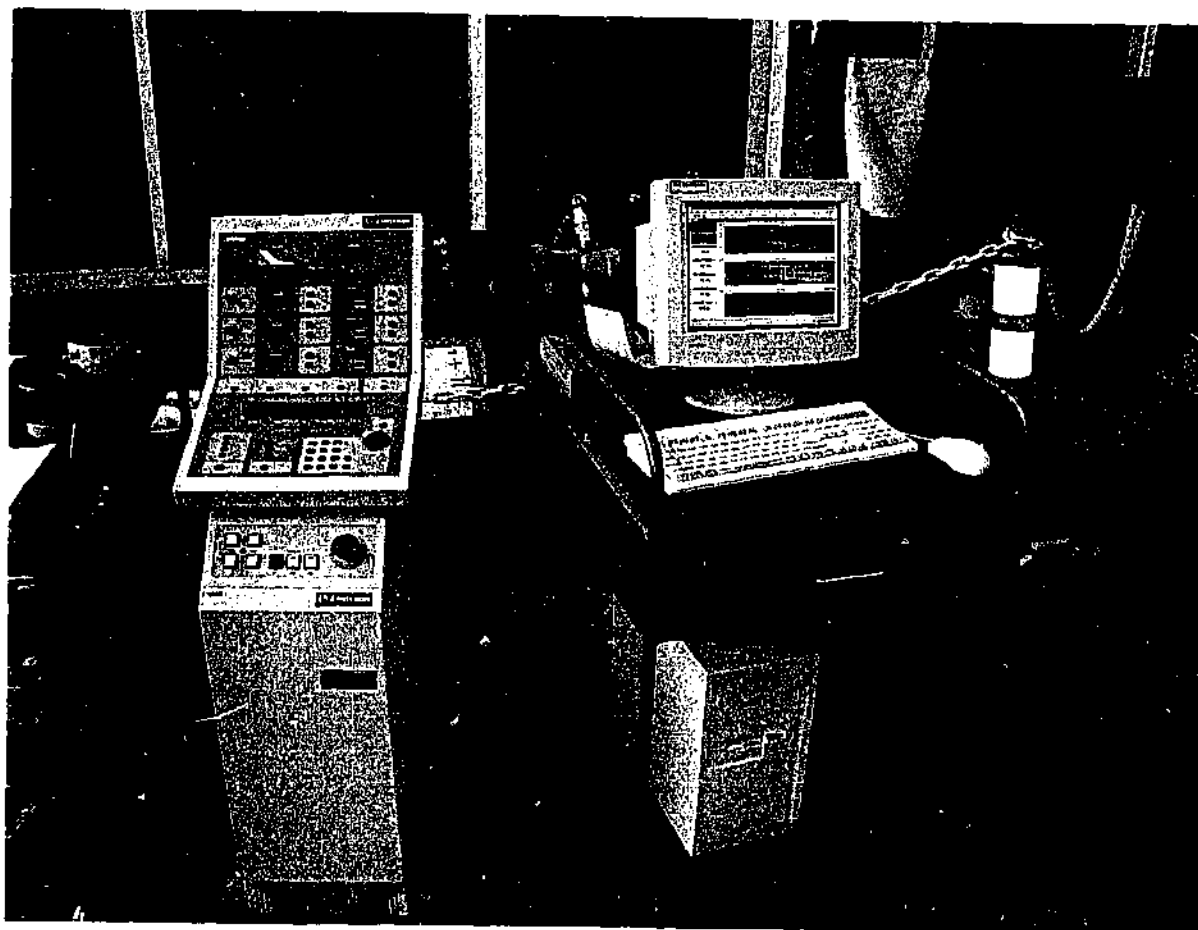
Figure 4.11 A typical data acquisition set up
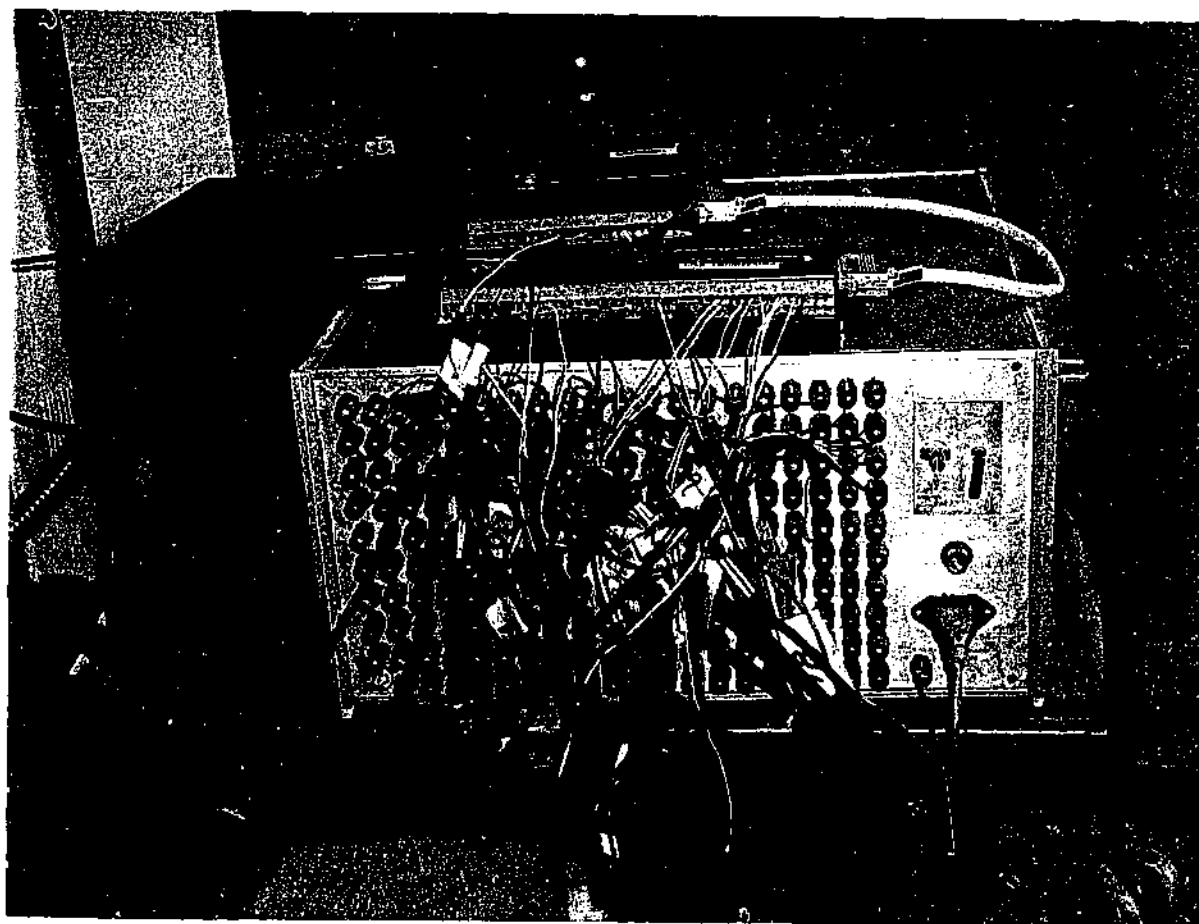
Figure 4.12 Data taker box

Figure 4.9 Slip measurement at the bottom of concrete plug
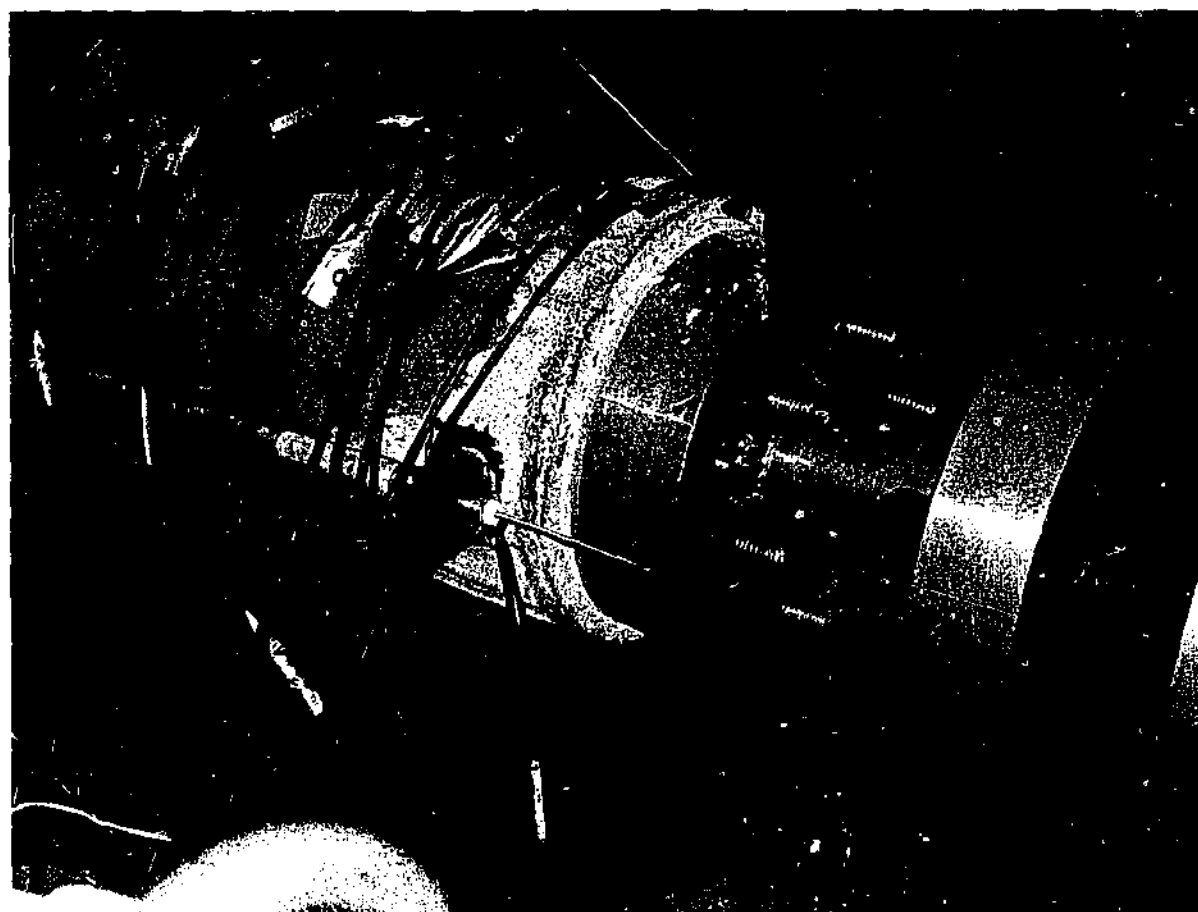
Figure 4.10 Slip measurement at the top of concrete plug

Figure 4.13: Wired strain gauges

4.7 Strain Gauges

Strain gauges are useful devices for monitoring strain/stress at certain points along a specimen's face. Longitudinal gauges and hoop gauges were used in combination to record strains in the principal directions (longitudinal and transverse plane) of the specimen. Using the two dimensional form of Hookes' law, stresses in the principal directions would then be calculated. Longitudinal gauges were also used on alternate sides of the specimen; these gauges were used to confirm that the applied load contained no eccentricity.

CEA- student series were used. These gauges are in the general purpose family of constantan alloy strain gauges widely used in experimental stress analysis. Extremely thin and flexible [0.0022 in (0.056mm)], CEA-Series gauges feature polyimide - encapsulated grids and exposed copper-coated integral solder tabs to which lead wires could be soldered directly. The normal use temperature range

for static strain measurement is –75 C to +175 C and strain limits of approximately 5% for 240 in gauge length apply on each strain gauges. M-Bond 200 was used to provide required bonding between steel surface and a strain gauge.

Strain gauges were positioned such that a detailed understanding of stress distributions could be obtained within a particular interest. Strain gauge locations for each specimen can be seen in Appendix A.

The cyclic loading test results are presented in the next chapter.

5 PRESENTATION OF CYCLIC LOADING TEST RESULTS

5.1 Introduction

This chapter presents the results of Stages 1 and 2 of experimental work, and subsequent analysis of these results. The primary focus of this discussion is to isolate the effect of cyclic loading on the ultimate bond strength of the concrete plug and the steel tube.

5.2 Key findings from the test results

The following are key findings from the cyclic loading test results

1. The average bond strength between concrete plug and the steel tube
2. The ultimate pull-out strength
3. The ultimate push-out strength
4. The longitudinal and transverse strains on steel tube
5. Slip at the top and bottom of concrete plug (only for stage two) into the steel tube, and the rate of slip growth per cycle increased with the pick load.
6. Cyclic reduction factor
7. The failure mechanisms
8. The relationships were obtained between the load and the rate of slip growth per cycle under repeated load.

5.3 Test Results For Stage 1

This stage aimed to evaluate the effect of initial cyclic loading on ultimate pull-out strength. Three specimens each of two different concrete plug lengths of 1.0D and 1.5D were tested. The first specimen of each plug length group was tested for

static tension capacity to enable the assessment of cyclic load effects. The other two specimens were then initially subjected to two ten cycles of 150 and 250 for series 1.0D specimens and 250 and 400 for series 1.5D specimens. This was followed by monotonic pull-out tests.

5.3.1   Summary of the tests conducted in Stage 1

A total of six successful tests were conducted, comprising two monotonic tests to determine the pull-out strength of the concrete plug and four pull-out tests with initial symmetric cyclic loadings. Table 5.1 summarizes the Stage 1 tests.

Table 5.1 Summary of the test conducted at the stage 1

Specimen ID	Test Number	Type of test	Load Range	Each cycle time/No of cycle	Date
S1.0D-1	1	Monotonic (tension)	-	-	15/11/1999
	2	Monotonic (compression)	-	-	15/11/1999
S1.0D-2	3	Symmetric Cyclic	±150 kN	4min / 10	9/11/1999
	4	Symmetric Cyclic	±250 kN	4min / 10	9/11/1999
	5	Monotonic (tension)	-	-	9/11/1999
S1.0D-3	6	Symmetric Cyclic	±150 kN	4min / 10	9/11/1999
	7	Symmetric Cyclic	±250 kN	4min / 10	9/11/1999
	8	Monotonic (tension)	-	-	9/11/1999
S1.5D-1	9	Monotonic (tension)	-	-	12/11/1999
	10	Monotonic (compression)	-	-	12/11/1999
S1.5D-2	11	Symmetric Cyclic	±250 kN	4min / 10	11/11/1999
	12	Monotonic (tension)	-	-	11/11/1999
S1.5D-3	13	Symmetric Cyclic	±250 kN	4min / 10	11/11/1999
	14	Symmetric Cyclic	±400 kN	4min / 10	11/11/1999
	15	Monotonic (tension)	-	-	11/11/1999

5.3.2 Ultimate bond strength

In order to calculate the ultimate pull out capacity of the specimens, it was decided that specimen S1.0D-1 and S1.5D-1 be subjected to a static pull out test at first and then to a static push out test.

The Instron machine was set at a displacement rate (as measured by the linear variable differential transducer inside the actuator) of 0.015 mm/sec. Specimen S1.0D-1 failed at an ultimate pull out strength of 665 kN, giving an average ultimate bond strength of 4.2 MPa. This was followed by a push out test, which resulted in ultimate push out capacity of 525 kN, giving average ultimate bond strength of 3.3 MPa.

Specimen S1.5D-1 achieved ultimate pull out strength of 1000 kN at slip of 1.7 mm. This was followed by a push out test, which resulted in ultimate push out capacity of 1000 kN at slip of 1.5 mm. The corresponding ultimate bond strength of 4.0 MPa was achieved in both pull out and push out.

The Instron machine was set to the load control for cyclic tests. Specimens S1.0D-2 and S1.0D-3 then were initially subjected to ten symmetric cycles of ±150 kN followed by another 10 symmetric cycles of ±250 in tension and compression. This was followed by pull out tests, which resulted in ultimate load 711 kN and 405 kN for specimens S1.0D-2 and S1.0D-3, respectively corresponding ultimate bond strengths are 4.5 and 2.6 MPa.

Specimen S1.5D-2 was initially subjected to ten symmetric cycles of ±250. This was followed by a pull out test, which resulted in ultimate load of 500 kN, and an ultimate bond strength of 2.2 MPa. Specimen S1.5D-3 was initially subjected to ten symmetric cycles of ±250 kN followed by another 10 symmetric cycles of ±400 kN. The specimen failed at the end of the cyclic loading test, giving average ultimate bond strength of 1.8 MPa.

Table 5.2 lists the value of peak loads achieved and corresponding average bond strength. The slip values at peak load, initial cyclic loading test situations and age of the concrete on date of test are also tabulated.

Table 5.2 Summary of the Stage 1 test results

Specimen ID	Type of test	Measured Peak Load kN	Bond Strength MPa	Max. of slip (mm)	Each cycle time/No of cycle	Concrete Age (days)
S1.0D-1	Monotonic (tension)	665	4.2	2.3	-	32
	Monotonic (compression)	525	3.31	7.5	-	
S1.0D-2	Symmetric Cyclic	150	0.94	0.6	4min / 10	
	Symmetric Cyclic	250	1.58	1.0	4min / 10	26
	Monotonic (tension)	711	4.49	12.2	-	
S1.0D-3	Symmetric Cyclic	150	0.94.	0.2	4min / 10	
	Symmetric Cyclic	250	1.58	0.7	4min / 10	26
	Monotonic (tension)	410	2.59	11.7	-	
S1.5D-1	Monotonic (tension)	1000	4.3	1.7	-	29
	Monotonic (compression)	1000	4.3	1.5	-	
S1.5D-2	Symmetric Cyclic	230	0.99	0.2	4min / 10	
	Monotonic (tension)	500	2.15	1.8	-	28
	Monotonic (compression)	400	1.72	6.8		
S1.5D-3	Symmetric Cyclic	230	0.99	0.1	4min / 10	
	Symmetric Cyclic	400	1.72	2.4	4min / 10	28
	Monotonic (tension)	404	1.74	9.2	-	

Average bond strengths of 4.25 MPa for static pull-out test and 2.77 MPa for pull-out test with cyclic loading effect were achieved. The test results indicated that pre-cyclic loading tests reduced the bond strength due to the prior damage to the plug pile interface.

5.3.3   Load-slip response

Figures 5.1 and 5.2 show the load-slip responses of specimen series S1.0D and S1.5D respectively.

In pull-out specimen S1.0D-1 exhibited a decay shear/bond load as slip increased after peaking at a slip of 1.0-1.5 mm. This is the expected result associated with a plug in a properly circular straight pile. In push out, the specimen exhibited some slip at an initial load of 300 kN. This is attributed to reversal of permanent slip created by the prior pull-out test. The initial slip of 2.0 mm is believed to be recovery of permanent pull-out slip. The specimen then exhibited a gradual increase in load transfer as slip increased after reaching an applied load of 450 kN at a slip of 1.0 mm. A possible explanation is that the initial pull-out test pre-stressed the interface. Macro interlock effects are then created when the slip becomes significant. These raise the contact stress between the steel tube and concrete plug, which increases the frictional resistance.

Specimen S1.0D-2 and S1.0D-3 exhibited a typical load-slip response in tension after initial cyclic loading. It was characterized by a gradual decrease in load transfer as slip increased after peaking at a slip of 1.0mm. The load-slip of specimen S1.0D-2 indicates that the initial cyclic loading may not have a significant effect on the load-slip behavior and the ultimate pull-out strength of the specimen. On the contrary, the load-slip response of specimen S1.0D-3 shows that the initial cyclic loading reduced the interface stiffness and shear transfer between concrete and the steel tube. This was due to the prior damage to the plug pile interface.

As can be seen from the figure, the load-slip response of specimen S1.5D-1 shows a typical behavior in pull-out test with peak load of 1000 kN at a slip of 1.7 mm. The test procedure stopped at 1000 kN as the specimen reached the limitation of the test instrumentation. The load-slip of the specimen in push-out shows gradual reversal slip to load level of 300 kN. This is attributed to the reversal of

permanent slip created by prior pull-out test. The specimen then reached a load level of 1000 kN at a slip of 1.0 mm.

Specimen S1.5D-2 exhibited a typical load-slip response in tension after initial cyclic loading. It was characterized by a gradual decrease in load transfer as slip increased after peaking at a slip of 1.0mm. The load-slip response of specimen S1.0D-3 shows that the initial cyclic loading reduced the interface stiffness and shear transfer. This was due to the prior damage to the plug pile interface.

Specimen S1.5D-3 failed at the end of the second ten cycles. The load-slip response of the specimen indicates that the initial cyclic loading reduced the ultimate strength of the specimen to the level of the second cyclic load of 400 kN. This was due to the significant damage to the plug pile interface. The post failure response shows an almost constant shear transfer in pull out test after cyclic loading. This behavior continued until the slip values reached 9.2 mm.

The load-slip response of the specimens indicated that the load slip curves of the pull-out test with cyclic effect is similar to the load slip curve obtained for monotonic static tests. The shifting between these two curves in the ordinate load axis is due to the different cyclic loading rate and concrete plug length. The effects of cycling rate and the damage model will be discussed in the following sections.

The ultimate capacity and load slip response of specimens under cyclic loading can be reasonably approximated from the ultimate strength and load slip of static test results by reducing the ultimate strength values of static test by a cyclic reduction factor. The cyclic reduction factor is defined as the factor by which the cyclic strength of a specimen may be obtained from the static strength for a given displacement. The cyclic reduction factor seems to depend on the rate of load, number of cycles, the concrete characteristics and shrinkage, the imperfection of the steel tube, the length of plug and perhaps the presence of reinforcement.

Load-slip response for specimen S1.0D-1

Load-slip response for specimen S1.0D-2

Load-slip response for specimen S1.0D-3
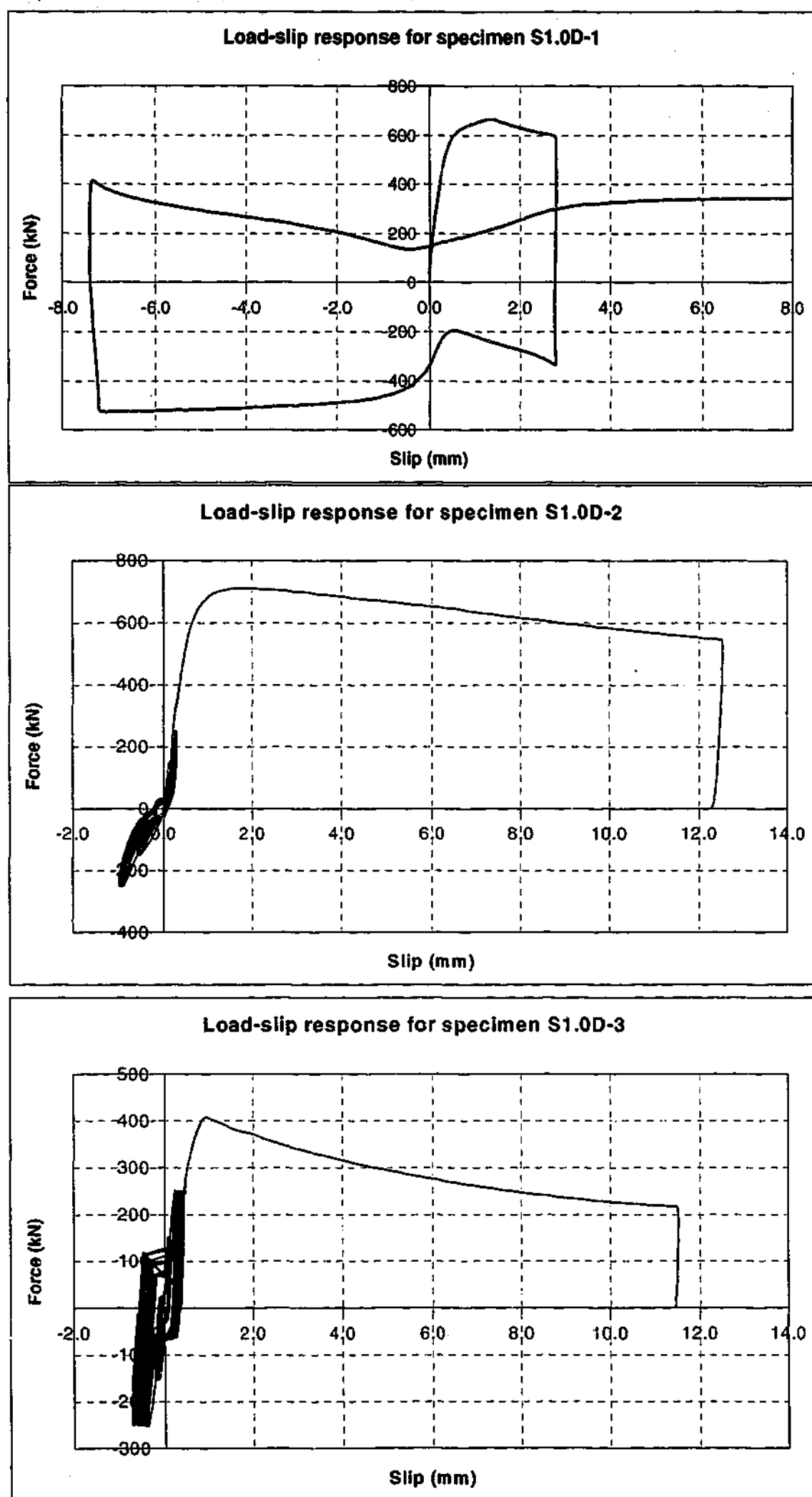
Figure 5.1 Load-slip response for specimens S1.0D

Load-slip response for specimen S1.5D-1

Load-slip response for specimen S1.5D-2

Load-slip response for specimen S1.5D-3
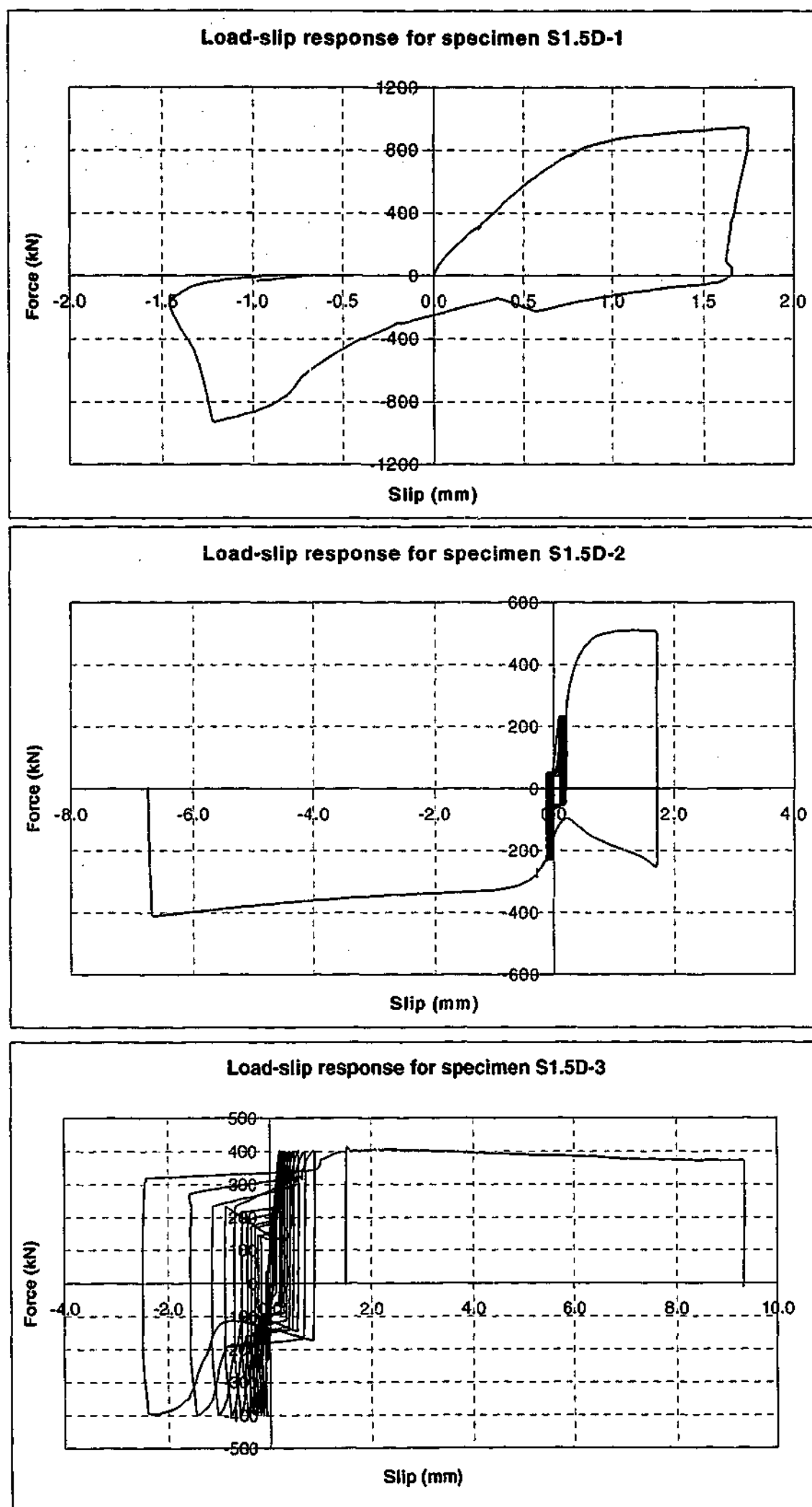
Figure 5.2 Load-slip response for specimens S1.5D

5.3.4   Slip versus cycles results for cyclic loading

During cyclic loading, damage to the concrete plug and the pile/plug interface became apparent either by progressive loss of stiffness through the accumulation of microcracking or by progressive plastification that appeared as an irreversible residual strain that increased with each additional cycle.

The slip versus cycles behavior for each of the specimens is plotted in Figures 5.3 to 5.6. The time for one load cycle was typically 4 minutes. The rate of loading increased as the load range increased in order to keep the cycle time constant. The load was applied for 10 cycles at each load range.
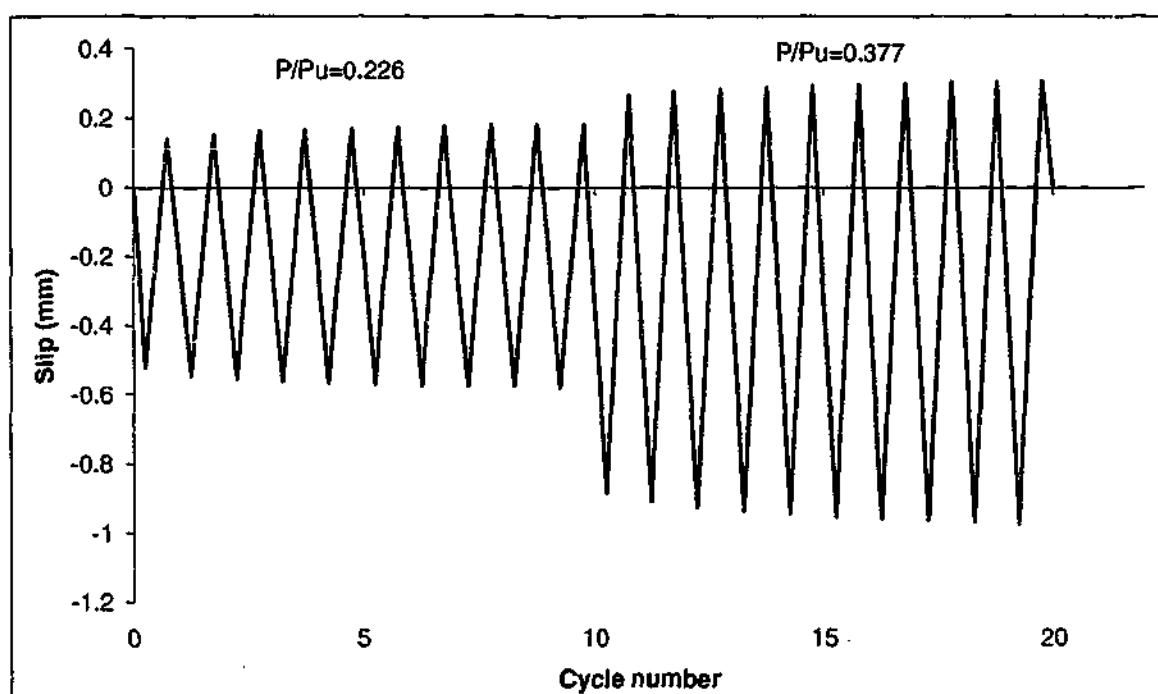
Figure 5.3 Slip versus cycles for specimens S1.0D-2
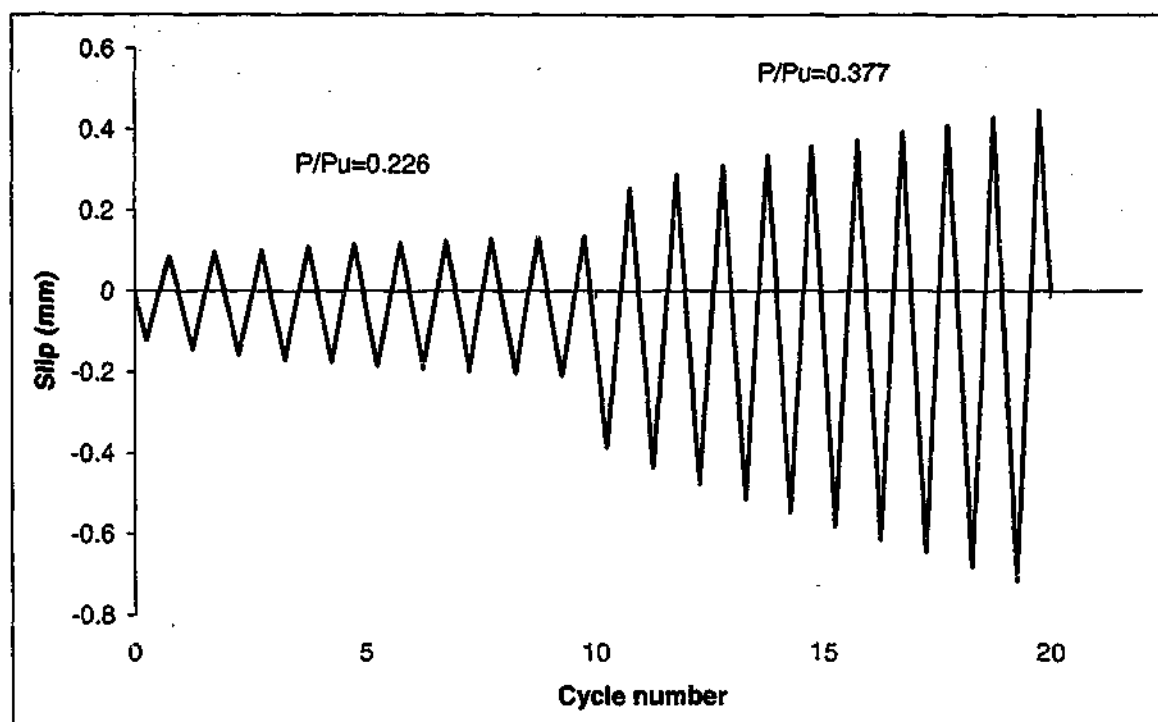
Figure 5.4 Slip versus cycles for specimens S1.0D-2
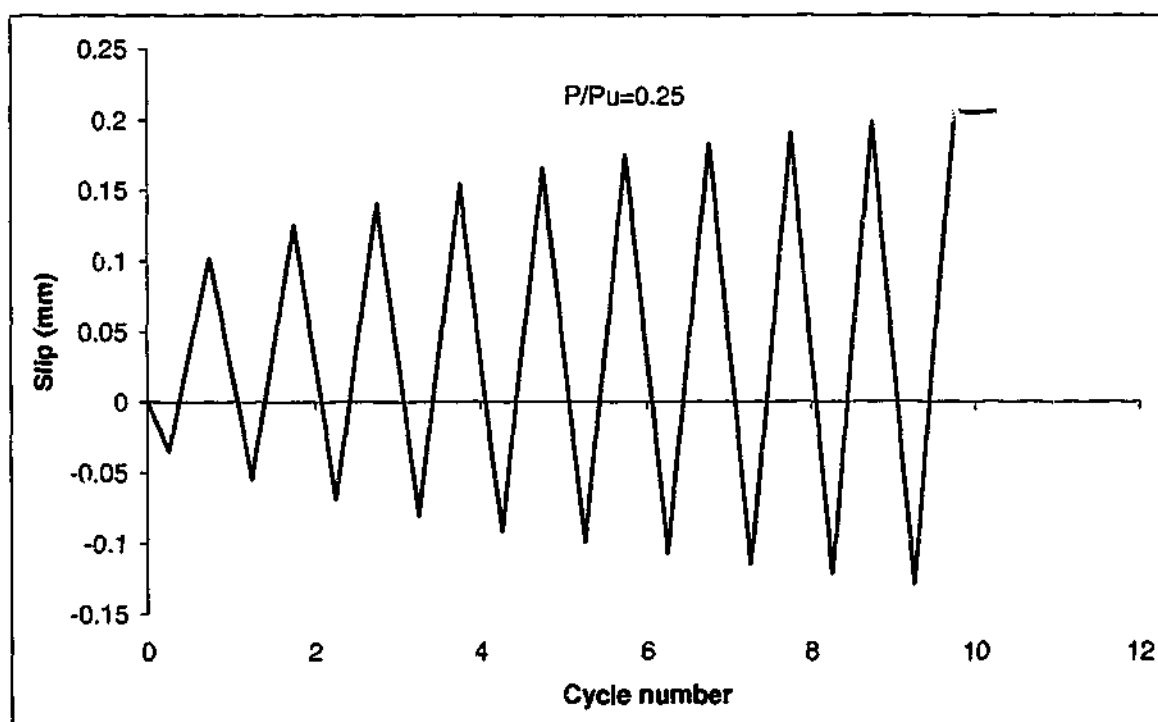
Figure 5.5 Slip versus cycles for specimens S1.5D-2
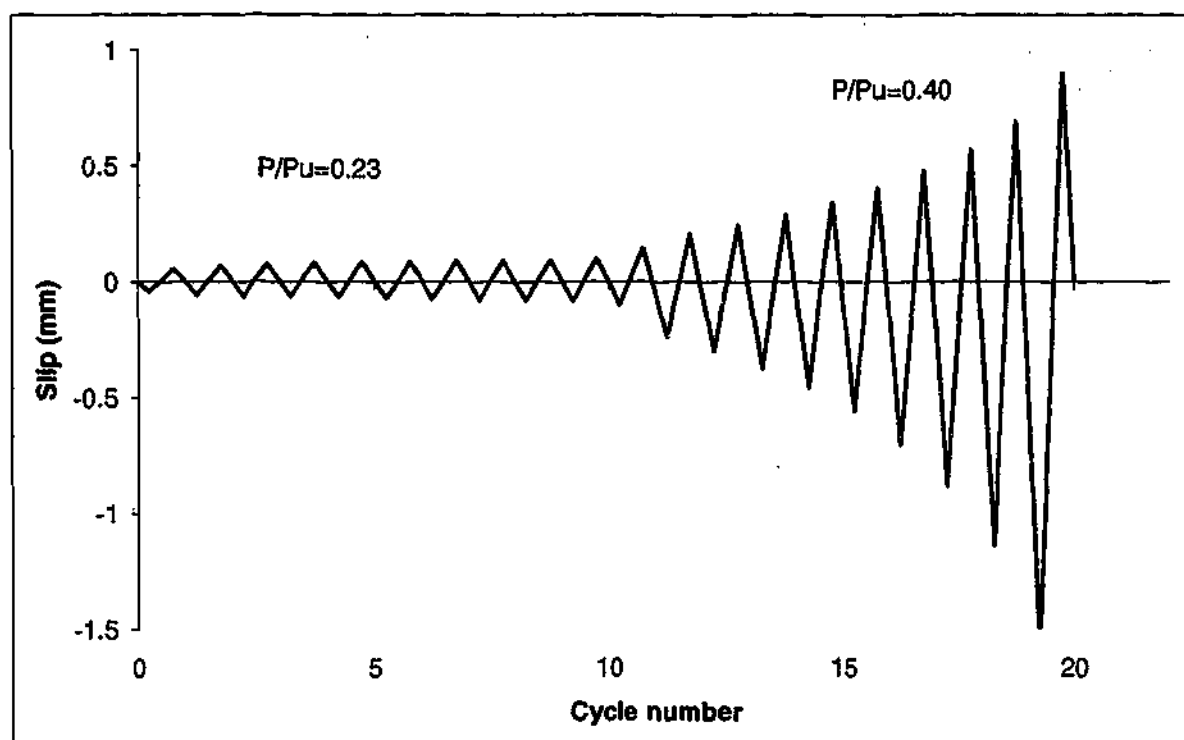
Figure 5.6 Slip versus cycles for specimens S1.5D-3

From the figures it is clear that slip increased with load cycles, and that the rate of slip growth increased with the peak load. The non-symmetric behavior may be due to differences in the local stiffness of the concrete plug adjacent to the steel tube. A concentration of coarse aggregate or of voids immediately adjacent to the top or bottom of the steel tube would have an effect on the concrete stiffness and on the rate of slip growth (decreasing and increasing it respectively).

5.3.5   Rate of slip growth under cyclic loading

It was observed from Figures 5.3 to 5.6 that, after the first few cycles at any load range, the slip increased approximately linearly with cycles. The exception to this is specimen S1.5D-3 at the second 10 cycles, where the slip increased more rapidly with cycles as the test approached failure.

A line of best fit to the rate of slip growth with cycles was calculated for every test at every load range. The values are presented in Table 5.3. These data are plotted in Figure 5.7, with the rate of slip growth plotted on a logarithmic scale. Although there is considerable scatter in the data, there is a clear trend that the rate of slip growth increased with the peak load. The scatter in the data is probably a reflection of the variation in the characteristics of the concrete plugs.

Table 5.3 Rate of slip growth for cyclic tests (Stage 1)

Specimen ID	Type of test	Load (kN)	P/Pu	Rate of slip growth (μmm/Cycle)	
				Positive slip	Negative slip
S1.0D-2	Symmetric Cyclic	150	0.226	4.06	5.71
	Symmetric Cyclic	250	0.337	3.91	8.86
S1.0D-3	Symmetric Cyclic	150	0.226	5.11	8.64
	Symmetric Cyclic	250	0.337	19.07	33.04
S1.5D-2	Symmetric Cyclic	230	0.23	9.68	9.547
S1.5D-3	Symmetric Cyclic	230	0.23	4.02	4.08
	Symmetric Cyclic	400	0.337	75.8	131.93

A line of best fit to the data (plotted in the figure) gave equation *(5.1)*,

$$\text{Symmetric cyclic loading, slip growth per cycle} = 10^{(0.3584\frac{P}{P_u}-0.0754)} \text{ mm/cycle}$$

(5.1)

Various forms of representing the data were trialed, including higher order functions to fit the log-linear representing of the data given in Figure 5.7.
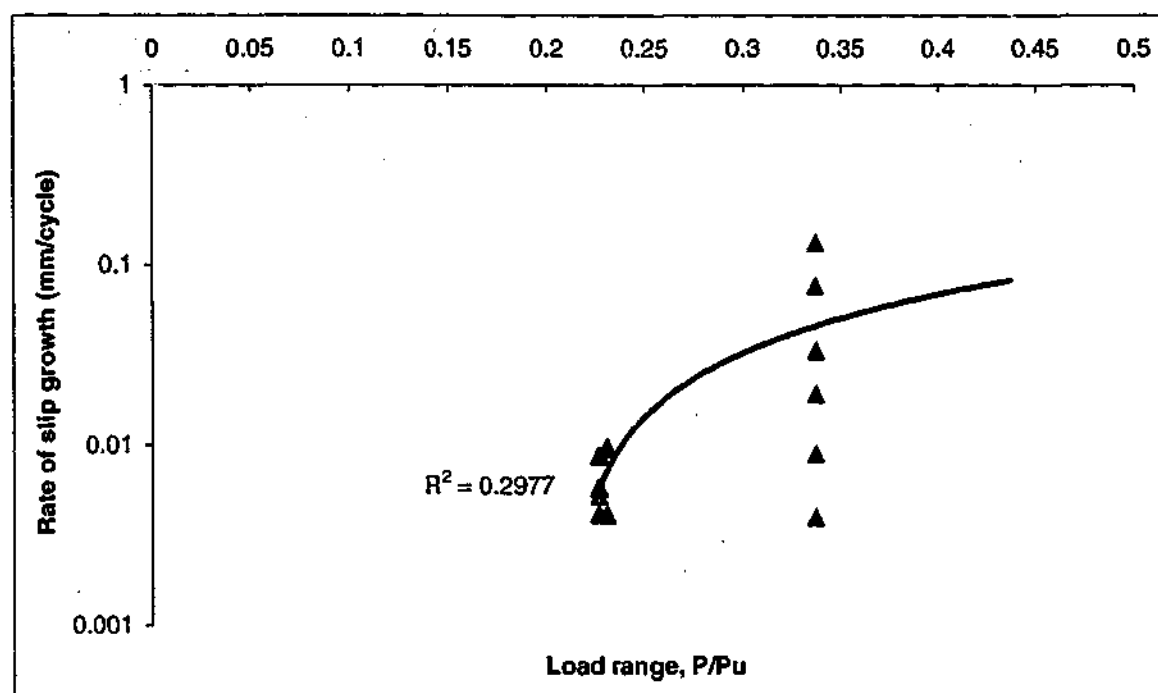
Figure 5.7 Load range versus rate of slip growth

While slightly higher correlation could be achieved using higher order functions, the correlation was not significantly better, and in the absence of a physical model, which supports a particular relationship, an exponential function was adopted as providing a simple function that could be consistently applied across different data series.

Equation (5.1) does not strictly satisfy the boundary condition for the rate of slip growth that when P=0, the slip growth per cycle could be zero. This is not possible with an exponential function. The discrepancy arises because the equation is derived empirically, and not from the fundamental physical model of the behavior. When P=Pu the slip growth per cycle, calculated from the equation, is finite (but large). This is consistent with the observed behavior – the slip does not approach infinity as the specimen approaches failure.

5.3.6   Load slip response for cyclic loading

The load-slip response for all specimens was plotted to show the relationship between load and slip. The specimens exhibited pinched hysteretic behavior. This is illustrated in Figures

Load-slip response of specimen S1.0D-2 for first 10 cycles

Slip (mm)

Load-slip response of specimen S1.0D-2 for second 10 cycles

Slip (mm)
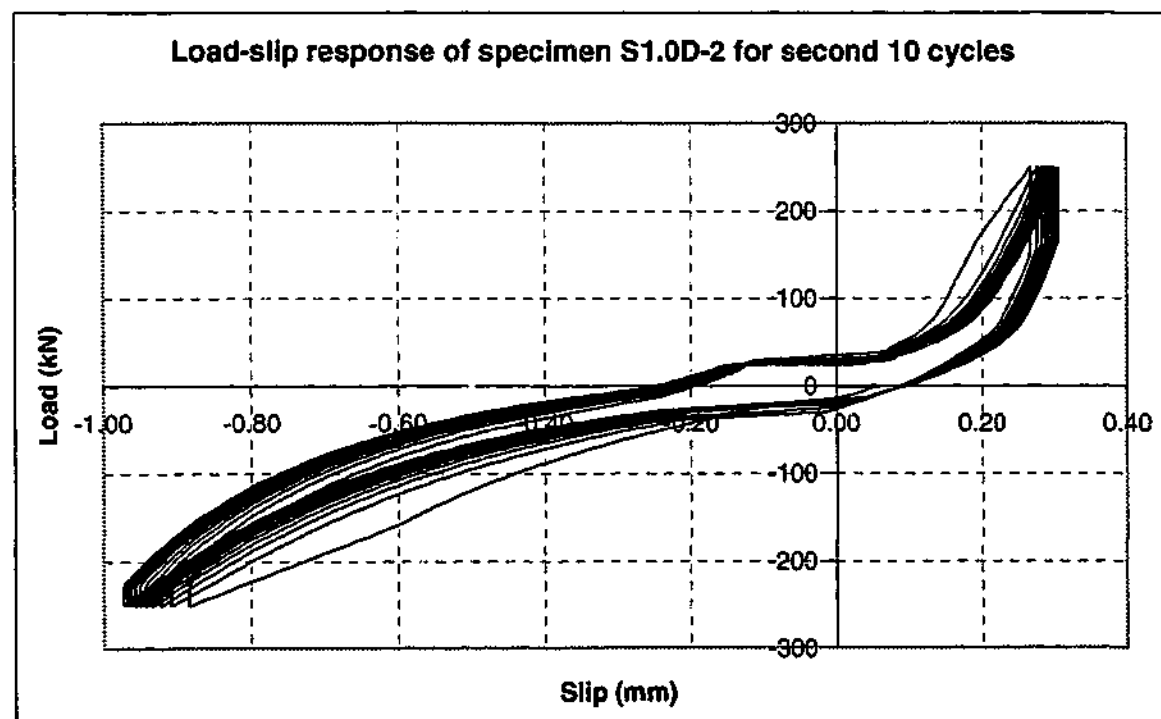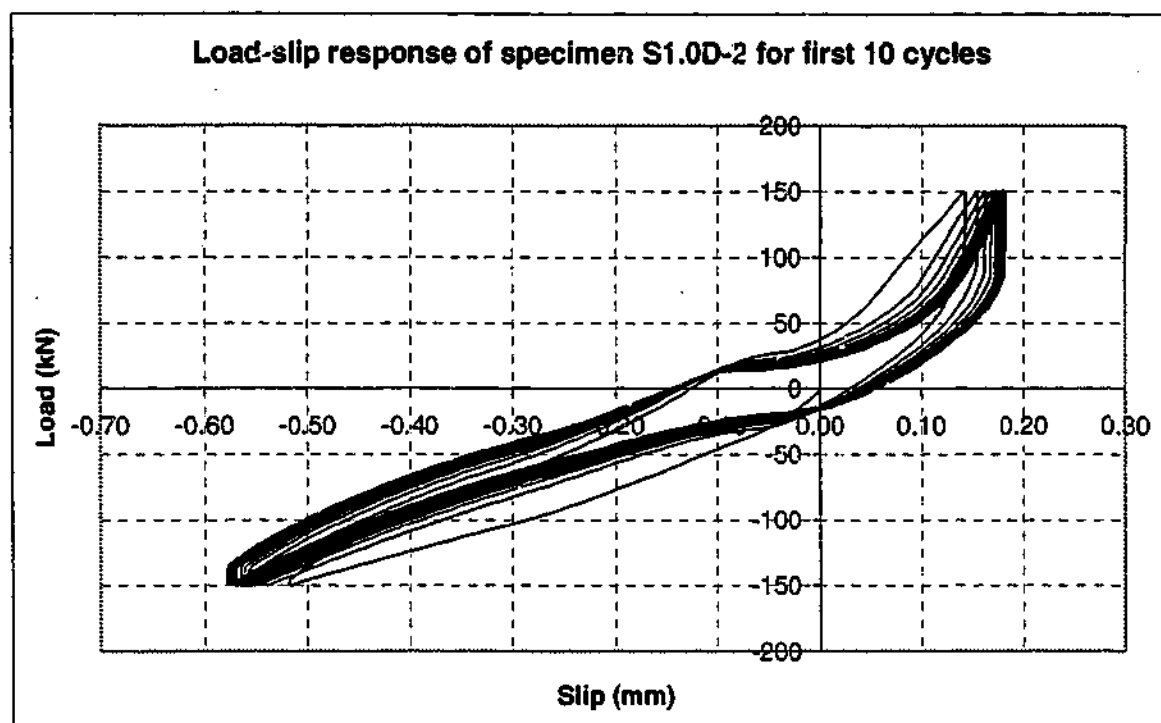
Figure 5.8 Hysteric load-slip behavior for specimens S1.0D-2
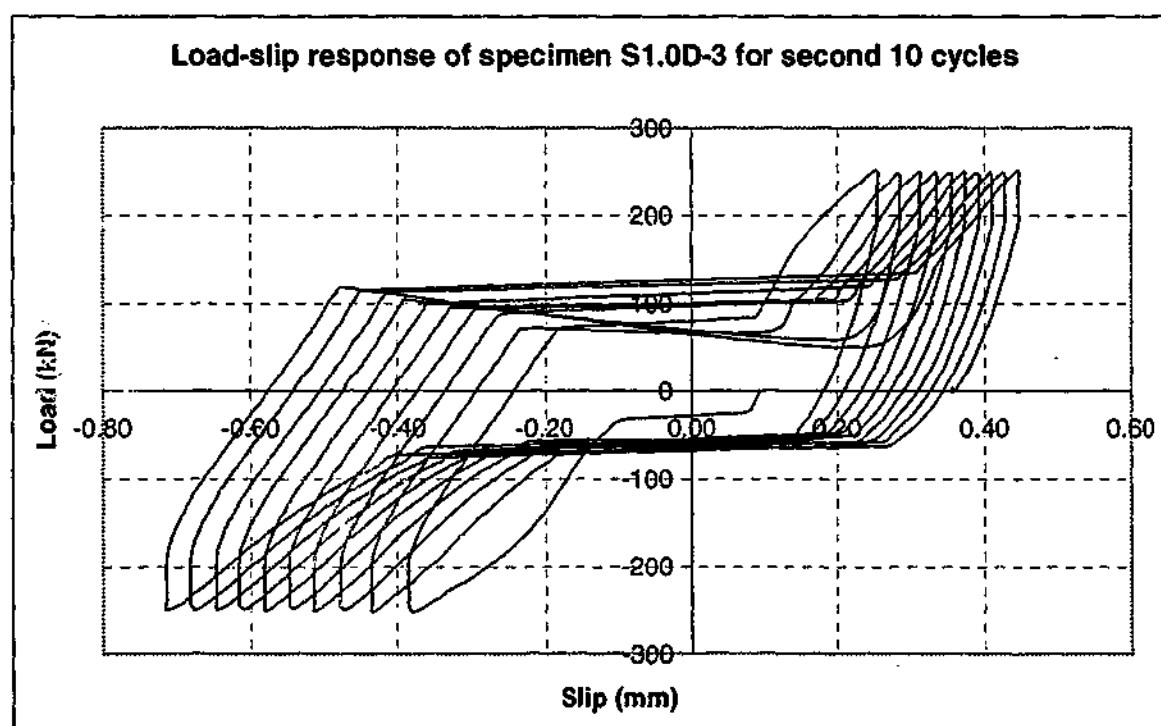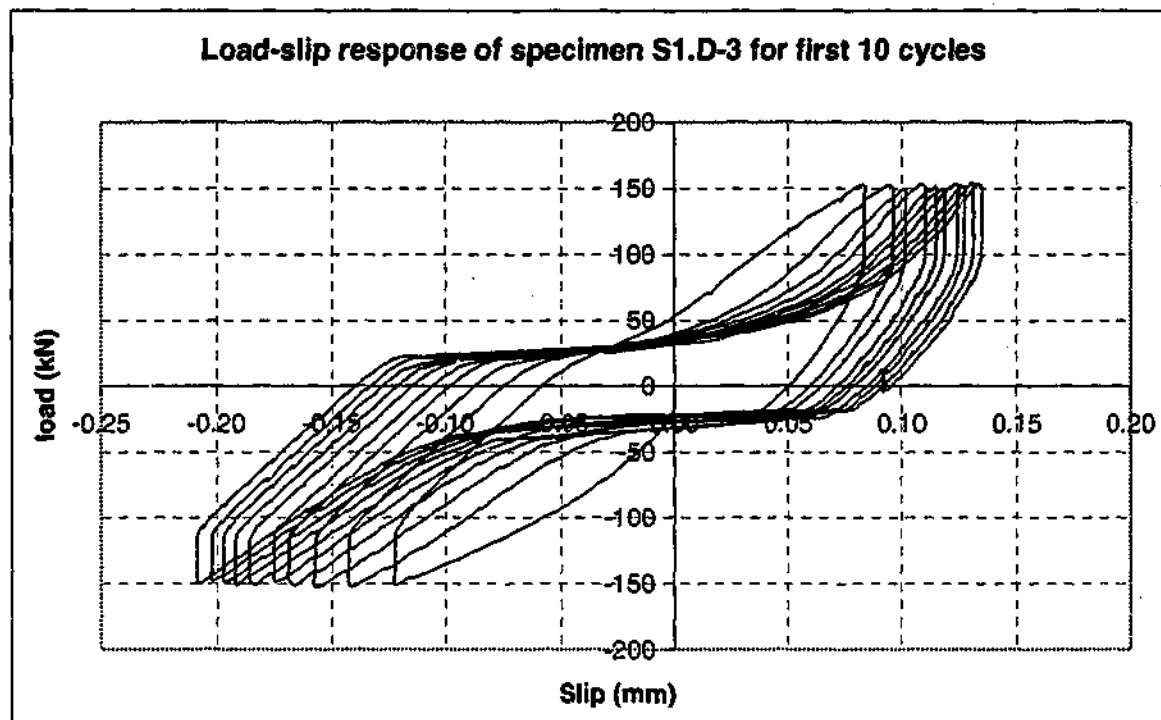
Figure 5.9 Hysteric load-slip behavior for specimens S1.0D-2
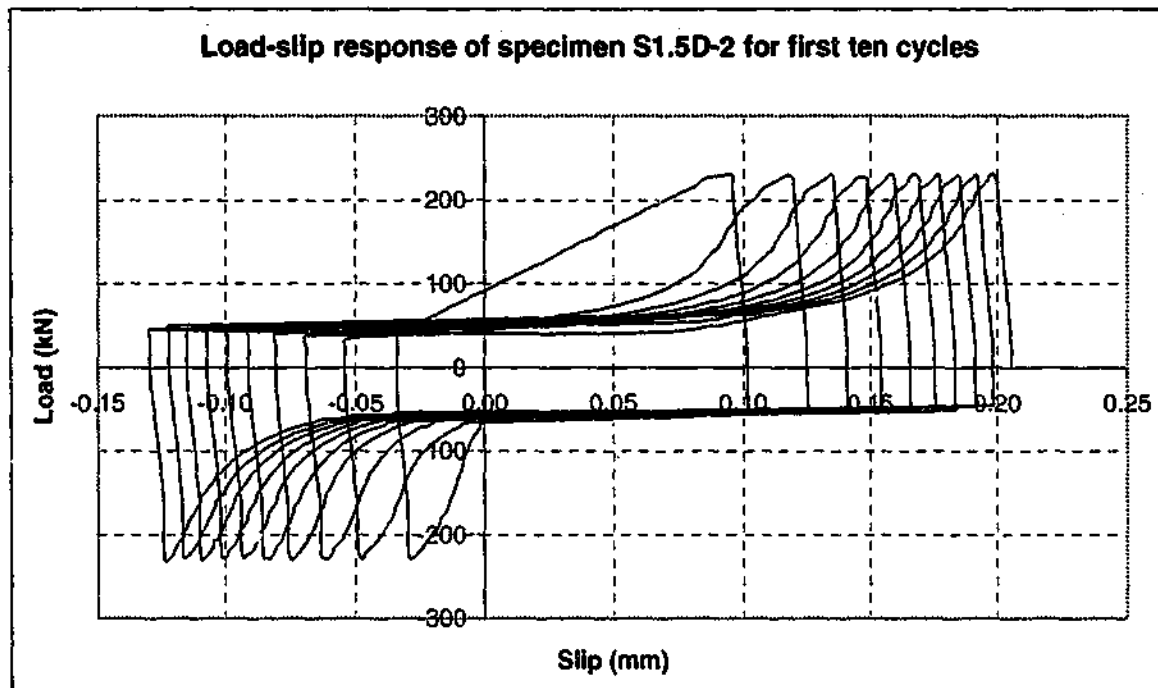
Figure 5.10 Hysteric load-slip behavior for specimens S1.5D-2
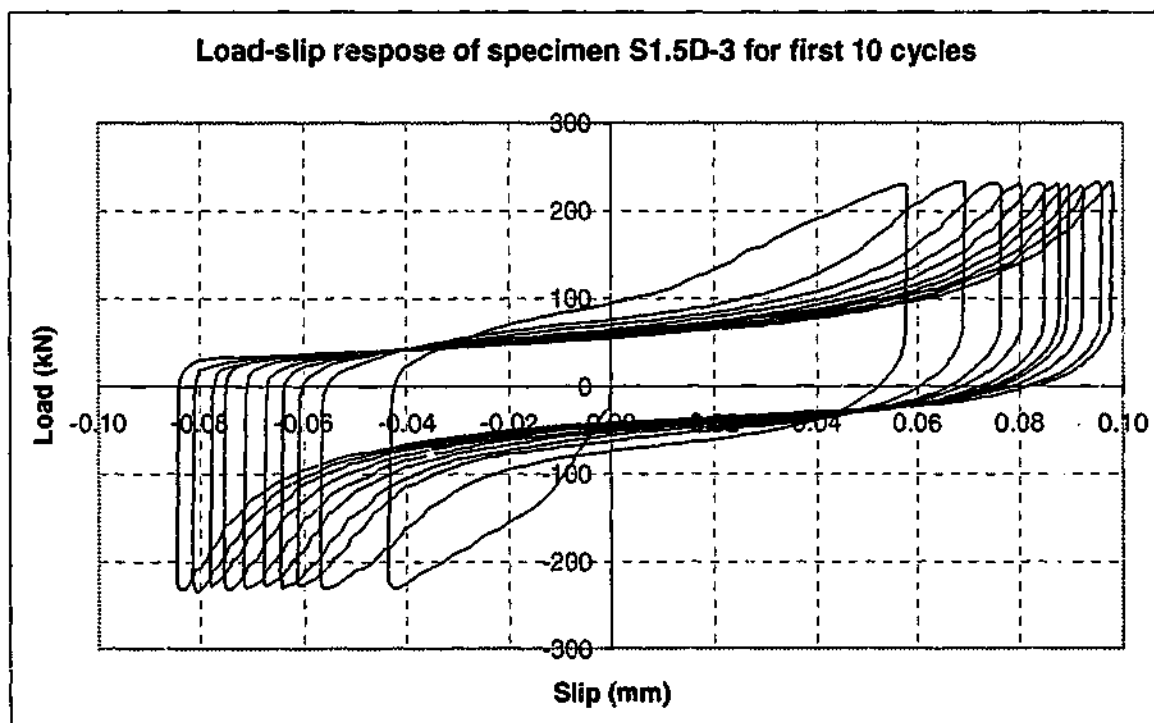
Figure 5.11 Hysteric load-slip behavior for specimens S1.5D-2

To understand this behavior better, Figures 5.12 to 5.14 plot three cycles (first, fifth and tenth) of loading for specimens S1.0D-3 at the same load range. These figures show that the region of low stiffness (the 'pinch' in the hysteresis curve) grows larger with increasing number of cycles, and at higher peak loads.

On each of the figures an idealized piecewise linear representation of the data is plotted, comprising a region of zero stiffness and a region of constant shear transfer between concrete plug and the steel tube. The value for the constant shear transfers is taken from monotonic tests (1000 kN/mm), and approximated the secant load transfer in loading and unloading segments of the load-slip curves.

Based upon this representation of the slip behavior, a simplified model for the behavior of concrete plugs embedded in steel tubular piles under repeated load was adopted as follows;

Under repeated loading the load-slip behavior of the specimen can be idealized as a region of slip with zero stiffness, followed by a constant shear transfer region. The constant shear transfer between concrete plug and the steel tube has the same value as the shear transfer of the linear region in the monotonic tests.

The region of zero stiffness in the model will be referred to as the *damage*. The damage accumulates with increasing numbers of cycles, and the rate at which it accumulates is a function of peak load. An empirical equation to calculate the rate of damage (or slip) growth per cycle was presented in equation 4.2 (Section 5.3.4), for the case of symmetric cyclic loading.

The piecewise linear representation of the load slip behavior under repeated loading will be used to develop the mathematical relationships necessary to describe the behavior of concrete plugs in steel tubes under repeated loading.
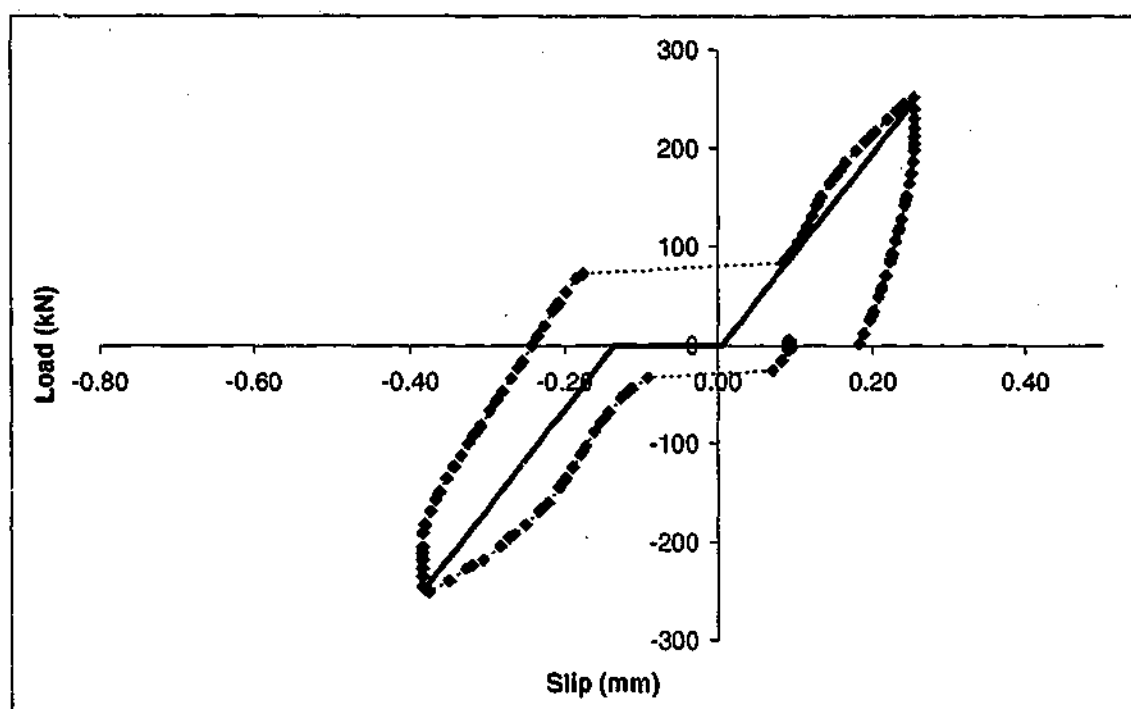
Figure 5.12 Load-slip behavior of specimen S1.0D-3, first cycle at ±250 kN
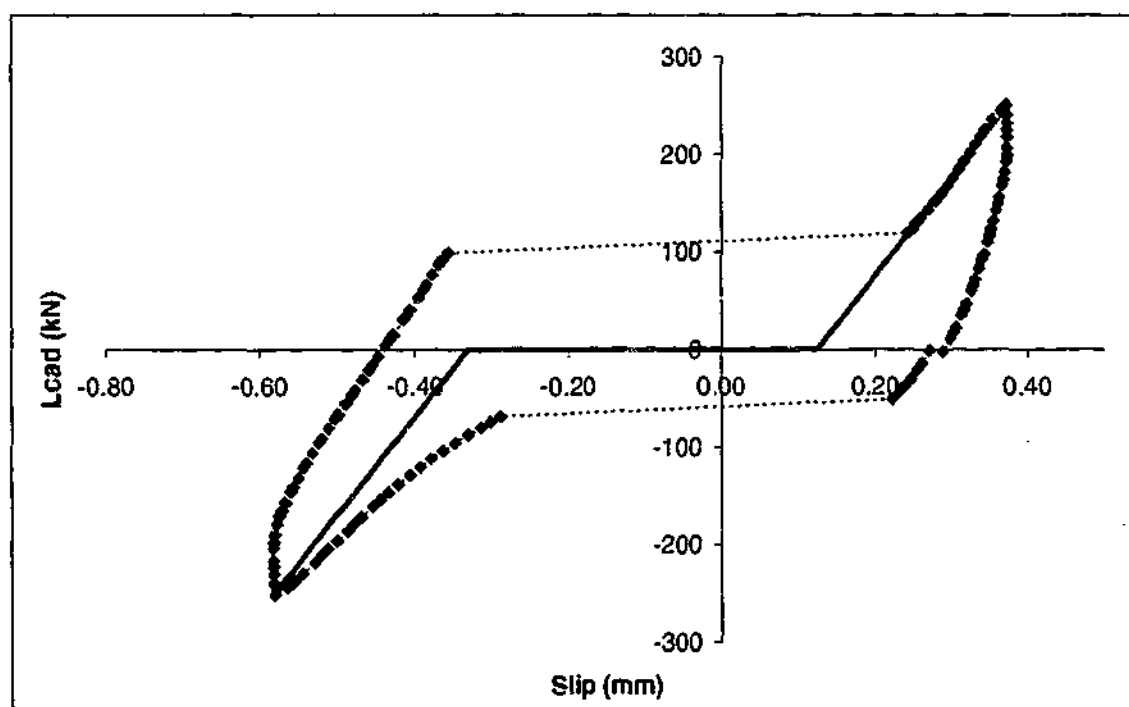
Figure 5.13 Load-slip behavior of specimen S1.0D-3, fifth cycle at ±250 kN
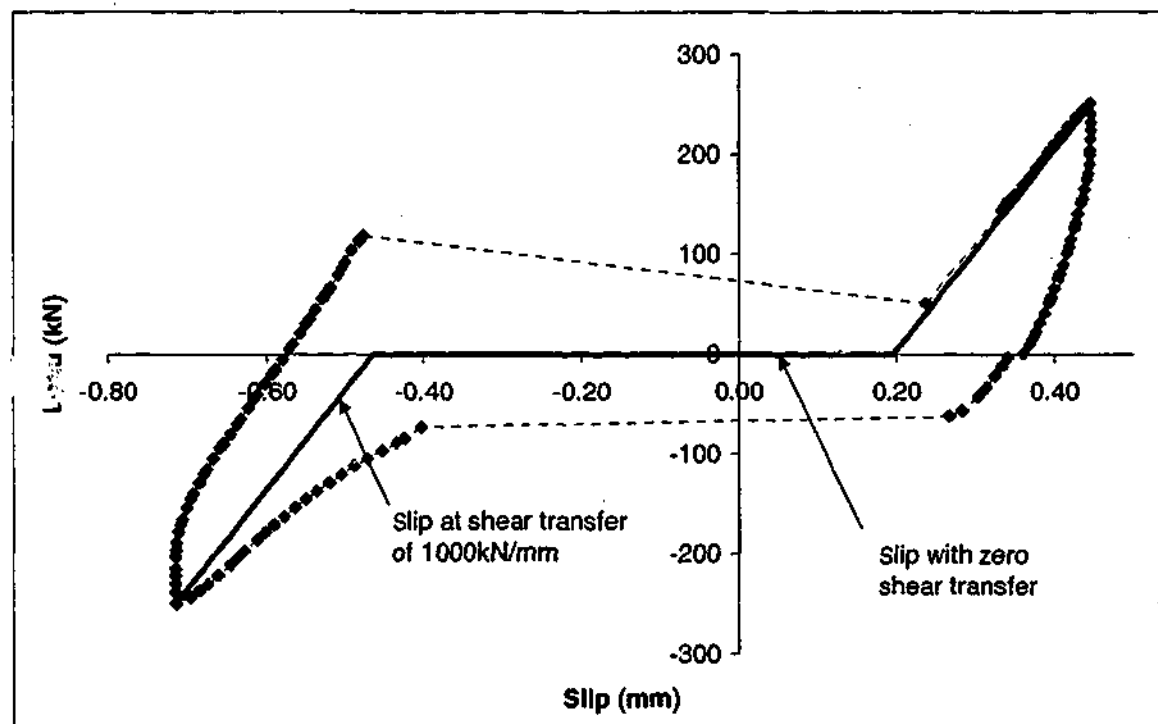
Figure 5.14 Load-slip behavior of specimen S1.0D-3, tenth cycle at ±250 kN

5.4   Test Results For Stage 2

This stage aimed to evaluate the effect of initial cyclic loading on ultimate push-out strength. Three specimens each of three different concrete plug lengths of 1.0D and 1.5D were tested. The first specimen of each plug length group was tested for static compression capacity to enable the assessment of cyclic load effects. The other two specimens were then initially subjected to a variety of different cyclic loading. This was followed by monotonic pull-out tests.

This stage of the experiment took place about two years after construction of the specimens. Therefore, the determination of the effect of shrinkage on bond strength of concrete plugs can also be evaluated with this set of test data.

5.4.1   Summary of the tests conducted in Stage 2

A total of nine successful tests were conducted, comprising three monotonic tests to determine the push out strength of the concrete plug, six tests with symmetric cyclic loading of the specimens, and three tests with extra pull out tests to evaluate effect of cyclic loading. Table 5.1 summarizes the tests.

Table 5.4 Summary of the tests conducted at Stage 2

Specimen ID	Test Number	Type of test	Load Range	Each cycle time/No of cycle	Date
S1.25D-1	1	Monotonic (compression)	-	-	22/11/2000
	2	Monotonic (tension)	-	-	22/11/2000
S1.25D-2	3	Symmetric Cyclic	260 kN	2min / 10	23/11/2000
	4	Symmetric cyclic	310 kN	4min / 5	23/11/2000
	5	Monotonic (tension)	-	-	23/11/2000
S1.25D-3	6	Symmetric Cyclic	245 kN	4min / 1.75	28/11/2000
	7	Monotonic (tension)	-	-	28/11/2000
S1.75D-1	8	Monotonic (compression)	-	-	29/11/2000
	9	Monotonic (tension)	-	-	29/11/2000
S1.75D-2	10	Symmetric Cyclic	100 kN	4min / 5	8/10/2001
	11	Symmetric Cyclic	125 kN	4min / 5	8/10/2001
	12	Symmetric Cyclic	150 kN	4min / 5	8/10/2001
	13	Symmetric Cyclic	175 kN	4min / 5	8/10/2001
	14	Symmetric Cyclic	200 kN	4min / 5	8/10/2001
	15	Symmetric Cyclic	225 kN	4min / 5	8/10/2001
	16	Symmetric Cyclic	250 kN	4min / 5	8/10/2001
	17	Symmetric Cyclic	275 kN	4min / 5	8/10/2001
	18	Symmetric Cyclic	300 kN	4min / 4	8/10/2001
S1.75D-3	19	Monotonic (tension)	-	-	9/10/2001
	20	Symmetric Cyclic	150 kN	4min / 5	9/10/2001
	21	Symmetric Cyclic	200 kN	4min / 5	9/10/2001
	22	Symmetric Cyclic	225 kN	4min / 5	9/10/2001
	23	Symmetric Cyclic	250 kN	4min / 3.5	9/10/2001

Specimen ID	Test Number	Type of test	Load Range	Each cycle time/No of cycle	Date
S2D-1	24	Monotonic (compression)	-	-	26/9/2001
	25	Monotonic (tension)	-	-	26/9/2001
	26	Symmetric Cyclic	500 kN	4min / 11	27/9/2001
	27	Symmetric Cyclic	550 kN	4min / 7	27/9/2001
	28	Symmetric Cyclic	600 kN	4min / 1.25	27/9/2001
	29	Symmetric Cyclic	600 kN	4min / 1.25	27/9/2001
	30	Symmetric Cyclic	600 kN	4min / 7.25	2/10/2001
S2D-2	31	Monotonic (tension)	-	-	2/10/2001
S2D-3	32	Symmetric Cyclic	200 kN	4min / 5	5/10/2001
	33	Symmetric Cyclic	250 kN	4min / 5	5/10/2001
	34	Symmetric Cyclic	300 kN	4min / 5	5/10/2001
	35	Symmetric Cyclic	350 kN	4min / 1	5/10/2001

5.4.2 Ultimate bond strength

In order to calculate the ultimate push out capacity of the specimens, it was decided that specimens S1.25D-1, S1.75D-1 and S2.0D-1 be subjected to a static push out test first and then to static pullout test.

The Instron machine was set at a displacement rate (as measured by the linear variable differential transducer inside the actuator) of 0.015 mm/sec. The push out test stopped at 2.75 mm slip of concrete plug with ultimate push out strength of 443 kN, giving average bond strength of 2.29 MPa. This was followed by a pull out test, which resulted in an ultimate pull out capacity of 460 kN, giving average bond strength of 2.38 MPa.

Specimen S1.75D-1 failed at an ultimate push out force of 395 kN and slip of 7.5 mm, giving an average bond strength of 1.45 MPa. This was followed by a pull-out test, which resulted in Ultimate push out force of 330 kN and average bond strength of 1.21 MPa.

Specimen S2.0D-1 achieved push out force of 1000 kN at slip of 1.9 mm, giving an average bond strength of 3.29 MPa. This was followed by a pull-out test, which resulted in a pull-out force of 1000 kN (instrumentation capacity) at slip of 1.2 mm. The specimen then was subjected to a set of cyclic loadings, which are listed in Table 5.5.

The Instron machine was set to the load control for cyclic tests. Specimen S1.25D-2 was initially subjected to ten symmetric cycles of ±260 kN followed by five symmetric cycles of ±310 kN in tension and compression. This was followed by a pull-out test, which resulted in ultimate pull-out force of 439 kN, giving an average bond strength of 2.27 kN. Specimen S1.25D-3 was initially subjected to 1.75 symmetric cycles of ±245 kN. The cyclic test stopped as the specimen reached slip of 8 mm. This was followed by a pull-out test, which resulted in an ultimate pull out force of 540 kN at slip of 20 mm. The corresponding ultimate bond strength of 2.79 MPa was achieved in pull-out.

Specimen 1.75D-2 was subjected to five symmetric cycles each of nine load ranges from ±100 to ±300kN. The specimen failed at the fourth cycle of 300 kN, giving an average bond strength of 1.11 MPa. Specimen S1.75D-3 initially was subjected to a pull-out test to evaluate the pull-out capacity of the specimen, and the pull-out test stopped at a load level of 431 kN whereas the concrete plug slip reached 1.37 mm. This was followed by five symmetric cycles each of four load ranges from ±150 kN to ±250 kN. The specimen failed at a cyclic load of 250 kN.

Specimen S2.0D-2 failed at a pull-out force of 479 kN before reaching the first cycle's peak load of the initial cyclic loading of ±500. Specimen S2.0-3 was subjected to five symmetric cyclic loadings, each of four cyclic loading ranged from 200 kN to 350 kN. The specimen failed at the first cycle of cyclic loading of 350 kN, giving an average bond strength of 1.15 MPa
Table 5.5 lists the value of peak loads achieved and corresponding average bond strength. The slip values at peak load, initial cyclic loading test and age of concrete on the date of test are also tabulated.

Table 5.5 Summary of the stage 2 test results

Specimen ID	Type of test	Ultimate Strength kN	Bond Strength MPa	Max. of slip (mm)	Each cycle time/No of cycle	Concrete Age (days)
S1.25D-1	Monotonic compression	443	2.29	2.75	-	403
	Monotonic tension	460	2.38	24.5	-	
S1.25D-2	Symmetric cycling	±260	1.34	1.05	2 min / 10	404
	Symmetric cycling	±310	1.60	7.95	4 min / 5	
	Symmetric cycling	±439	2.27	24.1	-	
S1.25D-3	Symmetric cycling	±245	1.26	8.02	4 min /1.75	409
	Monotonic tension	540	2.79	20.9	-	
S1.75D-1	Monotonic compression	395	1.45	7.48	-	410
	Monotonic tension	330	1.21	12	-	
S1.75D-2	Symmetric cycling	±100	0.37	0.12	4 min / 5	716
	Symmetric cycling	±125	0.46	0.17	4 min / 5	
	Symmetric cycling	±150	0.55	0.23	4 min / 5	
	Symmetric cycling	±175	0.65	0.30	4 min / 5	
	Symmetric cycling	±200	0.74	0.37	4 min / 5	
	Symmetric cycling	±225	0.83	0.56	4 min / 5	
	Symmetric cycling	±250	0.93	0.84	4 min / 5	
	Symmetric cycling	±275	1.01	1.67	4 min / 5	
	Symmetric cycling	±300	1.11	14.8	4 min / 4	
S1.75D-3	Monotonic tension	±431	1.59	1.37	-	717
	Symmetric cycling	±150	0.55	0.03	4 min / 5	
	Symmetric cycling	±200	0.74	2.16	4 min / 5	
	Symmetric cycling	±225	0.83	7.72	4 min / 5	
	Symmetric cycling	±250	0.93	18.6	4 min / 3.5	

Specimen ID	Type of test	Ultimate Strength kN	Bond Strength MPa	Max. of slip (mm)	Each cycle time/No of cycle	Concrete Age
S2.0D-1	Monotonic compression	1000	3.29	1.89	-	703
	Monotonic tension	1000	3.29	1.24	-	
	Symmetric cycling	±500	1.64	1.75	4 min / 11	
	Symmetric cycling	±550	1.81	2.95	4 min / 7	
	Symmetric cycling	±600	1.97	2.97	4 min / 1.25	
	Symmetric cycling	±600	1.97	3.25	4 min / 1.25	
	Symmetric cycling	±600	1.97	16.0	4 min / 7.25	
S2.0D-2	Symmetric cycling	±479	1.57	16.7	-	710
S2.0D-3	Symmetric cycling	±200	0.66	0.54	4 min / 5	713
	Symmetric cycling	±250	0.82	1.43	4 min / 5	
	Symmetric cycling	±300	0.99	2.97	4 min / 5	
	Symmetric cycling	±350	1.15	30.8	4 min / 1	

A total of 35 tests were carried out on 9 specimens. The pull-out bond strength was a maximum 3.29 MPa, minimum 1.21 MPa and average of 2.26 MPa for seven pull-out tests. The push out bond strength was a maximum 3.29 MPa, minimum 0.93 MPa and average of 2.34 for three push out tests. The cyclic bond strength was a maximum 1.97 MPa, minimum 0.93 MPa and average of 1.34 MPa for six cyclic loading tests.

The test results indicated that cyclic bond strength is lower than ultimate static pull-out or push out bond strengths. This is due to the incremental damage to the plug pile interface.

5.4.3   Load-slip response

Figures 5.15 to 5.17 show the load-slip response of specimen series S1.25D, S1.75D and S2.0D respectively.

In static push out tests, specimen S1.25D-1 exhibited a decay shear transfer after peaking at a slip of 1.0-1.5 mm. This is the expected result associated with a plug in a properly circular straight pile. This fretting of the cement matrix on the steel surface has a powdering effect, removing the interlock with asperities on the steel surface, and lowering the effective coefficient of friction. In the following pull-out test, the specimen experienced a reversal slip at a load level of 300kN. The slip is believed to be a recovery of permanent push out slip. The specimen then showed a gradual increase in load transfer as slip increased. This is due to the initial push out test, which consolidated the concrete into the steel tube. Macro interlock effects were then created when the slip became significant. These raised the contact stress between the steel tube and concrete plug, which increase the friction resistance.

Specimen S1.25D-2 reached its ultimate strength at the end of initial symmetric cyclic loading of ±310 kN. The specimen then showed a smooth decay shear transfer after peaking at a slip of 8 mm in the following pull-out test. This was due to significant damage to the plug / pile interface during the initial cyclic loading. Specimen S1.25D-3 failed at the second cycle of first cyclic loading range after reaching a slip of 8 mm. In the following pull-out test, the specimen exhibited a gradual increase in load transfer as slip increased.

Load-slip response of specimen S1.75D-1 shows that the push out load dipped after an early peak at about 2 mm slip but then recovered, indicating some macro effects previously discussed. In the following pull-out test, the plug locked into the steel tube with no reversal slip before peaking at a pull-out load of 330 kN. The shear transfer then dipped down but then partly recovered after reversal of the permanent push out slip. The locking of the plug was due to a mechanical interlock mechanism.

Specimens S1.75D-2, S1.75-3 and S2.0D-3 exhibited pinched hysteretic behavior and completely failed in the cyclic loading.

Push out load – slip curve of specimen S2.0D-1 was seen to exhibit a nearly bilinear response prior to peak load (set limitation of the test machine). The change of slope of the load-slip curve during the loading was assumed to commit with the breaking of chemical adhesion (non-slip mechanism) and activation of the mechanical interlock mechanism (very small – slip mechanism). In the following pull-out test, specimen experienced a reversal slip at a load level of 700 kN. The slip is believed to be a recovery of permanent push out slip. The specimen then showed a load transfer increase as slip increased before reaching the test machine limitation of 1000 kN. The specimen S2.0D-2 unexpectedly failed at the first pull-out force of cyclic loading. However, the specimen exhibited a decay shear transfer after peaking at a slip of 1.0-1.5 mm.

The load-slip response of the specimens indicated that the load slip curves of cyclic loading tests are similar to the load slip curve obtained for monotonic static tests. The shifting between these two curves in the ordinate load axis is due to the different cyclic loading rate and concrete plug length. The effects of cycling rate and the damage model will be discussed in following sections.

The ultimate capacity and load slip response of specimens under cyclic loading can be reasonably approximated from the ultimate strength and load slip of static test results by reducing the ultimate strength values of static test by cyclic reduction factor. The cyclic reduction factor is defined as the factor by which the cyclic strength of specimen may be obtained from the static strength for a given displacement. The cyclic reduction factor seems to depend on the rate of load, number of cycles, the concrete characteristics and shrinkage, the imperfection of the steel tube, the length of the plug and perhaps the presence of the reinforcement. However this rule does not apply to some of the specimens due to their irregular peak loads. These irregularities might be mainly caused by the effect of shrinkage.
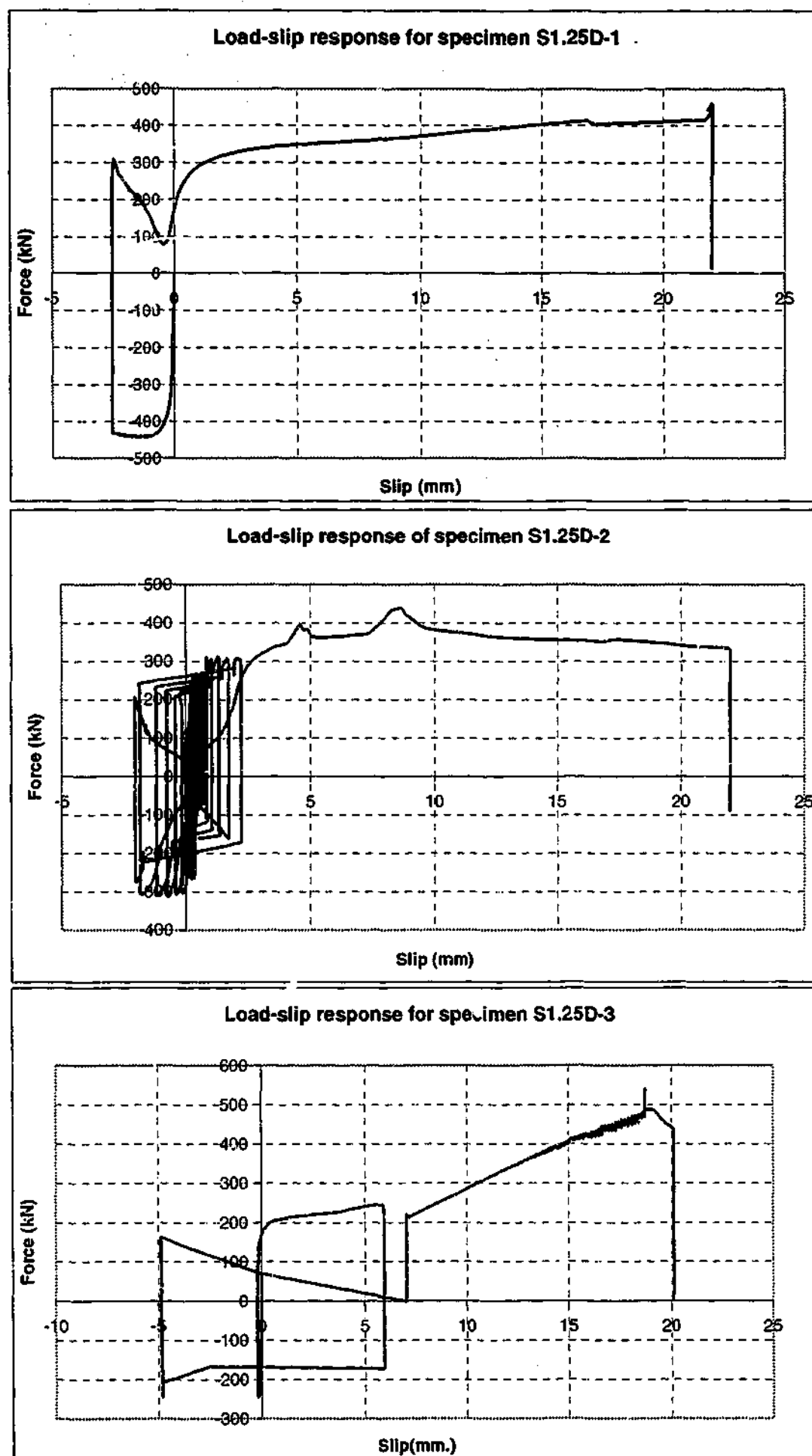
Figure 5.15 Load-response for specimens S1.25D
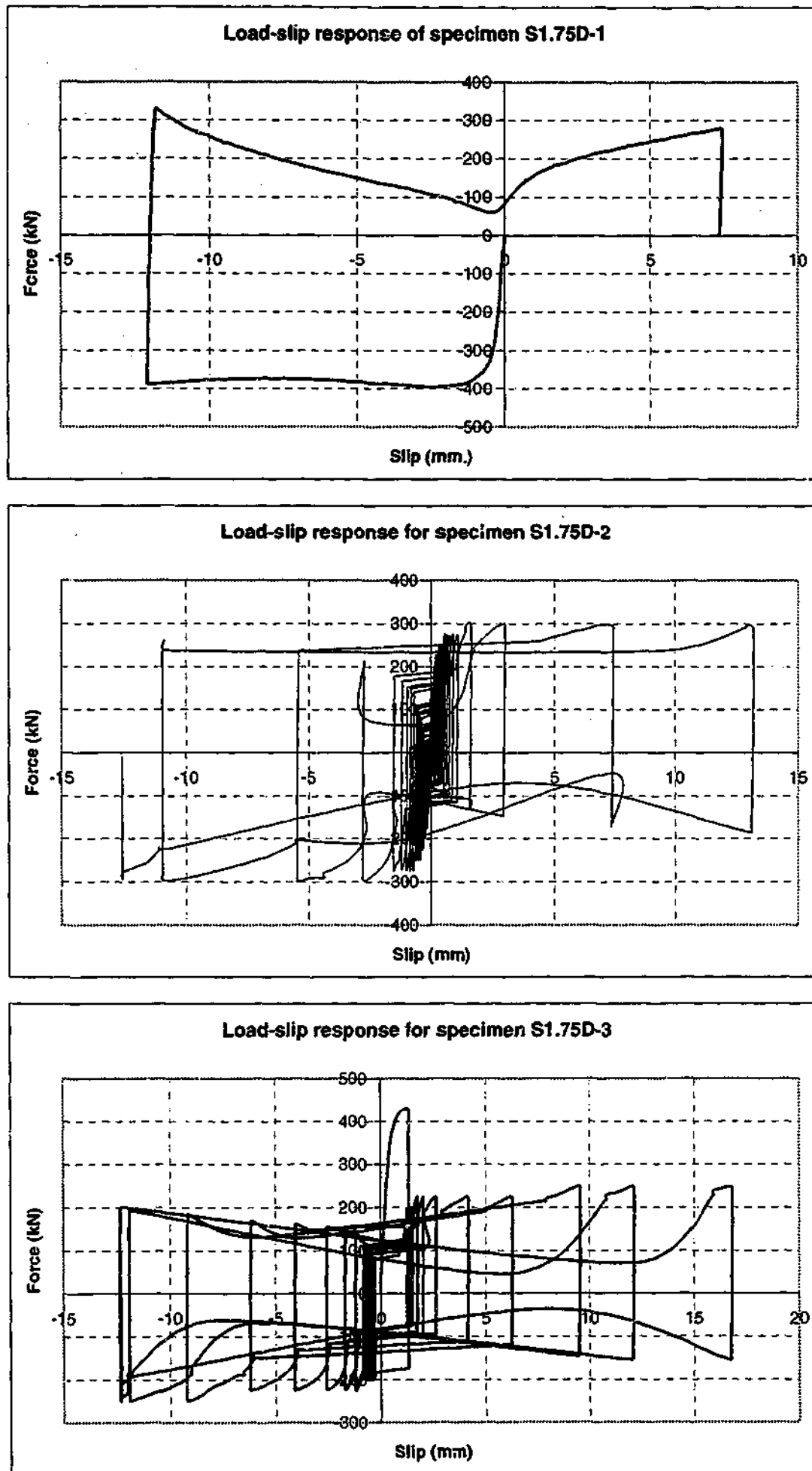
Figure 5.16 Load-response for specimens S1.75D
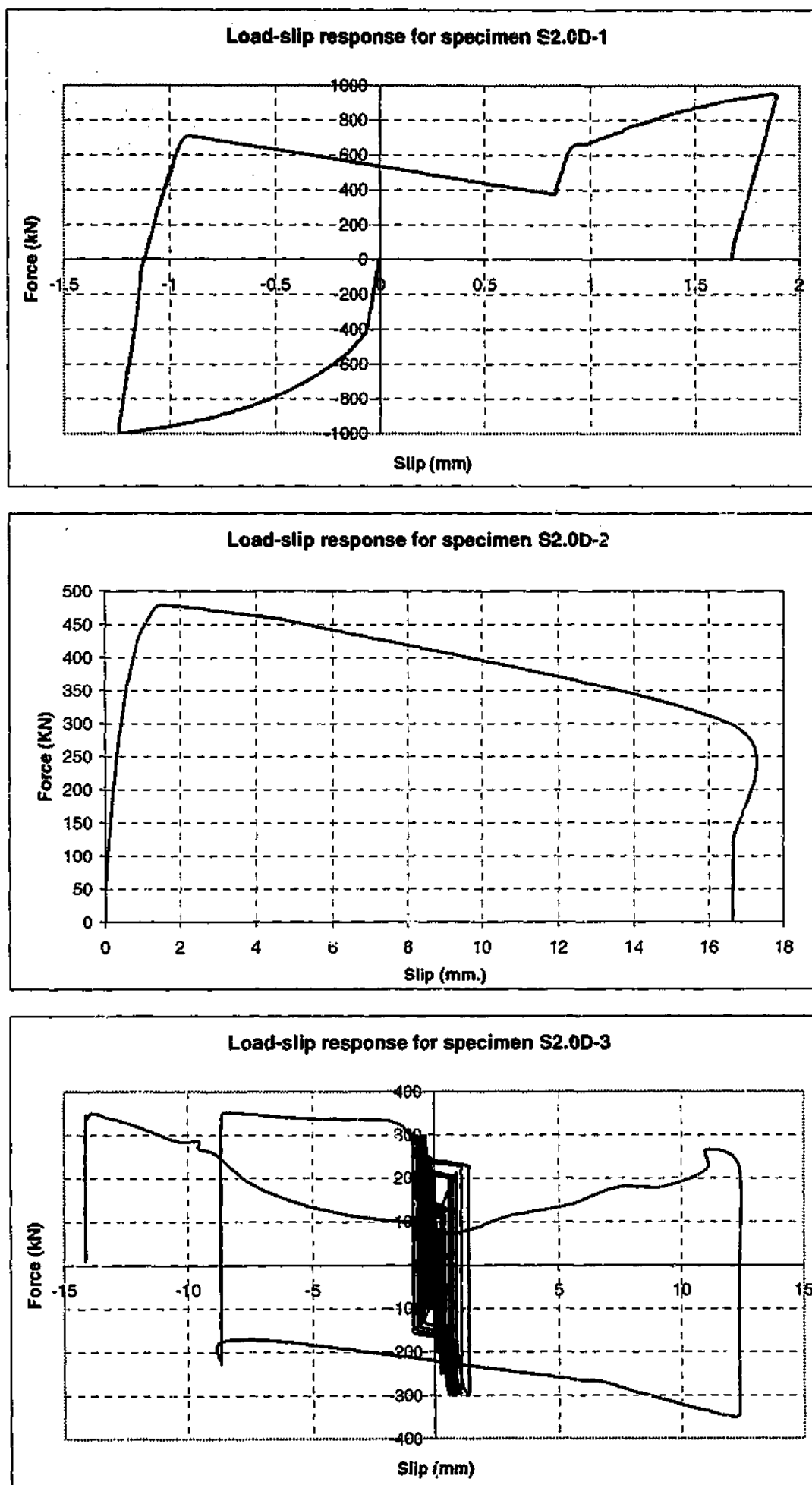
Figure 5.17 Load-response for specimens S2.0D

5.4.4 Slip versus cycles results for cyclic loading

Cyclic loading reduced the bond strength and ultimate capacity of the specimens. This was due to damage of the concrete plug and pile plug interface either by progressive loss of stiffness through the accumulation of microcracking or by progressive plastification that appears as an irreversible residual strain that increases with each additional cycle.

The slip versus cycles behavior for each of the specimens is plotted in Figures 5.18 to 5.22. The time for one load cycle was typically 4 minutes. The rate of loading increased as the load range increased in order to keep the cycle time constant.
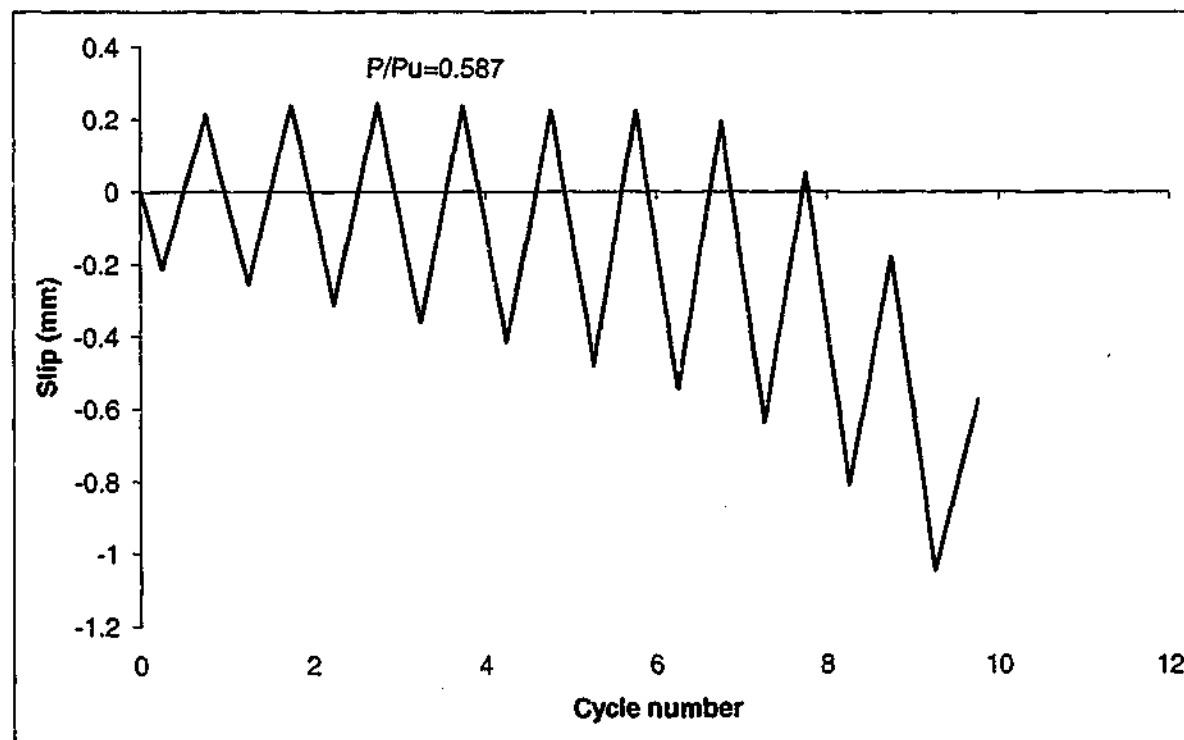
Figure 5.18 Slip versus cycles for specimens S1.25D-2
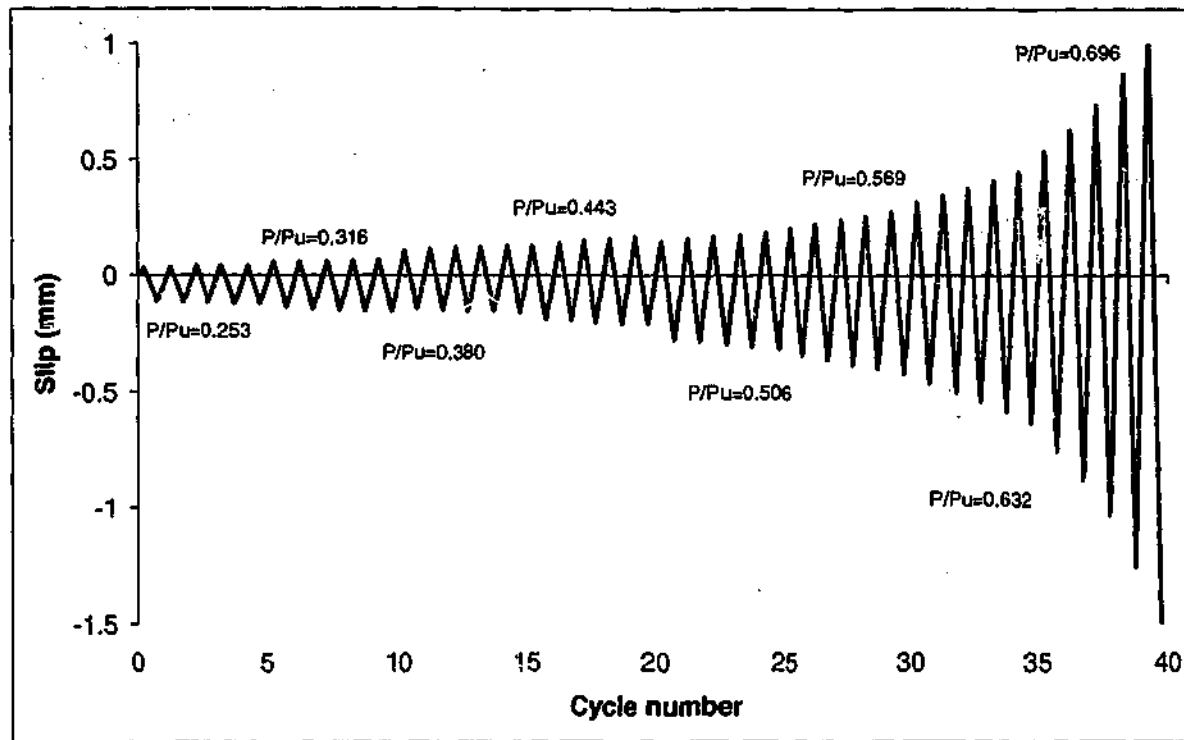
Figure 5.19 Slip versus cycles for specimens S1.75D-2
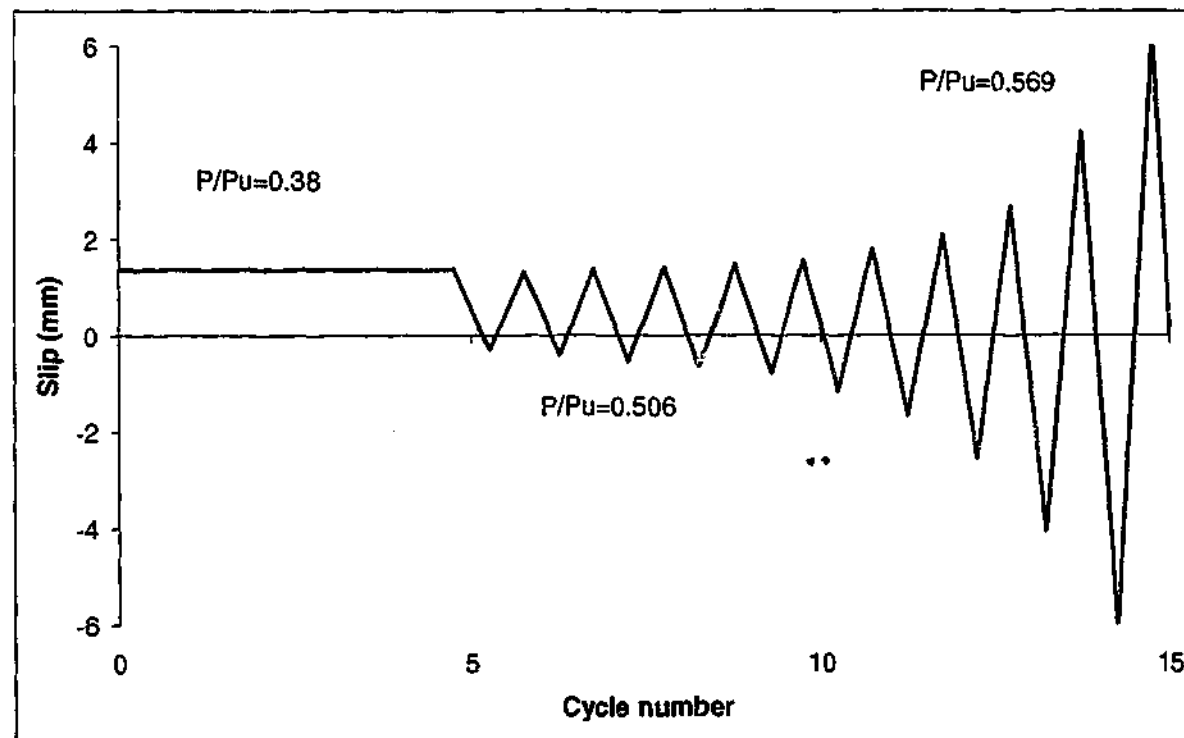
Figure 5.20 Slip versus cycles for specimens S1.75D-3
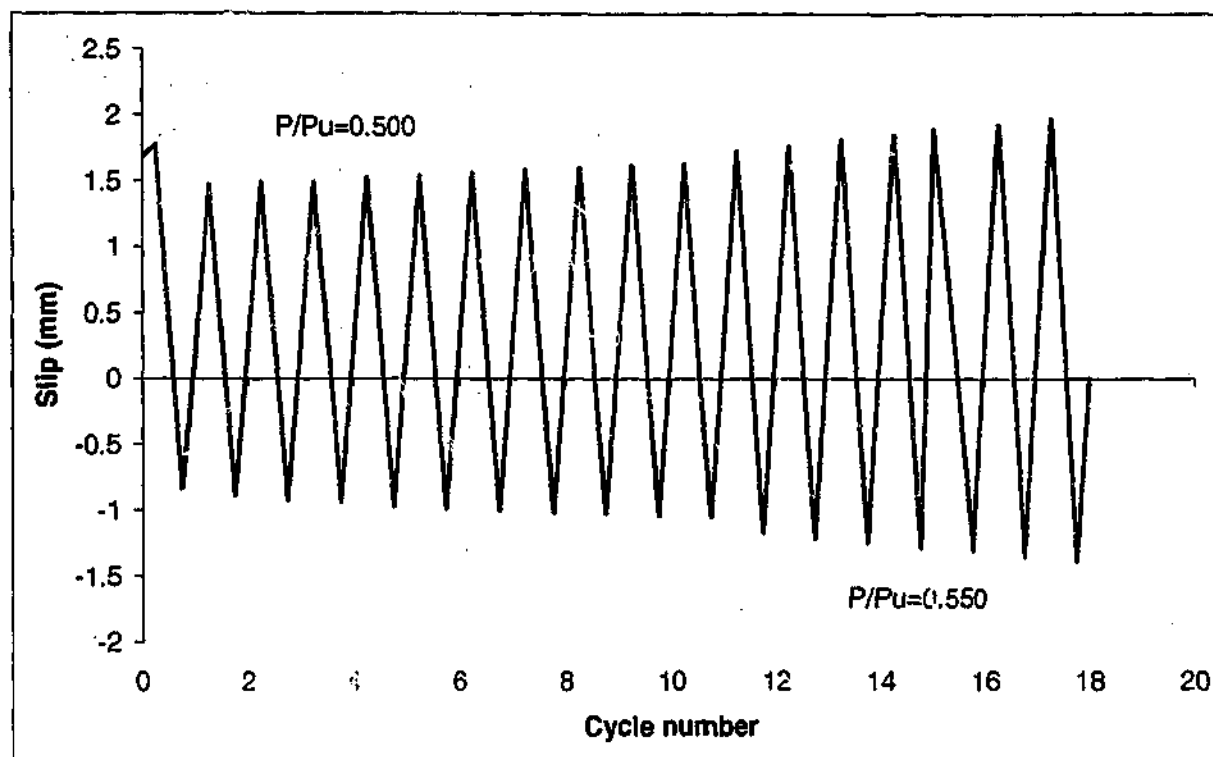
Figure 5.21 Slip versus cycles for specimens S2.0D-1
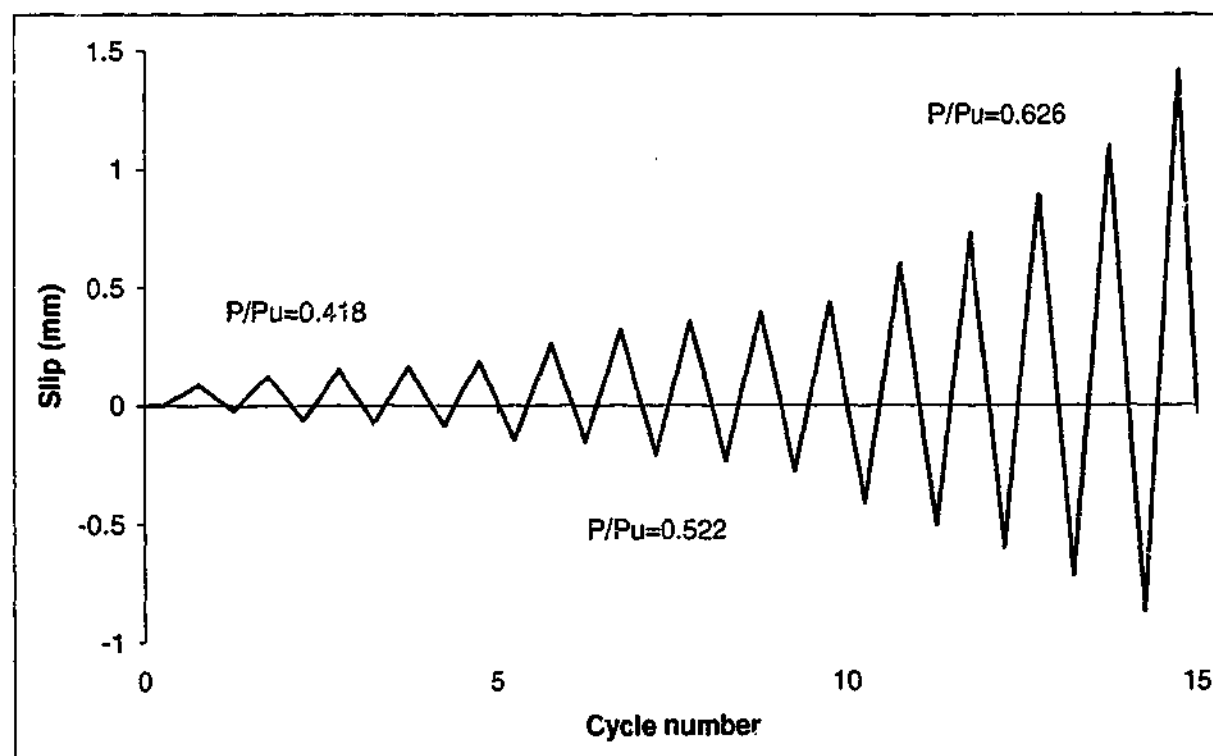
Figure 5.22 Slip versus cycles for specimens S2.0D-3

From the figures it is clear that slip increased with load cycles, and that the rate of slip growth increased with the peak load. The non-symmetric behavior in some specimens may be due to differences in the local stiffness of the concrete plug adjacent to the test tube.

A concentration of coarse aggregate or of voids immediately adjacent to the top or bottom of the steel tube would have an effect on the concrete stiffness and on the rate of slip growth. The different effective mechanical interlock mechanisms in pull out and push out also could have effects on the concrete stiffness.

5.4.5   Rate of slip growth under cyclic loading

It was observed from Figures 5.18 to 5.22 that, after the first few cycles at any load range, the slip increased approximately linearly with cycles. The exceptions to this are specimens S1.25D-2, S1.25D-3 and S2.0D-2.

The concrete plug of specimen S1.25D-2 slipped into the steel tube therefore the slip increased in the compression part and decreased in the tension part of each cycle. Specimens S1.25D-3 and S2.0D-3 failed at the start of the cyclic loading.

A line of best fit to the rate of slip growth with cyr' : was calculated for every test at every load range. The rate of slip values and load ranges are presented in Table 5.6. These data are plotted in Figure 5.23, with the rate of slip growth plotted on a logarithmic scale. Although there is considerable scatter in the data, there is a clear trend that the rate of slip growth increased with the peak load.

The scatter in the data is probably a reflection of the variation in the characteristics of the concrete plug and the effect of shrinkage.

Table 5.6 Rate of slip growth for Stage 2 of cyclic test

Specimen ID	Type of test	Load (kN)	P/Pu	Rate of slip growth (μmm/Cycle)	
				Positive slip	Negative slip
S1.75D-2	Symmetric cycling	±100	0.253	2.188	2.188
	Symmetric cycling	±125	0.316	2.188	3.282
	Symmetric cycling	±150	0.380	4.375	3.284
	Symmetric cycling	±175	0.443	7.657	3.282
	Symmetric cycling	±200	0.506	7.657	8.750
	Symmetric cycling	±225	0.569	13.127	15.316
	Symmetric cycling	±250	0.632	26.254	33.912
	Symmetric cycling	±275	0.696	105.015	164.086
S1.75D-3	Symmetric cycling	±150	0.380	0.406	1.094
	Symmetric cycling	±200	0.506	49.511	99.546
	Symmetric cycling	±225	0.569	903.433	1000.914
S2.0D-1	Symmetric cycling	±500	0.500	25.707	33.364
	Symmetric cycling	±550	0.550	29.692	33.911
S1.5D-3	Symmetric cycling	±200	0.418	19.690	17.502
	Symmetric cycling	±250	0.522	33.911	26.254
	Symmetric cycling	±300	0.626	164.087	91.888

A line of best fit to the data (plotted in the figure) gave equation (5.2);

$$\text{Symmetric cyclic loading, slip growth per cycle} = 10^{(0.255\frac{P}{P_u}-0.899)} \text{ mm/cycle}$$

(5.2)

Various forms of representing the data were trailed, including higher order functions to fit the log-linear representation of the data given in Figure 5.23.
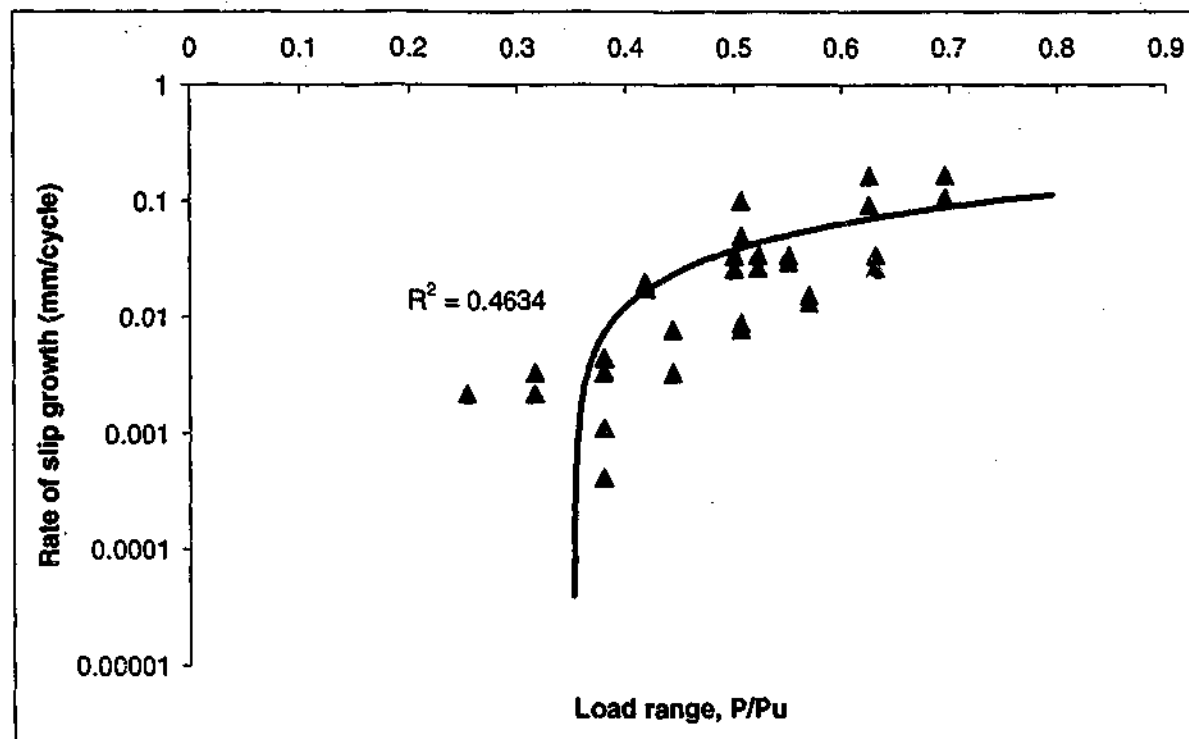
Figure 5.23 Load range versus rate of slip growth

While slightly higher correlation could be achieved using higher order functions, the correlation was not significantly better, and in the absence of a physical model, which supports a particular relationship, an exponential function was adopted as providing a simple function that could be consistently applied across different data series.

Equation (5.2) does not strictly satisfy the boundary condition for the rate of slip growth that when P=0, the slip growth per cycle could be zero. This is not possible with an exponential function. The discrepancy arises because the equation is derived empirically, and not from a fundamental physical model of the behavior. When P=Pu the slip growth per cycle, calculated from the equation, is finite (but large). This is consistent with the observed behavior – the slip does not approach infinity as the specimen approaches failure.

5.4.6   The observed effect of shrinkage

The results so far presented are all the peak values in a loading cycle – that is the peak load and slip between the concrete plug and the slip tube. When the behavior during a loading cycle is investigated, some unusual characteristics are revealed, all of which can be explained by concrete shrinkage.

Concrete shrinkage cracks at the interface on top of specimens were observed prior to testing of the specimens. Concrete shrinkage diminishes the mechanical interlocking, thereby reducing the ultimate capacity of the specimens. The average separation width was 0.1 mm.   This gap should be closed by lateral expansion of the concrete (Poisson's effect in push out and induced wedge action from reinforcement in pull-out). If this was not achieved, concrete would therefore behave in the unconfined state, and the beneficial effect of composite action would be severely reduced or lost entirely.

Because the specimens have axial symmetry, the compression or tension will cause radial deflection, Δ_{tube}, of the tube and $\Delta_{concrete}$, of the concrete plug. The radial forces and deflections of concrete plug and steel tube depend on applied axial force, viscosity and compressive strength of the concrete, length of concrete plug and the tube diameter. The shrinkage of the concrete will involve a radial reduction $\Delta_{shrinkage}$, of the concrete plug.

Three possible states exist along the interface:

- State A: $\Delta_{tube} - \Delta_{rugosity} < \Delta_{concrete} - \Delta_{shrinkage}$
- State B: $\Delta_{tube} - \Delta_{rugosity} = \Delta_{concrete} - \Delta_{shrinkage}$
- State C: $\Delta_{tube} - \Delta_{rugosity} > \Delta_{concrete} - \Delta_{shrinkage}$

Where $\Delta_{rugosity}$ is amplitude of the rugosity of the interior of the tube.

In State A, the concrete pressure persists on the interface after the shrinkage is complete, and the initial bond strength is provided by adhesion between the steel and the concrete. This is often termed chemical bond. With increasing shear, this chemical bond is exceeded, and the subsequent strength depends on the mechanical interlock characteristics at the interface. Here two features exist: the bond that depends on the interface pressure and the coefficient of friction, and the bond provided by the mechanical interlock of the concrete and steel.

State B is an intermediate condition. Adhesion is of reducing significance, and the mechanical bond progressively reduces in a unpredictable manner as the state approaches State C

In state C, separation of two materials exists after shrinkage, and relatively rigid body motion occurs with little bond strength or resistance.

The shrinkage radial reduction may be assumed to be linear and is calculated as follows (Roeder et al.1999):

$$\Delta_{shrinkage} = cd / 2 \qquad\qquad (5.3)$$

where c is the linear shrinkage strain of the concrete and d is the concrete plug diameter. The shrinkage also depends on the concrete components and the curing procedure.

Given c and d values of 0.0003 and 2220 mm, the minimum rugosity needed to avoid state C and separation is 0.33 mm. Actual surface roughness of the used tubes are between 0.2 to 0.4 mm. This indicated that the interface condition of the most unloaded specimens tend to be in State B. Further, these comparisons show that specimens with large amounts of shrinkage and smaller tube imperfections may be in State C.

State B produces variable behavior, based upon the degree of interlock between the surface irregularities of the steel and the concrete in its shrunken state. As noted earlier, the mechanical interlock will be smaller and possibly non-existent at

larger amounts of shrinkage, but the uncertainly about shrinkage, c, adds uncertainly to the ultimate capacity of CFT connections. The largely unpredictable interface conditions will vary along and inside the steel tube, which also adds uncertainly in the behavior of the concrete plug in the steel tube. The shrinkage also causes higher damage accumulation due to the cyclic loading and the higher slip growth per cycle. This leads to early failure of specimens in cyclic loading.

To sum up, the shrinkage reduces the contact area and increased separation between the concrete and the steel tube along the interface, which means less shear/bond transfer. This decreased the chemical bond and effect of mechanical interlock. Therefore specimens showed non-consistent and lower ultimate capacity.

5.5 Cyclic Reduction Factor

The ultimate capacity and load response of the specimens under pull-out, push out and cyclic loading are presented in Figures 5.1, 5.2, 5.15 to 5.17 and Tables 5.2 and 5.5. The ultimate capacity and load slip response of specimens under the cyclic loading can be reasonably approximated from the static ultimate strength and load slip of the specimen by reducing the ultimate strength values of static test by the cyclic reduction factor. The cyclic reduction factor is defined as the factor by which the cyclic strength of the specimen may be obtained from the static strength for a given displacement. The cyclic reduction factor seems to depend on the rate of load, number of cycles, the concrete characteristics and shrinkage, the imperfection of the steel tube, the length of the plug and perhaps the presence of reinforcement. However, this rule does not apply to all specimens due to irregular peak loads. These irregularities might be caused by either steel tube imperfections or the effect of shrinkage

Table 5.7 shows calculated cyclic reduction factors for specimens with different concrete plug lengths based on the ultimate pull-out, push out and cyclic strength of specimens. The slip values at peak point are also tabulated.

Table 5.7 Cyclic reduction factors

Specimen ID	Failure Regime	Ultimate Strength kN	Cyclic Ultimate Strength (kN)	Cyclic Reduction Factor	Slip at Peak load (mm)
S1.0D-2	Pull-out with pre-cyclic loading	665	711	1.07	12.2
S1.0D-3	Pull-out with pre-cyclic loading	665	410	0.62	11.7
S1.25D-2	Symmetric cycling loading	460	439	0.95	24.1
S1.25D-3	Pull-out with pre-cyclic loading	460	540	1.17	20.9
S1.5D-2	Pull-out with pre-cyclic loading	1000	500	0.50	1.8
S1.5D-3	Pull-out with pre-cyclic loading	1000	404	0.40	9.2
S1.75D-2	Symmetric cycling loading	395	300	0.76	14.8
S1.75D-3	Cycling with pre pull-out test	395	250	0.63	18.6
S2.0D-1	Cycling with pre pull-out test	1000	600	0.60	16.0
S2.0D-3	Symmetric cycling loading	479	350	0.73	18.6

The cyclic reduction factors for the above ten specimens indicate that the symmetric cyclic loading reduces the shear / bond transfer between concrete plug and the steel tube. This is due to the accumulation of damage to the plug pile interface. The exception to this is specimens S1.0D-2 and S1.25D-3. It may be caused by either the steel tube imperfections or effect of shrinkage. However an average (mean) cyclic reduction factor of 0.74 with standard deviation of 1.90 was achieved.

5.6   Comparison of the Test Results with Adopted Formulation

The following formulation was used to calculate the bond strength regarding the adopted equation (Section 3.2.5).

$$f_{buc} = 9KC_l C_s \left(f_{cu}\right)^{1/2}$$

f_{cu} is the characteristic concrete compressive strength (in N/mm^2) = 40 MPa regarding to the compressive strength test of the used concrete

K is the stiffness factor defined below

$$K = \left[m(D/t)_g\right]^{-1} + (D/t)_p^{-1}$$

Where:

m is the modular ratio of steel to plug

D_p is the pile diameter

t_p is the pile wall thickness

To adopt OTO's(2001) recommendations for this study, diameter to thickness of the concrete layer between steel bars and steel tube is taken as $(D / t)_g$. The modular ratio of m is also taken as $E_{steel} / E_{concrete}$ = 5.5 (short term loading)

C_l is the coefficient for concrete plug length to pile diameter ratio

The available data on the parameter C_l are limited. In the absence of data relating to a specific tubular geometry and with regard to the test results of previous pull-out and push out tests (Chapter 3), the following values of C_l were assumed.

$$L/D_p \qquad C_l$$
$$< 1.50 \qquad 1.0$$
$$1.5 - 2.0 \qquad 0.9$$

where L is the plug length.

C_s is the surface condition factor

For normal internal surface of the pile, then in the absence of the test data, Cs was taken as 0.6 for Stage 1 and 0.4 for Stage 2 to consider the effect of shrinkage and age of concrete, which reduce the contact area of the interface.

Table 5.8 shows calculated values for the bond stress and ultimate strength based on the adopted formulation. The calculated values of ultimate strength were then examined against measured values and the calculated / measured ultimate strengths. The cyclic reduction factor of 0.74 was used to adjust the cyclic bond strength. The adopted formulation assumes a uniform bond distribution along and around the inside perimeter of the steel tube at the ultimate load performance level. This is justified because it can be later used in practice.

The predicted results for specimens S1.0D show that the predicted static ultimate strength is 18% and cyclic ultimate strength is 28% lower than test results. For specimens S1.25D the predicted values are 2% and 33% lower than static and cyclic ultimate strengths respectively. The predicted static ultimate strength of specimens S1.5D is 28% lower than test results but the predicted cyclic strength is 17% higher than test results. For specimens S1.75D the predicted values are 32% and 38% higher than the average test results of ultimate static and cyclic strengths respectively. The predicted values for specimens S2.0D are 15% and 2% lower than the average test results of ultimate static and cyclic strengths respectively. The higher than predicted values of bond and ultimate strengths in the test results could be related to the irregularities in the diameter and shape of the steel tube used for the specimens. The lower than predicted values of bond and ultimate strengths in test results might be related to the imperfection of the steel tube, and the effects of shrinkage.

Table 5.8. The adopted formulation against experiments

Specimen ID	Failure type	Ultimate Strength kN	Average Bond Strength MPa	Calculated Bond stress MPa	Cyclic Reduction Factor	Calculated Ultimate Strength kN	Calculated / Measured Strength
S1.0D-1	Static	665	4.2	3.43	-	543	0.82
S1.0D-2	Cyclic / Static	711	4.5	3.43	0.74	401	0.56
S1.0D-3	Cyclic / Static	410	2.6	3.43	0.74	401	0.98
S1.25D-1	Static	460	2.38	2.29	-	436	0.95
S1.25D-2	Cyclic / Static	439	2.27	2.29	0.74	323	0.74
S1.25D-3	Cyclic / Static	540	2.79	2.29	0.74	323	0.60
S1.5D-1	Static	1000	4.3	3.09	-	718	0.72
S1.5D-2	Cyclic / Static	500	2.15	3.09	0.74	531	1.062
S1.5D-3	Cyclic / Static	404	1.74	3.09	0.74	531	1.31
S1.75D-1	Static	395	1.45	2.06	-	561	1.42
S1.75D-2	Cyclic	300	1.11	2.06	0.74	415	1.38
S1.75D-3	Static / Cyclic	250	0.93	2.06	0.74	415	1.66
S2.0D-1	Static	1000	3.28	2.06	-	627	0.63
S2.0D-1	Static / Cyclic	600	1.97	2.06	0.74	464	0.77
S2.0D-2	Static	479	1.57	2.06	-	627	1.30
S2.0D-3	Cyclic	350	1.15	2.06	0.74	464	1.32

An average calculated / measured strength of 1.01 with standard deviation of 0.34 indicated that the predicted values and the test results of bond and ultimate strengths are in a reasonable correlation. The cyclic reduction factor also predicts very well the effect of cyclic loading. The variation between the test results and predicted values illustrates an important point to understanding the effect of shrinkage on the behavior of the concrete plug in steel tubular piles under axial loading.

5.7   Failure Mechanisms

Figures 5.24 to 5.26 show the completely pulled out concrete plug from steel tube for specimen S2.0D-1. The specimen reached the set limitation of 1000 kN in static pull-out and push out tests and failed in cyclic loading of 600 kN. The main failure mechanism displayed by the specimen was at the base of the concrete plug, where the steel tube contraction in pull-out is much higher than that of the concrete core, causing it to grip the concrete plug. The diagonal tension crack that formed in the concrete layer between the longitudinal reinforcement and the steel tube extended to the end of the embedded longitudinal reinforcement where it began running in hoop direction. This crack appeared to correspond to a tension splitting of the concrete plug at ultimate pull-out capacity of the specimen. This type of failure was discussed in Chapter 3.

The secondary failure mechanism displayed by the specimen was at the top of the concrete plug where the expansion of the concrete in push out is much higher than that of the steel tube, causing an increase in radial contact pressure. The micro-cracks formed and developed at the interface extended to the top of concrete plug. This type of mechanism was discussed in Chapter 3.

In cyclic loading the initial top and bottom cracks formed at the certain P/Pu and then developed and extended at each cycle. This resulted in an incremental slip of the concrete plug into the steel tube. However the damage on the concrete plug indicated that the failure was a combination of the above failure mechanisms, which were observed at the top and bottom of the specimen.

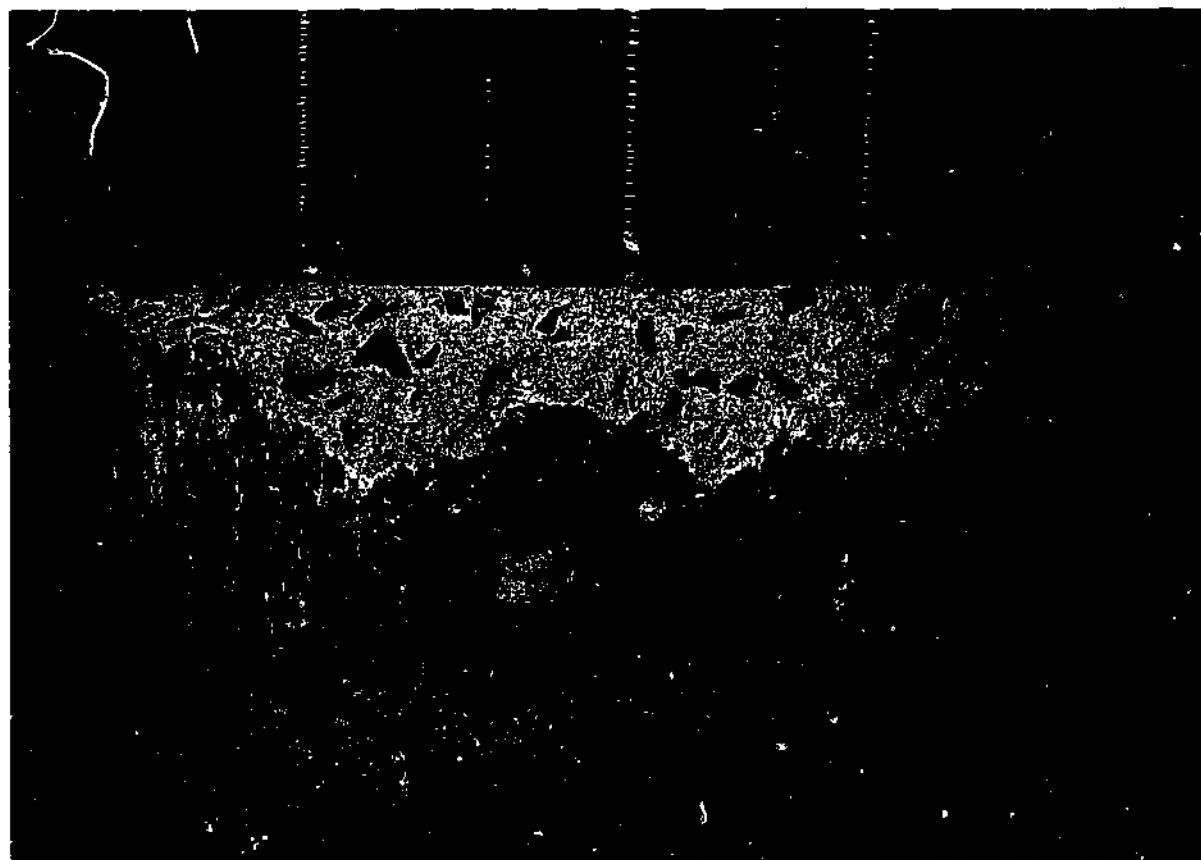Figure 5.24. Completely pulled out concrete plug

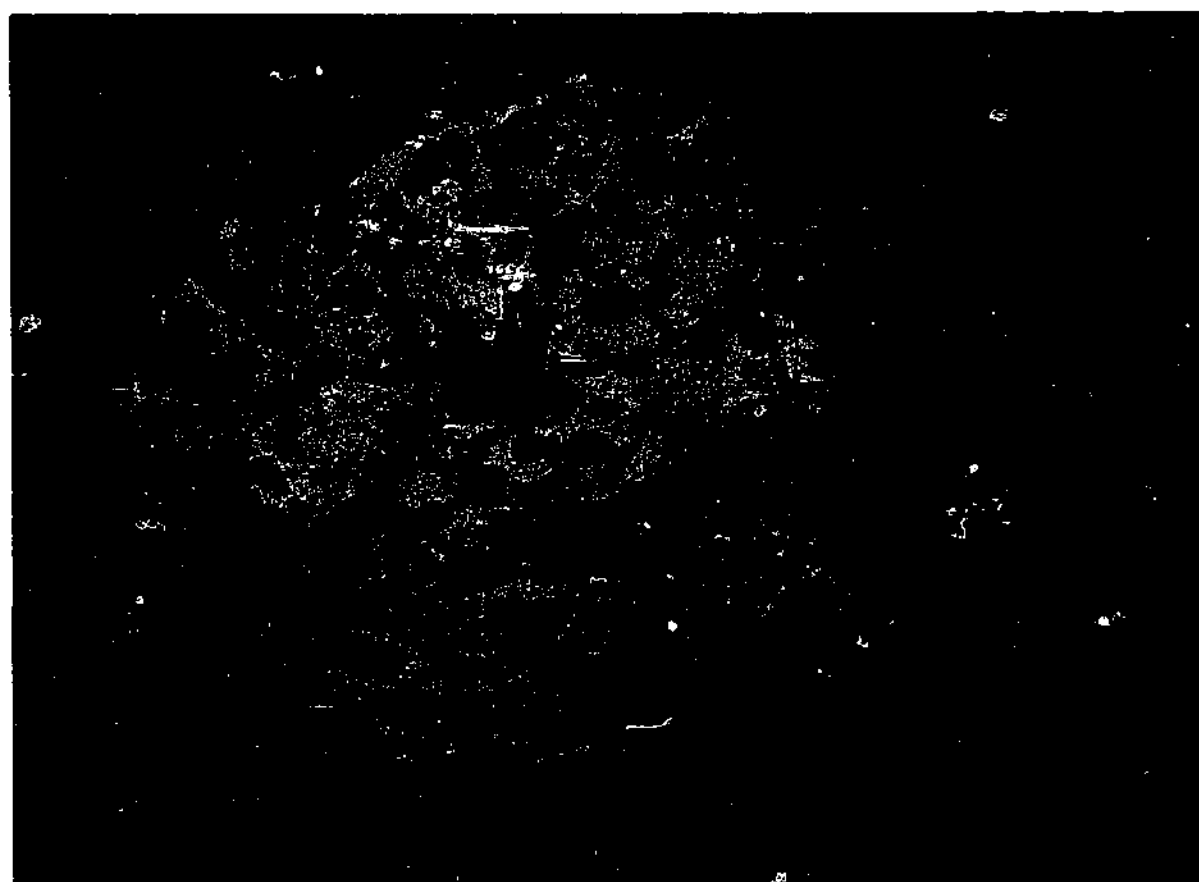Figure 5.25. Damage at top of the concrete plug

Figure 5.26. Damage at the base of concrete plug

5.8   Summary of Chapter 5

1.   The average ultimate bond strength of 4.25 MPa for static load and 2.77 MPa for cyclic load for Stage 1 and the average static bond strength of 2.37 MPa and average cyclic bond strength of 1.70 MPa for Stage 2 were achieved.

2.   The push-out and pull-out tests conducted under symmetric cyclic loading demonstrated that slip between concrete plug and the steel tube increased with repeated loading, and the rate of slip growth increased with the peak load.

3.   Empirical relationships between the load and the rate of slip growth (mm/cycle) were obtained from the experimental data as follows,

$$\text{Symmetric cyclic loading, slip growth per cycle} = 10^{(0.255\frac{P}{P_u}-0.899)}$$

$$(5.2)$$

4.   The ultimate capacity and load slip response of specimens under cyclic loading can be reasonably approximated from the static ultimate strength and load slip of the specimen by reducing the ultimate strength values of the static test by the cyclic reduction factor. The cyclic reduction factor is defined as the factor by which the cyclic strength of specimen may be obtained from the static strength for a given displacement. The average cyclic reduction factor of 0.74 was achieved.

6 NUMERICAL MODELLING USING NON LINEAR FINITE ELEMENT ANALYSIS

6.1 Introduction

The finite element method (FEM) has become an effective tool used in virtually every field of engineering analysis. It provides a powerful and general analytical tool for studying the behavior of the structure in a cost-effective manner.

The finite element method involves the analytical modeling of a continuous structure that is idealized as an assemblage of smaller discrete elements, interconnected at joints called nodes or nodal points. In its entirety, the elements simulate the behavior of the real structure but like any other numerical method, is an approximation with a certain margin of error that is inherent in the method itself. It allows variables to be varied conveniently and systematically, greatly reducing the number of costly experimental tests over the full range of variables. Internal forces, stresses, strains and displacements at any location on the structure can be obtained at any stage of the loading.

Experimental results would be used to calibrate the variables and for comparison against the results of the finite element analysis. FEM analysis then allows important parameters to be varied systematically and conveniently, which greatly reduces the number of costly large-scale testing whilst gaining new insights into the behavior. In the past, the majority of analyses have been restricted or carried out only in the linear elastic range. Concrete is a heterogeneous material with a complex behavior that is closely related to the grain size and shape, and the physical characteristics of its constituents. Therefore, Linear elastic analysis is simply inadequate in describing the complete behavior of concrete and hence non-linear analysis is required. In a concrete plug embedded in a steel tubular pile, non-linear behavior is due primarily to cracking and time dependent effects such

as creep, shrinkage of the concrete, nonlinear behavior of the interface and loading history.

6.2   Scope

Experimental work performed using the procedures outlined in previous chapters produced results that indicated the effect of concrete plug length and presence of reinforcement on the bond strength of concrete plugs in steel tubular piles, as well as the effect of shrinkage and failure mechanisms in pull-out and push-out tests. The work prescribed in Chapters 3 and 5 produced results and formulation that gave an approximation of the level of ultimate bond strength and bond stress distribution along the pile/plug interface.

It should be noted that cyclic behavior was not considered in NLFEA

Although a necessary part of the investigation, the experimental work may have sources of potential error and variations in material properties and specifications. This makes it impossible to draw solid conclusions from the test results. Numerical modeling in this research was also used as an investigative method to aid in the assessment of key parameters in this investigation.

Two sets of finite element analysis studies were carried out. In the first set, models with a given set of material properties were generated and analyzed to verify whether or not the models were simulating the behavior of the concrete plug specimens properly. The development of a calibrated modeling strategy that uses nonlinear finite element analysis (NLFEA) has potential in the accurate evaluation of the structural behavior of concrete plugs into steel piles under axial pull-out and push out force.

In the second set of finite element analysis, selected material properties and specifications of the models of the first study were varied and the effects on bond strength investigated. The aim was to determine qualitatively the sensitivity of the results with respect to variations in the material properties adopted in the first set

of analyses. The effect of varying the steel tube aspect ratio on the ultimate load, effective bond length, load slip behavior and strain distribution profiles was investigated. The main aim of the investigation was to use the results and findings of the numerical analyses in the development and understanding of the finite element models of the actual concrete plugs embedded in steel tubular piles. It also aimed to justify the adopted formulation for bond strength calculation.

The commercially available non-linear finite element package Displacement method Analyzer or DIANA (version 7.2), developed by TNO Building and Construction Research in the Netherlands, was used to model and analyze the concrete plug specimens. An in-depth review of the mathematical basis of the finite element method, material model theories and formulations will not be presented. Although the package allows modifications to the physical and material models through the use of user-defined subroutines, this has not been carried out since Diana's built-in models were found to be adequate.

This chapter presents firstly the objectives of the implementation of NLFEA. Secondly, the development of the physical model, its geometry and simplifications are described. Following this, various relationships to describe the behavior of the materials are outlined. A parametric study using these relationships was performed and the details of this are given in this section. A discussion of the iteration scheme, and the mechanisms used to detect failure is given. Finally, the modeling procedure is described.

6.3 Objective of the Implementation of Non-Linear Finite Element Analysis

Numerical modeling (NLFEA) was developed in this investigation to predict the effect of variations in concrete plug geometry and its characteristics on bond strength. This also includes the effect of reinforcement, crack patterns, load deflection response, and the ultimate capacity of the connection.

To ensure that the procedure achieved satisfactory results, the specimens used in experimental work were modeled with this procedure. The following additional objectives were set to achieve satisfactory prediction of bond strength.

1. Determining the capability of NLFEA to predict the ultimate strength of the experimental specimens.

2. Determining the capability of NLFEA to predict the stiffness of the specimens as measured from the gradient of the load-slip response of the specimens.

3. Determining the capability of NLFEA to predict the effect of presence of reinforcement in the bond strength.

4. Determining the capability of NLFEA to predict the failure mechanisms at the ultimate load level.

5. Determining the capability of NLFEA to predict the bond stress distribution along the interface.

6. Determining the capability of NLFEA to predict the effect of shrinkage on structural behavior of the specimens.

6.4   Physical Model

The physical modeling required selection of an adequate representation of the structure, selection of a satisfactory representative loading and support scheme (boundary conditions), and selection of element sizes that were appropriate for the model. This section discusses these aspects of the modeling procedure. It should be noted that these parameters were fixed throughout the modeling procedure and were not investigated as part of the parametric study outlined in Section 6.6.

6.4.1   Model geometry and boundary conditions

The first step of finite element modeling is to define the geometry and boundary conditions. An axisymmetric model was developed by revolving a plane figure about the centerline of the concrete plug. In this case geometry, material properties, loads and supports are axisymmetric. Thus the analysis problem is mathematically two-dimensional.

The model boundaries were intended to model the specimens that were tested throughout the experimental work. Several factors were considered in ensuring this replication of the experimental specimens, as well as providing an efficient model to reduce computational time.

A schematic of the FE model and interface element are illustrated in Figure 6.1.
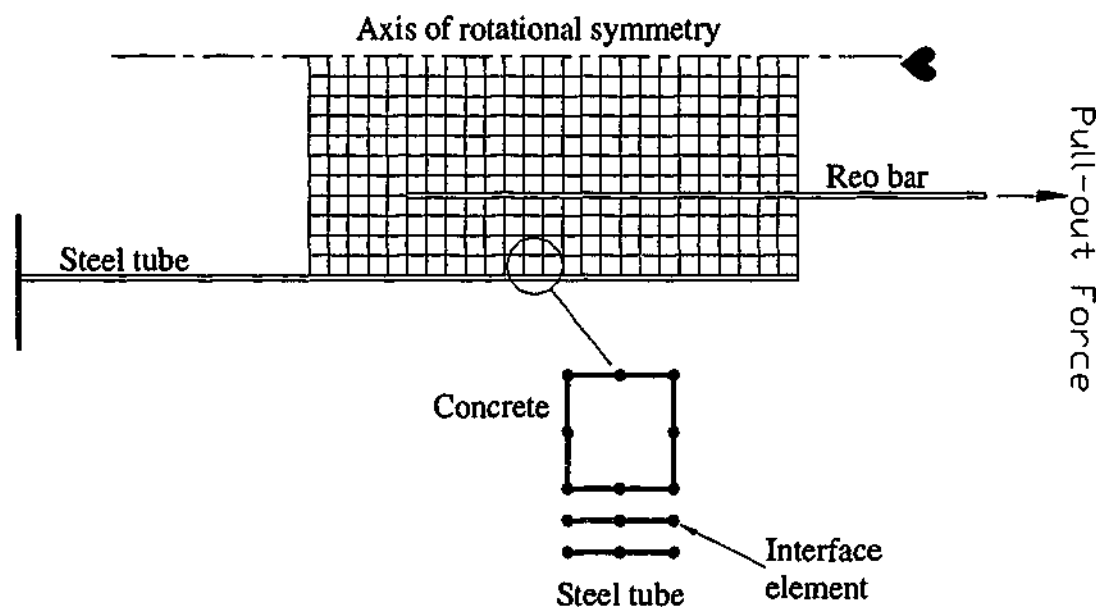
Figure 6.1. A schematic outline of the FE model

6.4.2   Element Selection

The next step would be to discretize the specimen into the appropriate type, number and size elements. To investigate the ability of the NLFEA solution to predict the behavior of the specimens, the models that were developed required distributions of stresses and strains to be produced in the axisymmetry plane of the concrete and the steel tube. It was therefore decided that axisymmetric elements be employed.

6.4.2.1 Concrete elements

The concrete was represented by the use of eight-node isoparametric axisymmetric solid ring element with quadrilateral cross section shown in Figure 6.2
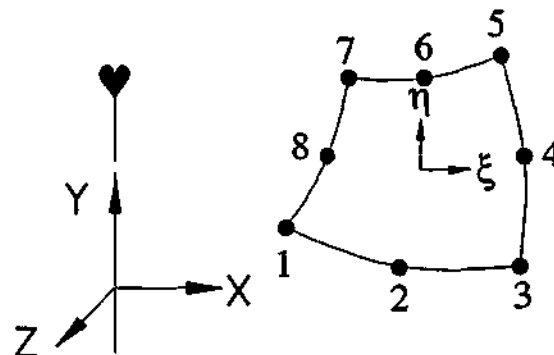

Figure 6.2 Eight-node quadrilateral isoparametric plane stress element

These elements have a node at each corner, as well as a midside node that is located at half of the length of each side of the element. Each element has sixteen degrees of freedom (DOF) with two displacements u_x and u_y, at each point. A 2 x 2 Gaussian integration scheme was employed. The polynomial for the displacements u_x and u_y can be expressed as:

$$u_i(\xi,\eta) = a_0 + a_1\xi + a_2\eta + a_3\xi\eta + a_4\xi^2 + a_5\eta^2 + a_6\xi^2\eta + a_7\xi\eta^2 \qquad (6.1)$$

This element is embedded within the DIANA software, has shape functions of the following characteristics.

(1)   The strain ε_{xx} varies linearly in the x-direction, and quadratically in the y direction.

(2)   The strain ε_{yy} varies linearly in the y-direction, and quadratically in the x direction.

(3)   The strain ε_{zz} varies quadratically in both x and y directions.

Selection of a mesh size that was capable of capturing the stress distributions in the regions required in a computationally efficient manner dictated the selection of the mesh density.

6.4.2.2 Steel elements

The steel tube and longitudinal reinforcement were represented by the use of a three-node numerically integrated axisymetical shell of revolution element shown in Figure 6.3. The longitudinal reinforcement was modeled as a circular ring.

These elements have a node at each end, as well as a middle node that is located at half of the length of the element. Each element has nine degrees of freedom (DOF) with three displacements u_x, u_y and ϕ_z at each point. A 2 x 2 Gaussian integration scheme was employed.
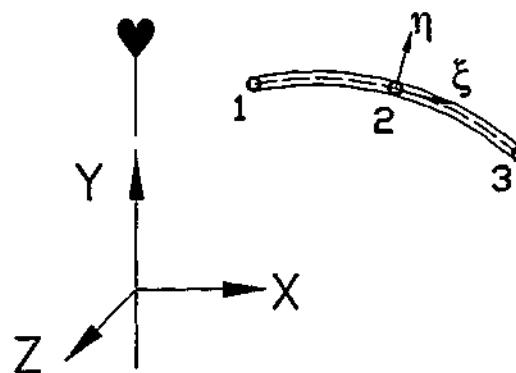

Figure 6.3 Three-node numerically integrated axisymetical shell of revolution

The interpolation polynomial for the translation u can be expressed as:

$$u_i(\xi) = a_0 + a_1\xi + a_2\xi^2 + (b_0 + b_1\xi + b_2\xi^2)\eta \qquad (6.2)$$

This element is embedded within the DIANA software. Typically this polynomial yields a strain ε_{xx}, which varies linearly in ξ direction.

Selection of a mesh size that was capable of capturing the stress distributions in the regions required in a computationally efficient manner dictated the selection of the mesh density.

6.4.2.3 Interface element

The structural interface elements describe the interface behavior in terms of a relation between the normal and shear tractions and the normal and shear relative displacements across the interface.

The pile/concrete plug interface was represented by the use of 3 + 3 nodes, two dimensional line structural interface element shown in Figure 6.4.
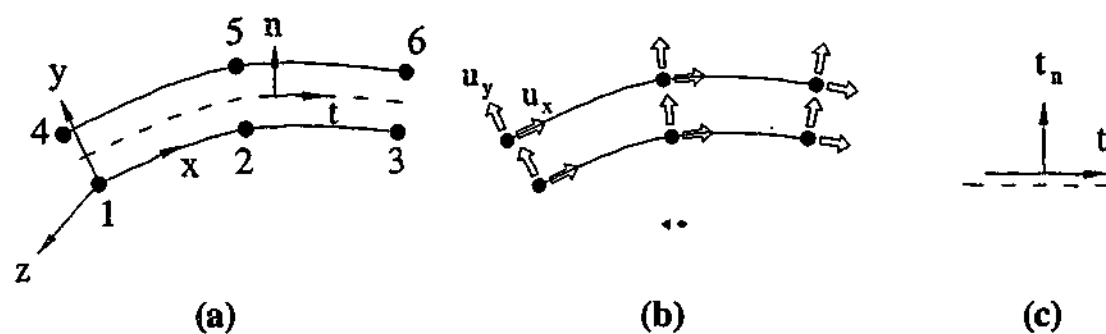

Figure 6.4 - 3+3 nodes structural interface elements (a) topology (b) displacements (c) tractions

The element describes a relation between the tractions (a stress), t, and the relative displacements, Δu, across the interface, based on quadratic interpolation. For this element type, the 4-point Newton-Cotes integration scheme was used.

This element is embedded within the DIANA software. Selection of a mesh size that was capable of capturing the stress distributions in the regions required in a computationally efficient manner dictated the selection of the mesh density.

6.5   Material Model

Aspects of the material behavior were obtained from the tensile tests on steel samples and the concrete cylinders. Instrumentation of the specimens provided information regarding the longitudinal and Hoop strains along the steel tube, therefore providing information into criteria required for a suitable constitutive model. This section summarizes the material models that were used in the solution scheme based on these results.

6.5.1   Concrete material model

The concrete embedded in the steel tube has a very complex material behavior: nonlinear stress-strain behavior in a triaxial state of stress where the confining pressure is not constant. Due to this complexity, selection of a proper constitutive model describing the concrete behavior under confining condition is a challenging task for developing an accurate finite element model.

DIANA provides several constitutive models that are appropriate in modeling the compressive response of concrete. These are divided into two categories, the plasticity based formulations, and the total strain formulations. It assumes that the tensile response of concrete is elastic prior to cracking, but offers a variety of constitutive modeling approaches to the post-cracking response of tension

concrete. These models can also be divided into two categories, linear tension softening models, and nonlinear tension softening models.

Owing to the lack of agreement of the constitutive relations in literature that exist describing the compressive and tensile response of concrete, and also the lack of agreement on the contribution of aggregate interlock to the resistance of shear, a parametric study of the above variables was performed as part of this research.

It should be noted that in both tension-softening models, the smeared crack approach developed by Litton (1974) was used to model the cracking that developed at the tensile strength of the concrete.

6.5.1.1   *The Drucker – Prager model*

The Drucker – Prager model was chosen as a representative model for the capability of the plasticity models to predict the response of the concrete in compression. This model describes the yield surface for plain concrete in terms of the first normal invariant of stress (I_1), the second deviatoric invariant of stress (J_2), and the hardening parameter (κ). The general form of the failure surface is given in Equation 6.3. The condition F=0 represents failure of concrete. It is noted that associative plasticity was considered in this implementation of the modelling so that the internal angle of friction (ϕ) is equal to the dilatancy angle (ψ).

$$F = \sqrt{J_2} - \alpha_f I_1 - \beta c = 0 \qquad (6.3)$$

The coefficient α_f is a scalar quantity that is dependent on the internal angle of friction (this angle is dependent on the hardening parameter, i.e. $\phi(\kappa)$) and is given in Equation 6.4. The coefficient β is also a scalar quantity that is dependent on the initial angle of internal friction (ϕ_o), it is shown in Equation 6.4. The parameter c is the cohesion and is defined in Equation 6.5.

$$\alpha_f = \frac{2\sin\phi(\kappa)}{3 - \sin\phi(\kappa)} \qquad ; \qquad \beta = \frac{6\cos\phi_o}{3 - \sin\phi_o} \qquad (6.4)$$

Strain hardening is included in the model by the relation of the cohesion to the equivalent plastic strain, κ. DIANA makes this relation within the software. This requires relation of the effective cohesion, and the equivalent plastic strain to a level of applied strain. The implementation of this requires an assumption regarding the stress strain response of the concrete. For the purpose of this analysis, it is assumed that the Thorenfeldt (1987) uniaxial curve describes the compressive response of all elements within a specimen. This assumption implies that the shape of the stress strain curve of the concrete elements within the model will not be affected by the existence of a multi-axial stress state. Application of this assumption yields the relation given in Equation 6.5 between the cohesion and the uniaxial compressive concrete stress (σ_c).

$$c = \sigma_c \frac{1 - \alpha_f}{\beta} \qquad (6.5)$$

Assuming that the friction angle (ϕ) and the dilatancy angle (ψ) remain constant for all states of stress, and equal to the initial values (ϕ_o and ψ_o), a relation of the equivalent plastic strain to the uniaxial plastic stress can be made. This is shown in Equation 6.6.

$$\dot{\kappa} = -\frac{\sqrt{1 + 2\alpha_g^2}}{1 - \alpha_g} \dot{\varepsilon}_3^p \qquad (6.6)$$

In this equation, α_g is equal to the scalar quantity α_f (this is since associative plasticity is assumed), and the strain ε_3^p is the plastic component of the principal compressive strain.

Mender et al.(1998) proposed a formulation to predict the pre-yield and post-yield behavior of confine concrete members subjected to axial compressive stresses. The model utilizes the equation given by Popovics (1973), originally developed to

represent the stress-strain response of unconfined concrete. This model is based on a constant confining pressure σ_R.

The peak-confined strength f'_{cc} is a function of the unconfined strength f'_c and the constant lateral pressure σ_R as follows

$$f'_{cc} = f'_c \left(2.254 \sqrt{1 + 7.94 \frac{\sigma_R}{f'_c}} - 2 \frac{\sigma_R}{f'_c} - 1.254 \right) \qquad (6.7)$$

The confined compressive strength of the concrete was then calculated   based on assuming constant lateral pressure of 10%. The yield condition of Drucker-Prager was expressed using the confined compressive strength.

6.5.1.2 Cracking Criteria

Cracking is specified as a combination of tension cut-off, tension softening and shear retention. The constant tension cut-off criterion was used in this modeling. The linear tension softening of concrete that was implemented into this modeling scheme was a simple formulation that relies only on knowledge of the cracking stress (f_{cr}), and ultimate strain (ε_u). The total tensile response of concrete using this model is shown below in Figure 6.5.
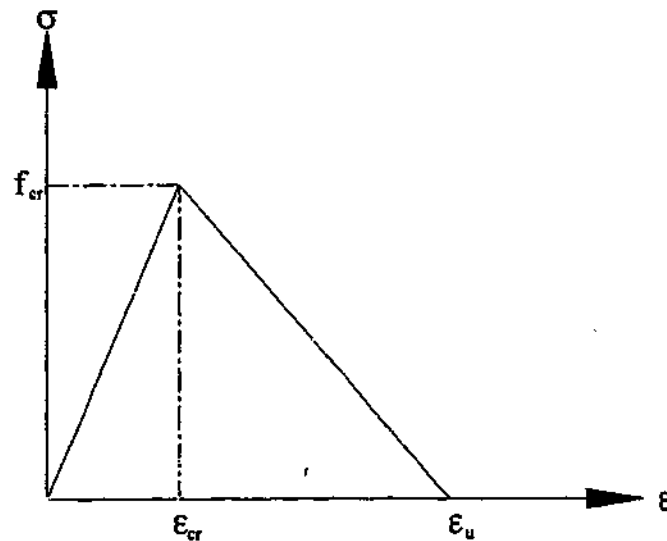

Figure 6.5 Linear tension softening response

By highlighting previous research, Stevens et al. (1991) demonstrated that cracked reinforced concrete can sustain tension forces beyond the yield stress of the steel. For the purpose of this model, the ultimate concrete tensile strain is calculated as the yield strain of the steel as follows:

$$\varepsilon_u^{cr} = \frac{\sigma_{y,steel}}{E_{steel}} \tag{6.8}$$

In smeared crack models, it is common to represent the shear stiffness of cracked concrete by means of a shear retention factor, β, which indicates the percentage of elastic shear capacity that remains after cracking. This factor is used to account for the effect of aggregate interlock in the concrete. In the current implementation in DIANA, only the constant stiffness reduction model is available, which is given by Equation 6.7 and illustrated in Figure 6.6. In reality, the shear stiffness that remains after cracking is a function of the strain normal to the crack. In the present study, the loading and deformation mechanism of the bond specimens is such that the effect of aggregate interlock is minor. For numerical stability of the finite element models, β is assumed to be 0.05 or 5%.
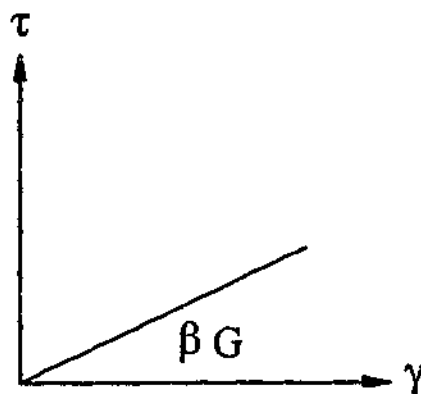
$$G^{cr} = \beta G \tag{6.9}$$

Figure 6.6 Shear after cracking

6.5.1.3 Material Properties

The 28 day cylinder strength for each concrete batch was obtained as part of the testing program. From this value, the basic properties consist of Young's modulus, Poisson's ratio, tensile and compressive strength was calculated using the following formulation. Young's modulus was determined in accordance with AS3600 (1995) reproduced herein as Equation 6.10. The density of concrete, ρ, was assumed as 2400kg/m^3. Poisson's ratio, ν, was taken as equal to 0.2. The tensile strength of the concrete was determined using Equation 6.8 using compressive strength, which is essentially a modification of the equation reported in AS3600 (1995). The concrete compressive strength of 50 MPa for pull-out and push-out tests and 40 MPa for Stage 1 and Stage 2 experimental sets were investigated.

$$E_c = \rho^{1.5}\left(0.043\sqrt{f'_{cm}}\right) \tag{6.10}$$

$$f_{cr} = 0.4\sqrt{f'_c} \tag{6.11}$$

These values of material properties were considered constant throughout the analysis procedure.

6.5.2   Steel material model

Results from instrumentation on the steel tube throughout the experimental work, as well as results of tensile tests on samples of the reinforcing batches and the reported specification for the steel tube indicated that if any reinforcing element had yielded, the strain on it was not enough to produce significant hardening. The level of stress on the steel tube also indicated that there was no significant hardening on the steel tube. This allowed the use of an elastic perfectly plastic constitutive model to be used that simulates a bilinear stress-strain curve. The Von Mises relation was considered appropriate to model these reinforcing and steel tube elements. Since this constitutive model is very accurate in the

prediction of the bilinear stress strain curve, any variations in this model were not considered in the parametric study. Poisson's ratio for steel was assumed to remain constant throughout the analysis at a value of $\nu=0.3$.

6.5.3   Interface material model

The interface element set a nonlinear relation between tractions (normal and tangential tractions) and relative displacement. The behavior of the interface between the steel pile and the concrete plug is governed by friction behavior. This behavior was modeled to the Coulomb friction model, which has closed resemblance with the Mohr-Coulomb plasticity model. Coulomb friction is illustrated in Figure 6.7.
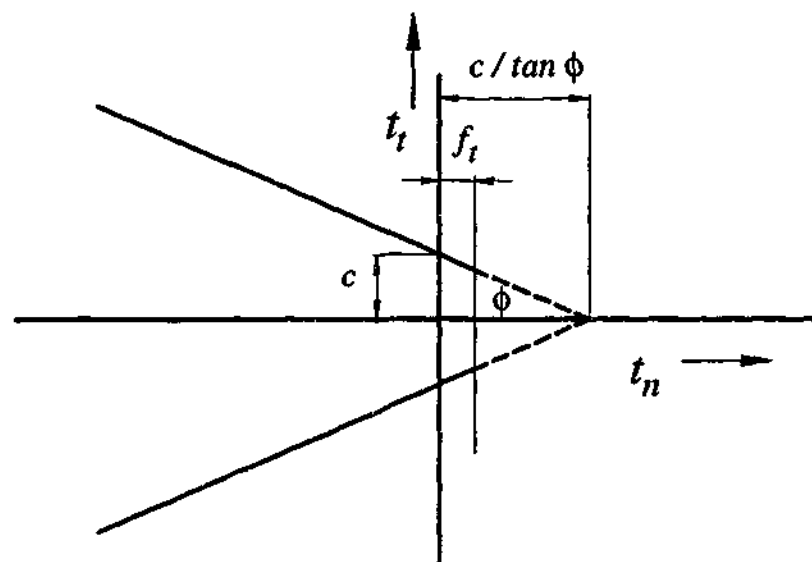
Figure 6.7 The coulomb friction criterion

The Coulomb friction model is basically given by the yield surface and the plastic potential surface.

$$f = \sqrt{t_t^2} + t_n \tan\phi(\kappa) - \overline{c}(\kappa) = 0 \qquad\qquad (6.12)$$

$$g = \sqrt{t_t^2} + t_n \tan\psi \qquad\qquad (6.13)$$

with $\tan\phi(\kappa)$ the friction coefficient as a function of the internal parameter κ, and $\overline{c}(\kappa)$ the cohesion as a function of the internal parameter κ. The direction of the irreversible displacements is given by the plastic potential function g where the "uplift" is determined by the dilatancy angle ψ.

To simulate the separation between concrete plug and steel tube, gap contact criterion was used with Coulomb friction criterion. DIANA assumes that a gap arises if the tensile traction t_n normal to the interface exceeds a certain value. After gap formation, t_n is reduced to zero immediately. The tensile strength of 1 MPa was used for bond between the concrete and steel tube in normal direction.

6.6   Modeling the Effect of Shrinkage

As discussed in Section 5.4.6, results from the tests showed evidence of the effect of concrete shrinkage on the deflection, slip and interface stiffness and shear/bond transfer between concrete plug and the steel tube. Therefore, to compare the measured results with the theoretical model and to evaluate the effect of shrinkage, it was necessary to model the effect of shrinkage in the analytical model.

The measurable effect of shrinkage had not been anticipated when the tests were planned, and therefore no shrinkage or creep had been measured for the concrete in these tests. The shrinkage and creep material properties were assumed based on computer compressive strength and measured slump of the concrete batch.

The finite element program "Diana" has the capability to do time dependent shrinkage and creep analysis. During the initial parametric study, it was found that the level of compressive stressing concrete is lower than the compressive strength of the concrete. Therefore, to minimize numerical errors, it was decided to model the shrinkage and creep of the concrete considering only cracking criteria and non-linearity of the interface. It assumes that the compressive response of the concrete is elastic prior to cracking.

In the analysis of the concrete plugs embedded into the steel tube using the finite element software DIANA, a method based on the European model code MC-1990 has been used to specify the creep and shrinkage behavior of the concrete material on the basis of the physical parameters involved. Following is the brief background of the model.

6.6.1 Theory for predicting shrinkage according to MC-1990

The mean shrinkage strain, which occurs within the time interval t_o to t is given by

$$\varepsilon_{sh}(t,t_o) = \varepsilon_{sho}[\beta_{sh}(t) - \beta_{sh}(t_o)]$$
(6.14)

where

ε_{sho} = basic shrinkage coefficient obtained from the product of 2 functions ε_{sh1} and ε_{sh2},

$$\varepsilon_{sh1} = 0.333(0.41\lambda^2 - 37.1\lambda - 372)x10^{-6}$$
(6.15)

$$\varepsilon_{sh2} = 0.7 + 1.42e^{(-0.18h_o + 0.45)}$$
(6.29)

$\beta_{sh}(t)$ = function describing the development of shrinkage with time, which is dependant on the notional thickness.

6.6.2   Analysis procedure

The time-dependent finite element analysis carried out in this investigation follows the sequence of events as they occurred in the test program. Material properties for concrete used in FE analysis were based on test results of concrete samples. Other properties, which were used for the shrinkage model, are as follows:

- Compressive strength 40 MPa for Stages 1 and 2, 50 MPa for pull-out and push-out tests
- Hypothetical thickness $h = 2A_g / u = 2$ x length of concrete plug
- Loading age   28 days
- Relative humidity RH   60 %
- Average ambient temperature   20 °
- Slump of 90 for pull-out and push out and 110 for Stage 1 and Stage 2 tests

The model allowed the specimens to undergo shrinkage after pouring the concrete into the steel tube.

6.7   The Iteration Scheme and Convergence

To account for the nonlinear response of the specimens to load, the NLFEA solution procedure uses an incremental scheme. This scheme requires applying incremental displacements to the specimen, and within each increment of displacement, iterating to ensure that the internal and external forces balance.

Section 6.7.2 outlines the method used to determine the magnitude of the increment of displacement, and this section outlines the iterations within each displacement increment.

6.7.1   The iteration scheme

Section 6.7.2 outlines the displacement increments that were investigated during the implementation of this numerical model. Within each increment of displacement, the solution was iterated until satisfactory convergence was achieved.

Through preliminary analysis, it was found that the Constant Stiffness Iteration procedure was the most stable prior to the peak load for this implementation. At each increment of displacement, the increment of external load is calculated using a value of stiffness equal to the initial stiffness of the previous load step. This stiffness is used to calculate the increment of applied external force (ΔF_{ext}) corresponding to the applied displacement increment ($\Delta \underline{u}$). Application of the shape functions leads to values of strain at the Gauss points which can be used to calculate the increment of stress, hence the increment of internal force (ΔF_{int}). The relative energy calculated from these quantities (described in Section 6.6.2 below) is used to determine if a correct estimate of the internal forces, hence stress field, has been achieved.

6.7.2 . Numerical convergence criteria

DIANA has three choices of criteria for checking convergence. These are the force norm method, the displacement norm method, and the energy norm method. The former of these two criteria check only the force convergence, and displacement convergence respectively. The latter of the options checks a combination of the both (as energy is the product of force and displacement), and was considered to be a stricter, hence more accurate means of checking convergence; therefore, the latter was adopted.

6.8   The Initial Parametric Study

The variables of the initial parametric study are of three types. Firstly the interface properties variable and then the concrete material properties variables as outlined in Section 6.4, and the size of the load step. This division broke up the parametric study on these variables into three parts. Firstly the material model variations for the interface were examined. Secondly, the material model variables for concrete were examined, and thirdly, the size of the load step was examined. The shrinkage model was introduced after the material models and load steps calibrated against test results. This section discusses the methodology of these studies.

It was considered that the experimental specimens that were chosen for the purpose of comparison with the results of this parametric study should have the failure mechanisms, ultimate strength and load-slip response that were obtained throughout the experimental work.

6.8.1   Interface elements parametric study

In the absence of the basis experimental data, the material model variations for interface outlined in Section 6.4.3 were varied as follows.

1) The values of initial stiffness were assigned values from 1×10^4 to 1×10^8 N/mm in normal direction and from 1×10^2 to 1×10^6 in   ngential direction.

2) The value of the cohesion c was varied from 0.1 to 3.0 MPa

3) The friction coefficient was varied from 0.2 to 1.3

The implementation considered firstly the value of the initial stiffness of the interface, secondly, the value of the cohesion was considered, and finally, the friction coefficient was considered

6.8.2   Displacement step size parametric study

The produced load-slip responses and ultimate strengths of the specimens from the parametric study were examined against the test results. The best combination of the material was then used to determine the effect of load step size on the load-slip response as well as ultimate strength predictions.

The size of the subsequent steps was governed by two issues; firstly, the size had to be reduced cracking and sudden slip on the interface influenced the results, and if this was not done solutions schemes were found to be unstable: secondly, the ratio between the initial step size when the specimen is uncracked, and that when the specimen is cracked could not be too large. Trial and error in preliminary analysis indicated that size of 0.01mm displacement increment resulted in a stable scheme.

6.9   Modeling Plan

As stated in the objectives in Section 6.2, this research used NLFEA to examine the results of ultimate strength, load-slip response, and bond/shear transfer along the interface of specimens with different concrete plug lengths. To do this, three stages of modeling were implemented as described below.

The first stage of modeling was the application of the solution scheme using the material models, shrinkage factors and incremental scheme found to be best suited using the parametric study outlined in Section 6.7 to representative specimens of the experimental work to determine the best combination of the material properties models as well as the best increment of displacement.

In the second stage of the modeling, the optimum combination of the above model characteristics was applied to the experimental specimens to determine the

capability of NLFEA to predict the results. In this thesis, static test results from pull-out, push-out, Stage 1 and Stage 2 were used to compare the ultimate strength, load slip response, longitudinal and Hoop strains along the outer surface of the steel tube and failure mechanisms. The NLFEA results then were used to determine the bond stress distribution along the interface and effective mechanisms in bond strength of the specimens.

The third and final stage of the modeling implemented the optimum modeling scheme determined in Stages 2 and 3 specimens of the same material properties model used in the experiments but with different aspect ratios for the steel tube. The final results also are used for implementation of the bond strength adopted formulation outlined in Sections 3.2.5, 3.4.5 and 5.6.

It should be noted that it was not possible to study the effect of varying the percentage of longitudinal reinforcement. This was due to use of the highest allowed percentage of reinforcement in the specimens. In NLFEA the incremental deflection applied through the end of longitudinal reinforcement to simulate the test procedure. Reduction of longitudinal reinforcement caused yielding of the reinforcement and therefore, NLFEA cannot predict the ultimate strength and complete load slip response of the specimens to be compared.

The specimens in stage two of the analysis (the experimental specimens) will be labeled with the same identifying mark that was used in the experimental work; e.g. Specimens S250 is the specimen with 250 length of concrete plug and specimen S1.25D is a specimen with concrete plug length of 1.25 times of the steel tube internal diameter. This is summarized in Tables 6.1.

Table 6.1 Specimen numbers and material properties for Stage 2 numerical mode

Specimen ID	Tube Length	Concrete Plug Length (mm)	L/D$_i$	f'_c MPa	Concrete Slump
S250	500	250	1.17	50	80
S500	750	500	2.34	50	80
S750	1000	750	3.51	50	80
S1000	1250	1000	5.85	50	80
S1.0D	600	222	1.00	38	110
S1.25D	600	277.5	1.25	38	110
S1.5D	600	333	1.50	38	110
S1.75D	600	377.5	1.75	38	110
S2.0D	600	444	2.0	38	110

The specimens in Stage three of the analysis (those models with different aspect ratio) will be given the same tags, but these will be followed with the letters AS and aspect ratio of the steel tube for variations of the aspect ratio of the steel tube. This is summarized in Table 6.2.

Table 6.2 Specimen numbers and material properties for final stage of numerical model

	Specimen ID	Tube Length (mm)	Concrete Plug Length (mm)	Tube Diameter (mm)	Tube Wall Thickness (mm)	Aspect Ratio
S250-Pull-out	AST-S250-15	500	250	222	14.8	15
	AST-S250-20	500	250	222	11.1	20
	AST-S250-25	500	250	222	8.9	25
	AST-S250-30	500	250	222	7.4	30
	AST-S250-35	500	250	222	6.3	35
	AST-S250-40	500	250	222	5.6	40
S500-Pull-out	AST-S500-15	750	500	222	14.8	15
	AST-S500-20	750	500	222	11.1	20
	AST-S500-25	750	500	222	8.9	25
	AST-S500-30	750	500	222	7.4	30
	AST-S500-35	750	500	222	6.3	35
	AST-S500-40	750	500	222	5.6	40
S750-Pull-out	AST-S750-15	1000	750	222	14.8	15
	AST-S750-20	1000	750	222	11.1	20
	AST-S750-25	1000	750	222	8.9	25
	AST-S750-30	1000	750	222	7.4	30
	AST-S750-35	1000	750	222	6.3	35
	AST-S750-40	1000	750	222	5.6	40
S750-Push-out	ASC-S750-15	1000	750	222	14.8	15
	ASC-S750-20	1000	750	222	11.1	20
	ASC-S750-25	1000	750	222	8.9	25
	ASC-S750-30	1000	750	222	7.4	30
	ASC-S750-35	1000	750	222	6.3	35
	ASC-S750-40	1000	750	222	5.6	40
S1000-Push-out	ASC-S1000-15	1250	1000	222	14.8	15
	ASC-S1000-20	1250	1000	222	11.1	20
	ASC-S1000-25	1250	1000	222	8.9	25
	ASC-S1000-30	1250	1000	222	7.4	30
	ASC-S1000-35	1250	1000	222	6.3	35
	ASC-S1000-40	1250	1000	222	5.6	40
S1.0D-Pull-out	AST-S1.0D-15	600	222	222	14.8	15
	AST-S1.0D-20	600	222	222	11.1	20
	AST-S1.0D-25	600	222	222	8.9	25
	AST-S1.0D-30	600	222	222	7.4	30
	AST-S1.0D-35	600	222	222	6.3	35
	AST-S1.0D-40	600	222	222	5.6	40

	Specimen ID	Tube Length (mm)	Concrete Plug Length (mm)	Tube Diameter (mm)	Tube Wall Thickness (mm)	Aspect Ratio
S1.5D-Pull-out	AST-S1.5D-15	600	333	222	14.8	15
	AST-S1.5D-20	600	333	222	11.1	20
	AST-S1.5D-25	600	333	222	8.9	25
	AST-S1.5D-30	600	333	222	7.4	30
	AST-S1.5D-35	600	333	222	6.3	35
	AST-S1.5D-40	600	333	222	5.6	40
S1.25D- Push-out	AST-S1.25D-15	600	277.5	222	14.8	15
	AST-S1.25D-20	600	277.5	222	11.1	20
	AST-S1.25D-25	600	277.5	222	8.9	25
	AST-S1.25D-30	600	277.5	222	7.4	30
	AST-S1.25D-35	600	277.5	222	6.3	35
	AST-S1.25D-40	600	277.5	222	5.6	40
S1.75D- Push-out	AST-S1.75D-15	600	388.5	222	14.8	15
	AST-S1.75D-20	600	388.5	222	11.1	20
	AST-S1.75D-25	600	388.5	222	8.9	25
	AST-S1.75D-30	600	388.5	222	7.4	30
	AST-S1.75D-35	600	388.5	222	6.3	35
	AST-S1.75D-40	600	388.5	222	5.6	40
S2.0D- Push-out	AST-S2.0D-15	600	444	222	14.8	15
	AST-S2.0D-20	600	444	222	11.1	20
	AST-S2.0D-25	600	444	222	8.9	25
	AST-S2.0D-30	600	444	222	7.4	30
	AST-S2.0D-35	600	444	222	6.3	35
	AST-S2.0D-40	600	444	222	5.6	40

7   COMPARISON OF EXPERIMENTAL RESULTS AND THE FINITE ELEMENT STUDY

7.1   Introduction

This chapter intends to verify the finite element analysis that was outlined in Chapter 6. The following steps summarize the methodology adopted in the finite element study.

1.   Determine the ability of the selected material model combination and step increment to predict the ultimate strength, load-slip response and failure mechanisms of four series of specimens tested in experimental work.

2.   Determine the ability of the solution scheme to predict bond/shear transfer distribution between the concrete plug and the steel tube along the interface by comparing longitudinal and hoop strains measured on the specimens.

3.   Determine the effect of aspect ratio of the steel tube on the ultimate strength, load slip response, failure mechanisms and bond stress distribution along the pile/plug interface.

4.   Knowing the limitations of the modeling strategy, determine the predicted values of the ultimate strengths and the load response of four series of concrete plug specimens that have two material properties.

7.2   Initial Parametric Study

This study applied to all specimens of each experimental set. These are specimens S250, S500 and S750 for pull-out tests, specimens S750 and S1000 for push-out tests, specimens S1.0D and S1.5D for Stage1 and S1.25 for Stage 2. Each experimental set displayed different behavior and bond strengths that were observed from the experimental work.   This is due to the different curing environments, specimen age (shrinkage), concrete characteristics and test arrangements. The material properties of the interface elements were calibrated against experimental results for each set of experiments to adjust these variations.

To determine the most suitable combination of material properties to describe the behavior of the concrete plugs in the steel tubes, the following comparisons were made regarding the procedure outlined in Section 6.7.

1.   Comparison of the load vs. slip of the concrete plug into the steel tube plots obtained for each of the material combinations with those produced in the experimental work.

2.   Comparison of the ultimate strength from experiment (P_u) with the peak load obtained from NLFEA, $(P_u)_{NLFEA}$.

3.   Comparison of the crack patterns from the experiments with those obtained from the finite element analysis.

It would be useful to compare the longitudinal and Hoop strains, however, the results from the experimental work only gave strains at a few points along the steel tube. It was also possible that eccentricity in the specimen caused different strains around the steel tube outside diameter. Therefore it was decided that these factors would not be considered in this parametric study.

Table 7-1 shows the most suitable material properties combinations for the interface resulting from the initial parametric study. D_{11} and $D22$ are initial stiffness in normal and tangential directions (N/mm), C_h is cohesion (MPa) and t_{ph}, t_{ps} are friction coefficients.

Table 7-1 The most suitable material properties combinations for the interface elements

Experimental stage	Initial Stiffness D_{11}, D_{22} (N/mm)	Cohesion C_h (MPa)	Friction t_{ph}, t_{ps}
Pull-out tests	1.0E7, 1.2E5	1.0	1.3, 1.3
Push-out tests	1.0E7, 7.5E4	0.2	0.4, 0.4
Pre Pull-out + Push-out tests	1.0E7, 7.5E4	0.3	0.5, 0.5
Stage1: Pull-out	1.0E7, 1.2E5	0.85	1.25, 1.25
Stage 2: S1.25D	1.0E7, 1.0E5	0.3	1.2, 1.2
Stage 2: S1.75D	1.0E7, 1.0E5	0.3	1.0, 1.0
Stage 2: S2D	1.0E7, 1.0E5	0.3	1.25, 1.25

Specimens S750-2 and S750-3 in the push out test series were subjected to prior pull–out load of 1000 kN. This is considered to be sufficient to partially overcome the effect of shrinkage and improve the interface behavior. Therefore two finite element models (push out and pre pull-out + pushout) with slightly different interface element properties were used for specimen S750 of the push-out tests.

Interface element properties of specimens S1.25D, S1.75D and S2.0D of Stage 2 tests each were calibrated. This was due to the different age of specimens at the time of testing and the unexpected high bond strength of specimen S2.0D-1.

The interface element properties for the rest of the specimens were calibrated to be equal in each test series.

7.3   Specimen Study

The present finite element model was verified by simulating four experimental programs conducted at Monash University as outlined in Chapters 3, 4 and 5. To verify the finite element models, which are simulating the behavior of concrete plug specimens, four items are compared between the experimental and numerical results. These are the ultimate strength, load-slip response, longitudinal and hoop strains along the steel tube and failure mechanisms.

Application of a combination of the crack model and shrinkage based on European code of MC1990 for the concrete and Coulomb friction model for the interface was applied for numerical modeling of all specimens in this stage. These models included exact properties of both materials as calculated from cylindrical and slump tests. The interface element properties were calibrated for each experimental set. This section present a comparison between the NLFEA results and those obtained from the experimental work.

7.3.1   Ultimate strength

Table 7-2 below shows the comparison between the peak loads obtained from experimental work with those obtained from the numerical analysis as well as the relative error between these. In general, the NLFEA procedure has closely predicted values of the peak load with a small amount of relative error; the average relative error was 8.5 %, with a standard deviation of 6.0%.

NFELA over predicted the peak load of specimens S250-1 and S250-2 of the push out test. This may be due to the higher effect of shrinkage on these specimens. However, the predicted ultimate strength for this set of specimens is very close to the experimental average ultimate strength of 855 kN for specimens S250. The ultimate load was under predicted for specimens S250-3, S750-1 and S750-2. Figure 3.7 in Chapter 3 shows that the ultimate strength for specimen S250-3 did not adhere to the usual trend displayed through experimental results, and was higher than the usual trend. Specimens S750-1 and S750-2 were subjected to prior

pull-out load. This was considered sufficient to overcome the effect of shrinkage and improve the interface behavior. The higher relative error from NLFEA for these specimens is thought to arise from this experimental inconsistency and might also be caused by inconsistency of shrinkage. The NEFLA predicted the ultimate load well for the rest of the specimens.

Table 7-2. Ultimate strength comparison

	SPECIMEN	P_U (kN)	$P_{U(NLFEA)}$ (kN)	$P_{U(NLFEA)}/P_U$	RELATIVE ERROR (%)
Pull-out tests	S250-1	810	896	1.11	10.6
	S250-2	720	896	1.24	24.4
	S250-3	1035	896	0.87	13.4
Push out tests	S750-1	3445	3196	0.93	7.2
	S750-2	3700	3196	0.86	13.6
	S750-3	2503	2747	1.10	9.7
	S1000-1	1360	1266	0.93	6.9
	S1000-2	1350	1266	0.94	6.2
St 1	S1.0D	665	671	1.10	0.9
	S1.5D	1000	1004	1.00	0.4
St 2	S1.25D	443	463	1.05	4.5
	S1.75D	395	368	0.93	6.8
	S2.0D	1000	948	0.95	5.2
Average				0.99	8.5
Standard Deviation					6.0

7.3.2   Load-slip response

For the purpose of this discussion, load-slip response comparisons for all specimens of each series are presented in this section. Figure 7-1 to Figure 7-10 below show the load-slip comparison between the numerical model and test results.   Note that the load presented in the finite element results is the sum of reactions.
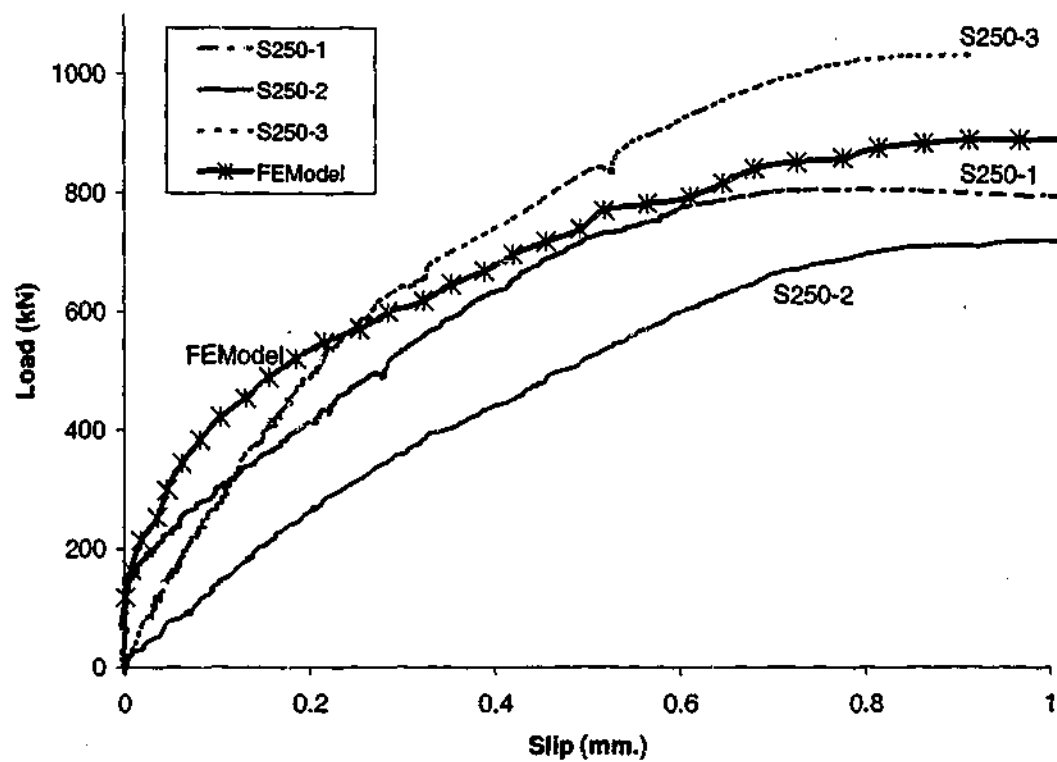
Figure 7-1: Comparison of load-slip response for specimen S250 in pull-out
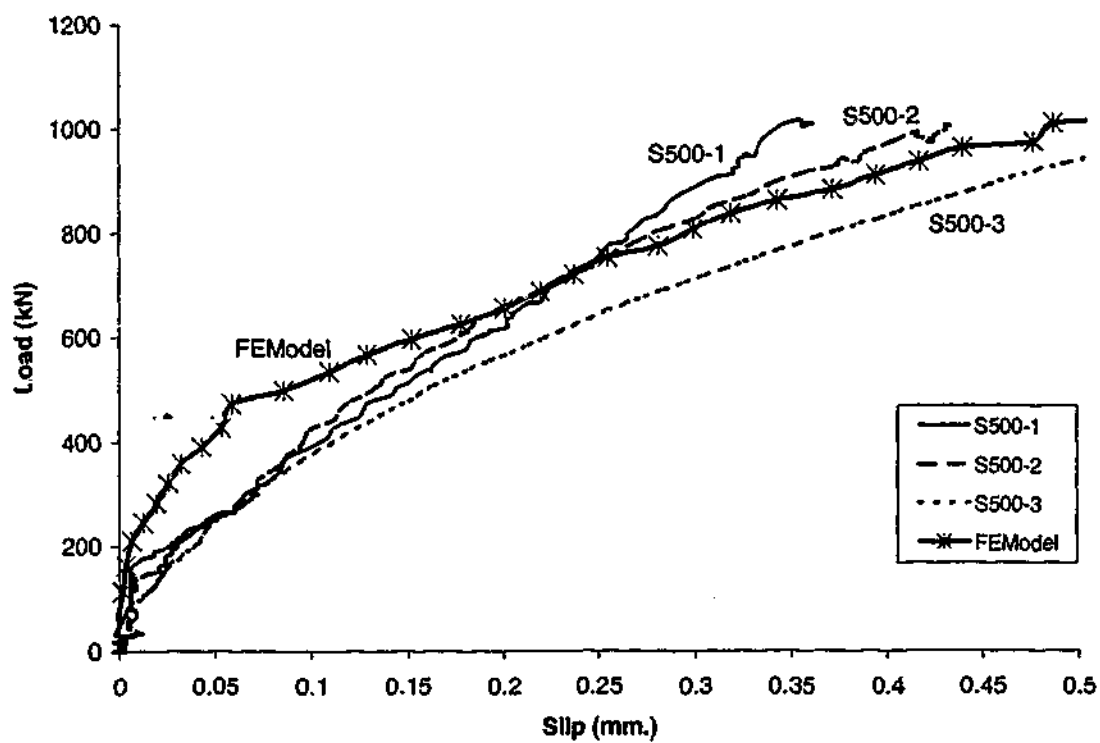
Figure 7-2: Comparison of load-slip response for specimen S500 in pull-out
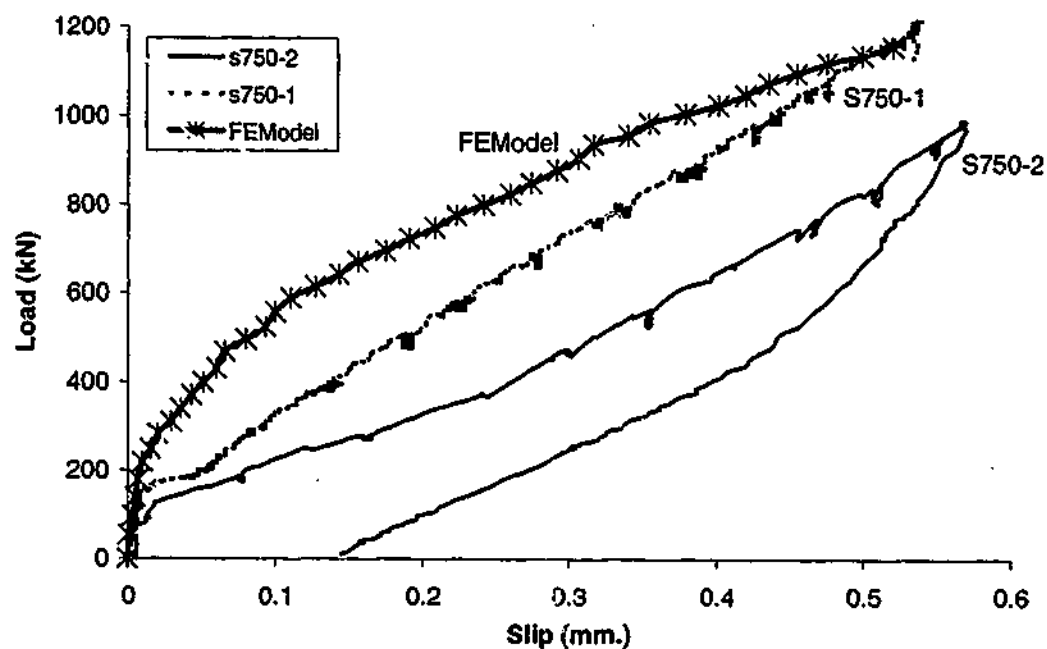
Figure 7-3: Comparison of load-slip response for specimen S750 in pull-out
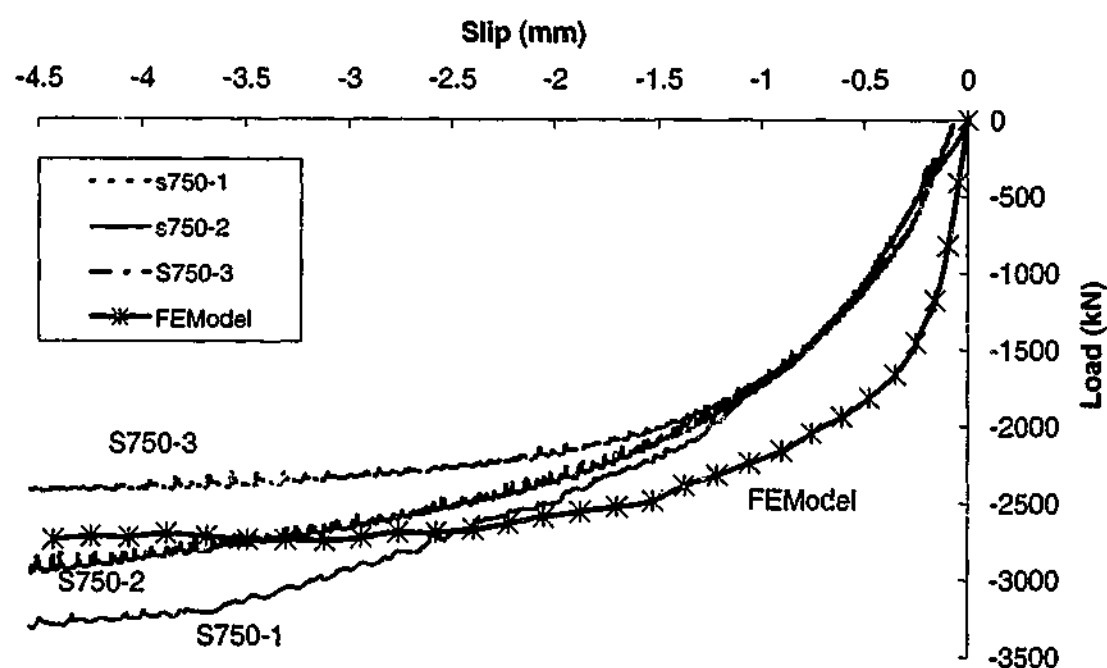
Figure 7-4: Comparison of load-slip response for specimen S750 in push-out
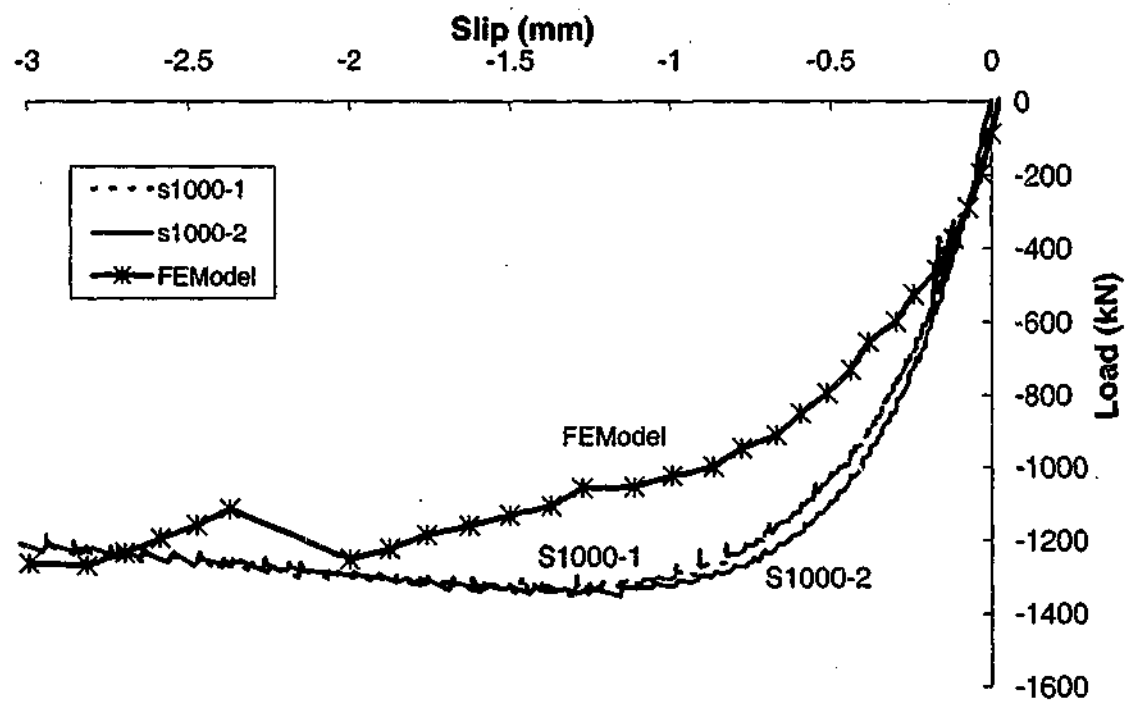
Figure 7-5: Comparison of load-slip response for specimen S1000 in push-out
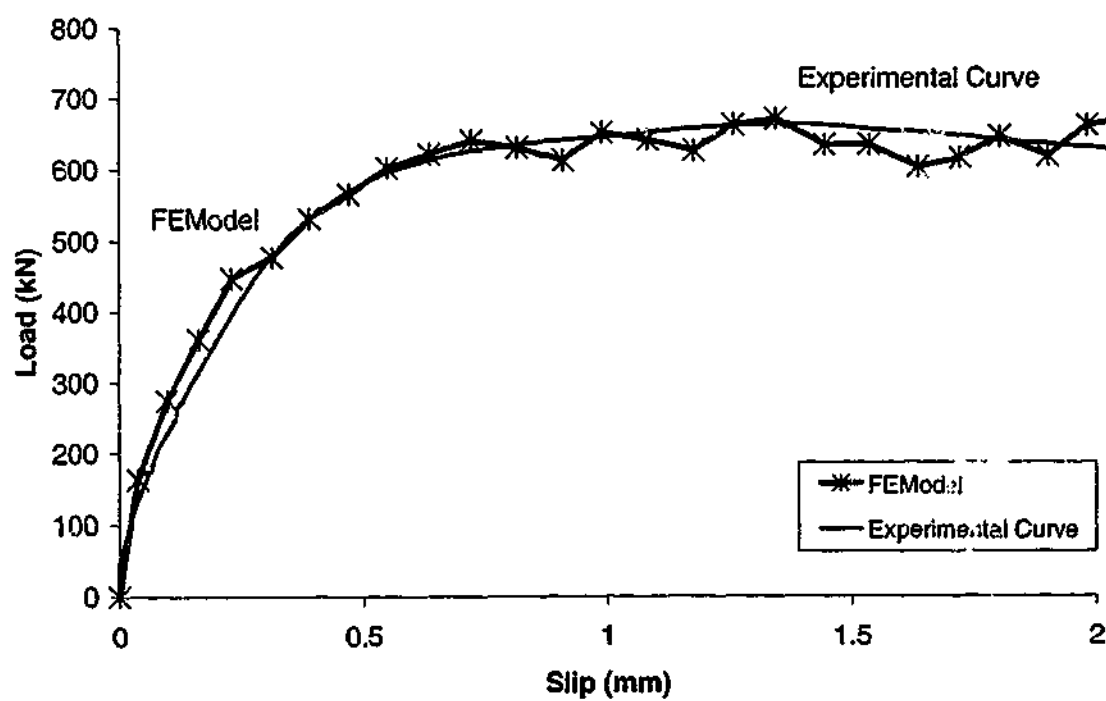
Figure 7-6 Comparison of load-slip response for specimen S1D (Stage 1)
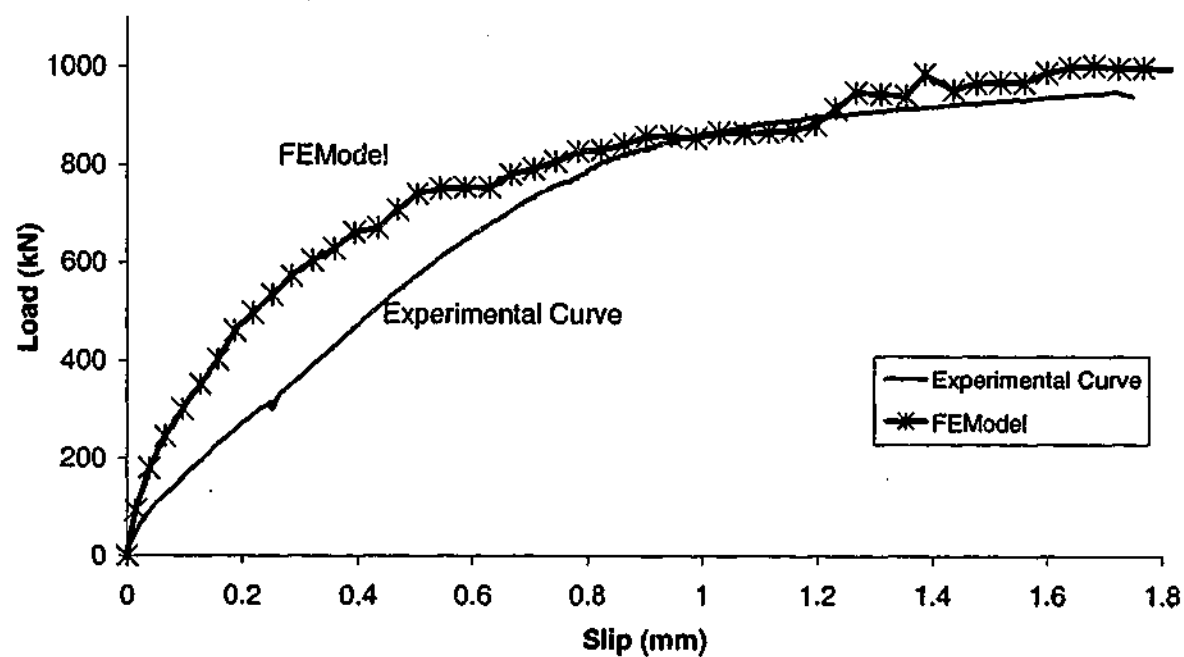
Figure 7-7 Comparison of load-slip response for specimen S1.5D (Stage 1)
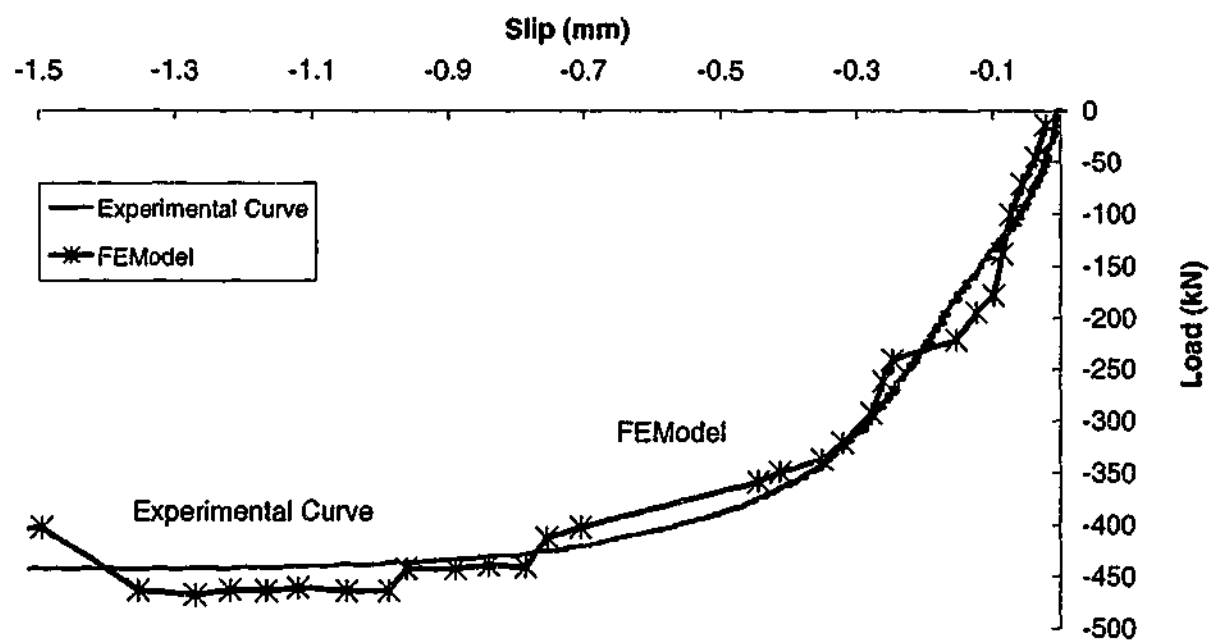
Figure 7-8 Comparison of load-slip response for specimen S1.25D (Stage 2)
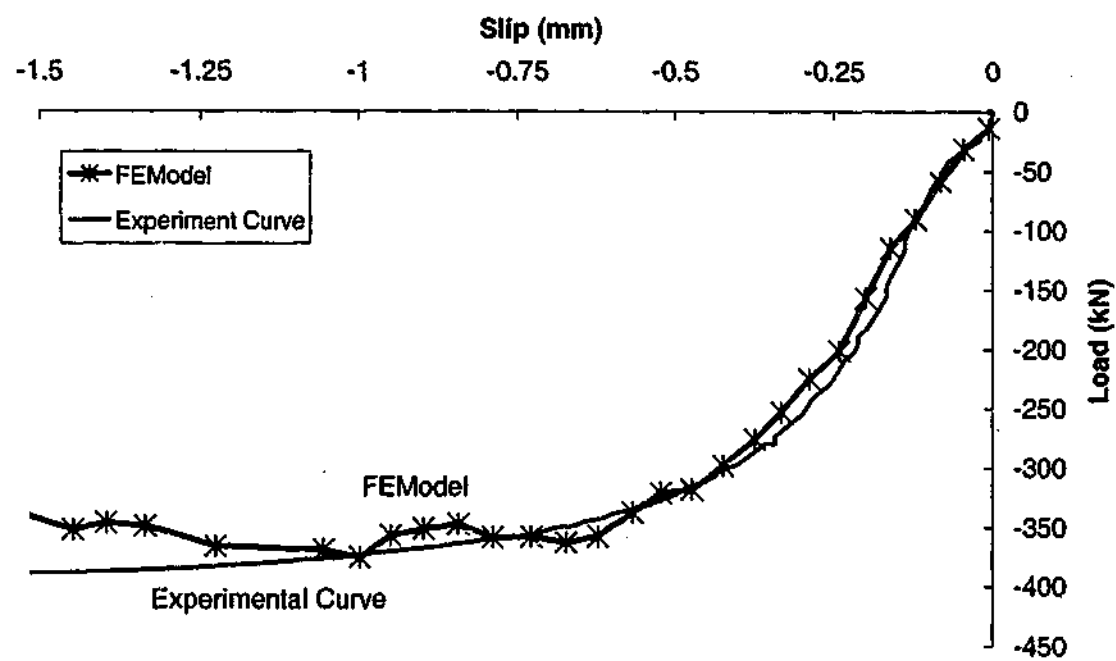
Figure 7-9 Comparison of load-slip response for specimen S1.75D (Stage 2)
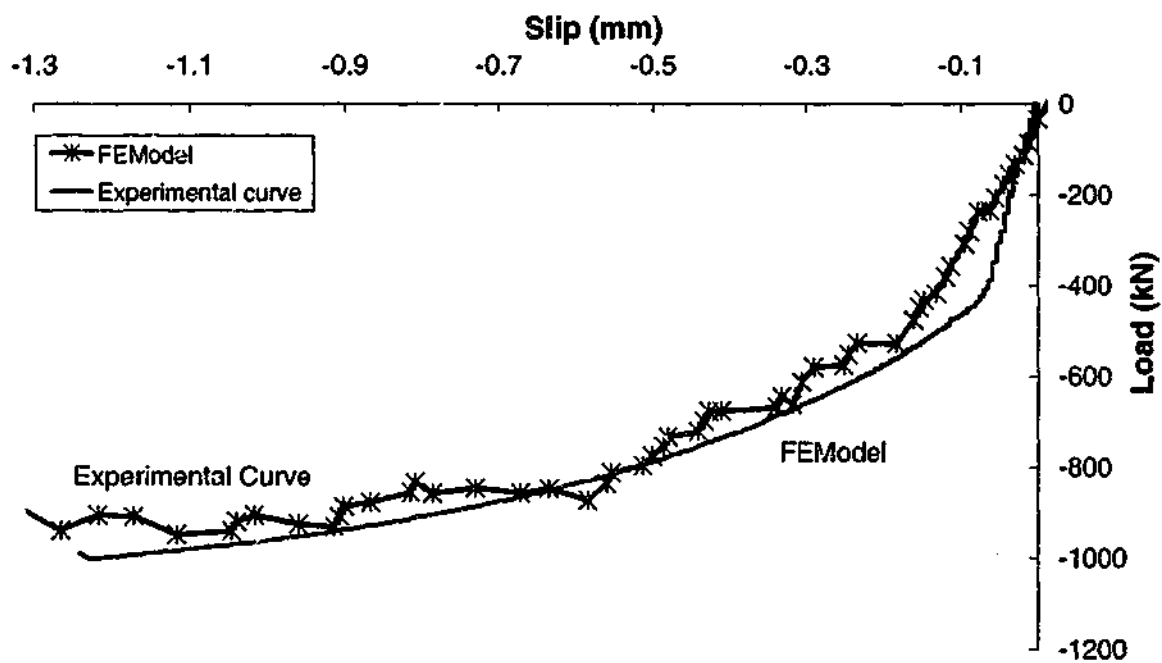
Figure 7-10 Comparison of load-slip response for specimen S2.0D (Stage 2)

In general NLFEA has produced results of the load slip response that capture the trend of the experimental results. The results of all the specimens shown above indicate that the slope of the load slip response from the NFELA is very close to that of the experiments.

The results can be divided into two groups. The first group are specimens with lower shrinkage effect, including S250, S500, S750 in pull out and S750 in push out tests. For this group, although the ultimate load was closely predicted, the initial stiffness was not as well predicted for the analytical model as it was for the test specimen. However both analysis and experiment suggest a simple bilinear relation. The position of the change of slope seems to indicate that the bond resistance of the specimen changes from a non-slip action (chemical adhesion between the interface of the concrete plug and the steel tube) to a very small slip action (mechanical macro locking between the concrete core and the steel surface). The higher initial stiffness (non-slip mechanism) in NFELA might be due to the higher effect of shrinkage of the concrete plug in the tests. It could also be due to different methods of slip measurements in NLEFA and the experiment. However the analytical model closely predicted the ultimate load and stiffness of the pile/plug interface after the mechanical macro interlock became active.

The second group are specimens with higher shrinkage effect due to the higher age of the specimens and slump of concrete at the time of pouring. In this group, both analysis and experiment suggest a simple bilinear relation. The position of the change of slope seems to indicate that the bond resistance of the specimen changes from a chemical adhesion to a mechanical macro locking between concrete core and the steel surface.

The analytical model exhibited the same trend as the test results. It also showed similar initial stiffness (non-slip mechanism), ultimate load and stiffness of pile/plug interface after the mechanical macro interlock became active. The results for specimens S1.25D, S1.75D and S2D from Stage 2 obtained from the finite element study show that the reactions decrease when the peak load is reached. This might be due to the limitation of NLFEA to model the post failure

behavior of these specimens with higher shrinkage and lower compressive strength of concrete. The rest of the load slip curves presented show that the reactions increased smoothly after the peak load achieved, which is in a good agreement with the experiment.

It was clear that the load–slip behavior of the analytical model was close to that of the experimental specimens, thereby providing an opportunity to investigate trends in shear/bond transfer between the concrete plug and the steel tube.

7.3.3   Failure Mechanisms

The failure mechanisms were studied only for specimens S250 and S1.5D by pulling the concrete plug out of the steel tube.

Figure 7-11 shows the completely pulled out concrete plug from the specimen after the specimen failed in pull-out tests, and Figure 7-12 shows the principal strain of the concrete plug after failure of the specimen from the finite element analysis.

The specimens exhibited very similar failure mechanisms in both analytical model and experiment. The failure mechanism displayed by the specimen in pull-out was at the base of the concrete plug, where the steel tube contraction is much higher than that of the concrete core, causing it to grip the concrete plug. The diagonal tension crack formed in the concrete layer between the longitudinal reinforcement and the steel tube. This crack appeared to correspond to a tension splitting of the concrete plug at ultimate pull-out capacity of the specimen.

In push out failure, it was not possible to accurately investigate the failure of the specimen due to damage of the interface by pulling the concrete plug out of the steel tube. However, the observation during the test and results from NLFEA both indicated that the failure occurred when the concrete plug separated at the interface.

It can be concluded that the analytical model reasonably predicted the failure of the specimen, particularly for the pull-out tests.
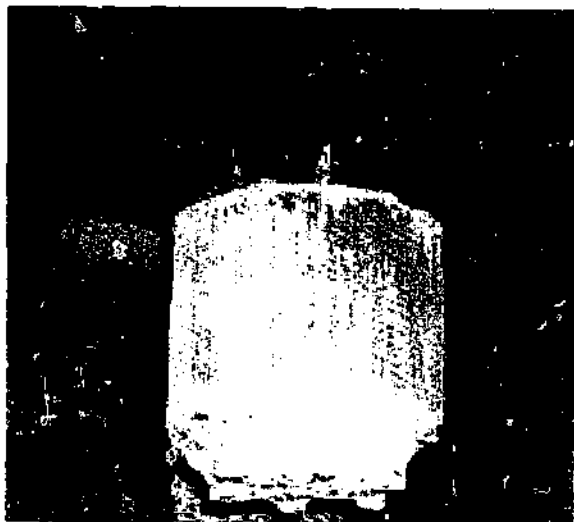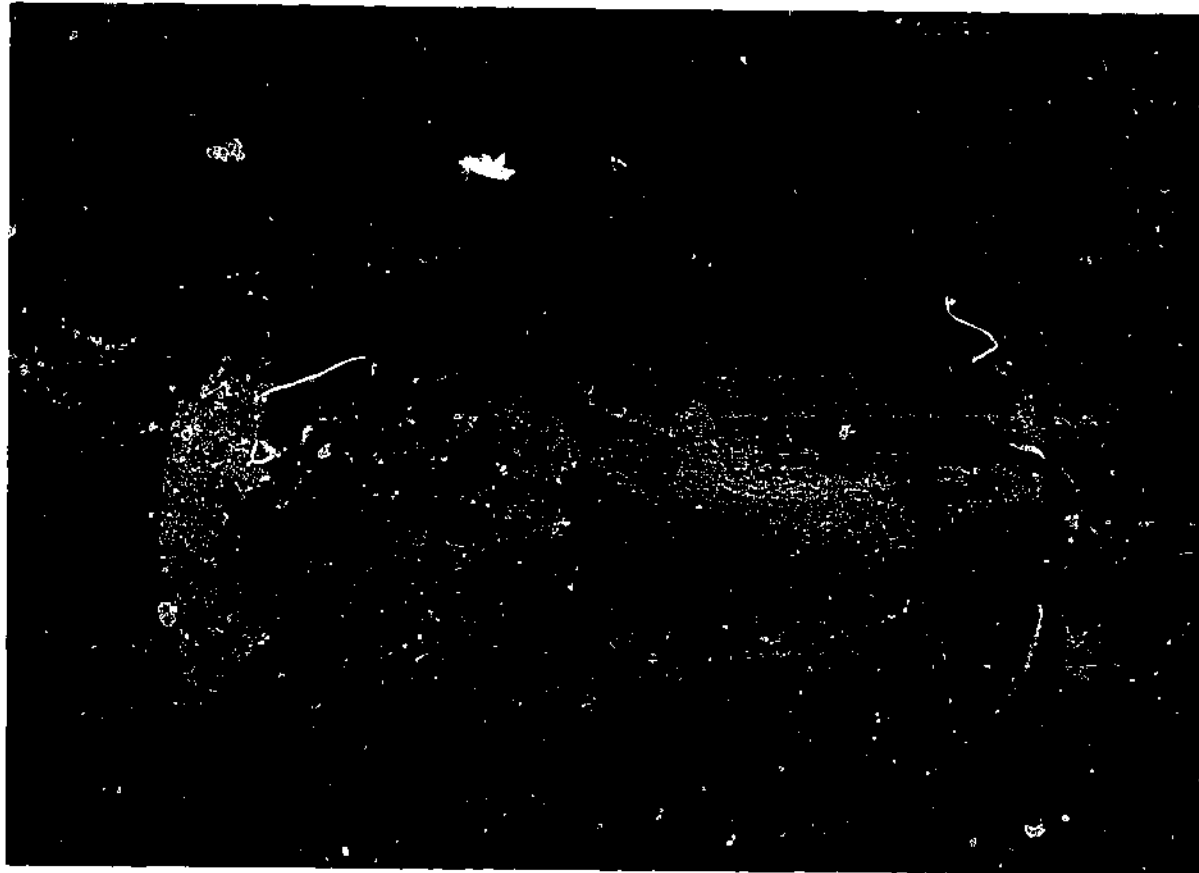
Figure 7-11 Failure mechanisms observed in experiment
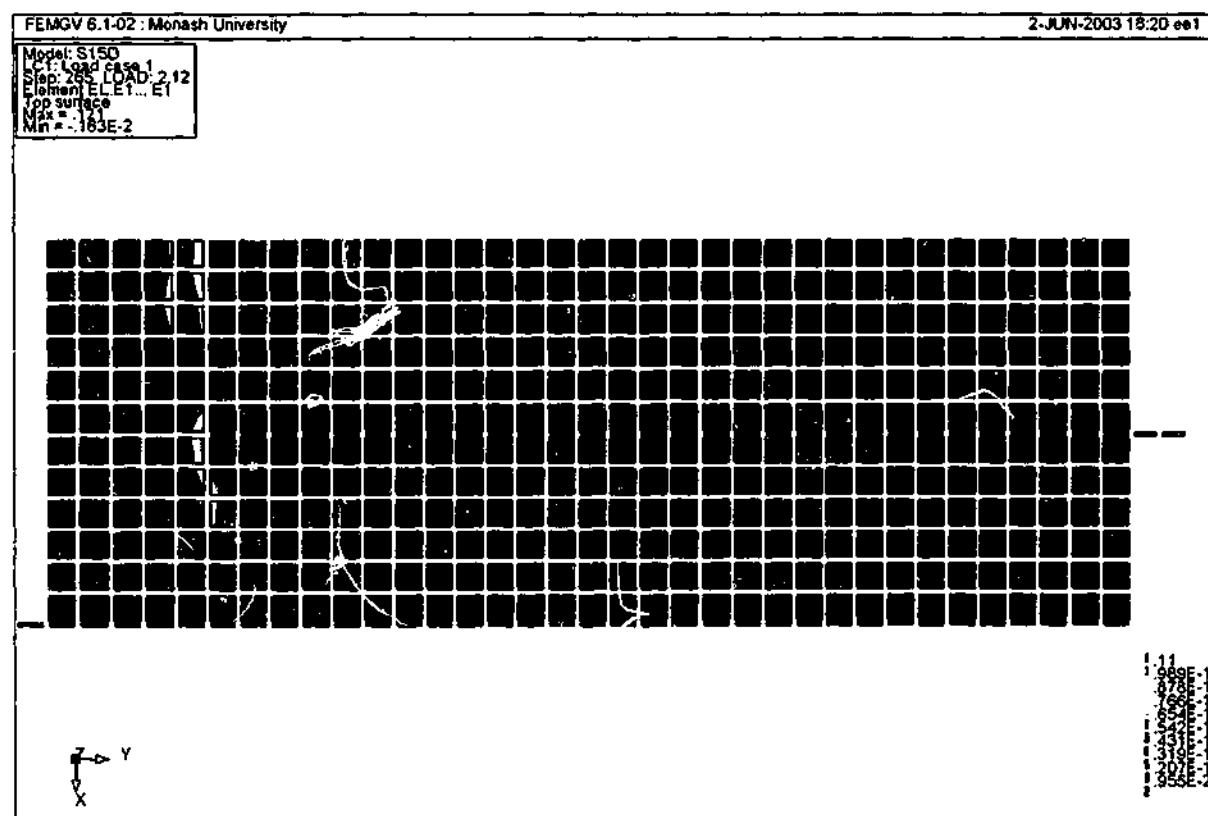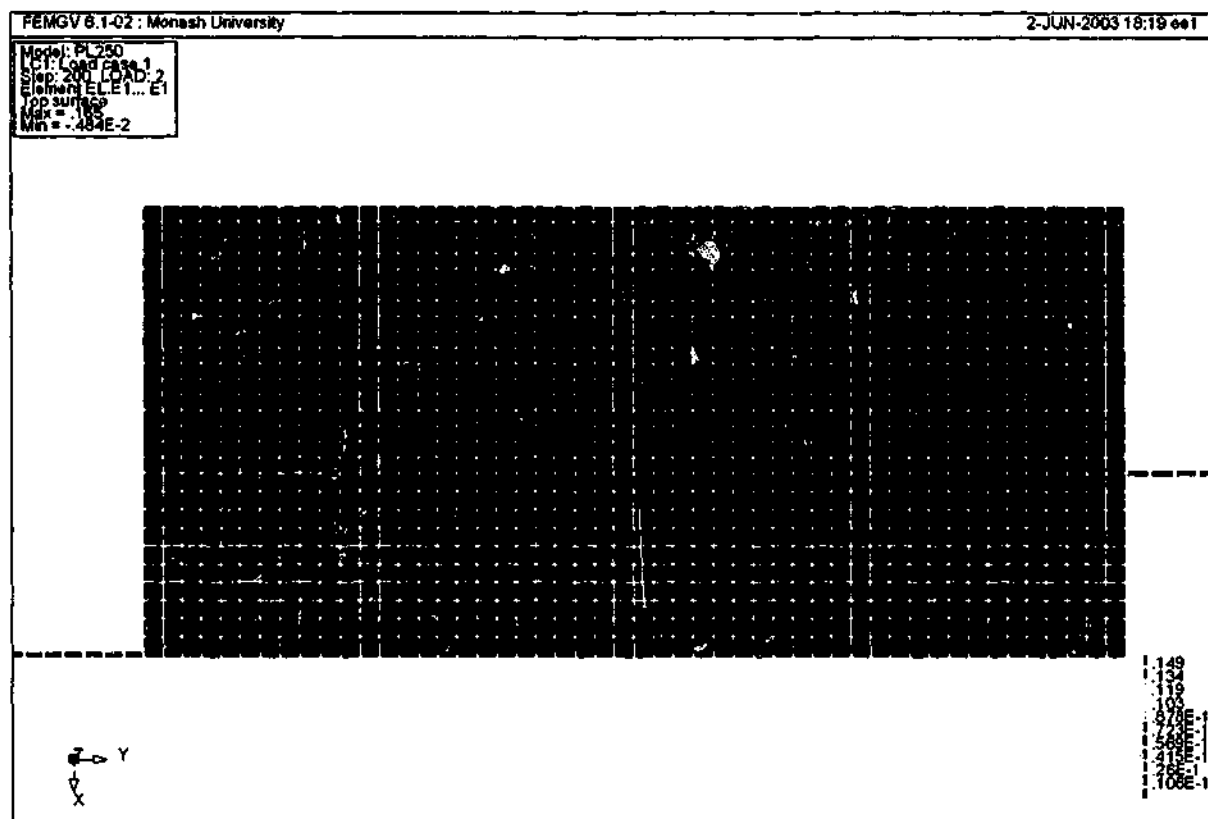
Figure 7-12 Principal strains of concrete plug from the NFELA

7.3.4 Longitudinal and Hoop strains

Most of the specimens were strain gauged along the outer surface of the steel tube within the length of the concrete plug. Both longitudinal and Hoop strain gauges were used. The purpose of these gauges was to determine the load transfer mechanism from the concrete plug to the steel tube. Figure 7-13 illustrates the strain gauge arrangements for specimens S1.0D and S1.5D. Appendix 1 shows the strain gauge arrangements for all specimens.
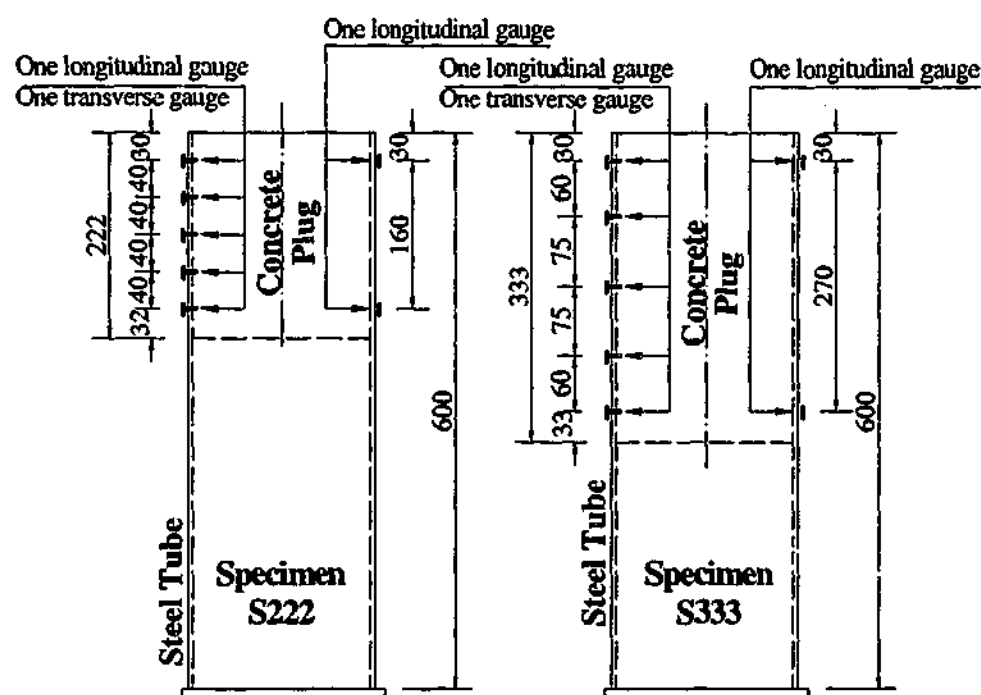
Figure 7-13 Strain gauge locations for specimens S1.0D and S1.5D

NLFEA also produced the longitudinal and Hoop strains along the outer surface of the steel tube. The experimental and numerical longitudinal and hoop strains along the outer surface of the steel tube element at two selected load levels for one specimen of each experimental set are compared in Figure 7-14 to Figure 7-21. At each load level, the experimental and numerical load levels are selected to be as close as possible.
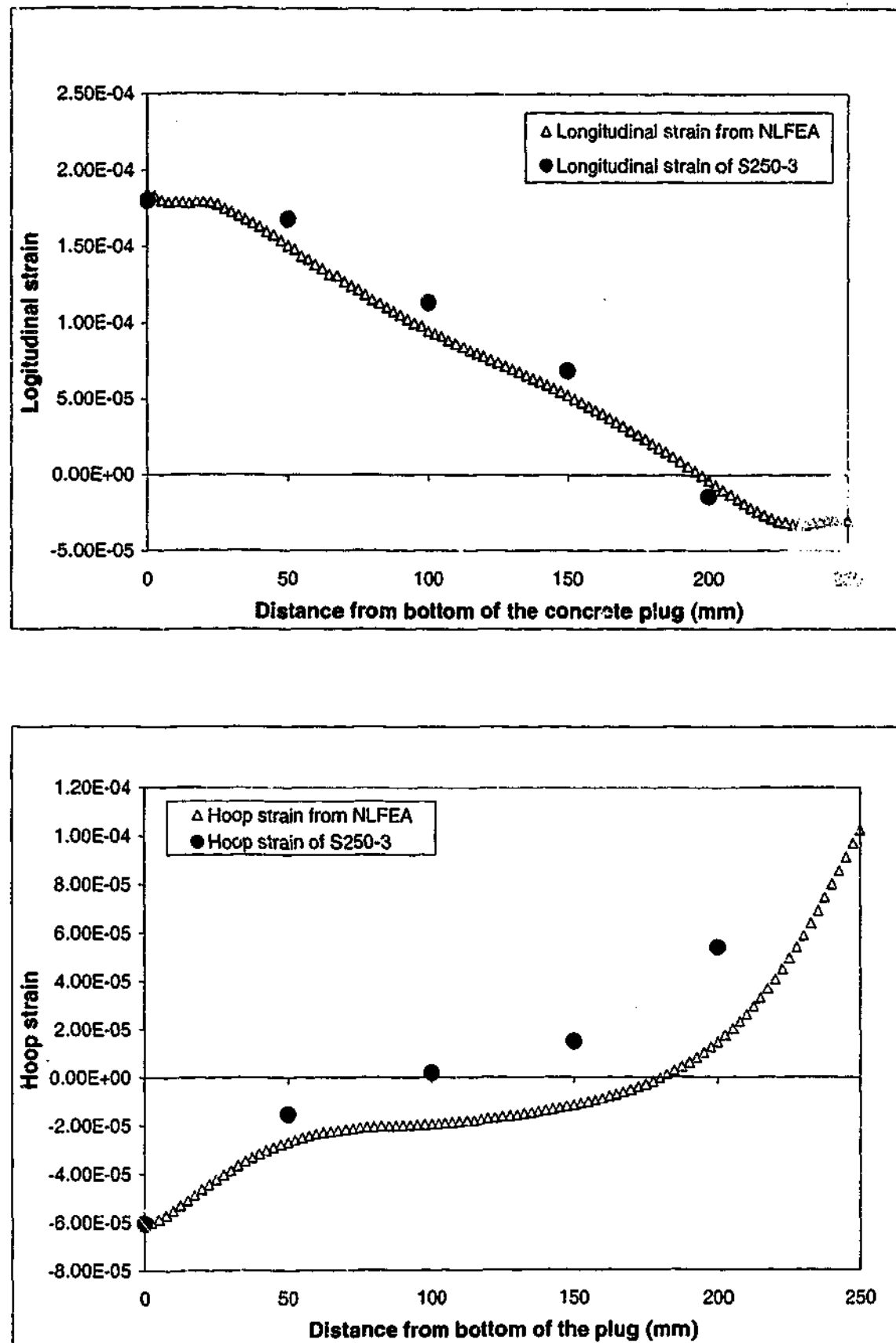
Figure 7-14 Comparison of longitudinal and Hoop strains along the outer surface of the steel tube for specimen S250 of the pull-out test at load level of 333 kN
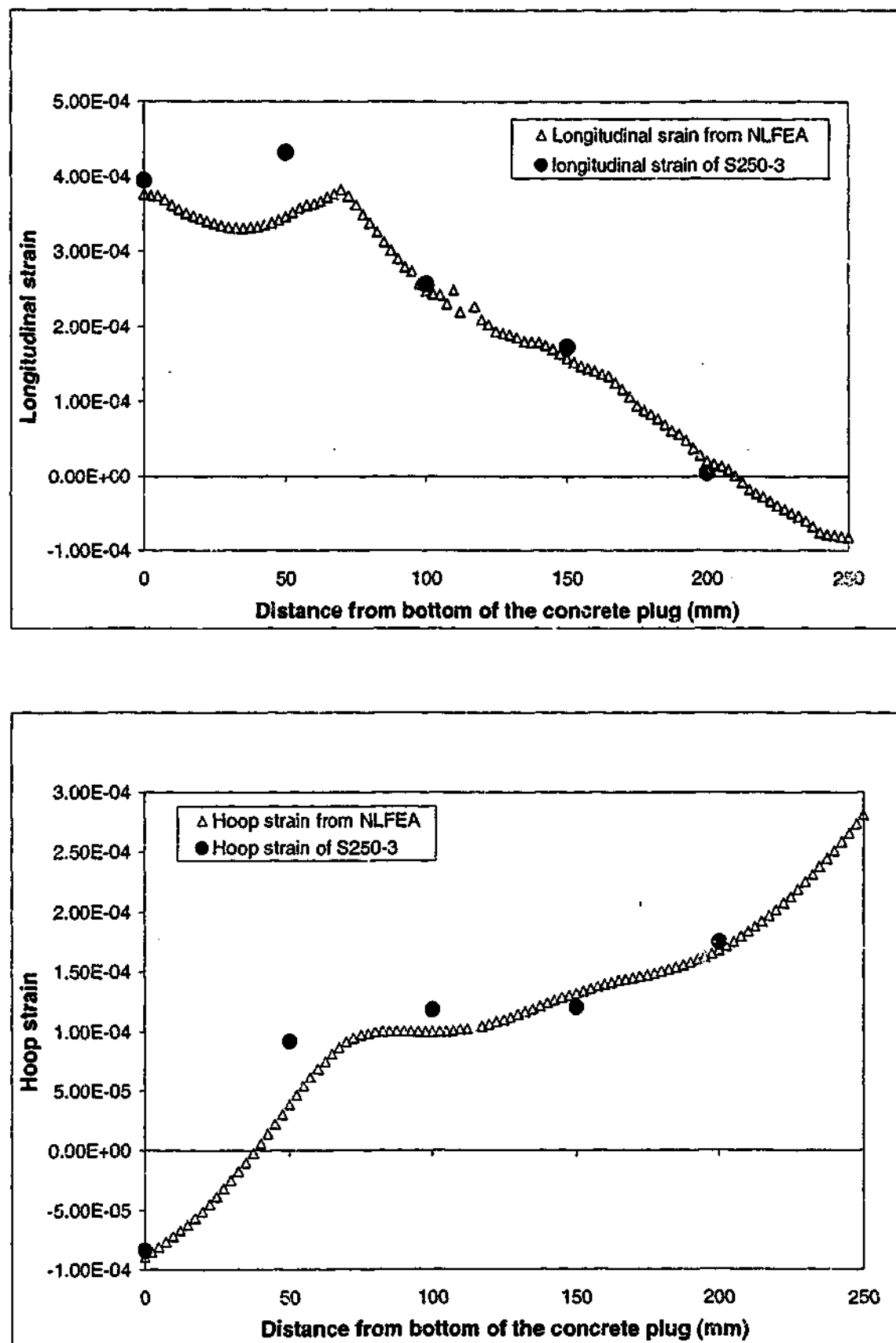
Figure 7-15 Comparison of longitudinal and Hoop strains along the outer surface of the steel tube for specimen S250 of the pull-out test at load level of 662 kN
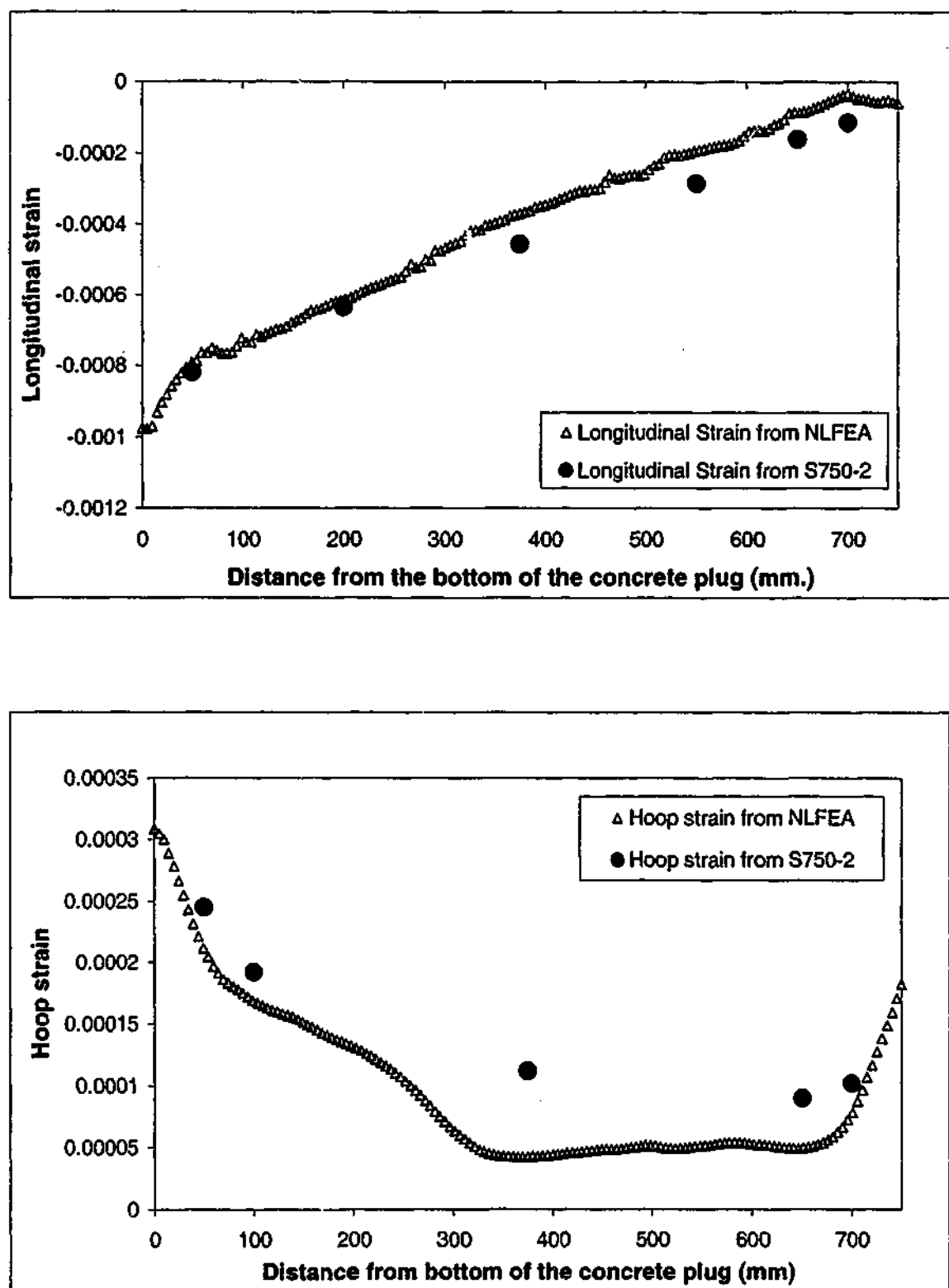
Figure 7-16 Comparison of longitudinal and Hoop strains along the outer surface of the steel tube for specimen S750 of the push-out test at load level of 1452 kN
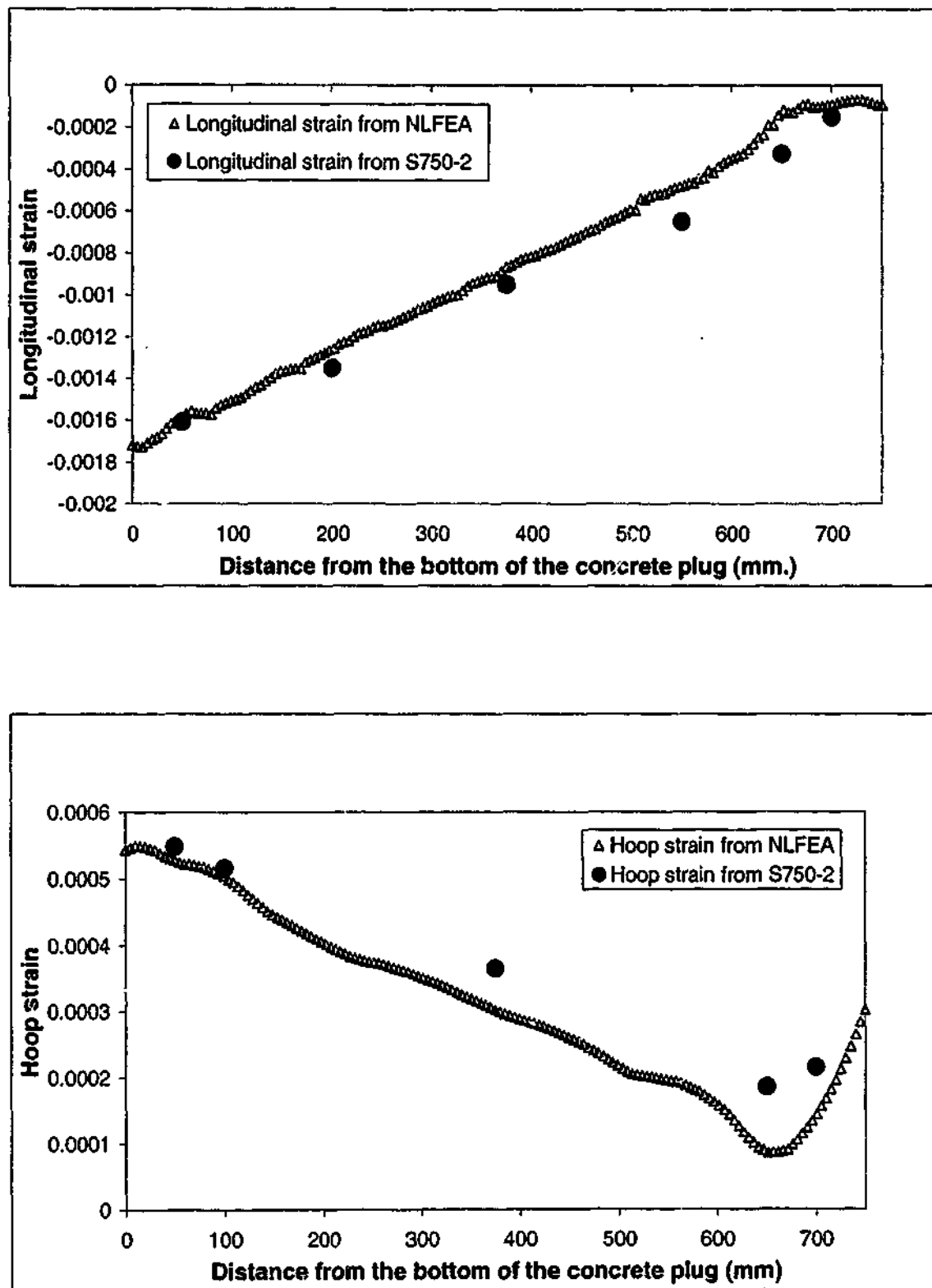
Figure 7-17 Comparison of longitudinal and Hoop strains along the outer surface
of the steel tube for specimen S750 of the push-out test at load level of 2747 kN
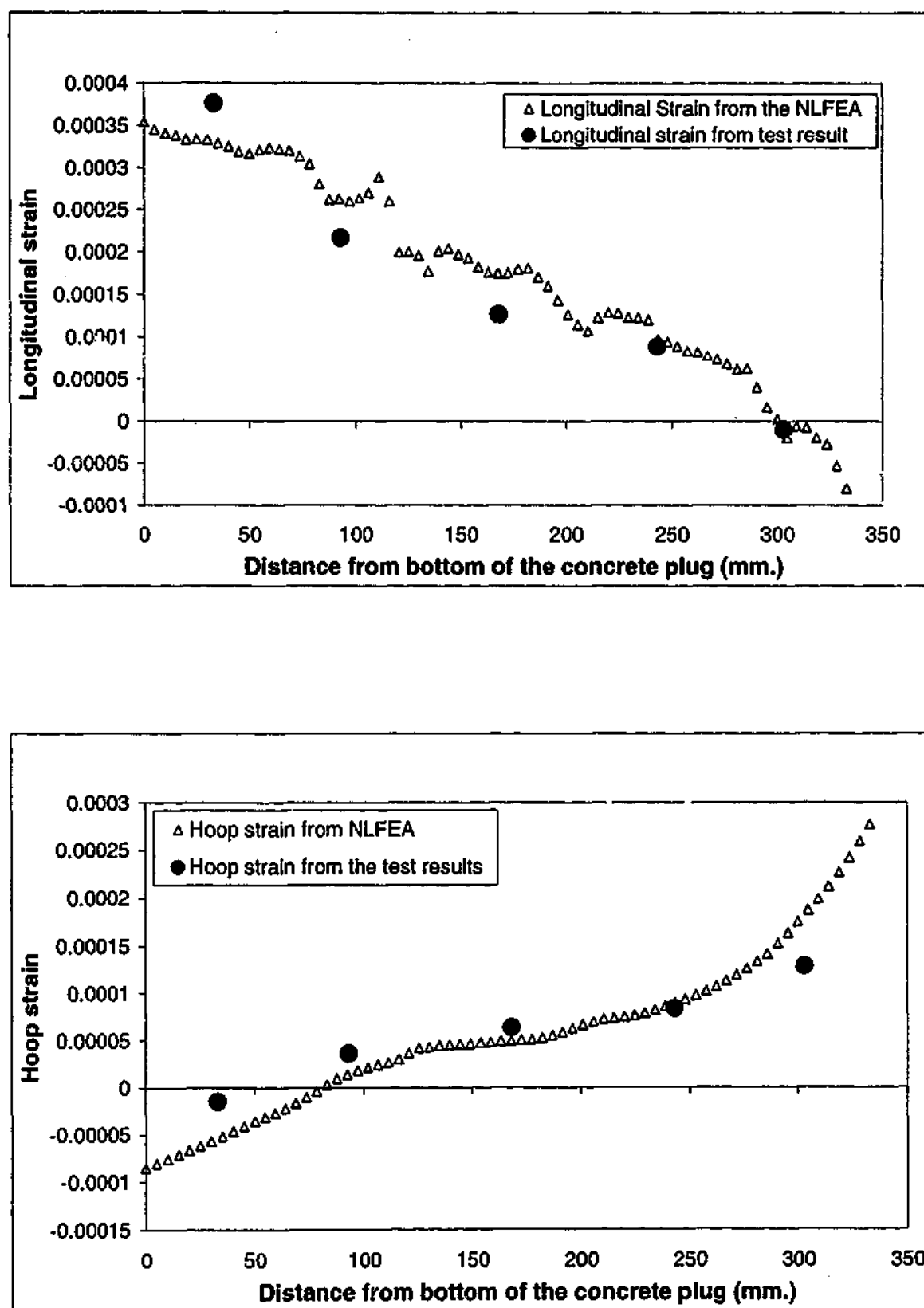
Figure 7-18 Comparison of longitudinal and Hoop strains along the outer surface
of the steel tube for specimen S1.5D of the Stage 1 at load level of 572 kN
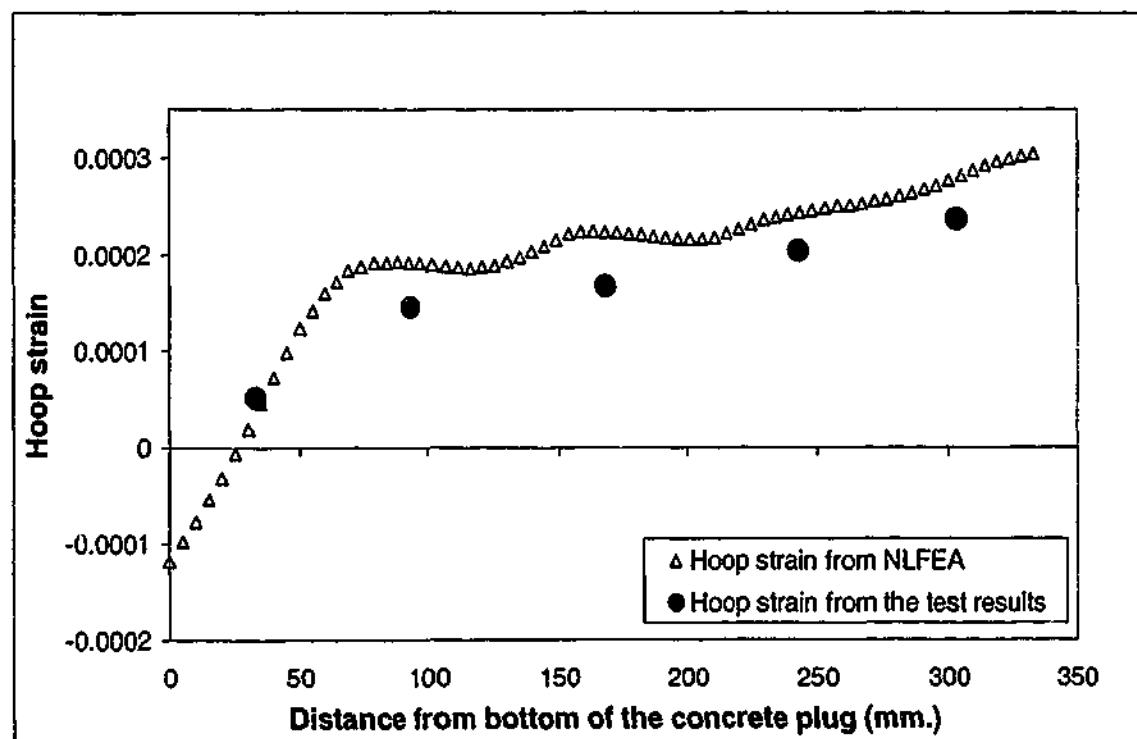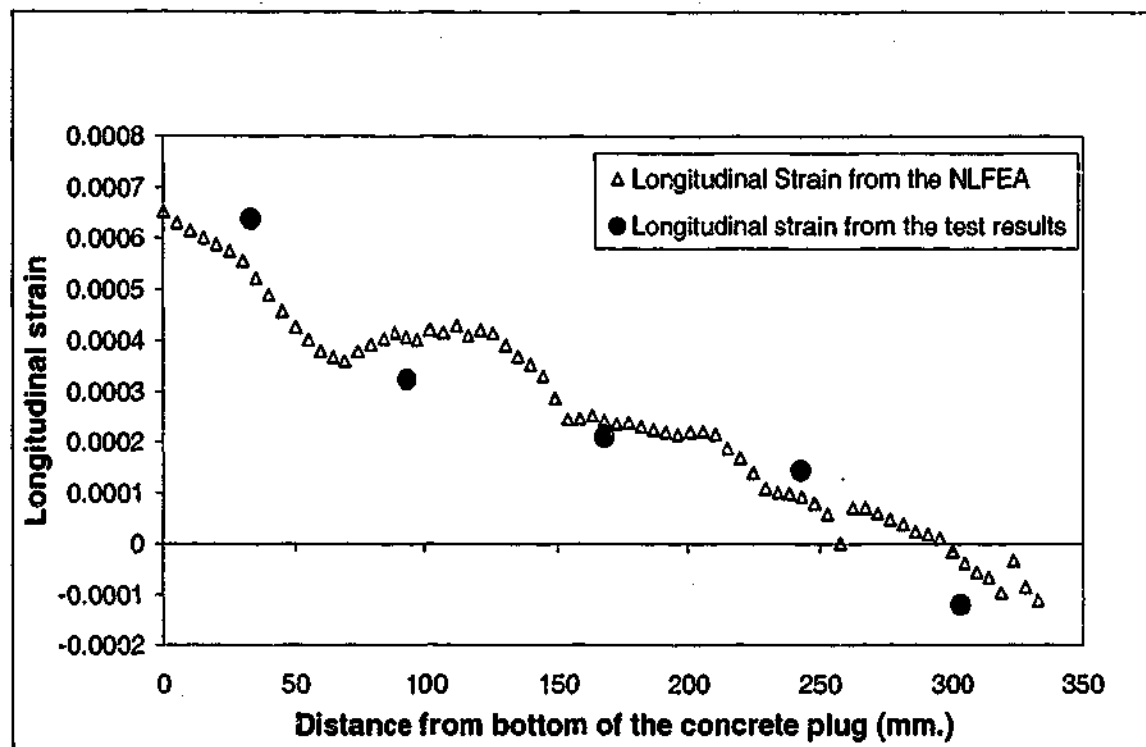
Figure 7-19 Comparison of longitudinal and Hoop strains along the outer surface of the steel tube for specimen S1.5D of the Stage 1 at load level of 1000 kN
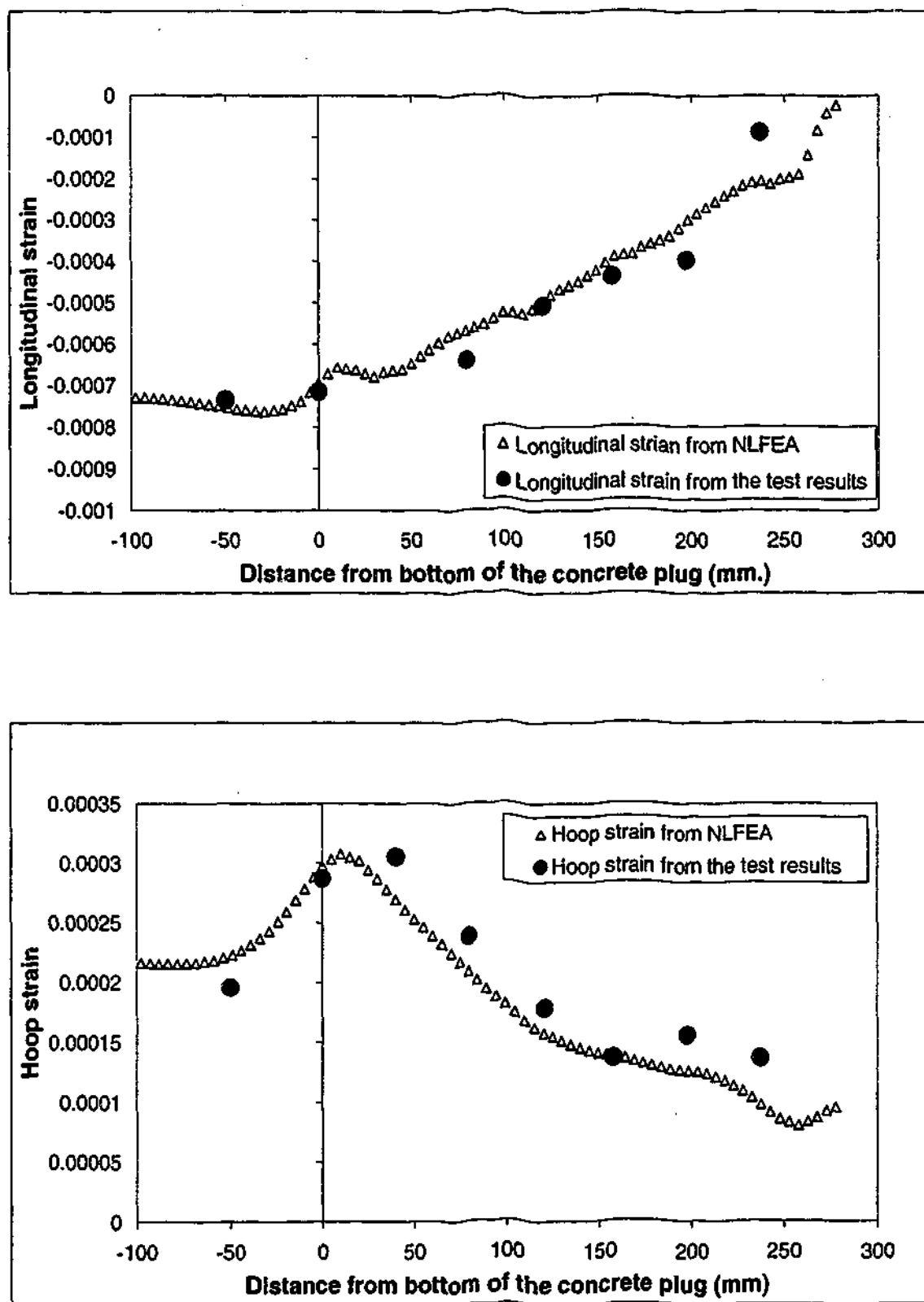
Figure 7-20 Comparison of longitudinal and Hoop strains along the outer surface of the steel tube for specimen S1.25D of the Stage 2 at load level of 222 kN
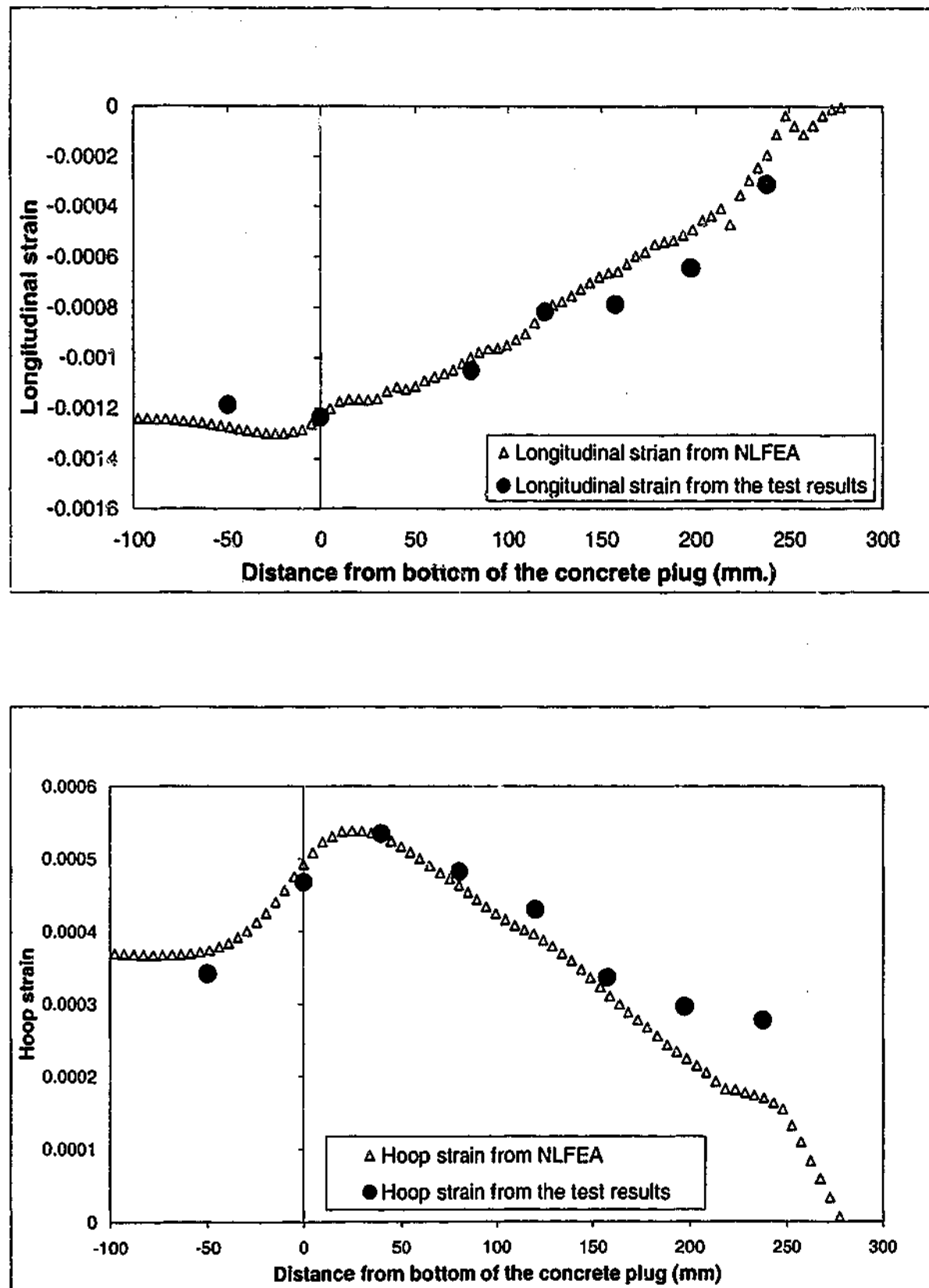
Figure 7-21 Comparison of longitudinal and Hoop strains along the outer surface of the steel tube for specimen S1.25D of the Stage 2 at load level of 440 kN

The load slip response curves indicate that the specimens exhibited a bilinear response of two bond resistance mechanisms of an early micro locking (non-slip action) and later a mechanical interlocking mechanism. The comparisons between numerical and experimental longitudinal and Hoop strains were made first at a load level before change of slope in load slip response (micro locking mechanism) and then at the peak load (mechanical macro interlocking mechanism).

In most cases, gauge readings from the experiments are in better agreement with the numerical model at the peak load. The reason might be the application of the Coulomb friction model for the interface element. In other words, the Coulomb friction model for the pile/plug interface closely predicted the behaviour after the macro mechanical interlocking mechanism became active.

In general, NLFEA has produced results of the longitudinal and hoop strains that follow the trend of the experimental results. The results of the specimens shown above indicate that the strain distributions from the analytical model were close to that of the experimental specimens, thereby providing an opportunity to investigate trends in shear transfer distribution along the interface. Appendix 2 shows the longitudinal and Hoop strain comparisons for all specimens.

7.3.5   Validity of the FEmodel

The finite element models with the material models and properties adopted produced comparable results to the experiment. The numerical peak loads were in very good agreement with the experimental peak loads. The load-slip response, failure mechanisms and longitudinal and hoop strain distributions along the outer surface of the steel tube profiles of the numerical models were similar to the experimental results, with the trends simulated adequately. Therefore, the results of the finite element models are valid. In the sections to follow, the bond stress distribution along the interface is studied and a parametric study is carried out using the models with material properties outlined earlier as the basis for comparison.

7.4   Bond Stress Distribution

The bond strength of a reinforced concrete plug embedded in a steel tube is a function of both chemical adhesion of the steel-concrete interface and mechanical interlock between the concrete core and steel surface. To overcome mechanical interlock a small dilation of the tube occurs as it rides over the asperities of the interface, generating radial contact pressure, which enhances frictional resistance. In addition, in push-out dilation of the concrete plug at the top of the connection due to Poisson's effect, where the compression in the concrete is high, and in the steel low, enhances radial pressure and therefore frictional resistance. At the base contact pressure between concrete and steel is reduced, due to Poisson's effect, and effective bond is therefore reduced at this location.

In the pull out case, the reverse is expected to occur. That is, near the base of the concrete plug, the steel tube contraction is much higher than that of the concrete core, causing it to grip the concrete plug. Near the top part of the plug, the tension force is transferred to the concrete through the reinforcing bars embedded in the concrete core and in the pile cap. The tensile stresses that develop in the concrete core result in contraction of the concrete, while the steel tube contraction is relatively small. This should result in separation occurring between the steel tube and the concrete. Considering the fact that deformed bars are used as reinforcement, the ribs on the bars tend to impart wedge pressure on the outer concrete layer, causing dilation of this layer. This dilation enhances the frictional stresses between the steel tube and the concrete along of the length equal to embedment of the longitudinal reinforcement from the top of the specimen.

Consider that the steel tube is subjected to radial contact forces along an arbitrary circle of the tube. Because of the symmetry of such loading, every section normal to the axis will remain circular, while the radius R will undergo a change $\Delta R = y$, varying along the length of the plug. The radial displacement y can be regarded as deflection for a longitudinal element of the tube, and hence it is seen that the

assumed loading will set up bending stresses in the longitudinal elements. This situation is analogous to the case of beams on elastic foundations (Heteyni, 1964).

Figure 7-22 to Figure 7-25 show computed longitudinal and circumferential bending moment along the steel tube at selected load levels for one specimen of each experimental set. Appendix 3 shows computed longitudinal and circumferential bending moment along the steel tube for all specimens in two load levels each.

It can be seen that mechanical macro interlock mechanisms at the top and bottom of the specimens caused the radial pressure on the steel tube. The differential of radial pressure along the steel tube applied longitudinal bending moment on the tube. Since the bending of the tube wall is a plane strain environment, it follows that $M_c = -\mu M_y$ in the circumferential ring, where M_y is the longitudinal bending moment and μ is Poisson's ratio for the steel tube. The analytical model clearly demonstrated this phenomenon.

Distribution of bending moment along the steel tube indicates that at an early stage of loading, the pronounced Poisson's ratio effect increases radial contact stress and mechanical interlock at the top and bottom of the interface. In pull-out at top, the dilation of the concrete increased the contact pressure between the steel bars and the steel tube, due to the wedging action exerted by the deformed steel bars against the concrete layer.

The bending moment distribution at ultimate load level indicated that the diagonal tension crack had formed and extended in the concrete layer between the longitudinal reinforcement and the steel tube before the failure of the specimens.

It should be noted that the measured longitudinal and Hoop strains on the outer surface of the steel tube from the experiment is due to the axial pull out force, together with longitudinal bending moment along the steel tube. Therefore, the measured strain could not be used to obtain the bond stress distribution along the interface.
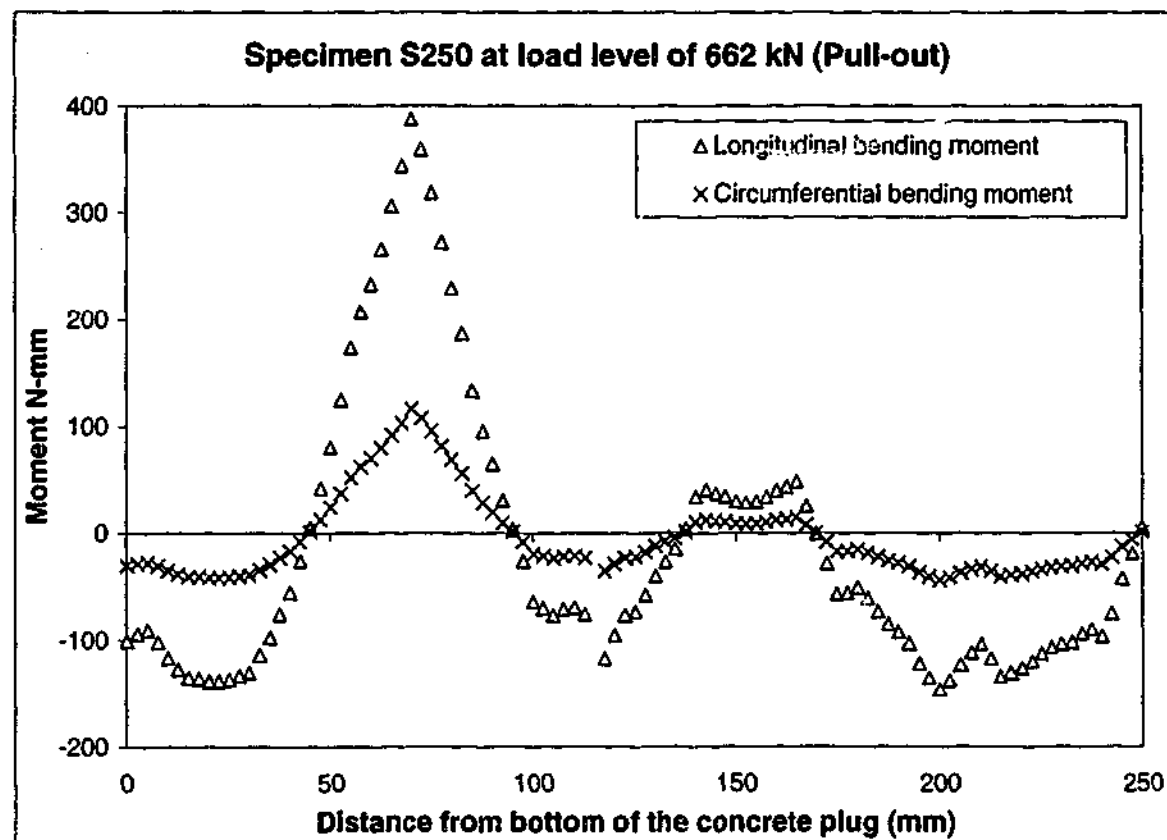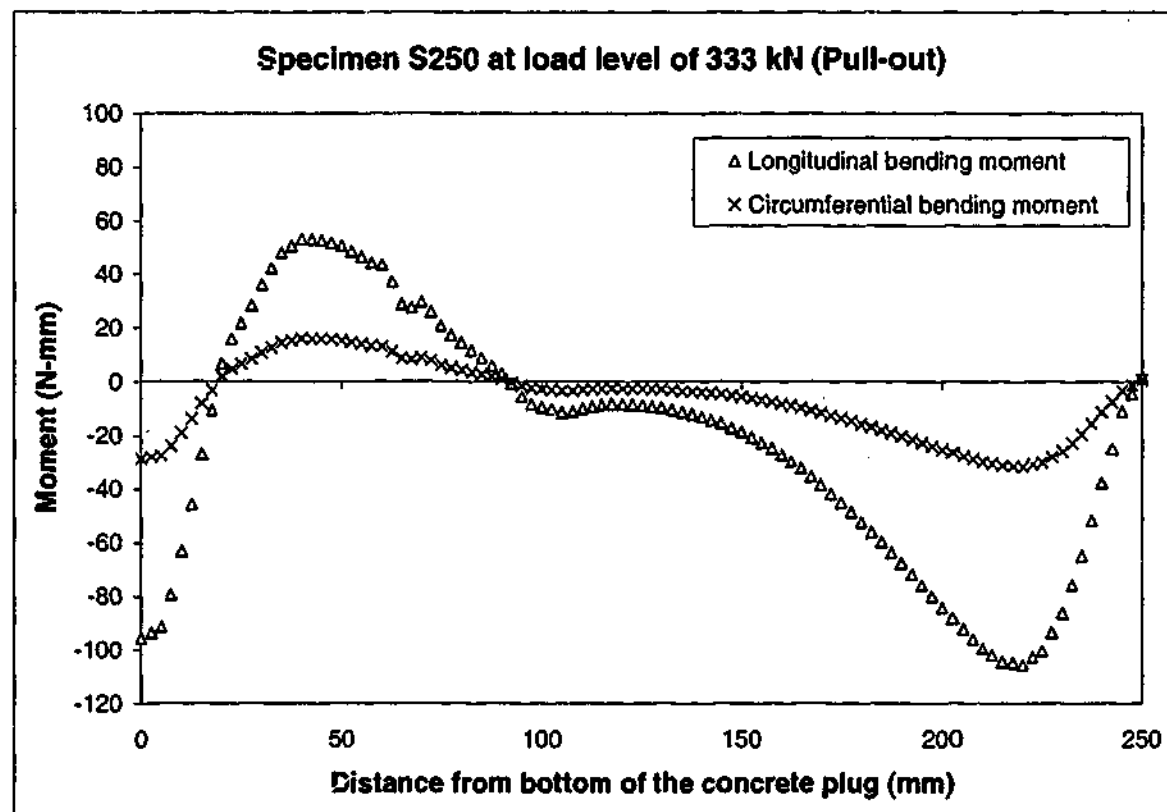
Figure 7-22 Bending moment distribution along the steel tube for specimen S250
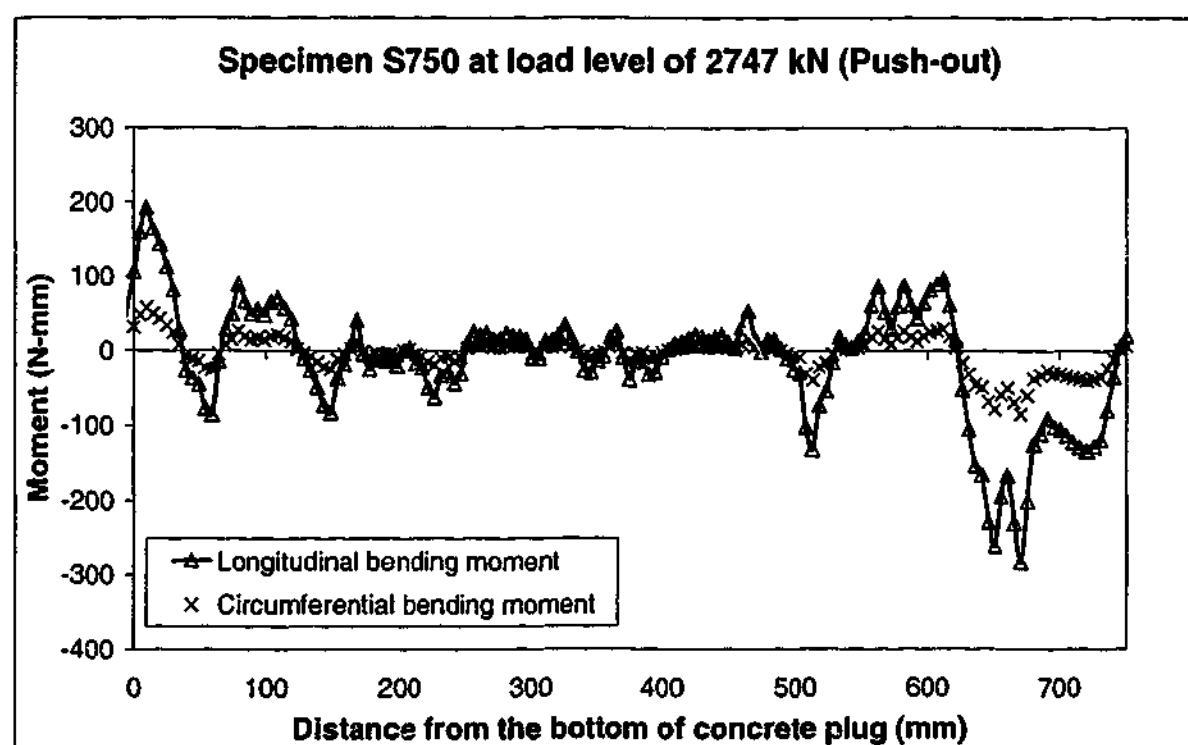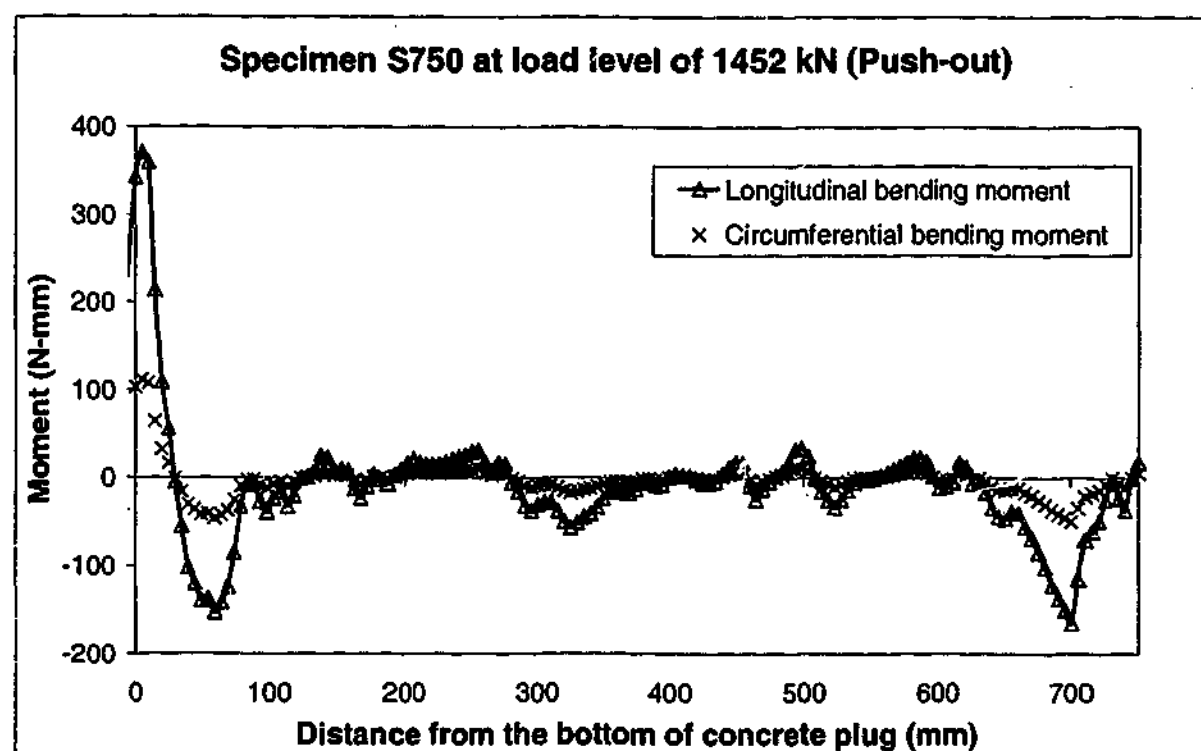
of the pull-out test

Figure 7-23 Bending moment distribution along the steel tube for specimen S750 of the push-out test
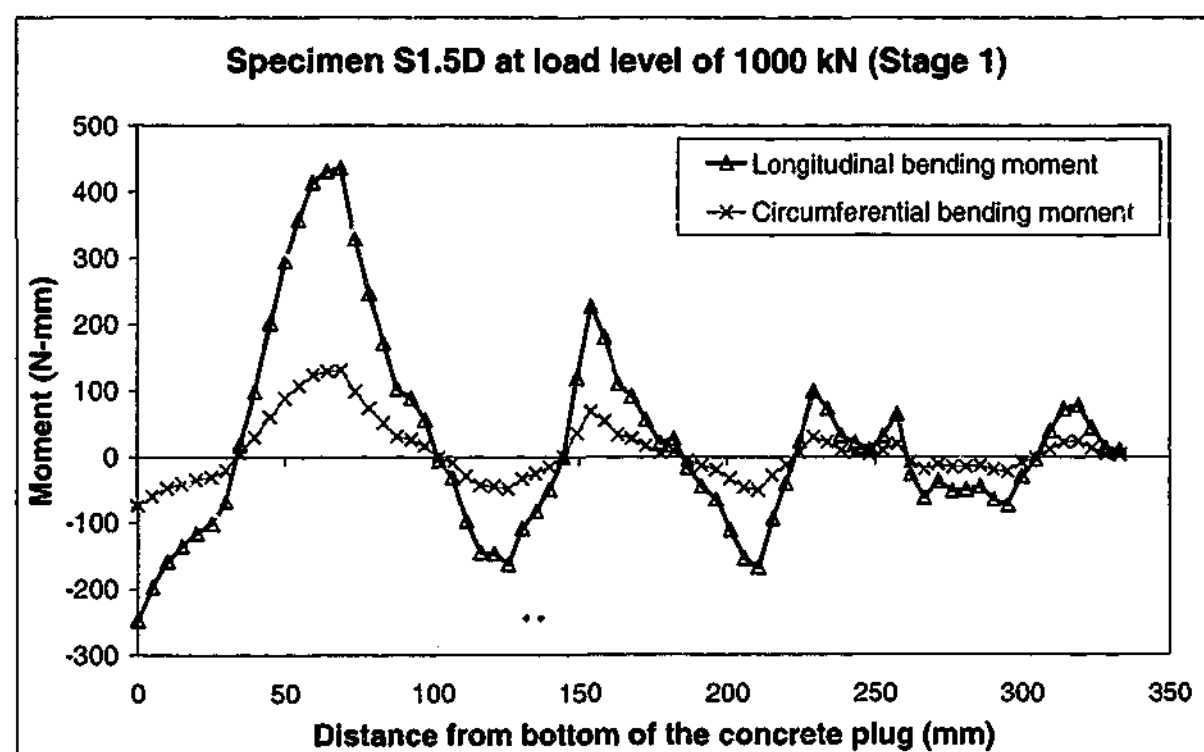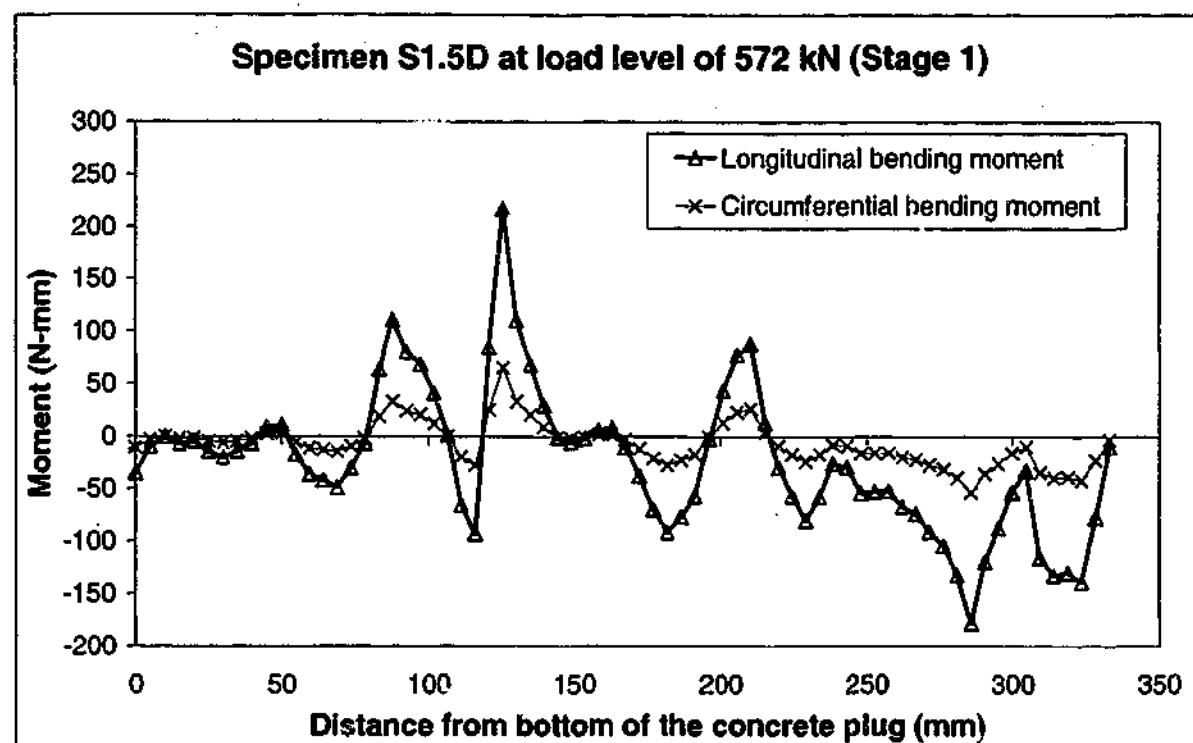
Figure 7-24 Bending moment distribution along the steel tube for specimen S1.5D
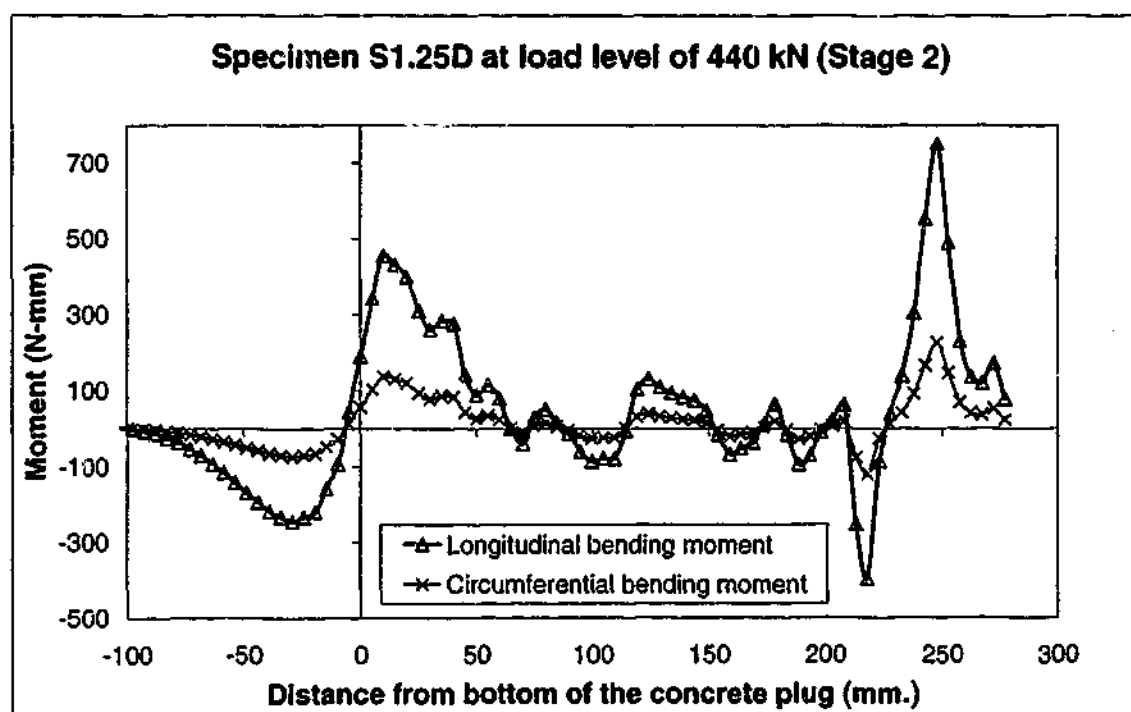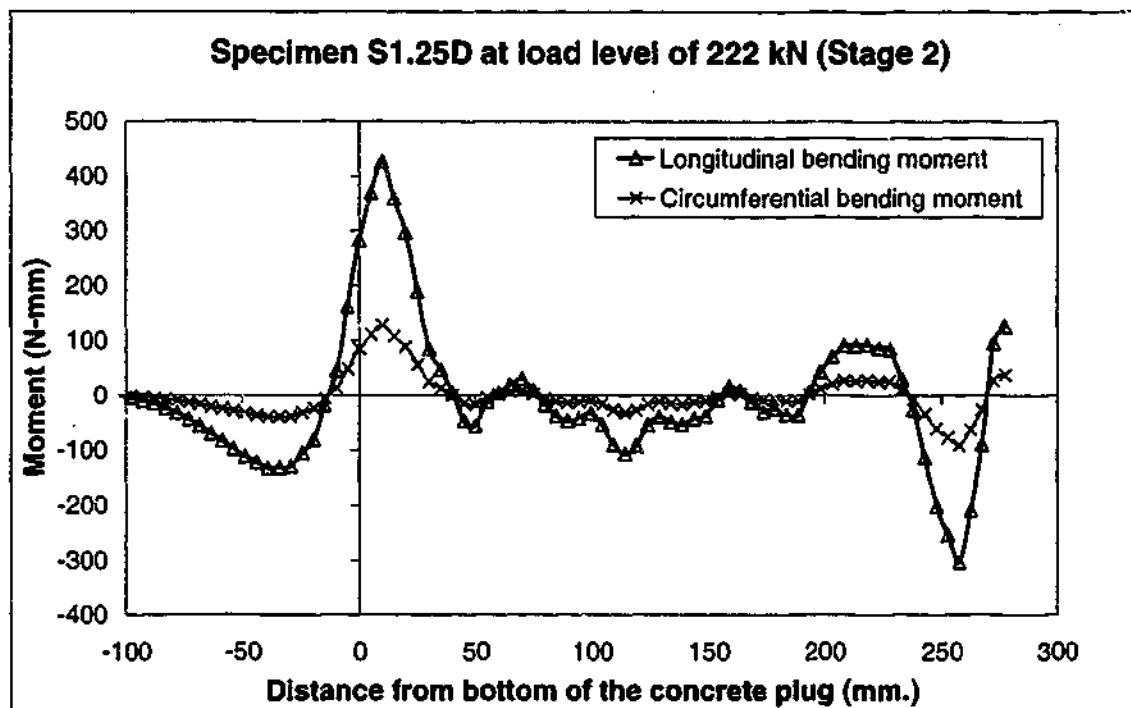
(Stage 1)

Figure 7-25 Bending moment distribution along the steel tube for specimen S1.25D (Stage 2)

To calculate the bond stress distribution along the interface, longitudinal stress along the steel tube at outer surface, centre line and inner surface of steel tube's wall are plotted. Figure 7-26 to Figure 7-29 illustrate the computed longitudinal stress distribution for one specimen for each experimental set. Appendix 4 shows the longitudinal stress distribution for all specimens at ultimate load level and at load level of changing the slope of load-slip response. The longitudinal stress distributions are shown at outer and inner surfaces and centre of the steel tube's wall. The stress distribution at the outer and inner surfaces of the steel tube cannot present the bond stress distribution due to the effect of bending moment. The stress distribution at the centre of the steel tube wall is used to determine the shear/bond stress distribution along the interface.

In the pull-out case, there is little shear transfer at the top of the specimens at an early stage, which indicates that the main mechanism is the pronounced Poisson's effect increasing radial contract stress at the base of the concrete plug. The longitudinal stress distributions at ultimate load level show that the cracking of the concrete at the base of the concrete plug due to tension splitting, reducing the shear transfer. The main mechanism which is believed to contribute to the bond strength in pull out tests was the dilation of the concrete due to the wedge action exerted by the deformed steel bars against the concrete layer between the steel bar and the steel tube. For the push-out tests and specimens with longer length of concrete plug, the longitudinal stress distributions illustrated almost a uniform bond stress distribution along the steel tube.

In general, the results of longitudinal stress distribution from the NLFEA at the centre of the steel tube's wall show almost a linear distribution along the length of the tube. Therefore, it can be adopted and idealized that the shear/bond stress distribution is a uniform distribution along the interface, particularly at ultimate load level. The slope of the longitudinal stress distribution along the steel tube at the centre of the steel tube's wall can be used to determine the value of uniform bond stress between the steel tube and the concrete plug along the pile/plug interface.
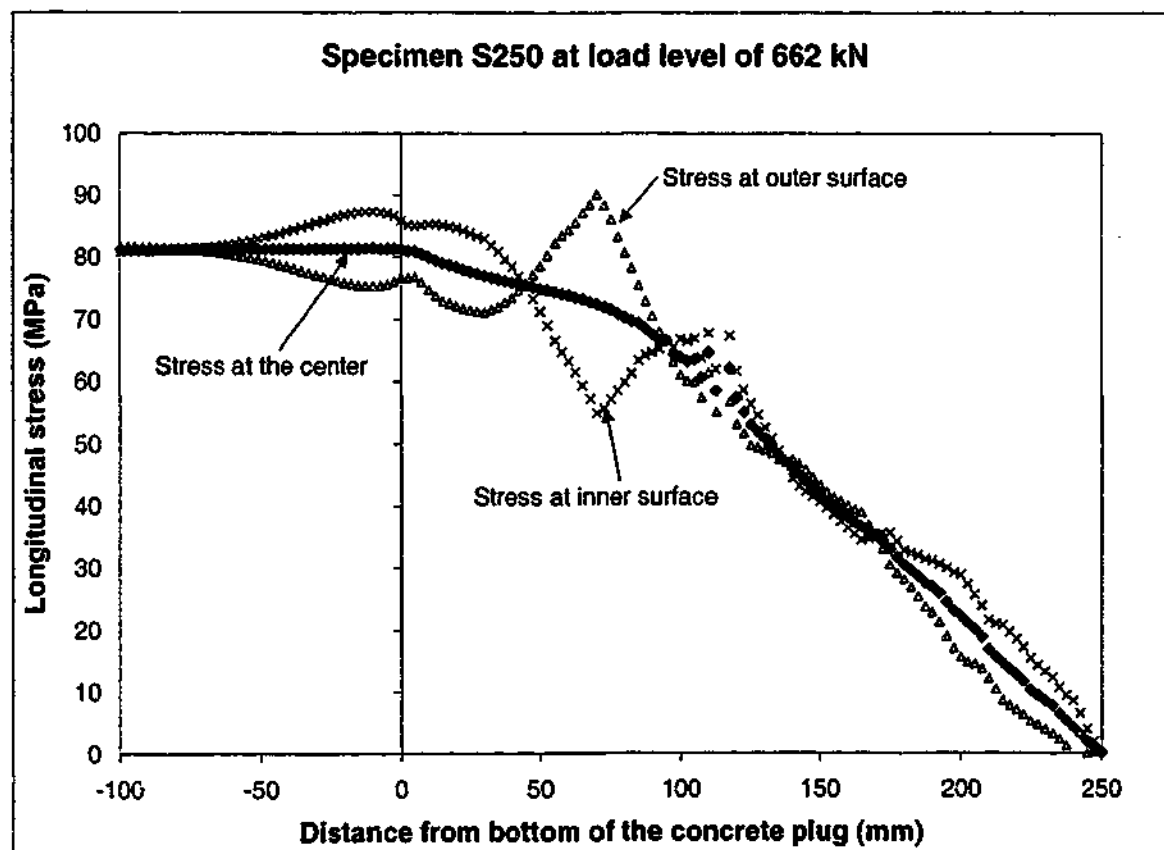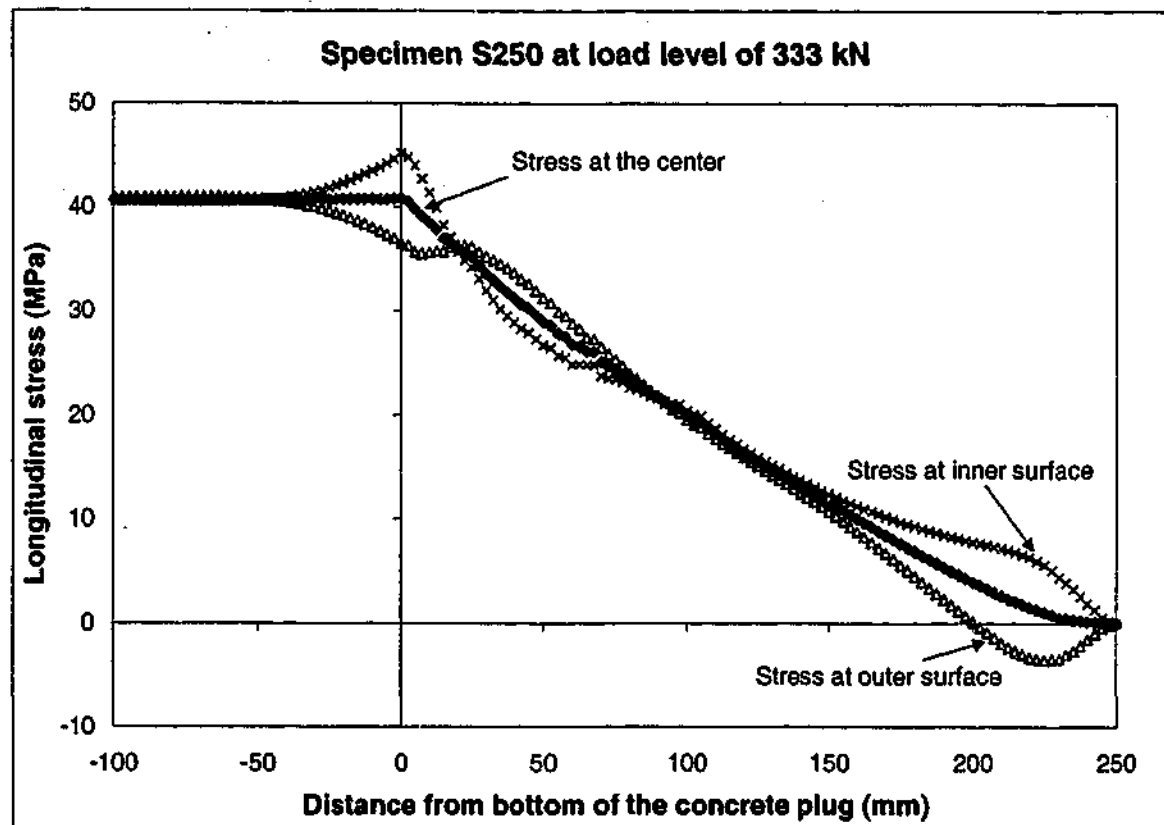
Figure 7-26 Longitudinal stress distributions along the steel tube for specimen
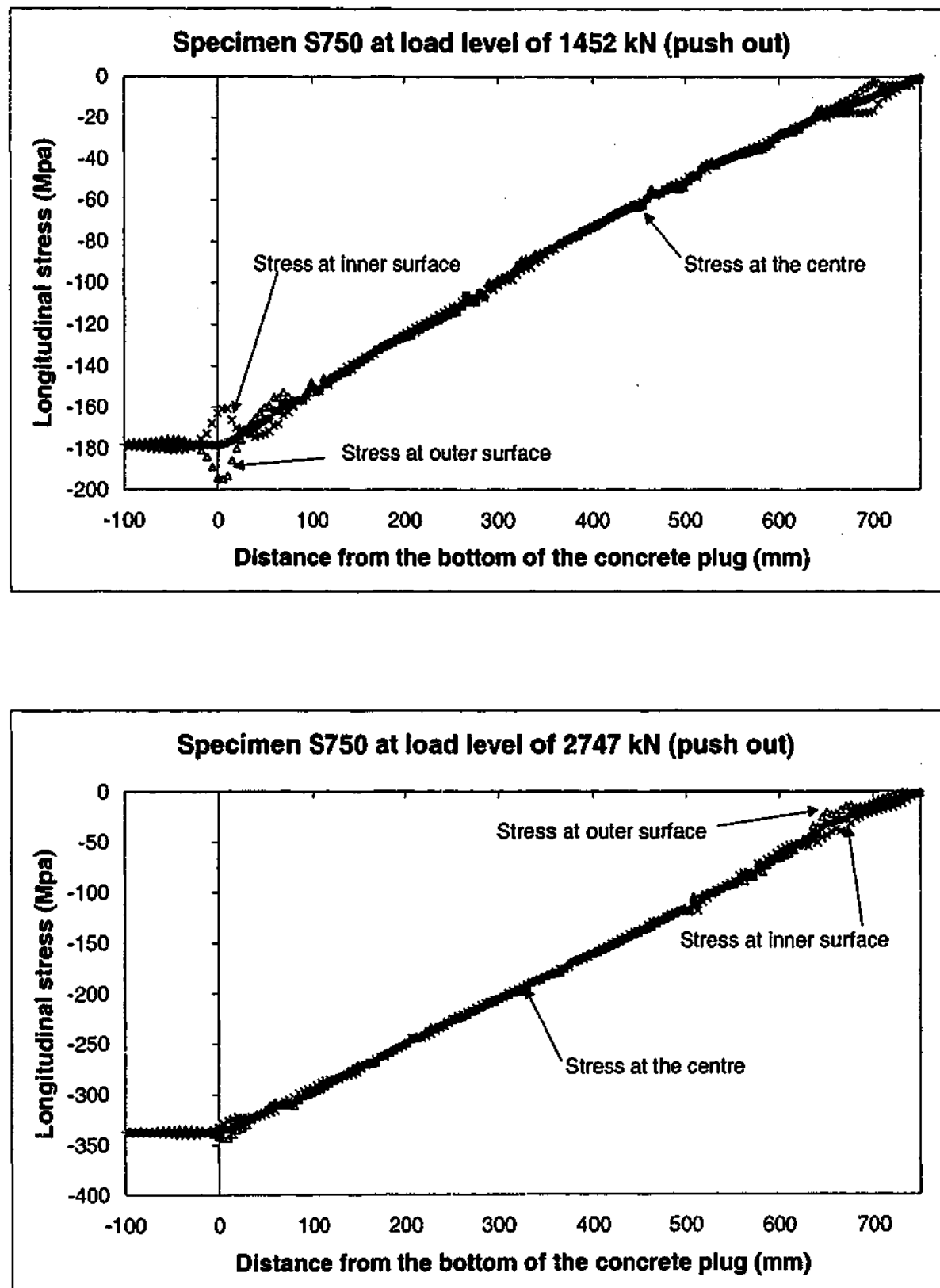S250 of pull-out test

Figure 7-27 Longitudinal stress distribution along the steel tube for specimen S750 of push-out test
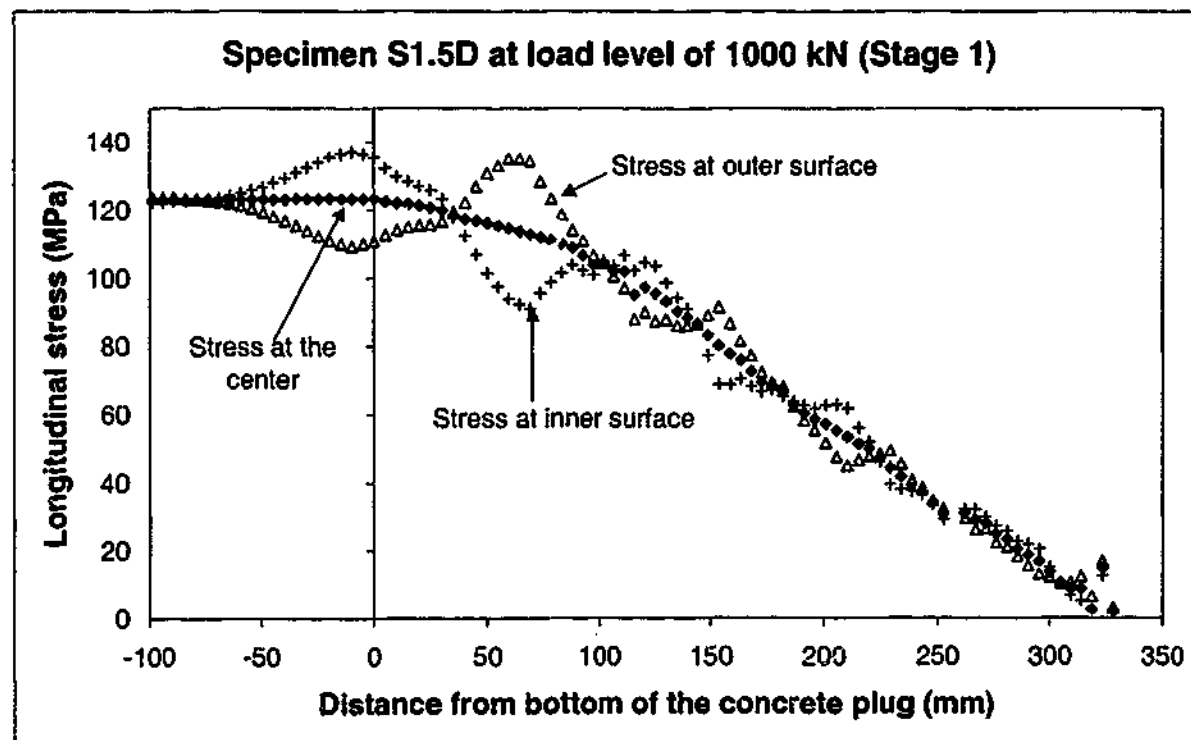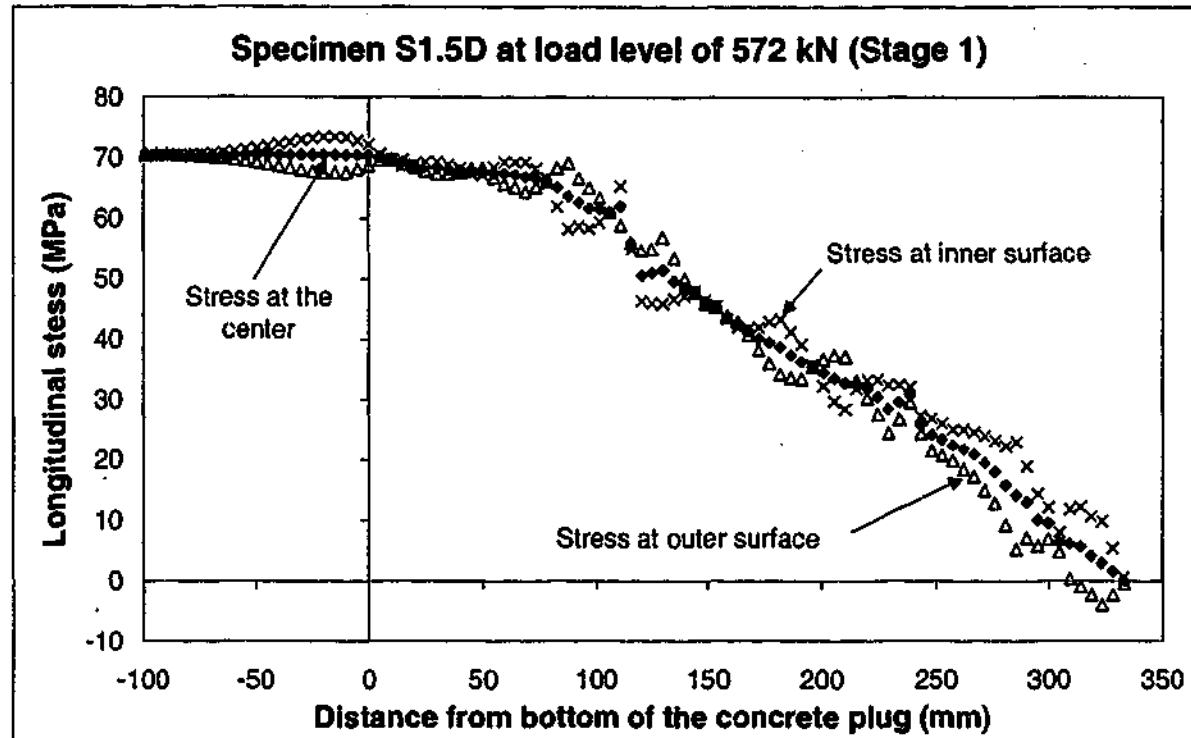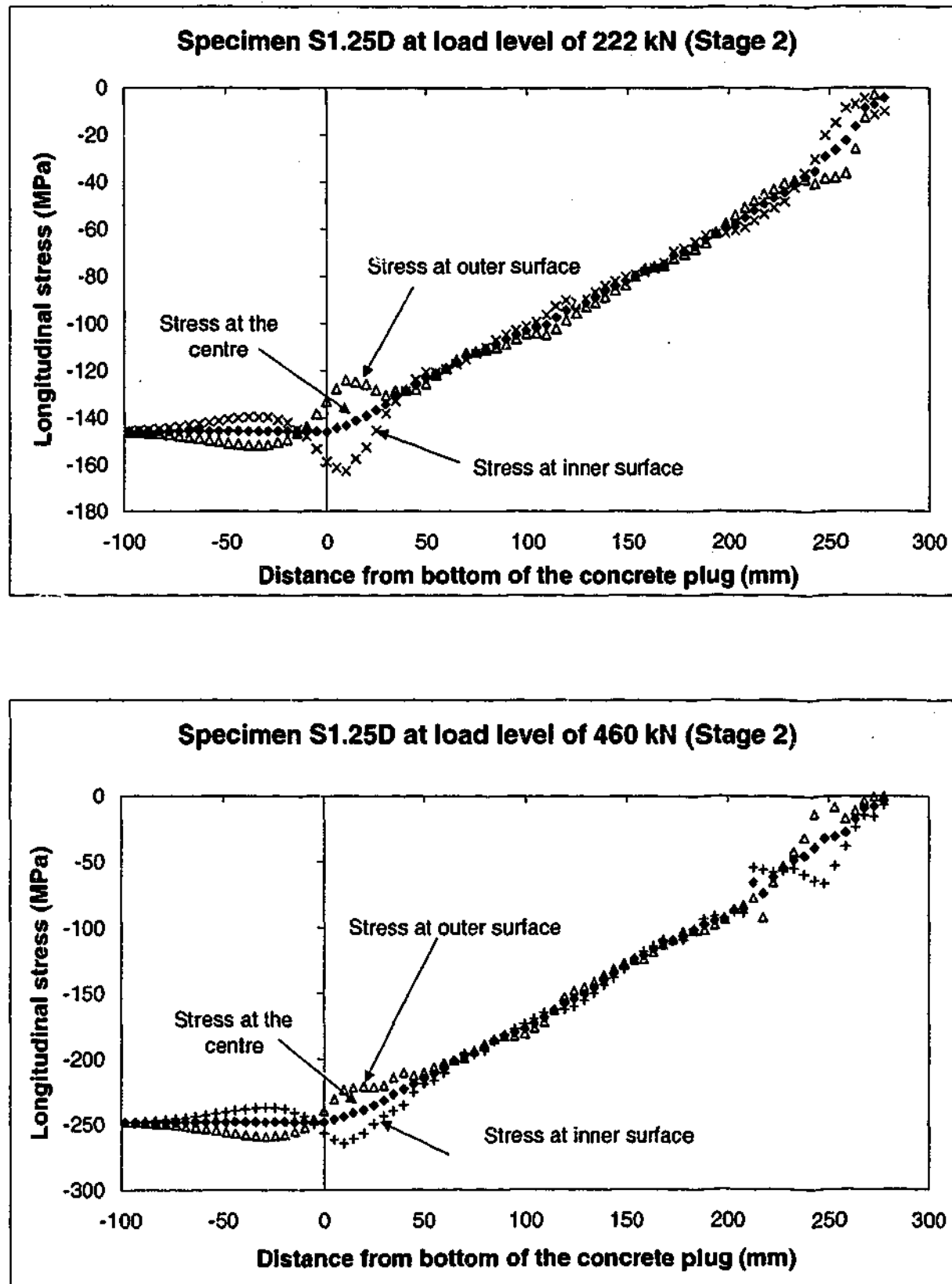
Specimen S1.5D at load level of 572 kN (Stage 1)

Specimen S1.5D at load level of 1000 kN (Stage 1)

Figure 7-28 Longitudinal stress distribution along the steel tube for specimen

S1.5D of Stage 1 test

Figure 7-29 Longitudinal stress distribution along the steel tube for specimen S1.25D of Stage 2 test

Examination of the results of NLFEA from the modelling of the specimens tested as part of the experimental work in this research indicates the following:

1. The ultimate strength predicted by the numerical simulation is in close agreement with the values obtained from the experimental work.

2. The numerical solution scheme predicts load-slip response of the specimens with close agreement. For some of the specimens, NLFEA predicted a stiffer response at the early stage of non-slip mechanism.

3. Failure pattern, obtained from numerical simulation are un close agreement with the failure mechanisms observed in experimental work (Chapters 3 and 5).

4. The NLFEA solution procedure has shown reasonable correlation in the prediction of longitudinal and hoop strain along outer surface of the steel tube. The numerical analysis showed that the measured longitudinal and Hoop strains on the outer surface of the steel tube from the experiment is due to the axial pull out force, together with longitudinal bending moment along the steel tube.

5. The numerical solution procedure has shown that a uniform shear/bond stress distribution can be adopted particularly at ultimate load level. The slope of the longitudinal stress distribution along the steel tube at the centre of the tube's wall can be used to determine the value of uniform bond stress between the steel tube and the concrete plug along the pile/plug interface.

7.5 Parametric Study on the Aspect Ratio of Steel Tube

Since good correlation between NLFEA and the test results was obtained in regards to the ultimate strength, load-slip response and longitudinal and Hoop strain, the solution scheme was applied to specimens identical to those of the experiments but without the unintentional variations in the material properties. This study investigates the effect of varying the aspect ratio of the steel tube on the ultimate strength and load-slip response of the specimens outlined in Section 6.7. The failure, ultimate strength and slip were determined based on the criterion used for the base models described earlier.

As established in Section 7.3.2, the load slip curves give an indication of the bond mechanisms and behaviour of the concrete plug in the steel tube that is predicted by implementation of the NLFEA procedure. Figure 7-30 to Figure 7-33 illustrate the load-slip relationship produced from the numerical models for one specimen from each experimental set with aspect ratio of 15 to 40 for steel tube. Appendix 5 shows the produced load-slip response form NFLEA for all specimens with aspect ratios of 15 to 40.

It can be seen that the specimens with higher aspect ratio show smaller relative slip at the same displacement increments. Consequently, the relative slip between the concrete plug and the steel tube at the end of the numerical procedure is smaller for higher aspect ratios. This was due to the lower circumferential stiffness of the steel tube with higher aspect ratio, which allows the concrete plug and the steel tube to expand laterally and reduce longitudinal deflections.

The load-slip curves also indicated that the specimens with shorter concrete plug length and higher shrinkage are more sensitive to variation of the aspect ratio of the steel tube.
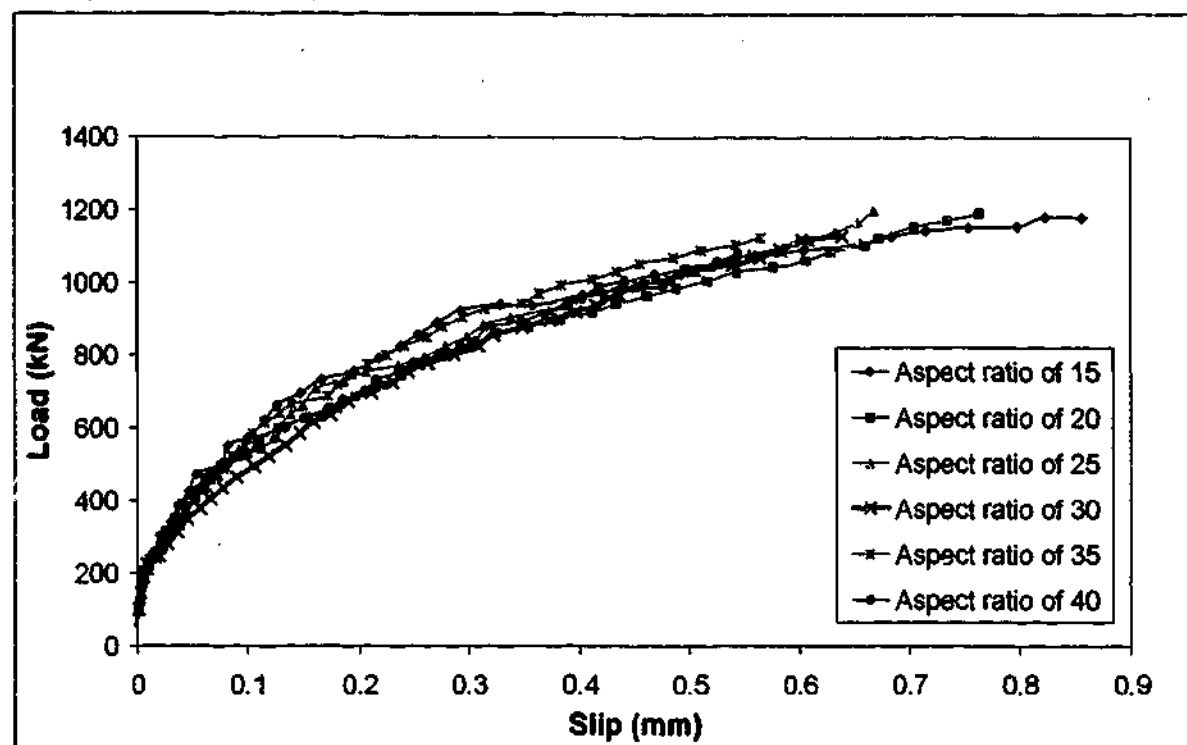
Figure 7-30 Load-slip behaviours of varying the aspect ratio of the steel tube for specimen S500 in pull-out test
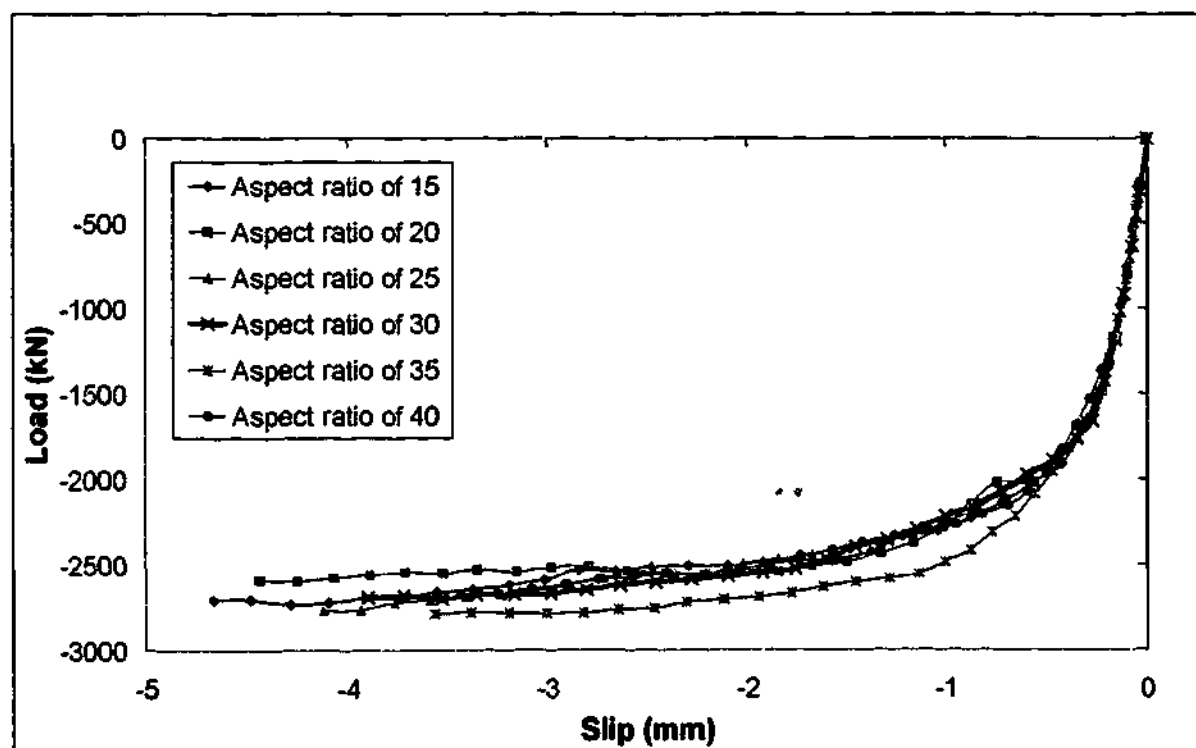
Figure 7-31 Load-slip behaviours of varying the aspect ratio of the steel tube for specimen S750 in push-out test
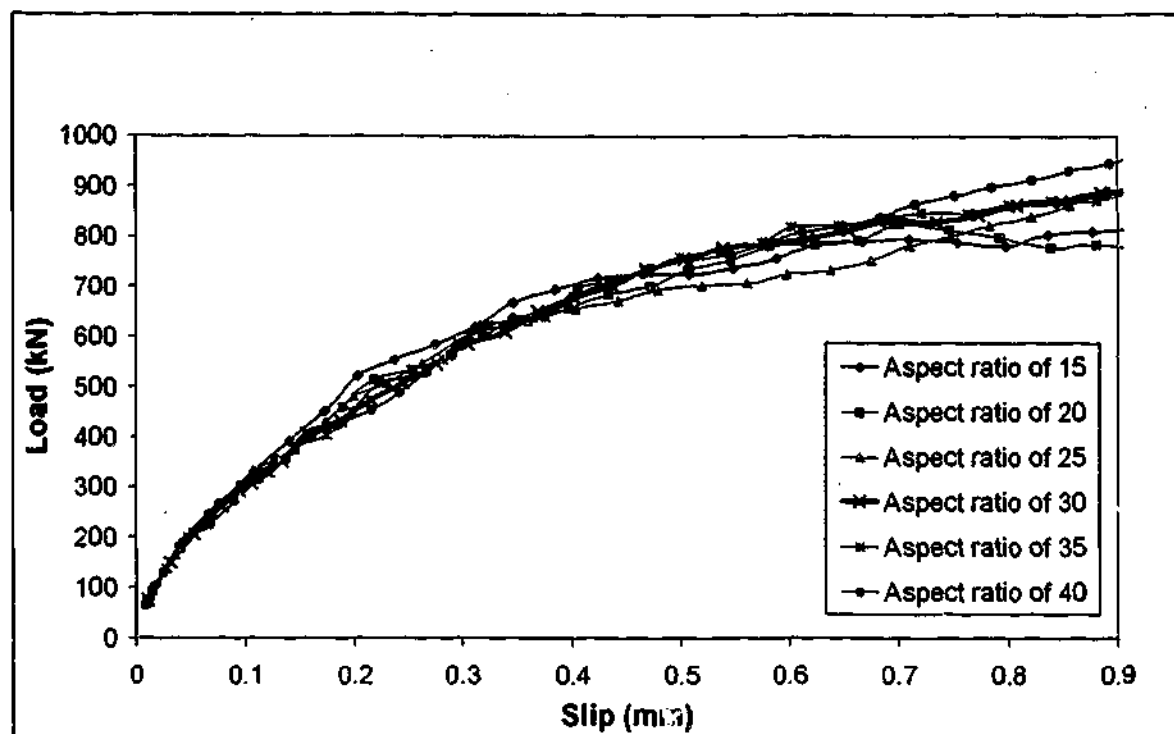
Figure 7-32 Load-slip behaviours of varying the aspect ratio of the steel tube for specimen S1.5D in Stage1 test
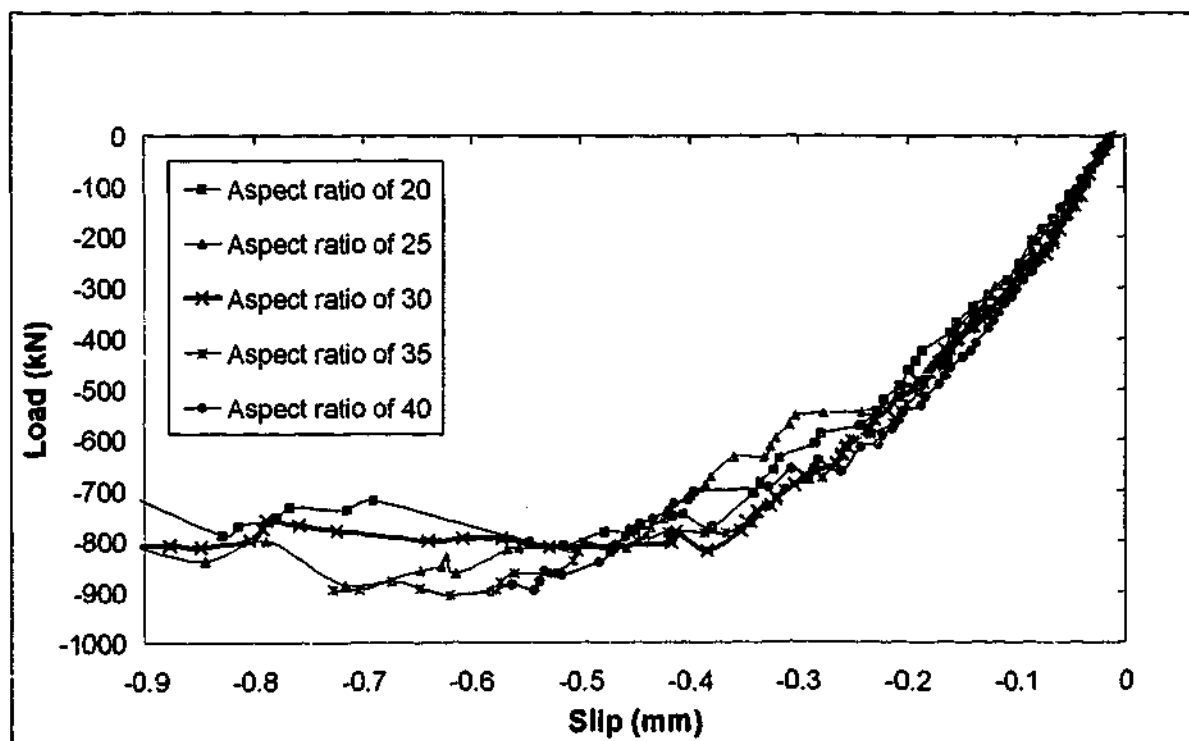

Figure 7-33 Load-slip behaviours of varying the aspect ratio of the steel tube for specimen S750 in push-out test

In general, the solution procedure does not predict any significant variation in the ultimate strength of the specimens due to variation of the steel tube aspect ratio of 15 to 40. It can also be seen that the load slip responses of specimens with aspect ratios ranging from 15 to 40 exhibited a similar trend. The solution scheme predicts a smaller relative slip for specimens with the greater aspect ratio. However, it might be concluded that the variation of the steel tube aspect ratio ranging from 15 to 40 has no major influence on ultimate strength and load slip behaviour of the concrete plug embedded in the tubular steel pile.

7.6   Conclusions From the Finite Element Analysis

The above sections presented an investigation into the suitability of non linear finite element analysis to predict the response of concrete plugs embedded into the steel tubular piles subjected to a pull-out or push-out load regimes. The study examined the sensitivity of the solution scheme to combinations of the material models that described the tension and compression response and shrinkage of the concrete as well as the frictional behaviour of the interface and displacement increment on the solution obtained. Once the optimum combination of these was established, the procedure was implemented to investigate the accuracy of predicting ultimate strength, load slip response, failure mechanisms and longitudinal and Hoop strains along the steel tube as compared with the experimental work. After the capabilities and limitations of the numerical scheme were established, it was applied to a set of specimens with only the aspect ratio of the steel tube as the variable. The following were concluded from this study:

1. The accuracy of the scheme and the prediction of the load deflection response are highly dependent on the choice of the frictional behaviour of the interface and shrinkage of the concrete. It is concluded that an application of a combination of the crack model and shrinkage based on European code of MC1990, for the concrete and Coulomb friction model for the interface are most suited to the specimen above.

2. The ultimate strength results predicted from NLFEA modeling of the experimental specimens are in a very close agreement with those recorded during the experimental work.

3. NLFEA predicted a failure mechanism, particularly in pull-out cases, consistent with those observed from the experimental specimens as evidenced by examining the completely pulled out concrete plugs.

4. NLFEA produced good predictions of longitudinal and hoop strains on the outer surfaces of steel tubes. It appears that the numerical solution predicted the strain distributions with better agreement at the ultimate load level.

5. NLFEA has shown that mechanical macro interlock mechanisms at the top and bottom of specimens caused the radial pressure on the steel tube. The differential of radial pressure along the steel tube applied longitudinal and circumferential bending moment on the tube. The measured longitudinal and Hoop strains on the outer surface of the steel tubes are due to the axial pull out force, together with longitudinal bending moment along the steel tube.

6. NLFEA has shown that the longitudinal stress distribution at the centre of the tube's wall is almost a linear distribution along the length. Therefore, it can be assumed that the shear/bond stress distribution is a uniform distribution along the interface particularly at ultimate load level.

7. NLFEA predicts that varying the aspect ratios of the tubes from 15 to 40 has no significant effect on ultimate strength and load slip response of a concrete plug.

8   BOND STRENGTH FORMULATION

8.1   Introduction

In the 'Pull-out and push-out tests' (Chapter 3) and 'Presentation of cyclic loading test results' (Chapter 5), the OTO's formulation (2001) was adopted to calculate bond stress between the concrete plug and the steel tube. The bond stress was assumed to be distributed uniformly around the inside diameter and along the interface. This was also suggested by NLFEA results.

The following formulation was suggested to calculate characteristic bond strength

$$f_{buc} = 9KC_l C_s (f_{cu})^{1/2}$$ (8-1)

where:

f_{cu} is the characteristic concrete compressive strength (in N/mm^2)

K is the stiffness factor defined below

$$K = \left[m(D/t)_g\right]^{-1} + (D/t)_p^{-1}$$ (8-2)

Where:

m is the modular ratio of steel to plug

D_p is the pile diameter

t_p is the pile wall thickness

To adopt OTO's(2001) recommendations for this study, diameter to thickness of the concrete layer between steel bars and steel tube is taken as $(D / t)_g$. The modular ratio of m is also taken as $E_{steel} / E_{concrete} = 5.5$ (short term loading)

C_l is the coefficient for plug length to pile diameter ratio

The available data on the parameter C_l are limited. In the absence of data relating to a specific tubular geometry and with regard to the test results of previous pull-out and push out tests (Chapter 3), the following values of C_l were assumed:

$$L/D_p \qquad C_l$$

$$< 1.50 \qquad 1.0$$

$$1.5 - 3.0 \qquad 0.9$$

$$> 3.0 \qquad 0.8$$

where L is the plug length.

Table 8.1 Calculated factors and bond strength from formulation

SPECIMEN	K	L/D	C_L	COMPRESSIVE STRENGTH (MPA)	C_S	BOND STRESS MPA
S250-1	0.1	1.06	1.0	50	0.6	4.07
S250-2	0.1	1.06	1.0	50	0.6	4.07
S250-3	0.1	1.06	1.0	50	0.6	4.07
S750-1*	0.1	3.37	0.9	50	0.6	3.46
S750-2*	0.1	3.37	0.9	50	0.6	3.46
S750-3	0.1	3.37	0.9	50	0.6	3.46
S1000-1	0.1	4.50	0.8	50	0.4	2.04
S1000-2	0.1	4.50	0.8	50	0.4	2.04
S1.0D	0.1	1.0	1.0	40	0.6	3.43
S1.5D	0.1	1.5	1.0	40	0.6	3.43
S1.25D	0.1	1.25	1.0	40	0.4	2.29
S1.75D	0.1	1.75	0.9	40	0.4	2.06
S2.0D*	0.1	2.0	0.9	40	0.6	3.09

C_s is the surface condition factor,

For normal internal surface of the pile, in the absence of the test data, C_s was taken as 0.6 for pull-out and Stage 1 pull-out tests and 0.4 for push out and Stage 2 push out tests to consider the effect of shrinkage and age of concrete, which reduce the contact area of the interface. Table 8.1 shows factors and bond strength calculated from previous chapters.

Table 8-2 Comparison of bond strength from different methods

Specimen	P_U (kN)	Bond Strength from Experiment	Bond Strength from NLEFA	Bond Strength from Formulation	Calculated / Measured Bond	Relative Error (%)
S250-1	810	4.8	5.31	4.07	0.85	15.2
S250-2	720	4.3	5.31	4.07	0.95	5.3
S250-3	1035	6.2	5.31	4.07	0.66	34.3
S750-1	3445	6.83	6.33	3.46	0.70	30.2
S750-2	3700	7.33	6.33	3.46	0.47	52.8
S750-3	2503	4.96	5.45	3.46	0.51	49.3
S1000-1	1360	2.06	1.91	2.04	0.99	1.0
S1000-2	1350	2.02	1.91	2.04	1.01	1.0
S1.0D	665	4.2	4.24	3.43	0.82	18.3
S1.5D	1000	4.3	4.31	3.43	0.80	20.2
S1.25D	443	2.38	2.48	2.29	0.96	3.8
S1.75D	395	1.45	1.35	2.06	1.42	42.1
S2.0D	1000	3.27	3.10	3.09	0.94	5.5
				Average	0.85	21.5
				Standard Deviation		17.8

This formulation will be calibrated again based on test results and new findings from the NLFEA. Table 8-2 shows comparisons of bond strength obtained from the experiment, numerical procedure and formulation and relative errors between the experiment and the calculated bond strength. The bond strength formulation has closely predicted values of the bond stress with a small relative error of 21.5 and standard deviation of 17.8.

8.2   Formulation Review

In this section, the factors in the Eq. *(8-1)* will be reviewed and calibrated against experimental results and NLFEA results and findings.

8.2.1   Stiffness factor

Stiffness factor is defined by the following formulation:

$$K = \left[m(D/t)_g \right]^{-1} + (D/t)_p^{-1}$$

NLFEA predicts that varying aspect ratios of the steel tubes from 15 to 40 has no significant effect on ultimate strength and load slip response of a concrete plug in the steel tube (Section 7.6).

In the absent of experimental results to cover a wide range of aspect ratios, it is suggested here that a value of K based on Eq. *(8-2)* be adopted to apply to aspect ratios close to the one tested. Substituting this value of K in formulation results in:

$$f_{buc} = 0.9 C_l C_s \left(f_{cu} \right)^{1/2} \quad \text{(for short term loading)} \qquad (8\text{-}3)$$

In the case of long-term loading, the values of m must be modified to account for creep effect of concrete. A creep factor of 2 is considered acceptable. This results in an m value of m = 2 x 5.5 = 11. Accordingly, Eq. *(8-3)* may be written as:

$$f_{buc} = 0.68 C_l C_s \left(f_{cu} \right)^{1/2} \text{ (for long term loading)} \qquad (8-4)$$

8.2.2   Compressive strength of concrete

The compressive strength of concrete appeared to be an important parameter in calculating the bond strength. Although there were not adequate test results on the variation of the compressive strength of concrete to accurately calibrate the formulation for this parameter, the good correlation between the calculated and experimental bond strength indicated that the compressive strength effectively was considered.

8.2.3   Surface condition factor

The test results and NLFEA study indicated that the surface condition is a very important parameter in calculating the bond strength of the specimen. This is due to the effect of surface condition on macro mechanical interlock between the concrete and the steel tube. The study shows that the shrinkage highly reduces the surface condition factor. The most suitable material properties for the interface element were obtained from the initial parametric study of numerical modeling (Section 7.2).

The results of the initial study are used to calibrate the surface condition factor. Specimens S750, two of which were subjected to prior pull-out load were excluded

Table 8.3 shows the calibrated value for surface condition factors and comparison between new calculated bond strength using Equation *(8-3)* and the experiment.

The comparison of the experimental bond strength with calculated bond strength from Equation *(8-3)* using the calibrated surface condition factors shows that the calculated values for the bond stress are in a better agreement with the experimental results. The relative error is 13.7 with a standard deviation of 15.1.

Table 8-3 Comparison of bond strength from calibrated surface condition factor with experiment

SPECIMEN	C_L	C_s	CALCULATED BOND STRENGTH (MPA)	BOND STRENGTH FROM EXPERIMENT	CALCULATED / MEASURED BOND	RELATIVE ERROR (%)
S250-1	1.0	0.7	4.45	4.8	0.93	7.2
S250-2	1.0	0.7	4.45	4.3	1.04	3.6
S250-3	1.0	0.7	4.45	6.2	0.72	28.1
S750-1	0.9	0.7	4.01	6.83	0.59	41.3
S750-2	0.9	0.7	4.01	7.33	0.55	45.3
S750-3	0.9	0.7	4.01	4.96	0.81	19.2
S1000-1	0.8	0.4	2.04	2.06	0.99	1.1
S1000-2	0.8	0.4	2.04	2.02	1.01	0.8
S1.0D	1.0	0.7	3.98	4.2	0.95	5.1
S1.5D	1.0	0.7	3.98	4.3	0.93	7.3
S1.25D	1.0	0.45	2.56	2.38	1.08	7.6
S1.75D	0.9	0.3	1.54	1.45	1.06	6.0
S2.0D	0.9	0.6	3.07	3.27	0.94	6.0
Average					0.89	13.7
Standard Deviation						15.1

It may be suggested that in application of Equation *(8-3)* the surface condition of 0.3 to 0.7 can be used. Due to inconsistency of the effect of shrinkage and

variation of the material properties, this study suggests that no reliable surface condition factor can be achieved. Therefore, in the absence of experimental and numerical analysis results, it is recommended to use minimum values of surface condition factors for design purposes.

8.2.4   Coefficient of concrete plug length

The test results and the NLFEA study showed that the coefficient of concrete plug length is also an effective parameter in the bond strength of the specimen. This is due to the effect of concrete plug length on maximizing the macro mechanical interlock between the concrete and the steel tube.

The comparison of calculated bond strength from Equation *(8-3)* using the calibrated surface condition factors and the OTO's(2001) recommendations for coefficient of plug length with experimental bond strength shows that the calculated values for the bond stress are in a good agreement with the experiment. Therefore the OTO's recommendations would be used in the bond strength formulation.

8.3 Conclusions on the review of the formulation

The sections above presented a revision of the suitability and calibration of the bond strength formulation, which was initially developed in Chapters 3 and 5. The formulation was examined to match the experimental results with NLFEA results. The following formulation was concluded from this study:

$$f_{buc} = 0.9 C_l C_s \left(f_{cu}\right)^{1/2} \quad \text{(for short term loading)} \tag{8-3}$$

And

$$f_{buc} = 0.68 C_l C_s \left(f_{cu}\right)^{1/2} \text{ (for long term loading)} \tag{8-4}$$

where :

f_{cu} is the characteristic concrete compressive strength at 28 days (in N/mm^2)

C_l is the coefficient for plug length to pile diameter ratio

L/D_p	C_l
< 1.50	1.0
$1.5 - 3.0$	0.9
> 3.0	0.8

and

C_s is the surface condition factor,

The surface condition factor from 0.3 to 0.7 is proposed in this investigation. In the absence of experimental and numerical analysis results, it is recommended to use minimum values of surface condition factor for design purposes.

9 CONCLUSIONS AND FURTHER WORK

9.1 Overview of the Research Undertaken

The research presented in this thesis implemented strategies to examine the bond strength of concrete plugs embedded in tubular steel piles subjected to pull-out, push-put and cyclic loadings. This task was undertaken in four tiers of work, as follows.

- Determination of the variation in ultimate strength, bond strength and failure mechanisms obtained from four groups of specimens with varying concrete plug length, but constant concrete strength, steel tube properties and reinforcing ratio to examine overall behavior in pull-out, push out and cyclic loadings.

- Evaluation of the bond strength and bond stress distribution along the interface in different loading regimes, by development of an experimental technique, associated analytical relation and a bond strength formulation that enable calculation of the bond strength.

- Implementation of the non linear finite element analysis procedure to predict both the ultimate strength, load-slip behavior, failure mechanisms, distribution of longitudinal and hoop strains along the steel tube and bond stress distribution along the interface.

- Evaluation of the mechanisms that contribute to bond strength of the concrete plug in the steel tube, and the effect of shrinkage in ultimate load, load-slip response and bond stress distribution along the interface.

9.2 Conclusions From This Research

It is the purpose of this section to draw general conclusions from this research. The conclusions specific to each of the four tiers of the work are presented at the end of the relevant section. These general conclusions are as follows:

The pull-out and push-out bond strength

The pull-out bond strength tested in specimens having concrete plug embedment length to tube inner diameter L/D =1 ranged from 4.3 to 6.2 MPa with an average of 5.1 MPa. The push-out bond strengths ranged from 2.0 to 7.3 MPa with an average of 3.89 MPa.

Bond strength mechanisms

Bond strength is a function of both chemical adhesion of the steel-concrete interface and mechanical interlock between the concrete core and steel surface. To overcome mechanical interlock a small dilation of the tube occurs as it rides over the asperities of the interface, generating radial contact pressure, which enhances frictional resistance. The main mechanism that is believed to contribute to the bond strength in pull-out was the dilation of the concrete due to the wedging action exerted by the deformed steel bars against the concrete layer between the bars and the steel tube. This dilation increased contact pressure, which enhances friction resistance. A secondary factor was the pronounced Poisson's ratio effect increasing radial contact stress at the base of the concrete plug. The main mechanism that is believed to contribute to the high bond strength push-out tests was the pronounced Poisson effect increasing radial contact stress at the top of the connection. A secondary factor was the presence of reinforcement in the plug.

The load slip behavior

The load-slip curves of the specimens showed a nearly bilinear response. The change of slope of the load-slip curves during loading is assumed to occur with the breaking of micro chemical adhesion and the activation of the mechanical macro interlocking mechanism.

Failure Mechanisms

The failure mechanism displayed by the specimen in pull out was at the base of the concrete plug, where the steel tube contraction is much higher than that of the concrete core. The diagonal tension crack formed in the concrete layer between the longitudinal reinforcement and the steel tube, where it extended to the end of the steel bars and then in the hoop direction. This crack appears to correspond to a tension splitting of the concrete plug at ultimate pull-out capacity of the specimen.

Bond stress distribution along the interface

At the ultimate load level, a uniform bond/shear load transfer distribution over whole interface of steel and concrete may be assumed.

Effect of cyclic loading on bond strength and load slip behavior

The average ultimate bond strength of 4.25 MPa for static load and 2.77 MPa for cyclic load for Stage 1 and the average static bond strength of 2.37 MPa and average cyclic bond strength of 1.70 MPa for Stage 2 were achieved. The push-out and pull-out tests conducted under symmetric cyclic loading demonstrated that slip between concrete plug and the steel tube increased with repeated loading, and the rate of slip growth increased with the peak load.

Effect of shrinkage

Shrinkage in the concrete plug was shown to contribute to loss of composite action and ultimate strength. Shrinkage caused an increase in slip, and a reduction in shear/bond transfer and stiffness of the interface. Shrinkage increased the effect of repeated loading on the rate of slip growth between the concrete plug and the steel tube.

Rate of slip growth

The rate of slip growth between the concrete plug and the steel tube under repeated loading was determined. Empirical relationships between the load and

the rate of slip growth (mm/cycle) were obtained from the experimental data as follows:

$$\text{Symmetric cyclic loading, slip growth per cycle} = 10^{(0.255\frac{P}{P_u}-0.899)}$$

Where,

P is the applied cyclic peak load

P_u is the static ultimate strength

Cyclic reduction factor

The ultimate capacity and load slip response of specimens under cyclic loading can reasonably be approximated from the static ultimate strength and load slip of the specimen by reducing the ultimate strength values of the static test by the cyclic reduction factor. The cyclic reduction factor is defined as the factor by which the cyclic strength of the specimen may be obtained from the static strength for a given displacement. The average cyclic reduction factor of 0.74 was achieved.

Implementation of the NLFEA solution scheme

Implementation of the NLFEA solution scheme with axi-symmetric elements, a time dependant shrinkage model based on European code MC1990, and a linear tension softening for the concrete and Coulomb friction model for the interface has shown the ability to predict the ultimate strength, load-slip response and longitudinal and hoop strains along the outer surface of the steel tube. This tool is suitable for the investigation of the effect of parameter variations on the ultimate strength of a concrete plug in a steel tube specimen subjected to a static pull-out and push-out force.

Variation of aspect ratio of steel tube

NLFEA predicted that varying aspect ratios of the steel tubes from 15 to 40 has no significant effect on ultimate strength and load slip response of a concrete plug in the steel tube.

Bond strength formulation

The bond stress is assumed to be distributed uniformly along the concrete tube interface. The following formulation was concluded from this study:

$$f_{buc} = 0.9 C_l C_s (f_{cu})^{1/2} \quad \text{(for short term loading)}$$

And

$$f_{buc} = 0.68 C_l C_s (f_{cu})^{1/2} \text{ (for long term loading)}$$

where :

f_{cu} is the characteristic concrete compressive strength at 28 days (in N/mm^2)

C_l is the coefficient for plug length to pile diameter ratio

L/D_p	C_l
< 1.50	1.0
1.5 – 3.0	0.9
> 3.0	0.8

and

C_s is the surface condition factor,

The surface condition factor from 0.3 to 0.7 is proposed in this investigation. In the absence of experimental and numerical analysis results, it is recommended to use minimum values of surface condition factor for design purposes.

9.3   Further Work

9.3.1   Experimental Testing

1. The work of this thesis is based on steel tube with 244 mm diameter and aspect ratio of 22. Tests need to be undertaken on 200 to 600mm steel tube, and aspect ratio of 20 to 50, as these are the sizes used by industry, to see if the phenomenon exists to the same degree.

2. The tests in this thesis were all aimed at two concrete strengths, when the other parameters varied. A range of tests should be conducted with concrete strength as the variable to investigate the effect that concrete has on ultimate strength, bond strength, load slip response and shear transfer distribution along the interface in pull-out and push-out tests as well as incremental slip in cyclic loading.

3. The twelve specimens tested in cyclic loading were only tested under symmetrical cyclic loading. Tests should be undertaken on specimens with different cyclic load regimes.

4. The tests in this thesis were all aimed at similar interface surface condition. Tests need to be undertaken on different conditions of the interface surface to study the effect that surface condition has on bond strength, load slip response and bond stress distribution along the interface.

5. The specimens in this investigation were all tested under concentric axial loads. Tests should be undertaken on specimens under eccentric loads.

9.3.2   Theoretical modeling

1. The simulation of a cyclic loading history for a concrete plug specimen requires a damage model to be employed in the NLFEA procedure. Further work needs to be carried on calibration of the material model to account for cumulative damage.

2. Shrinkage effects were modeled by assuming shrinkage parameters for the concrete plug that fitted with the measured values of bond strength and load slip response. However, if measured shrinkage data were available for the concrete material, it would be possible to accurately investigate the effect of shrinkage on bond strength and structural.

3. To model eccentric loading, three dimensional finite elements models need to be used.

REFERENCES

ACI committee 318, "Building Code Requirements for structural Concrete (ACI 318-99) and commentary (318R-99)," *American Concrete Institute,* Farmington Hill, Mich., 1999, pp391

ACI committee 340, "ACI Design Handbook: Design of Reinforced Concrete in Accordance with the Strength Design Method of ACI 318-83," *American Concrete Institute*, Farmington Hill, Mich.,

Al-Mahaidi, R., Grundy, P., Bean, W. (1999) " Pullout Strength of Concrete Plugs in Tubular Piles" Proceeding, International Offshore and Polar Engineering Conference, Brest, France. pp. 24-29

AS3600 (2001) *Concrete Structures,* Standards Australia, Sydney.

Aval, S. B. B.; Saadegvaziri, M. A.; and Golafshani, A. A. (2002). "Compressive Composite Inelastic Fiber Element for Cyclic Analysis of Concrete-Filled Steel Tube Columns." *Journal of Structural Engineering,* ASCE, Vol. 128, No.4, April 2002, pp. 428-437

Baltay, P.; and Gjelsvik, A. (1990). "Coefficient of Friction for Steel on Concrete at High Normal Stress." *Journal of Material in Civil Engineering,* Vol. 2, No:1, February 1990, pp. 46-49

Bean, W. R. H. (1997). "Investigation of the Pull Out Bond Strength Within Concrete Filled Circular Steel Sections." *Forth Year Project,* Civil Engineering Department of Monash University, October 1997

BSI 1979, BS5400 Steel, Concrete and Composite Bridges. *Part 5 Code of practice for design of composite bridges,* British Standards Institution, London

CEB-FIP (1993) *CEB-FIP Model Code 1990.,* Comite Euro-International du Beton.

CEN 199?, Eurocode 4 (Adopted European Prestandard EVN 1994-1-1:1992, European Committee for standardization)

Dafalias, Y. F.; and Popov, E. P. (1975). " A Model of Nonlinearly Hardening Materials for Complex Loading." *Acta Mechanica,* 21(3), pp.173-191

Dafalias, Y. F.; and Popov, E. P. (1977). "Cyclic Loading for Materials with a Vanishing Elastic Region." *Nuclear Engrg. Des.,* 41(2), pp.293-302

DIANA (1998) *Finite Element Analysis User's Manual, Release 7.0,* TNO Building and Construction Research.

Fam, A. Z., and Rizkalla, S. H. (2001). "Confinement Model for Axially Loaded Concrete Confined by Circular Fiber-Reinforced polymer tubes." *ACI Structural Journal,* V. 98, No. 4, July-August 2001, 451-461

Furlong, R. W. (1967). " Strength of steel-encased concrete beam-columns." *J. Struct. Div.,* ASCE, 93(5), 113-124.

Furlong, R. W. (1968). " Design of steel-encased concrete beam-columns." *J. Struct. Div.,* ASCE, 94(1), 267-281.

Grassl, P., Lundgren, K., and Gylltoft, K. (2002) "Concrete in compression: a plastic theory with a novel hardening law" *International Journal of Solids and Structures,* V.39 (2002) pp. 5205-5223

Hajjar, J. F.; and Gourley, B. C. (1999). " A Cyclic Nonlinear Model for Concrete-Filled Tubes." *Journal of Structural Engineering,* ASCE, Vol. 123, No.6, June 1997, pp. 736-744

Hajjar, J. F.; Schiller P. H. and Molodan, A. (1998). "A Distributed Plasticity Model for Concrete-Filled Steel Tube Beam-Columns with Interlayer Slip." *Journal of Engineering Structures,* Elsevier Science, Vol. 20, No.8, 1998, pp. 663-676

Hilmy, S. I.; and Abel, J. F. (1985). "A Strain-Hardening Concentrated Plasticity Model for Nonlinear Dynamic Analysis of Steel Building." *META 85, Numerical Methods in Engineering: Theory and Applications,* 1, pp.305-314

Johansson, M., and Akesson, M. (2001). "Finite Element Study of Concrete-Filled Steel Tubes Using a New Confinement-Sensitive Concrete Compression Model." *Nordic Concrete Research,* Publication No. 27 (5), 2001

Kilpatrick, A. E., and Rangan, B. V. (1999). " Influence of Interfacial Shear Transfer on Behavior of Concrete-Filled Steel Tubular Columns." *ACI Structural Journal,* V. 96, No. 4, July-August 1999, 642-648

Knowels, R. B., and Park, R. (1969). " Strength of concrete filled steel tubular columns." *J. Struct. Div.,* ASCE, 95(12), 2565-2587

Knowels, R. B., and Park, R. (1970). " Axial load design for concrete filled steel tubes." *J. Struct. Div.,* ASCE, 96(10), 2125-2153

Lahlou, K.; Lachemi, M. ; and Aitcin. P.-C. (1999). " Confined High-Strength Concrete under Dynamic Compressive Loading." *Journal of Structural Engineering,* ASCE, Vol. 125, No.10, October.1999, pp. 1100-1108

Mei, H., Kiousis, P. D., Ehsani, M. R. and Saadatmanesh, H. (2001). " Confinement Effects on High-Strength Concrete." *ACI Structural Journal,* V. 98, No. 4, July-August 2001, 548-553

Mender, J. E.; Priestley, M. J. N.; and Park. R. (1988). " Observed Stress-Strain Behavior of Confined Concrete." *Journal of Structural Engineering.,* ASCE, V.114, No.8, Aug.1988, pp. 1827-1849

Mender, J. B.; Priestley, M. J. N.; and Park. R. (1988). "Theoretical Stress-Strain Model for confined concrete." *Journal of Structural Engineering.,* ASCE, V.114, No.8, Aug.1988, pp. 1804-1826

Morishita, Y, Tommil, L. and Yoshimura, K. (1979) "Experimental Studies on Bond Strength in Concrete Filled Steel Tubular Columns Subject to Axial Loads" *Transaction of the Japan Concrete Institute,* Vol. 1, pp 359-366

Morishita, Y, Tommil, L. and Yoshimura, K. (1980) "A Method of Improving Bond Strength between Steel Tube and Concrete Core Cast in Circular Steel Tubular Columns" *Transaction of the Japan Concrete Institute,* Vol. 2, pp 319-326

O'Loughlin, B. (1998). "Investigation of the Push Out Strength of Reinforced Concrete plugs in Circular Steel Sections." *Forth Year Project,* Civil Engineering Department of Monash University, November 1998

OFFSHORE TECHNOLOGY REPORT 2001 (OTO 2001 016). *Pile/Sleeve connections,* Health and Safety Exeecutive.

Okamato, T., and Maeno, T. (1988) "Experimental Study on Rectangular Steel Tube Columns Infilled with Ultra High Strength Concrete Hardened by Centrifugal Force." *Annual Meeting* of AIJ, *Proceedings,* Chiba, October 1988, pp. 1359

Popovics, S. (1973). "A Numerical Approach to the Complete Stress-Strain Curves for Concrete." *Cement and Concrete Research*, V. 3, No. 5, pp. 583-599

Richart, F. E., Brandtzaeg, A. and Brown, R. L. (1928). "A Study of the Failure of Concrete under Combined Compressive Stresses." *Bulletin No. 185,* University of Illinois, Engineering Experimental Station, Urbana, Illinois, USA, November1928, pp. 104

Roeder, C. W., Cameron, B. and Brown, C. B. (1999). " Composite Action in Concrete Filled Tubes." *J. Struct. Div.,* ASCE, 125(5), 477-484

Sakino, K. and Tomii, M. (1981). " Hysteretic Behavior of Concrete Filled Square Steel Tube Beam-Columns Failed in Flexure." *Trans., Japan Concrete Inst.,* Japan, 3, pp.439-446

Sakino, K., Tomii, M., and Wananabe, K. (1985). " Sustaining load capacity of plain concrete stub columns by steel tubes." *Proc., Int. Spec. Conference on Concrete-Filled Steel Tubular Struct.,* 112-118.

Schneider, S. P. (1998). " Axially Loaded Concrete-Filled Steel Tubes." *J. Struct. Div.,* ASCE, 124(10), 1125-1138

Shakir-Khalil, H., (1991) "Bond Strength in Concrete-Filled Steel Hollow Sections." *Proceedings, International conference on Steel and Aluminium Structures*, Singapore. Vol. Composite Steel Structures, pp. 157-168

Shakir-Khalil, H., (1993a) "Push-out Tests on Concrete-Filled Steel Hollow Sections" *The Structural Engineer*, July 1993. Vol. 71, No.13 pp. 230-233

Shakir-Khalil, H., (1993b) "Push-out Tests on Concrete-Filled Steel Hollow Sections" *The Structural Engineer*, July 1993. Vol. 71, No.13 pp. 234-243

Shams, M., and Saadeghvaziri, A (1997). " State of the Art of Concrete-Filled Steel Tubular Columns." *ACI Structural Journal*, V. 94, No. 5, September-October 1997, 558-571

Shams, M., and Saadegvaziri, M. A. (1999). "Nonlinear Response of Concrete – Filled Steel Tubular Columns under Axial Loading." *ACI Structural Journal*, V. 96, No. 6, November-December 1999, 1009-1017

Silva, P. F., and Seible, F. (2001). "Seismic Performance Evaluation of Cast-in-Steel-Shell (CISS) Piles." *ACI Structural Journal*, V. 98, No. 1, January-February 2001, pp.36-49

Taplin, G (1999). " THE BEHAVIOR OF THE COMPOSITE BEAMS UNDER REAPEATED LOADING." *PhD thesis,* Civil Engineering Department of Monash University, November 1998

Tomii, M., Yoshimura, K., and Morishita, Y. (1977). " Experimental studies on concrete filled steel tubular stub columns under concentric loading." *Proc., Int. Colloquium on Stability of Struct. Under Static and Dynamic Loads,* 718-741.

Viridi, K. S. and Dowling, P. J (1975) "Bond Strength in Concrete Filled Circular Steel Tubes" CESLIC Report CC11.

Wang, Y. C., and Restrepo, J. I. (2001). "Investigation of concentrically Loaded Reinforced Concrete Columns confined with Glass Fiber-Reinforced Polymer Jackets." *ACI Structural Journal,* V. 98, No. 3, May-June 2001, 377-385

Whitburn, J. (1999). "Investigation of the effects of cyclic loading on the Bond Strength of Concrete Filled Circular Steel Sections." *Forth Year Project,* Civil Engineering Department of Monash University, December 1999

Yoshioka, Y. (1992) "State of Art of Composite Steel Tube and Concrete Structures In Japan." *US-Japan Work Shop on Composite and Hybrid Structures, Proceedings*, September 10-12, Berkeley, California, 1992, pp. 119-130

A1   STRAIN GAUGE ARRANGEMENTS

This appendix presents the strain gauge arrangements for all specimens.
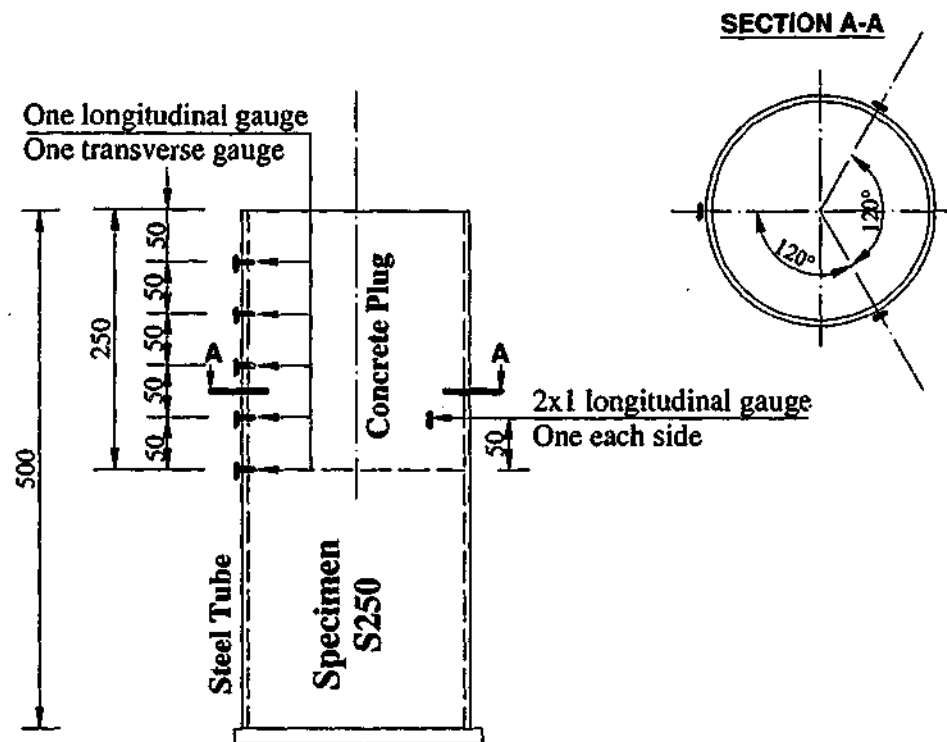
Figure A1-1: Strain gauge arrangement for specimen S250
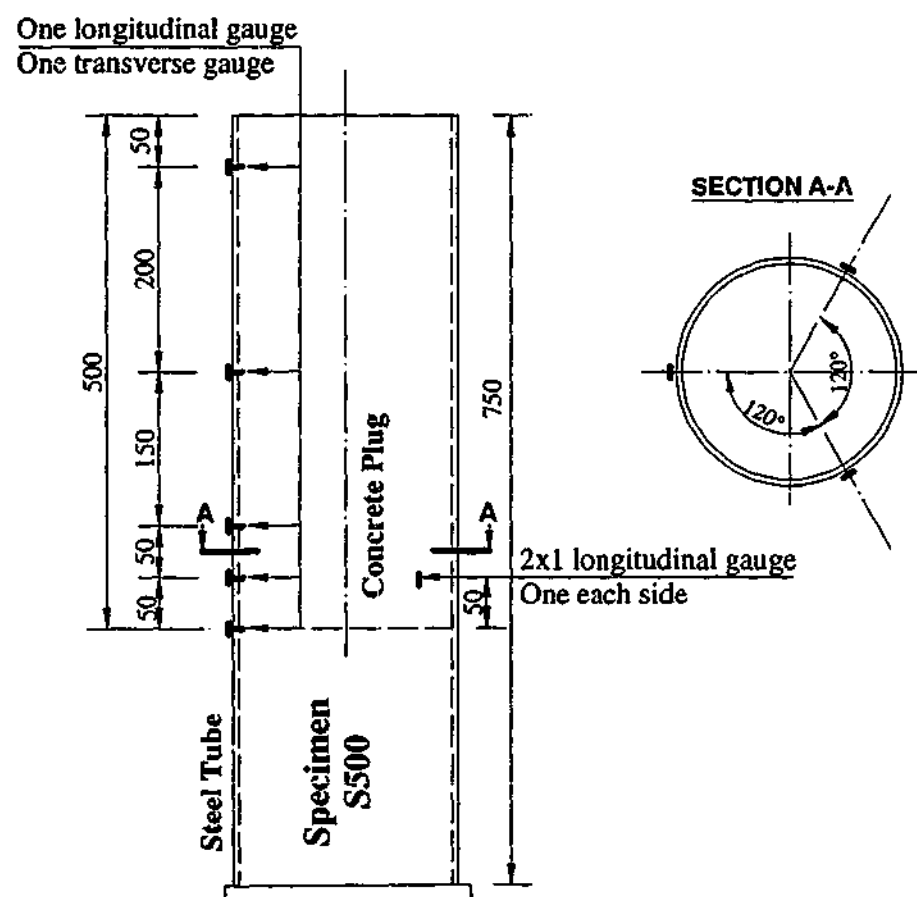
Figure A1-2: Strain gauge arrangement for specimen S500
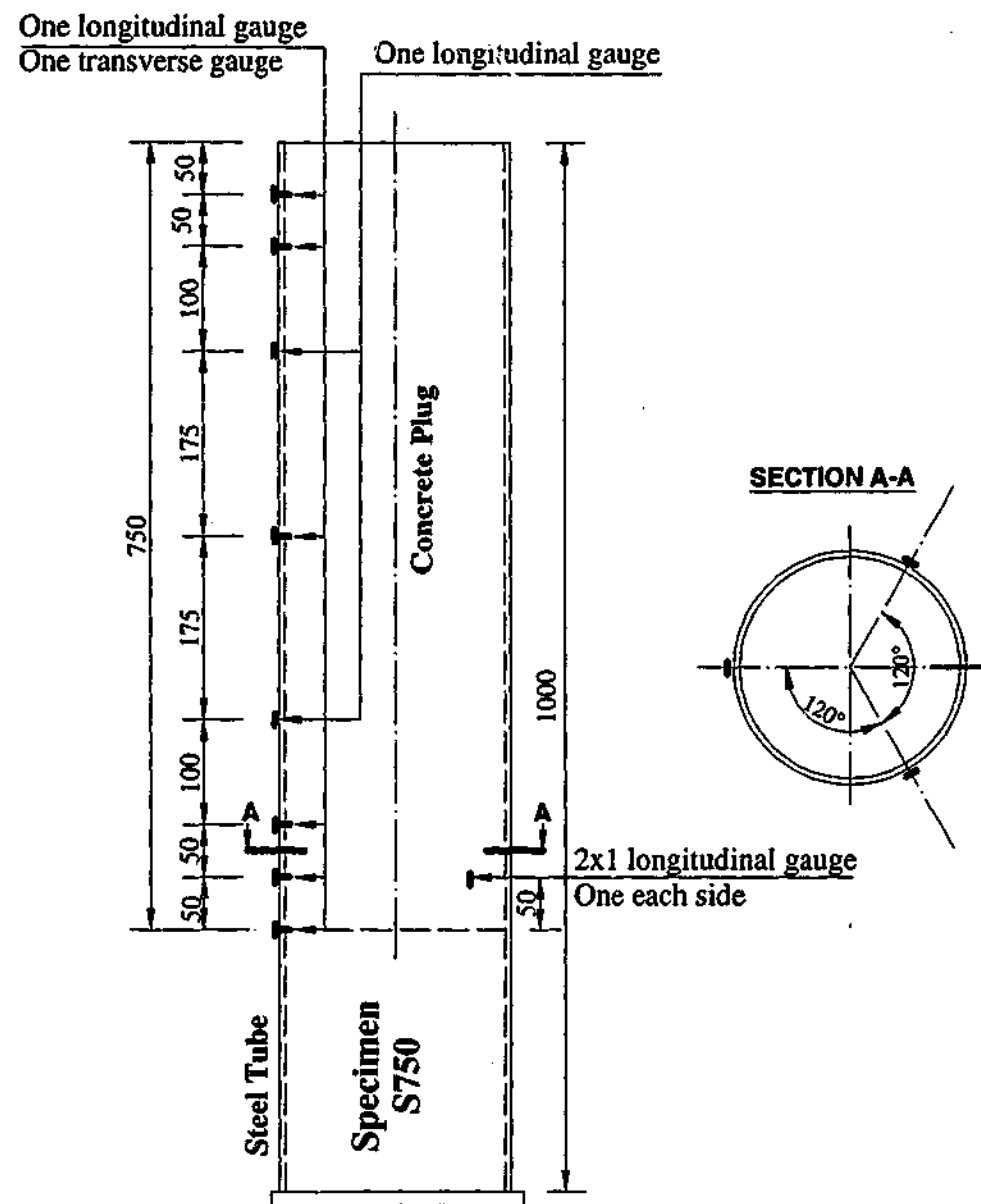
Figure A1-3: Strain gauge arrangement for specimen S750
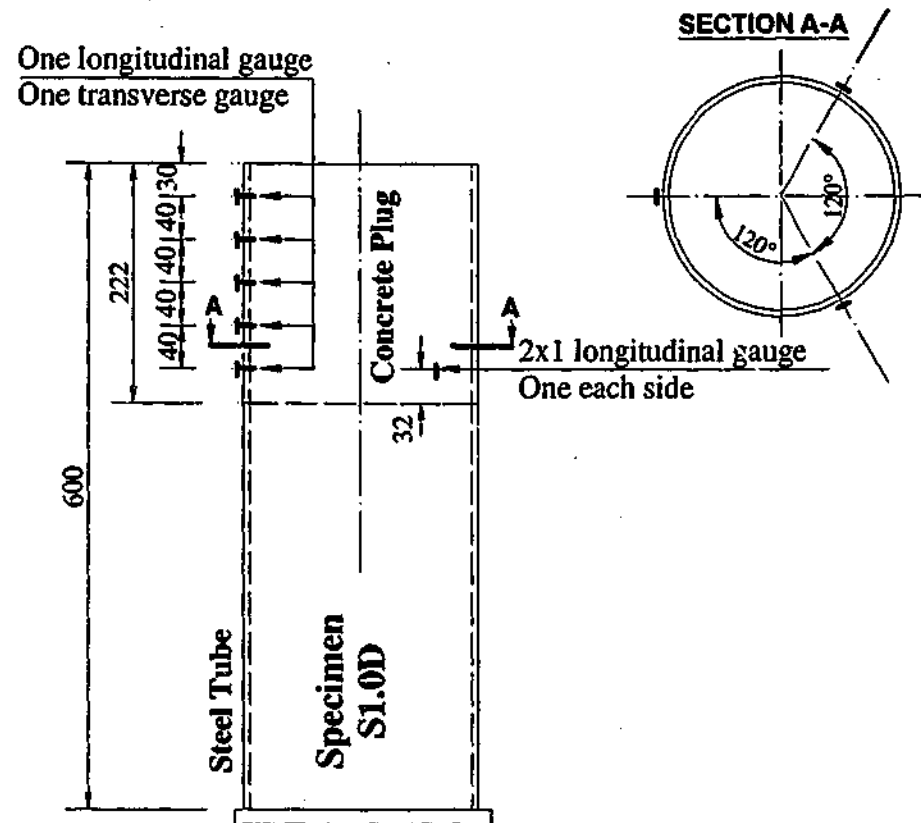
Figure A1-4: Strain gauge arrangement for specimen S1.0D
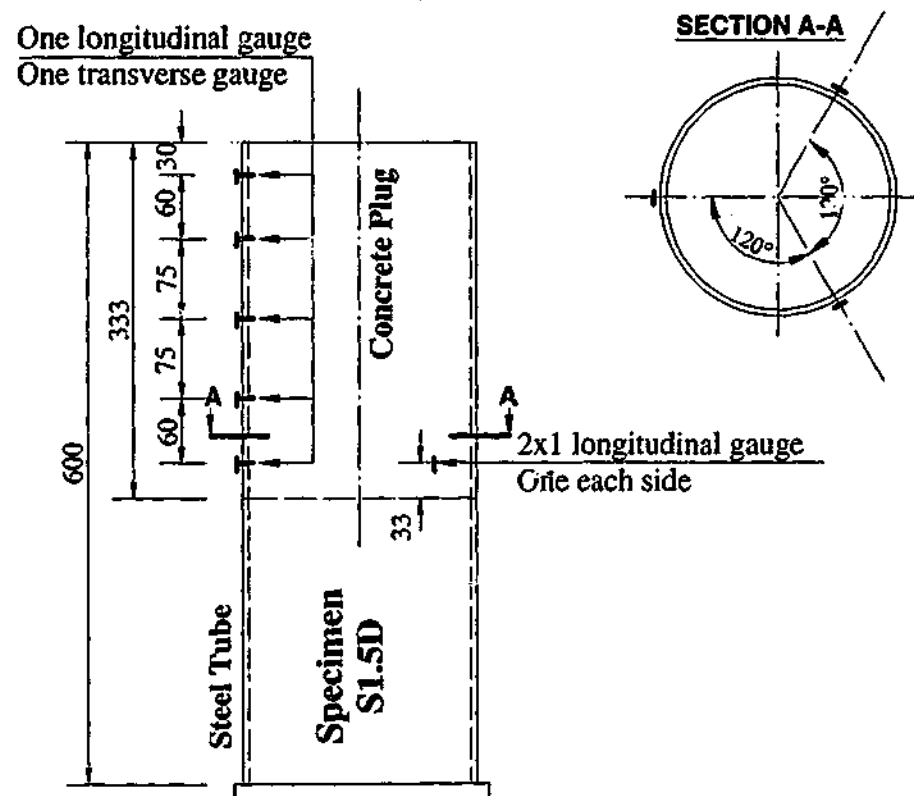
Figure A1-5: Strain gauge arrangement for specimen S1.5D
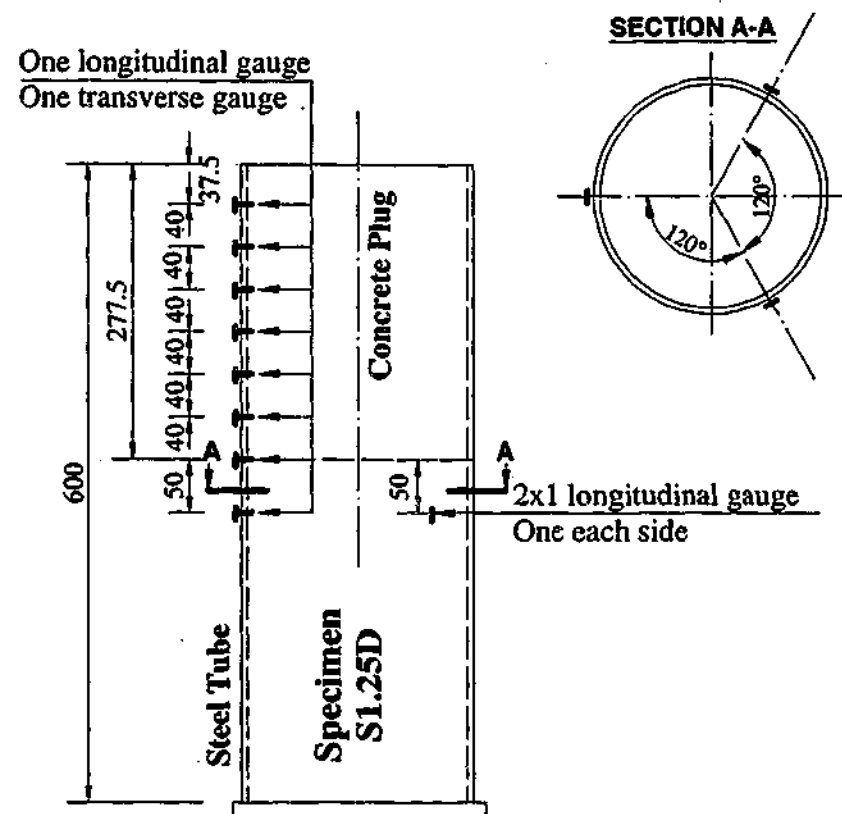
Figure A1-6: Strain gauge arrangement for specimen S1.25D
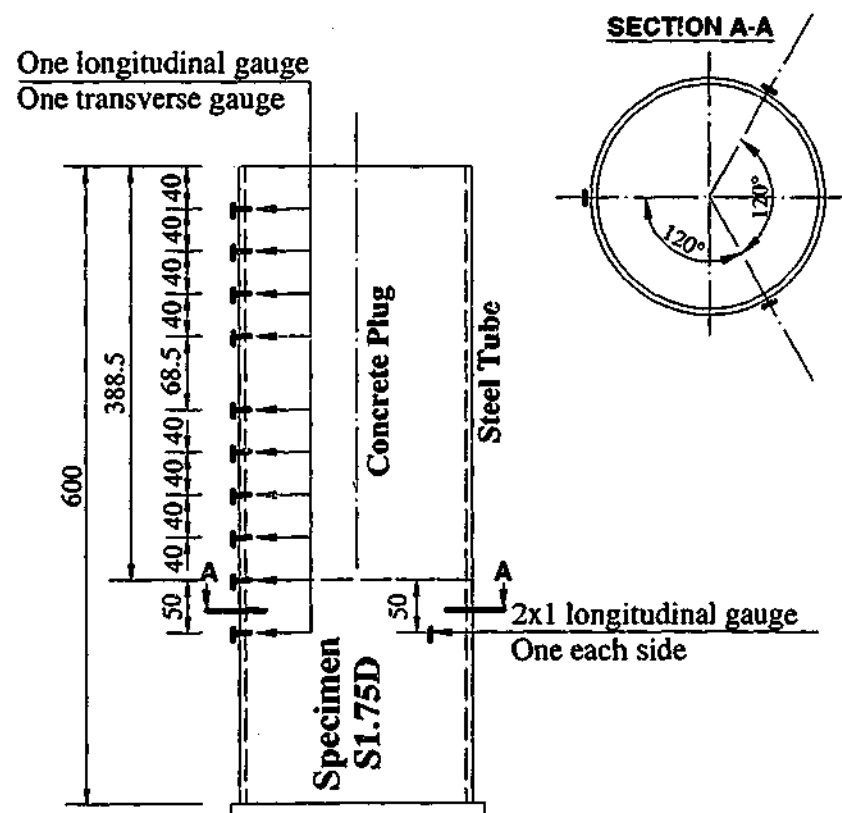
Figure A1-7: Strain gauge arrangement for specimen S1.75D
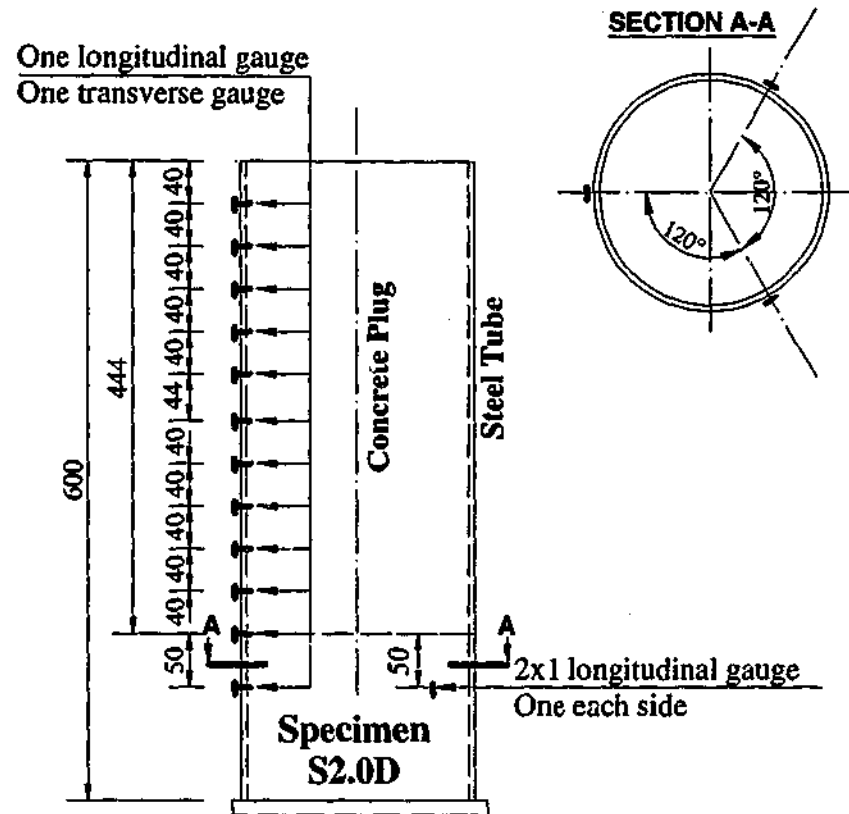
Figure A1-8: Strain gauge arrangement for specimen S2.0D

A2 COMPARISON OF LONGITUDINAL AND HOOP STRAINS BETWEEN NLFEA PREDICTION AND EXPERIMENT

The aim of this appendix is to give the reader a complete comparison of longitudinal and hoop strains of each strain gauged specimen in experimental work with the predicted strains as calculated using the NLFEA solution scheme. No discussion is provided in this appendix as the relevant discussion has been presented in Chapter 7.
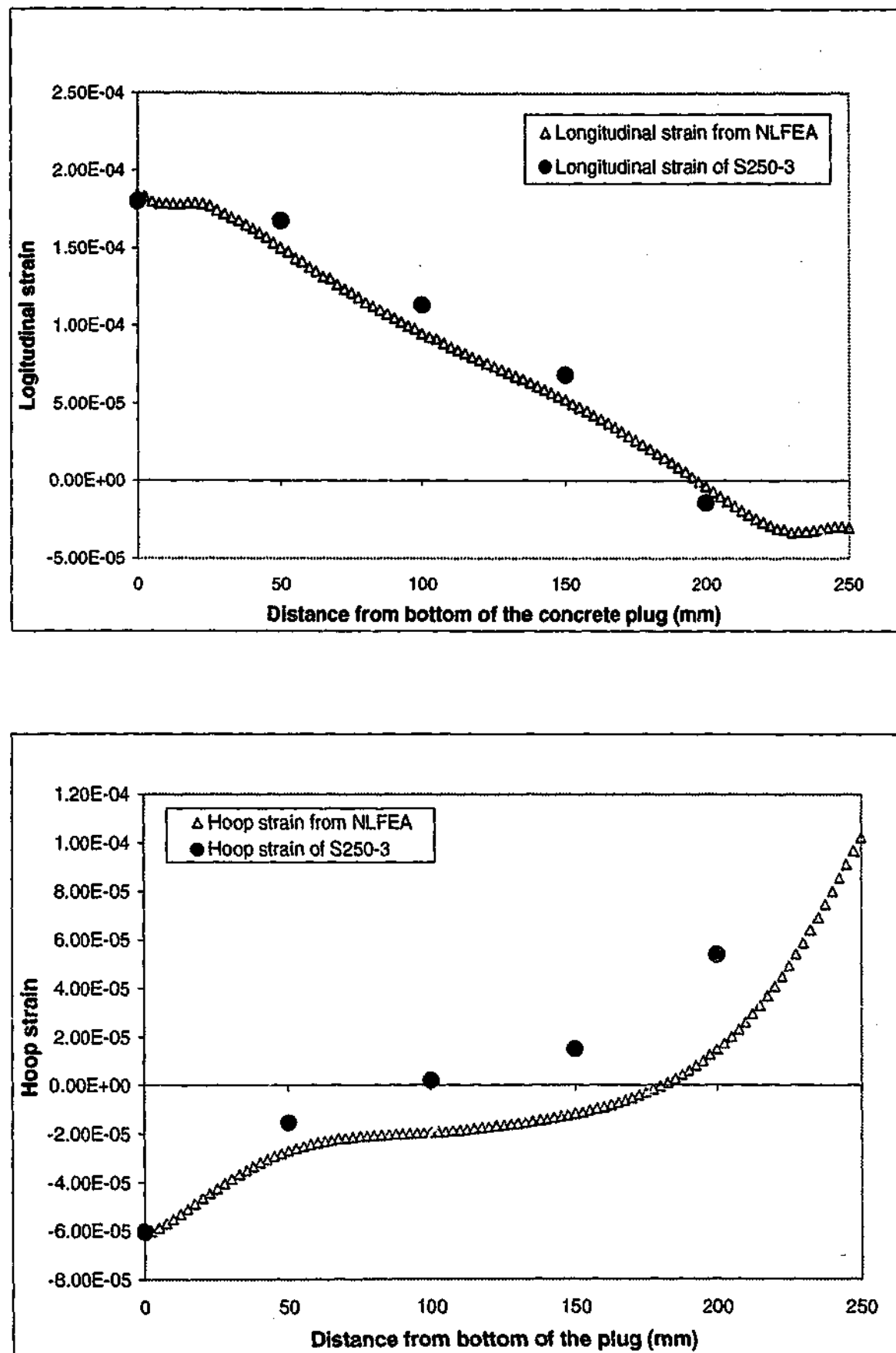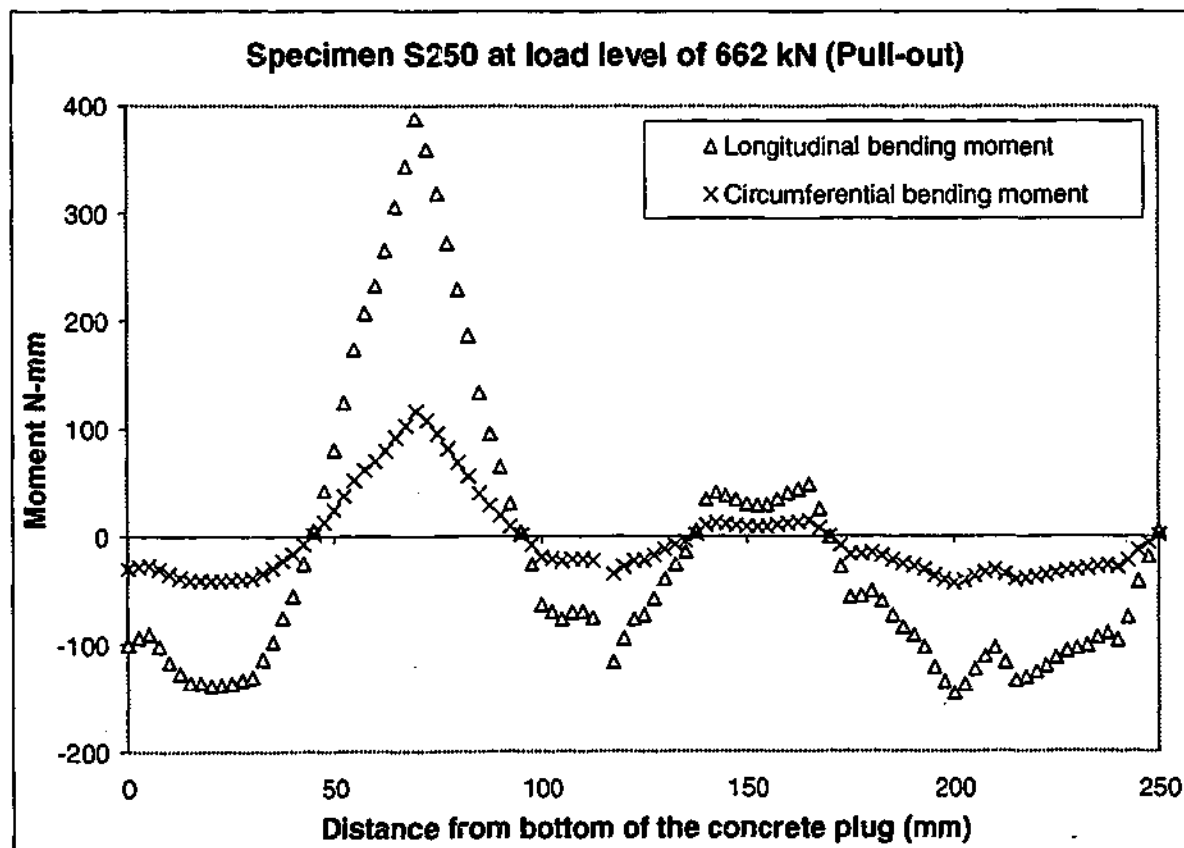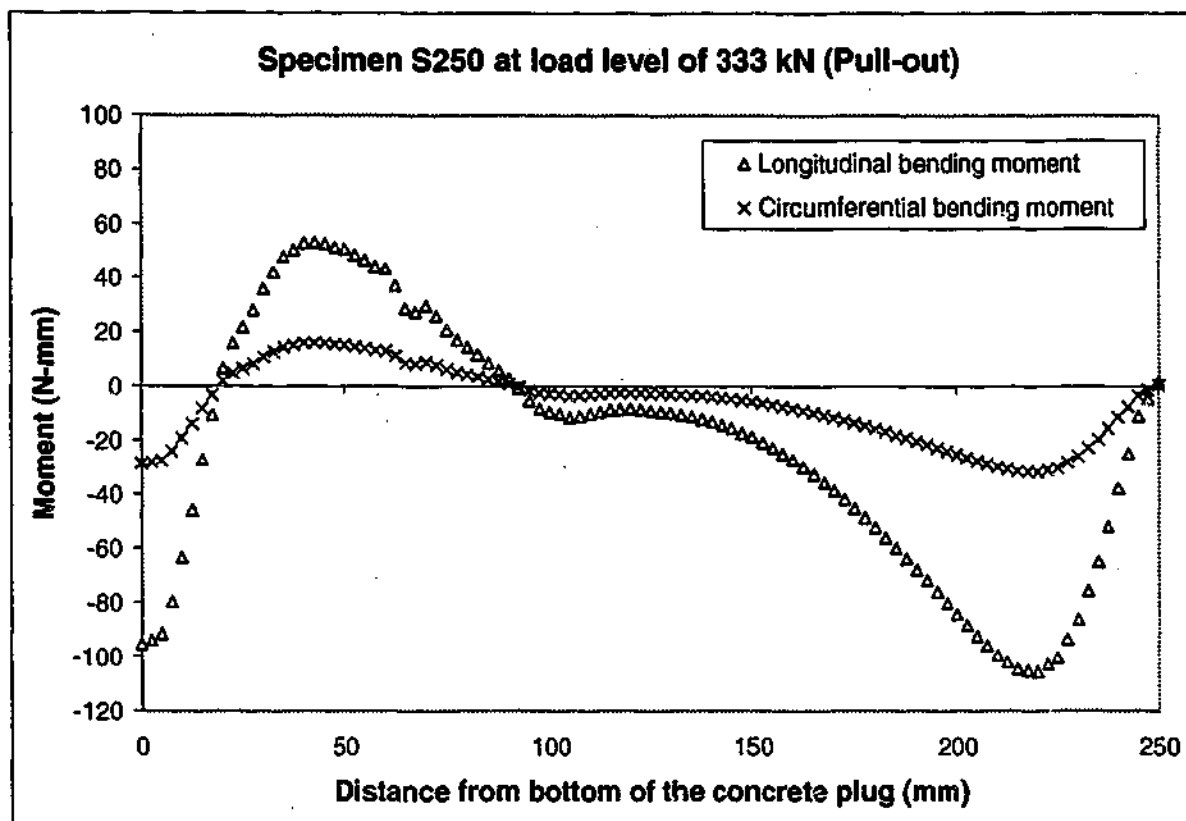
Figure A2-1 Comparison of longitudinal and Hoop strains along the outer surface
of the steel tube for specimen S250 of the pull-out test at load level of 333 kN
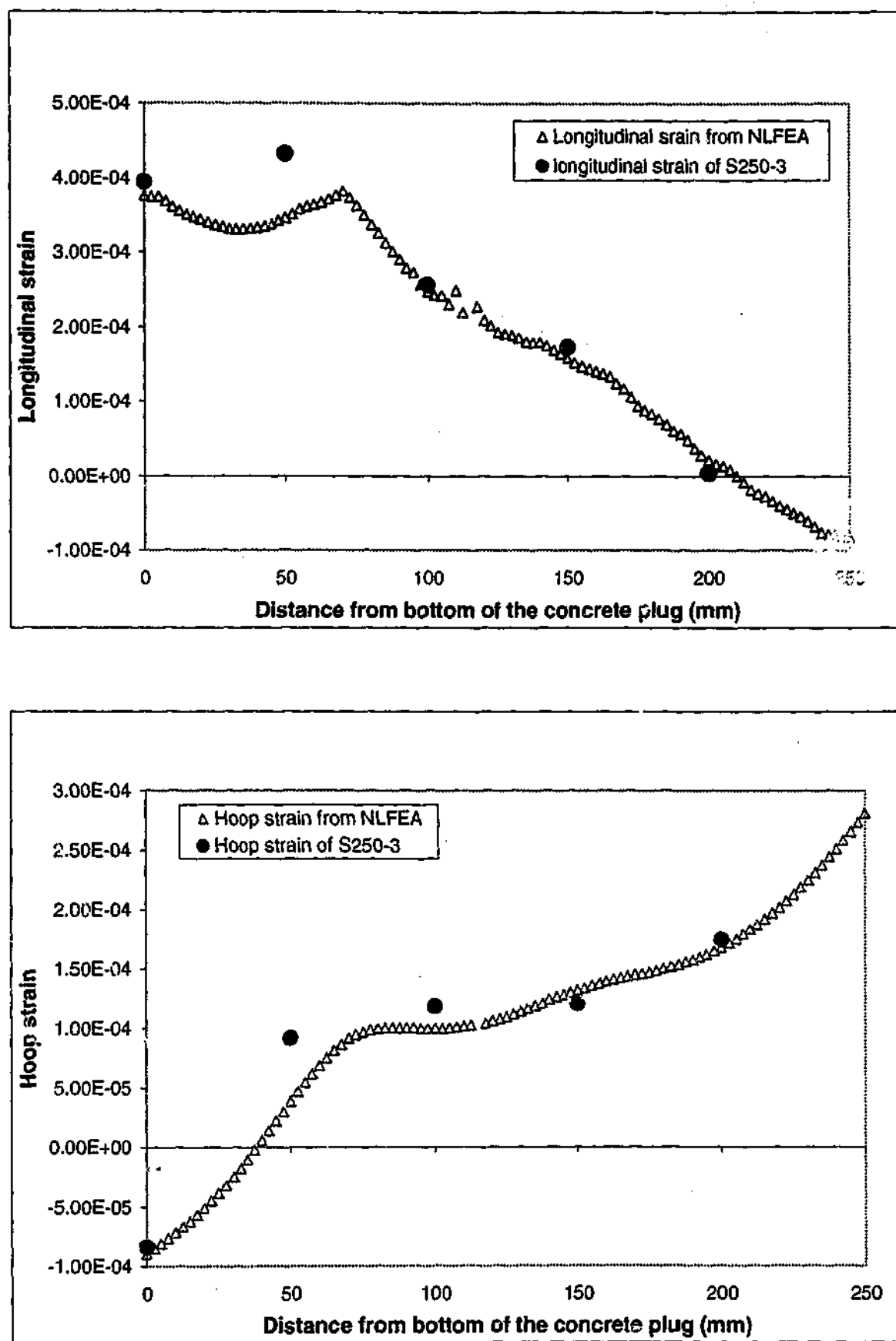
Figure A2-2 Comparison of longitudinal and Hoop strains along the outer surface of the steel tube for specimen S250 of the pull-out test at load level of 662 kN
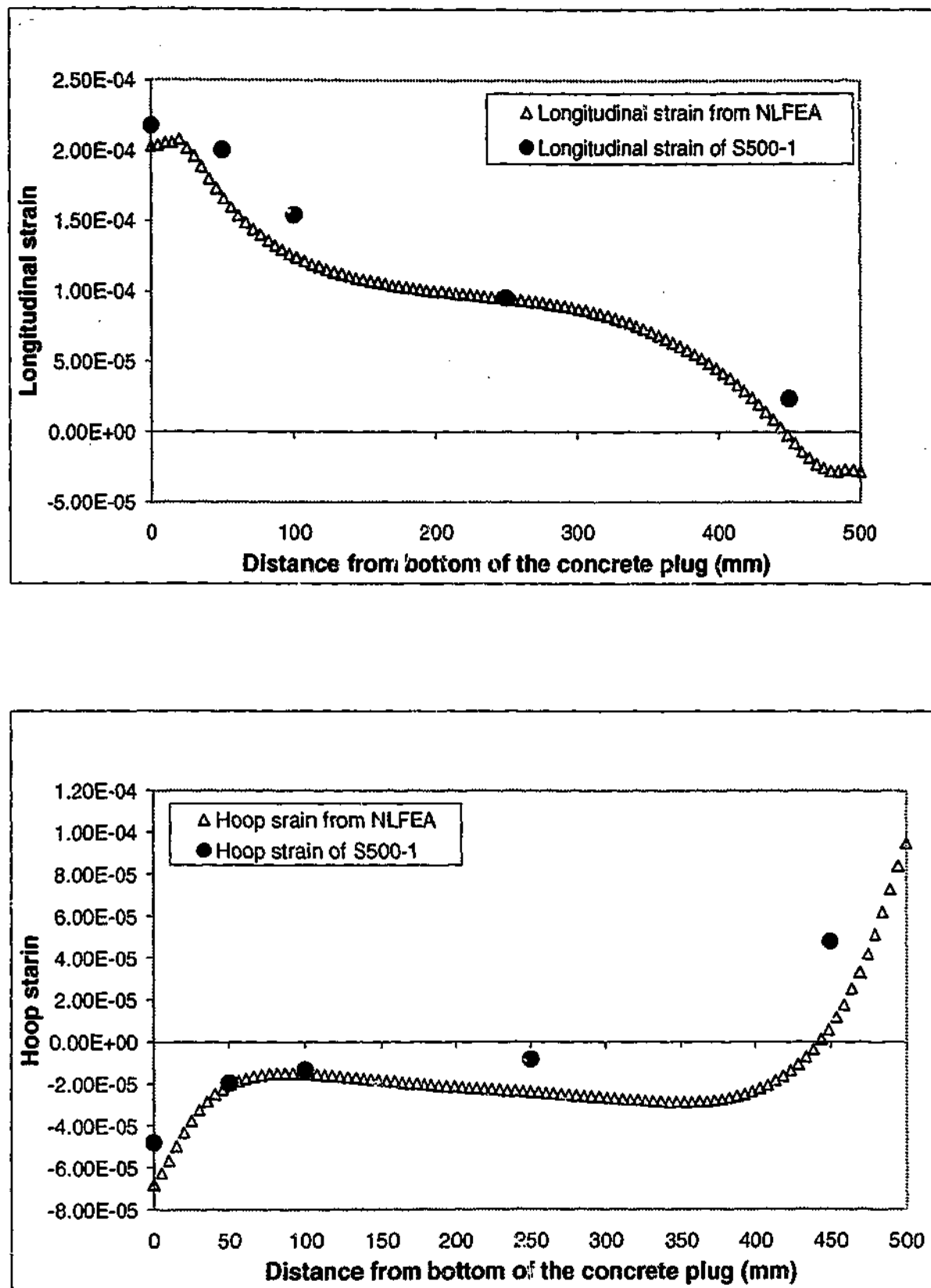
Figure A2-3 Comparison of longitudinal and Hoop strains along the outer surface
of the steel tube for specimen S500 of the pull-out test at load level of 334 kN
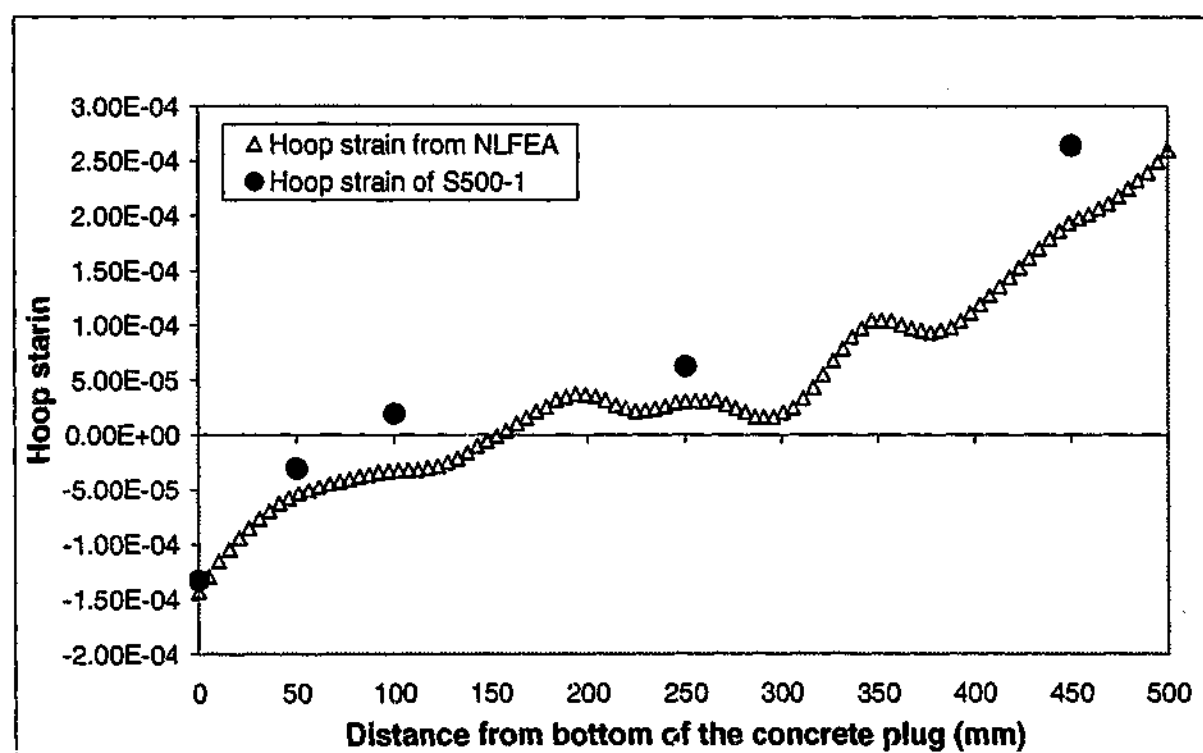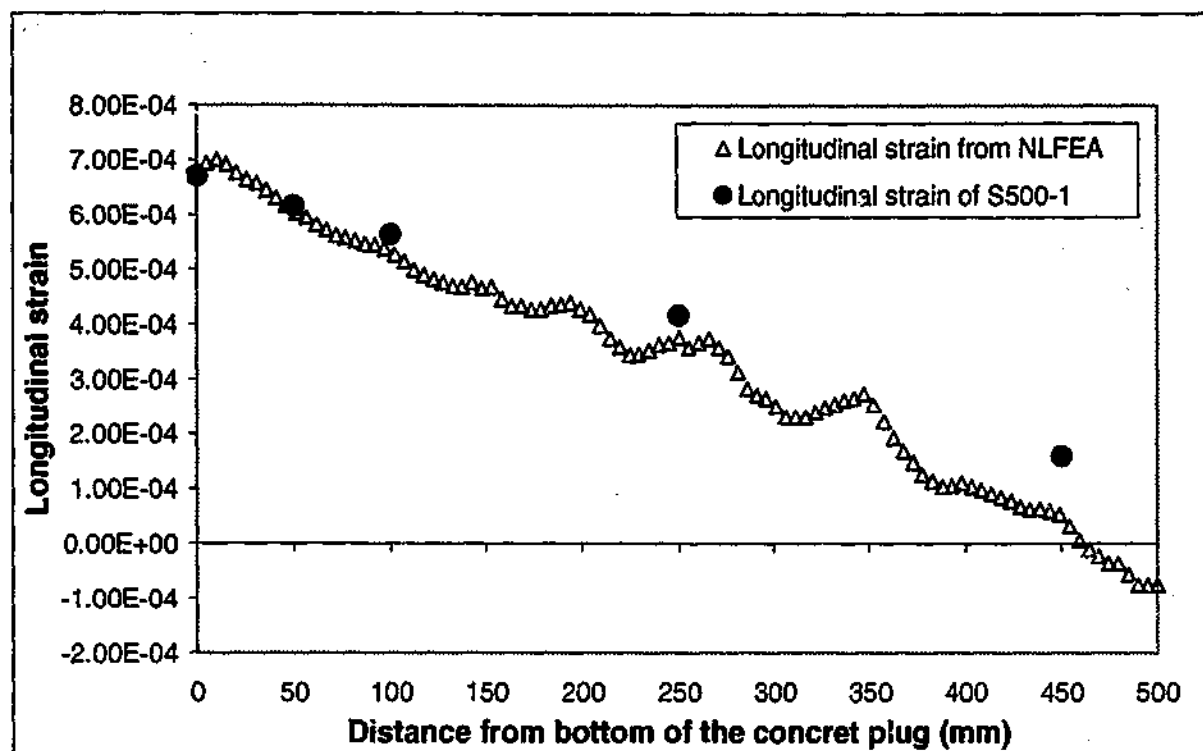
Figure A2-4 Comparison of longitudinal and Hoop strains along the outer surface
of the steel tube for specimen S500 of the pull-out test at load level of 1008 kN
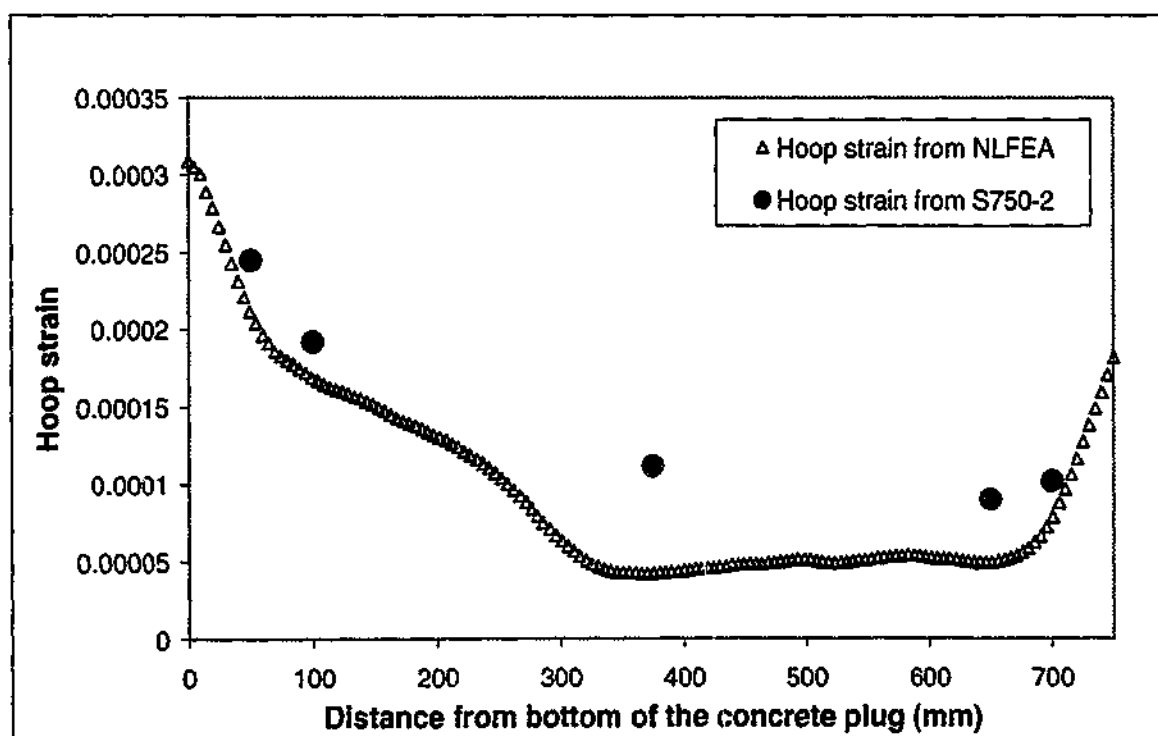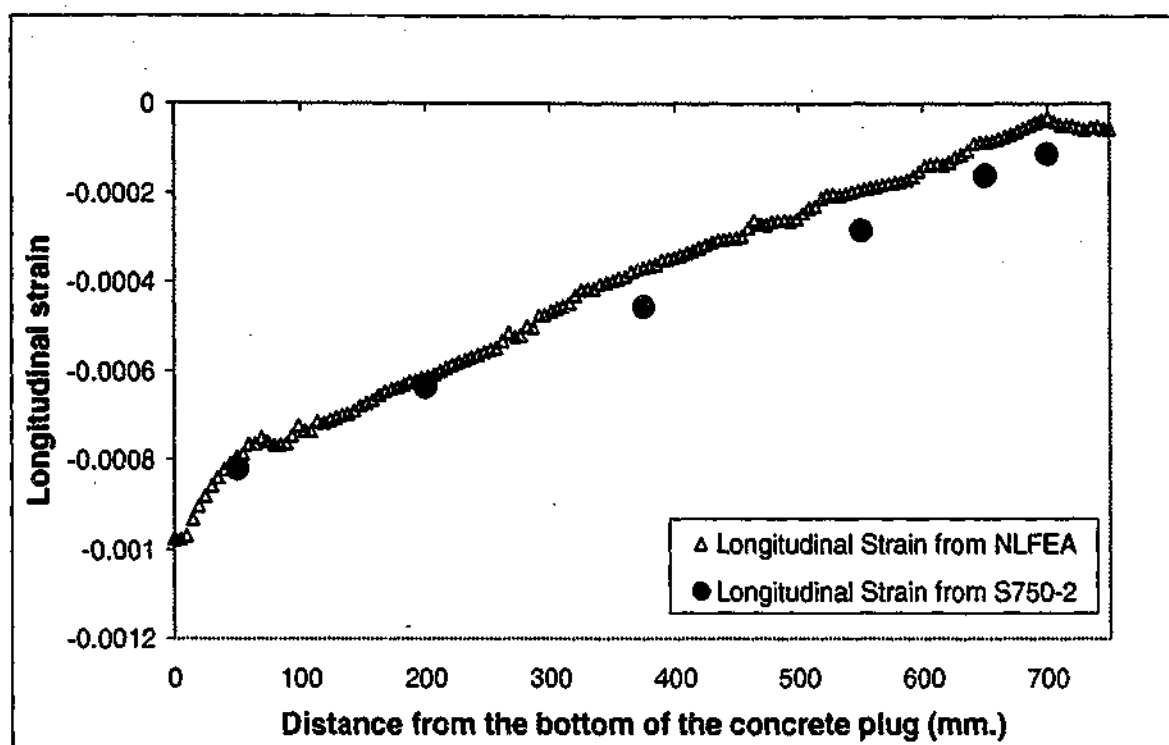
Figure A2-5 Comparison of longitudinal and Hoop strains along the outer surface of the steel tube for specimen S750 of the push-out test at load level of 1452 kN
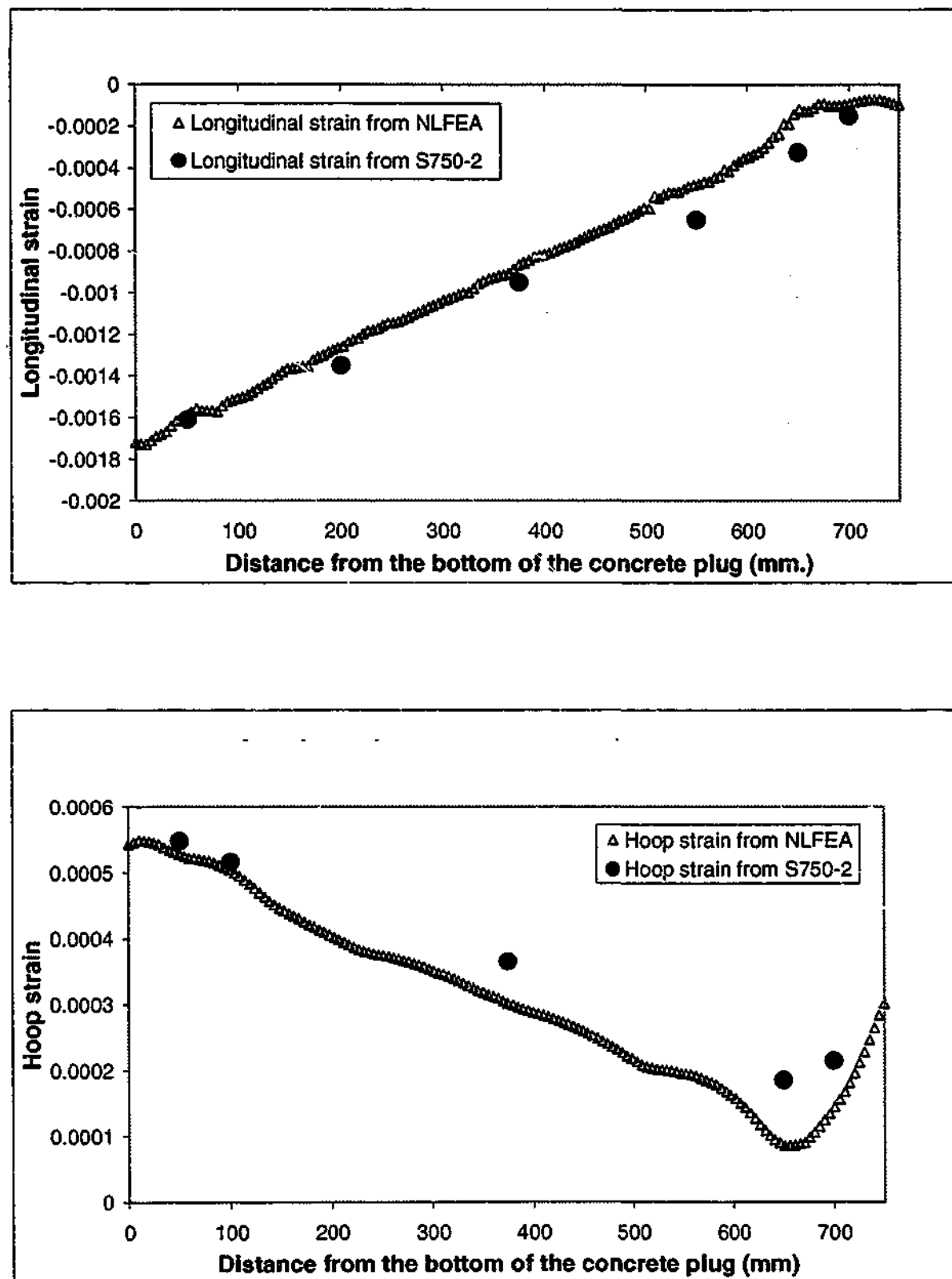
Figure A2-6 Comparison of longitudinal and Hoop strains along the outer surface of the steel tube for specimen S750 of the push-out test at load level of 2747 kN
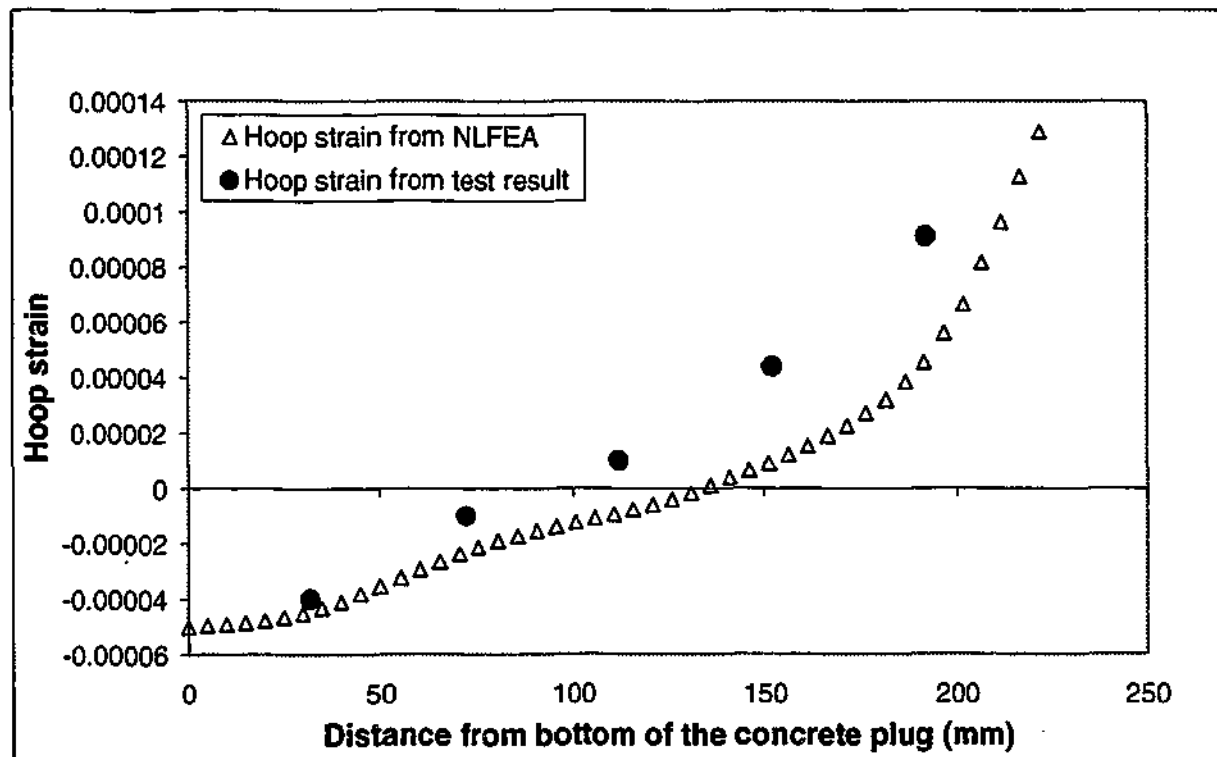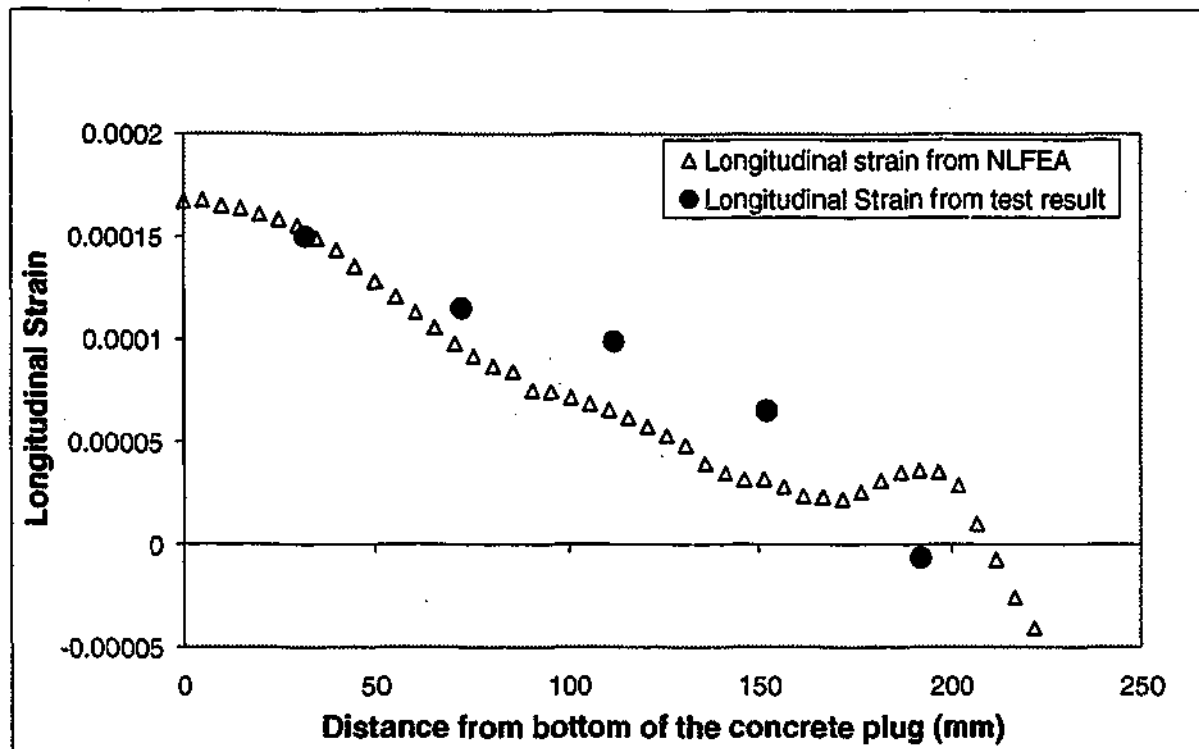
Figure A2-7 Comparison of longitudinal and Hoop strains along the outer surface
of the steel tube for specimen S1.0D of the Stage 1 at load level of 275 kN
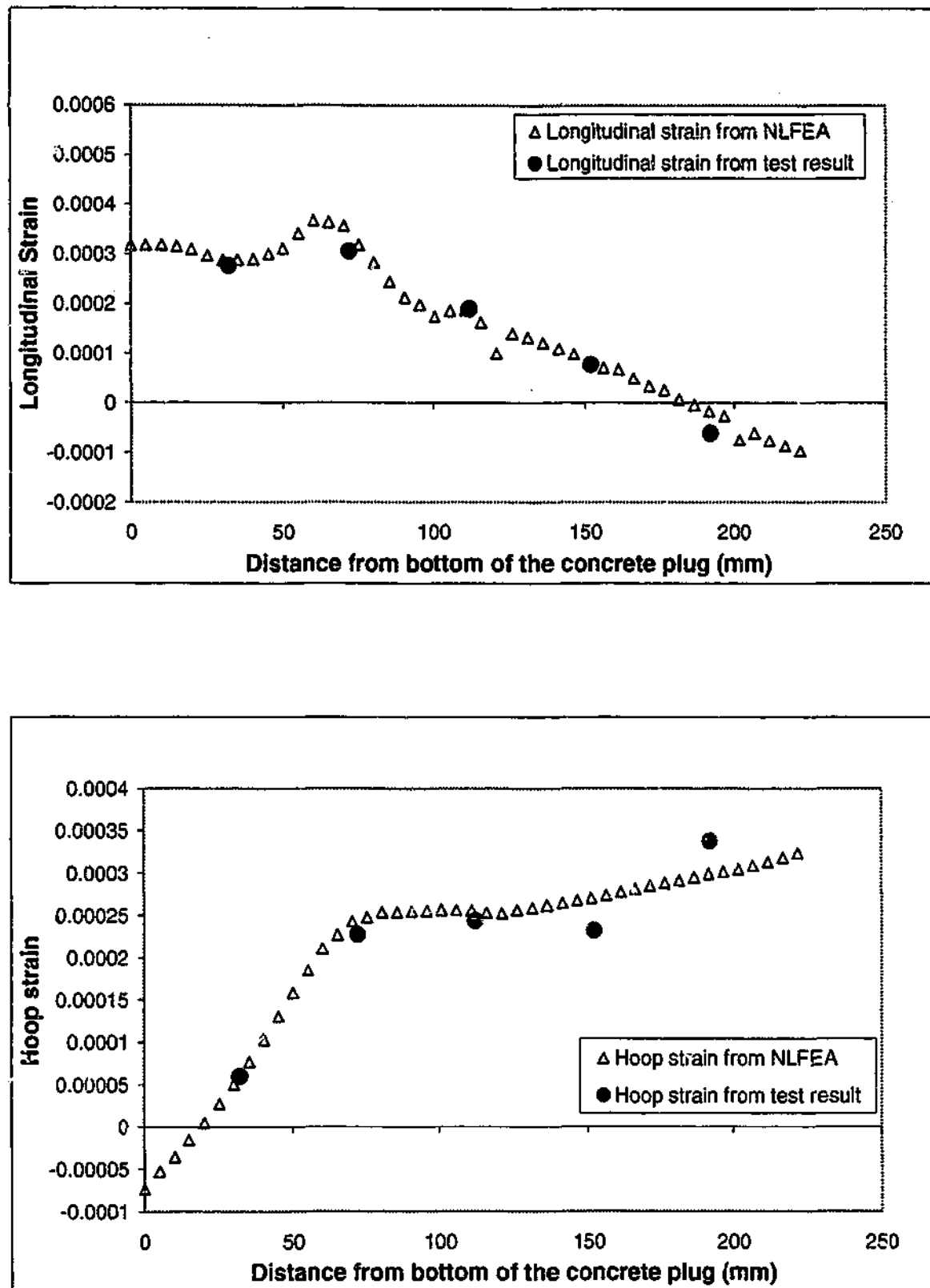
Figure A2-8 Comparison of longitudinal and Hoop strains along the outer surface of the steel tube for specimen S1.0D of the Stage 1 at load level of 663 kN
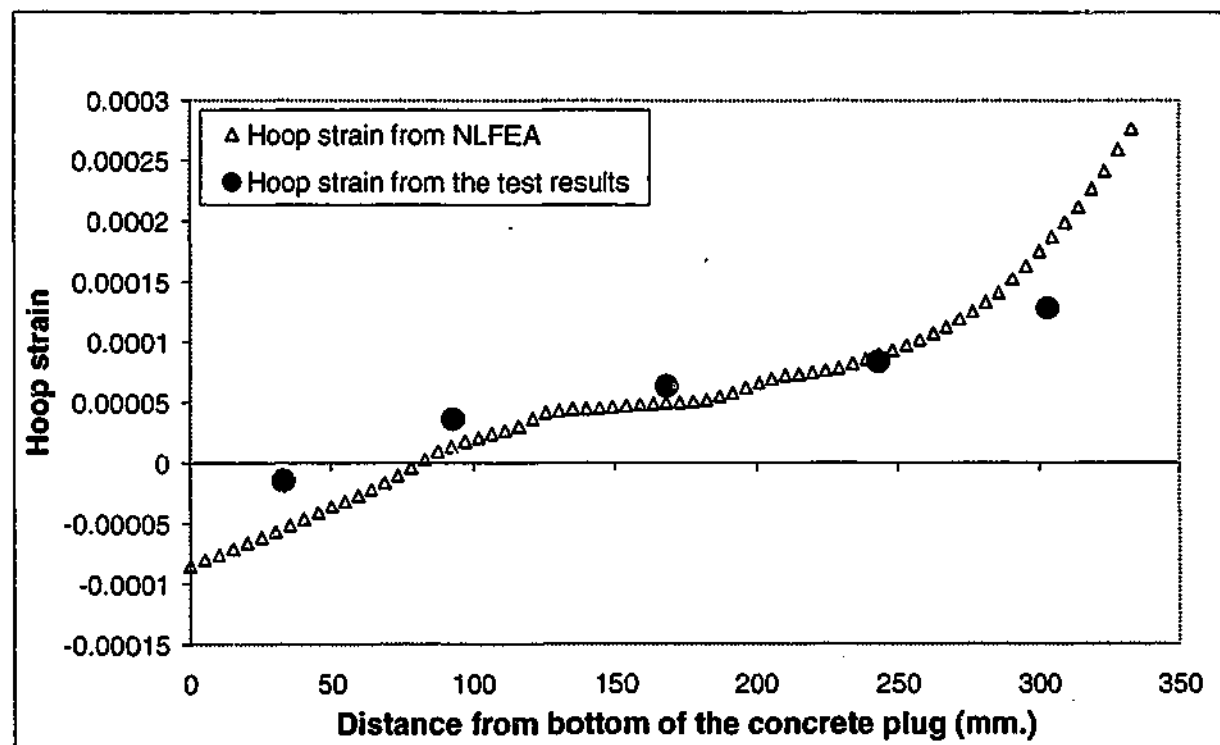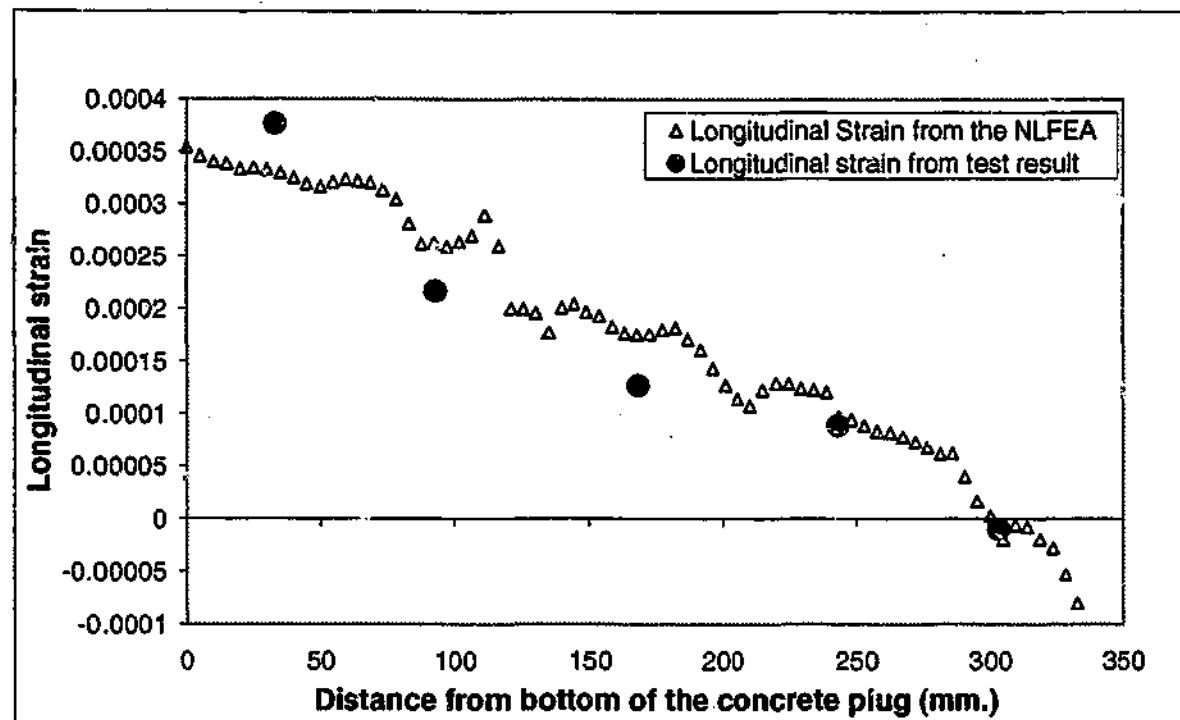
Figure A2-9 Comparison of longitudinal and Hoop strains along the outer surface

of the steel tube for specimen S1.5D of the Stage 1 at load level of 572 kN
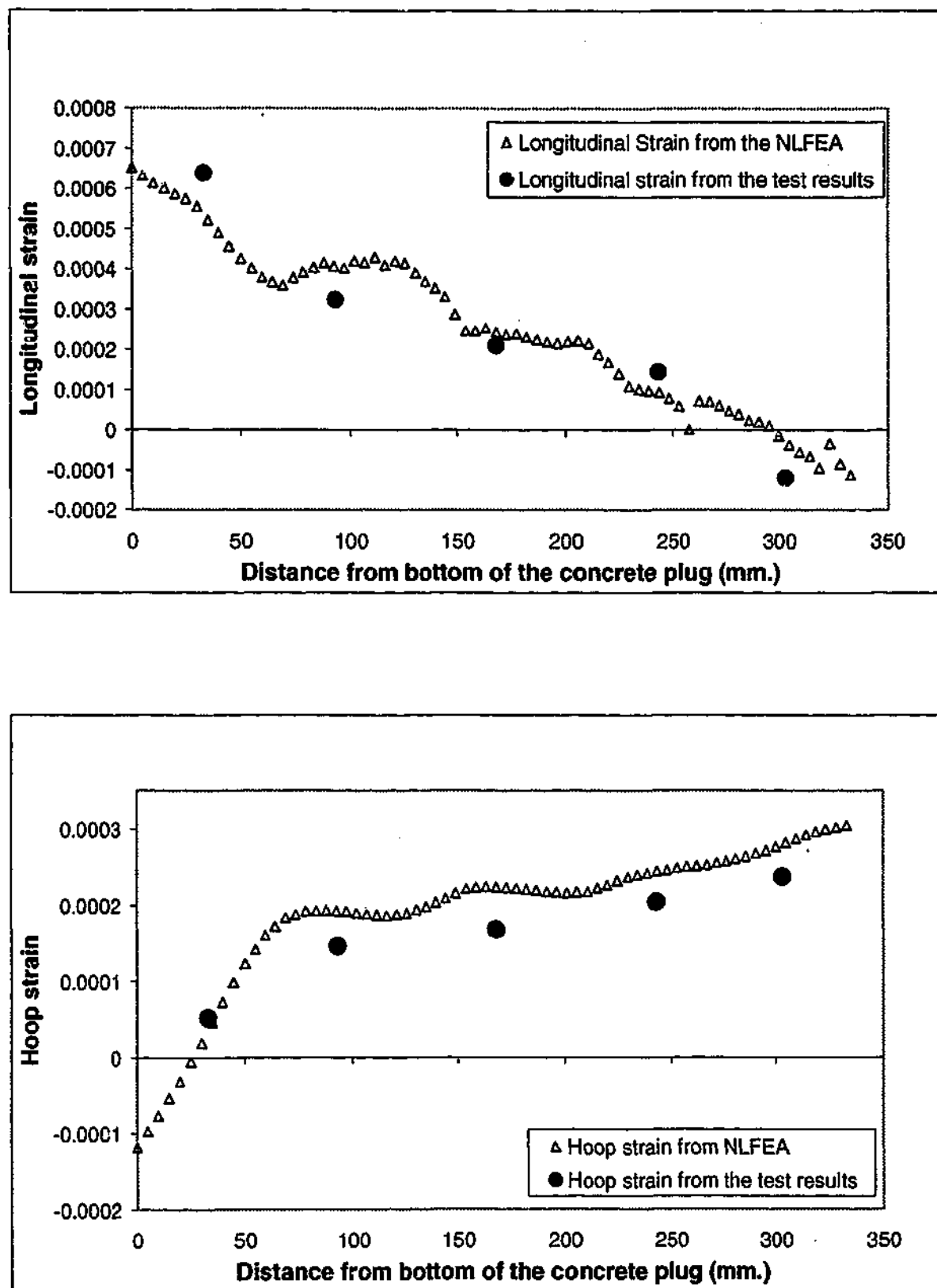
Figure A2-10 Comparison of longitudinal and Hoop strains along the outer surface
of the steel tube for specimen S1.5D of the Stage 1 at load level of 1000 kN
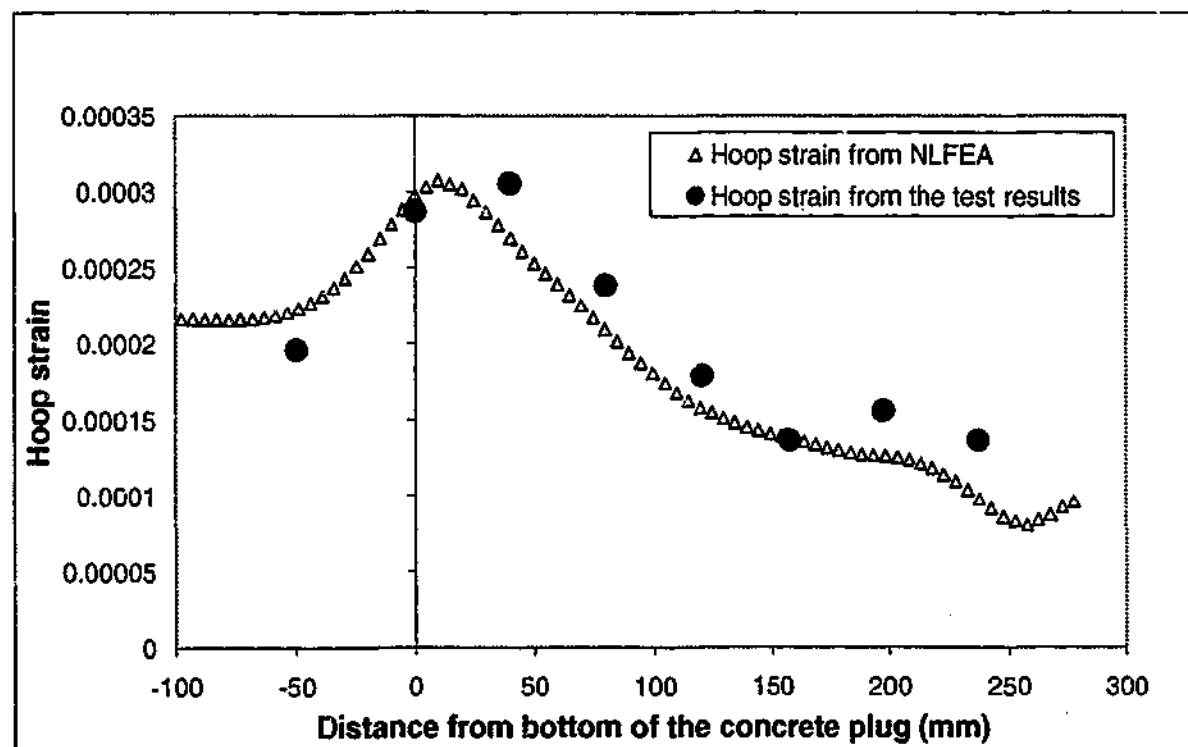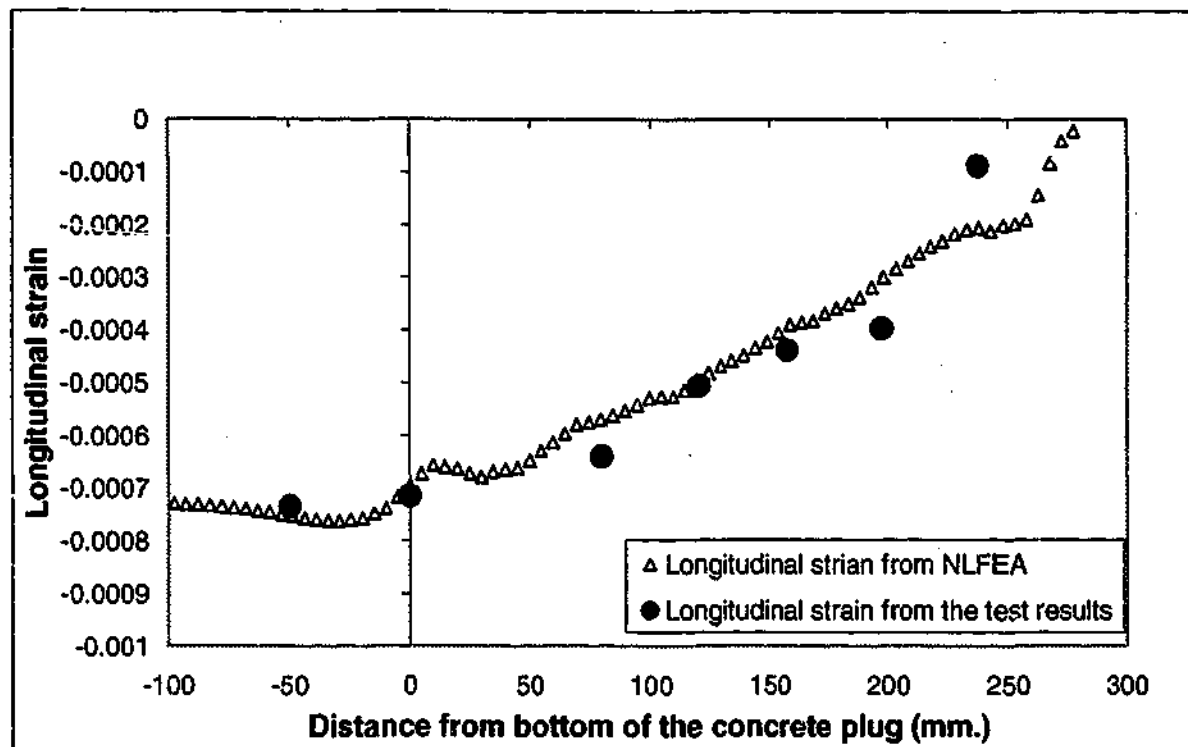
Figure A2-11 Comparison of longitudinal and Hoop strains along the outer surface
of the steel tube for specimen S1.25D of the Stage 2 at load level of 222 kN
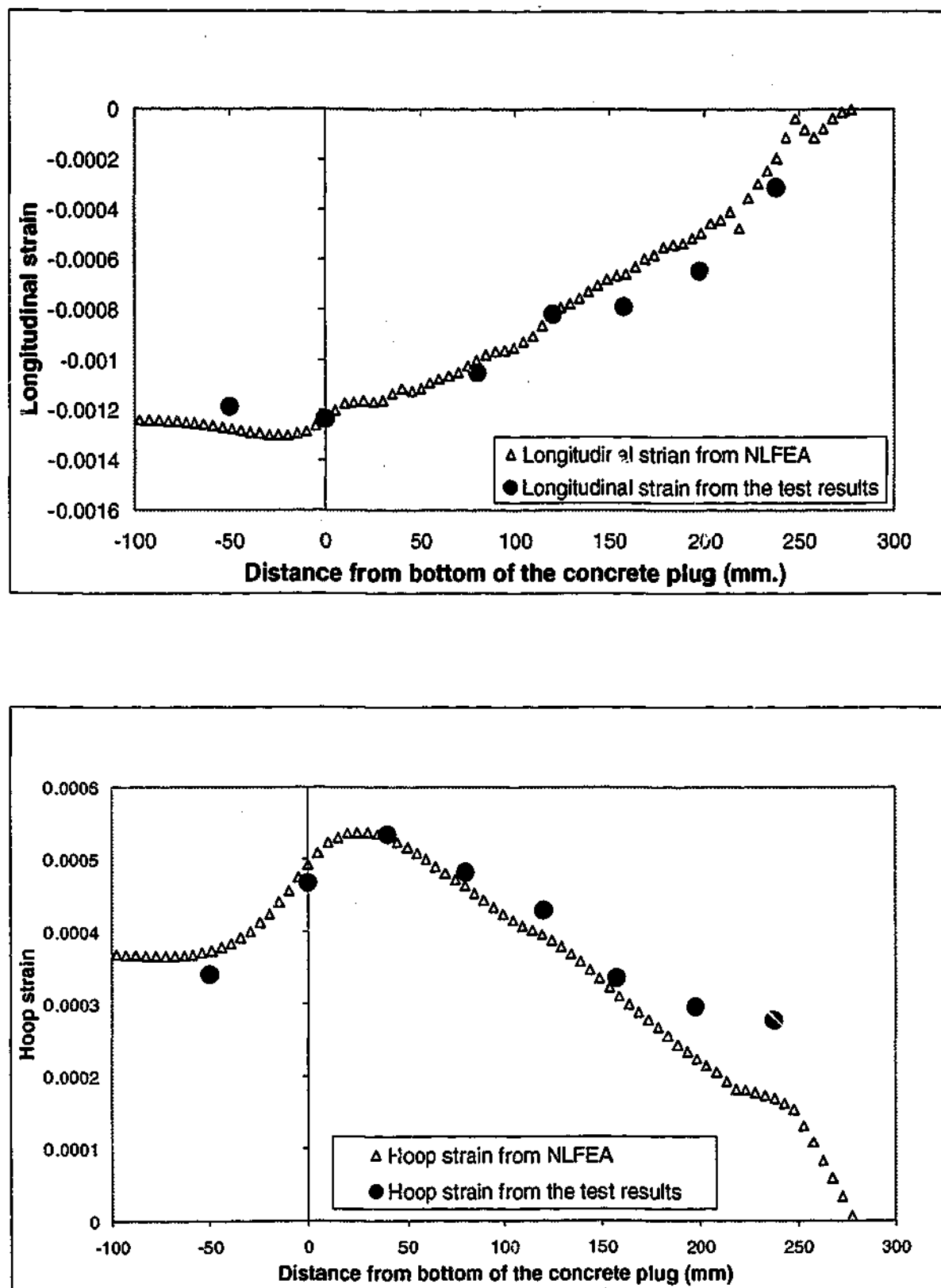
Figure A2-12 Comparison of longitudinal and Hoop strains along the outer surface of the steel tube for specimen S1.25D of the Stage 2 at load level of 440 kN
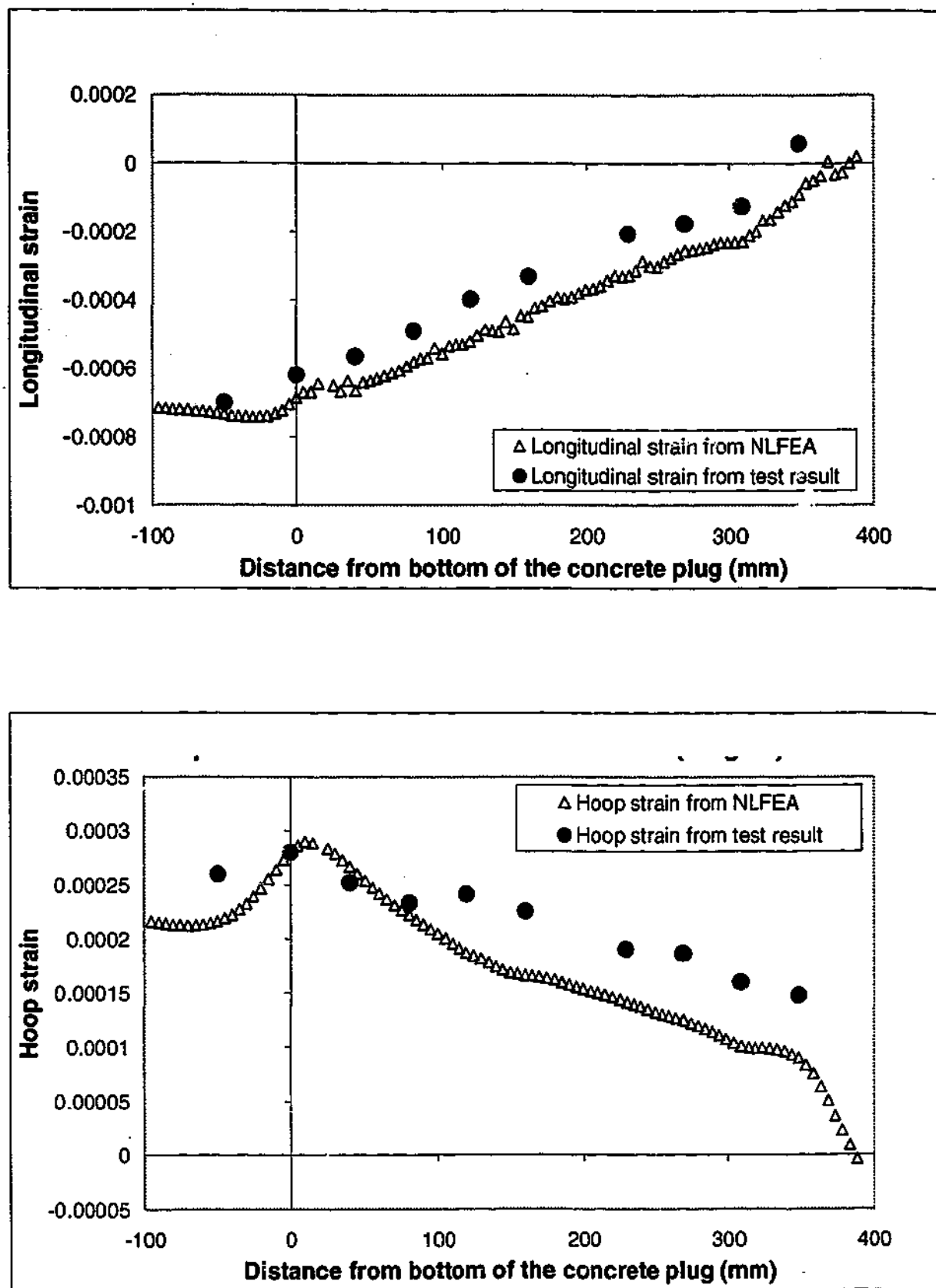
Figure A2-13 Comparison of longitudinal and Hoop strains along the outer surface of the steel tube for specimen S1.75D of the Stage 2 at load level of 225 kN
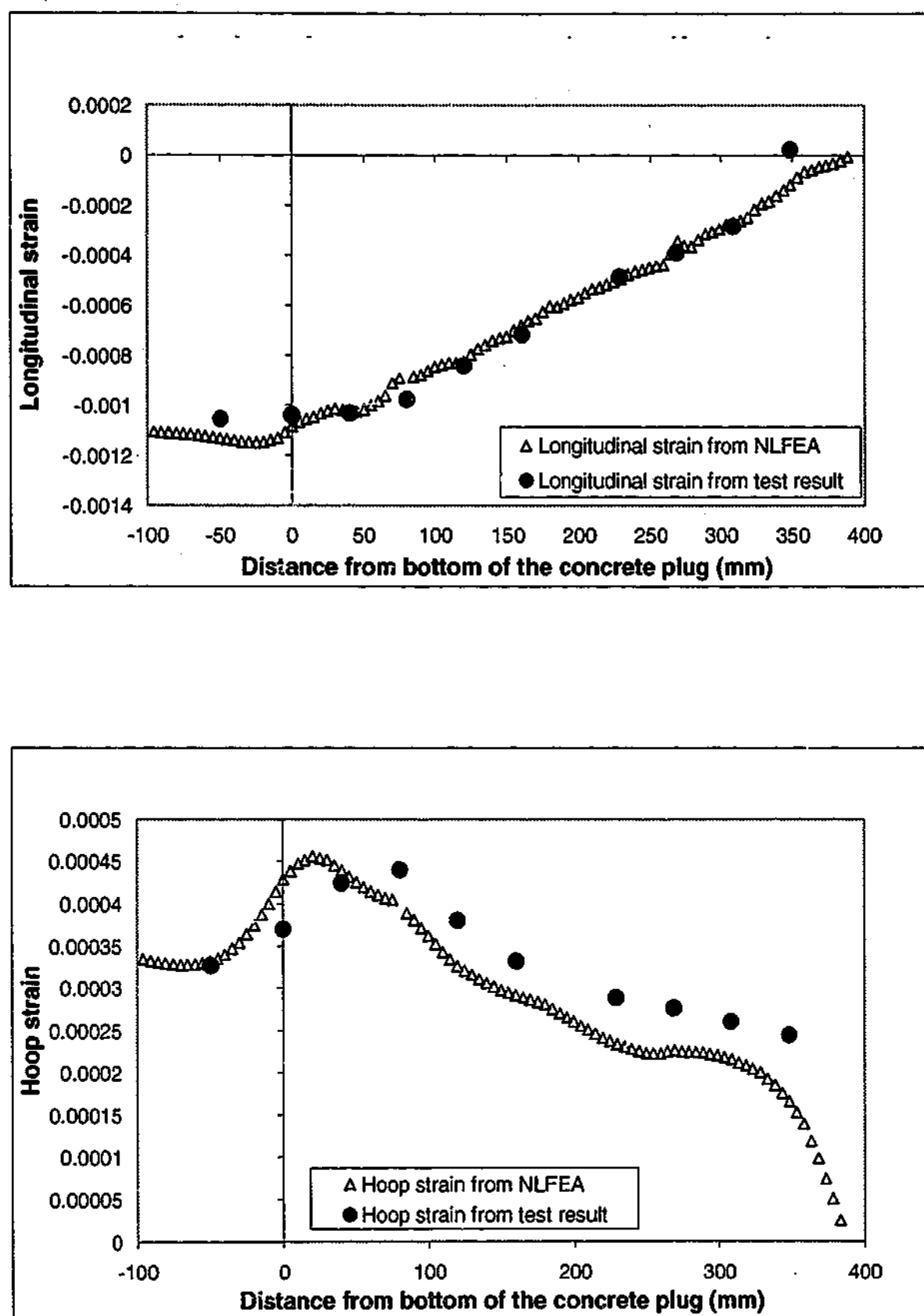
Figure A2-14 Comparison of longitudinal and Hoop strains along the outer surface
of the steel tube for specimen S1.75D of the Stage 2 at load level of 363 kN
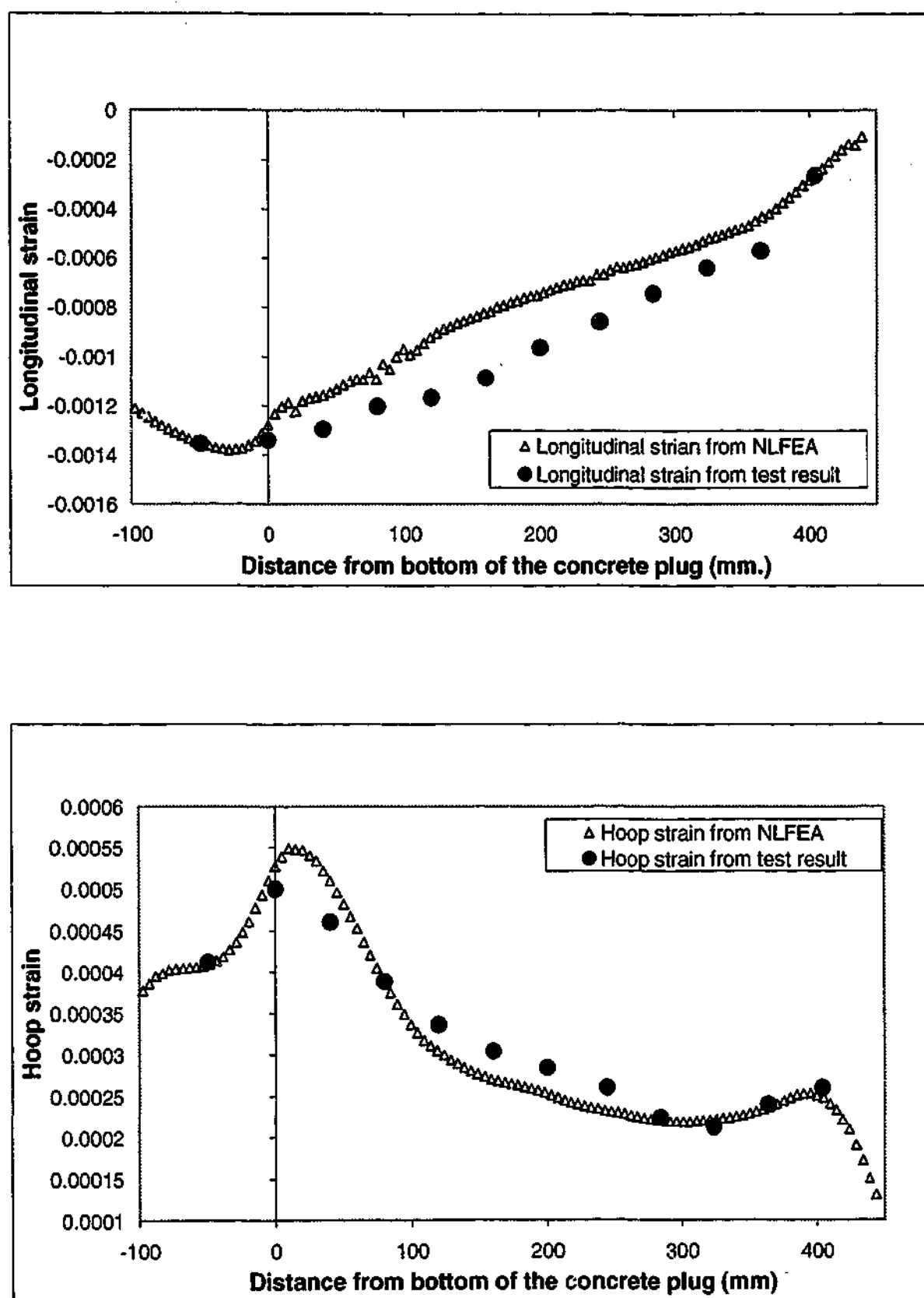
Figure A2-15 Comparison of longitudinal and Hoop strains along the outer surface
of the steel tube for specimen S2.0D of the Stage 2 at load level of 481 kN
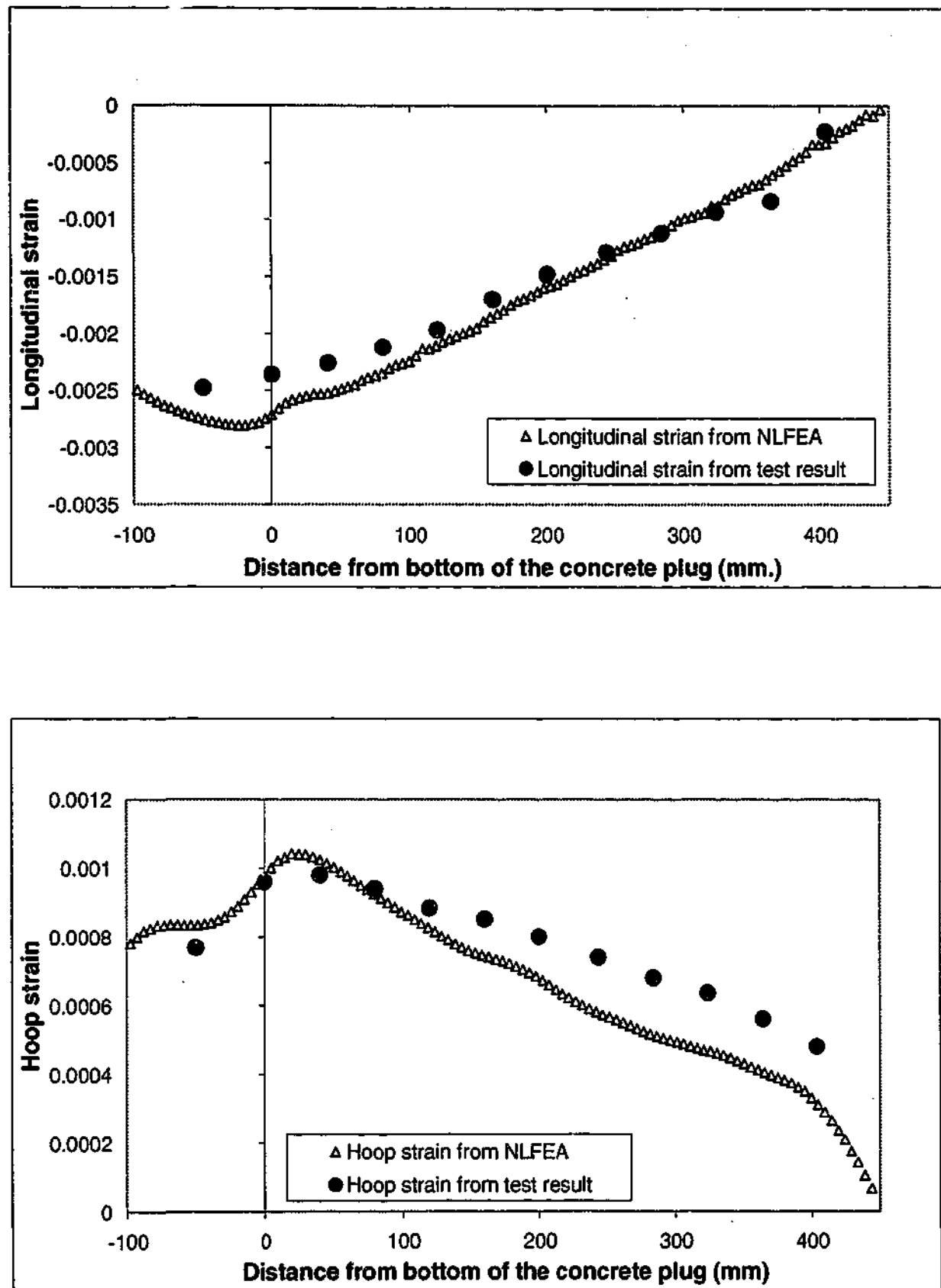
Figure A2-16 Comparison of longitudinal and Hoop strains along the outer
surface of the steel tube for specimen S2.0D of the Stage 2 at load level of 920 kN

A3   COMPUTED   LONGITUDINAL   AND CIRCUMFERENTIAL   BENDING   MOMENT ALONG THE TUBE'S WALL

This appendix presents computed longitudinal and circumferential bending moment along the steel tube for all specimens in two load levels each using the NLFEA solution scheme. No discussion is provided in this appendix as the relevant discussion has been presented in Chapter 7.

Specimen S250 at load level of 333 kN (Pull-out)

Legend:
△ Longitudinal bending moment
× Circumferential bending moment

Y-axis: Moment (N-mm)
X-axis: Distance from bottom of the concrete plug (mm)

Specimen S250 at load level of 662 kN (Pull-out)

Legend:
△ Longitudinal bending moment
× Circumferential bending moment

Y-axis: Moment N-mm
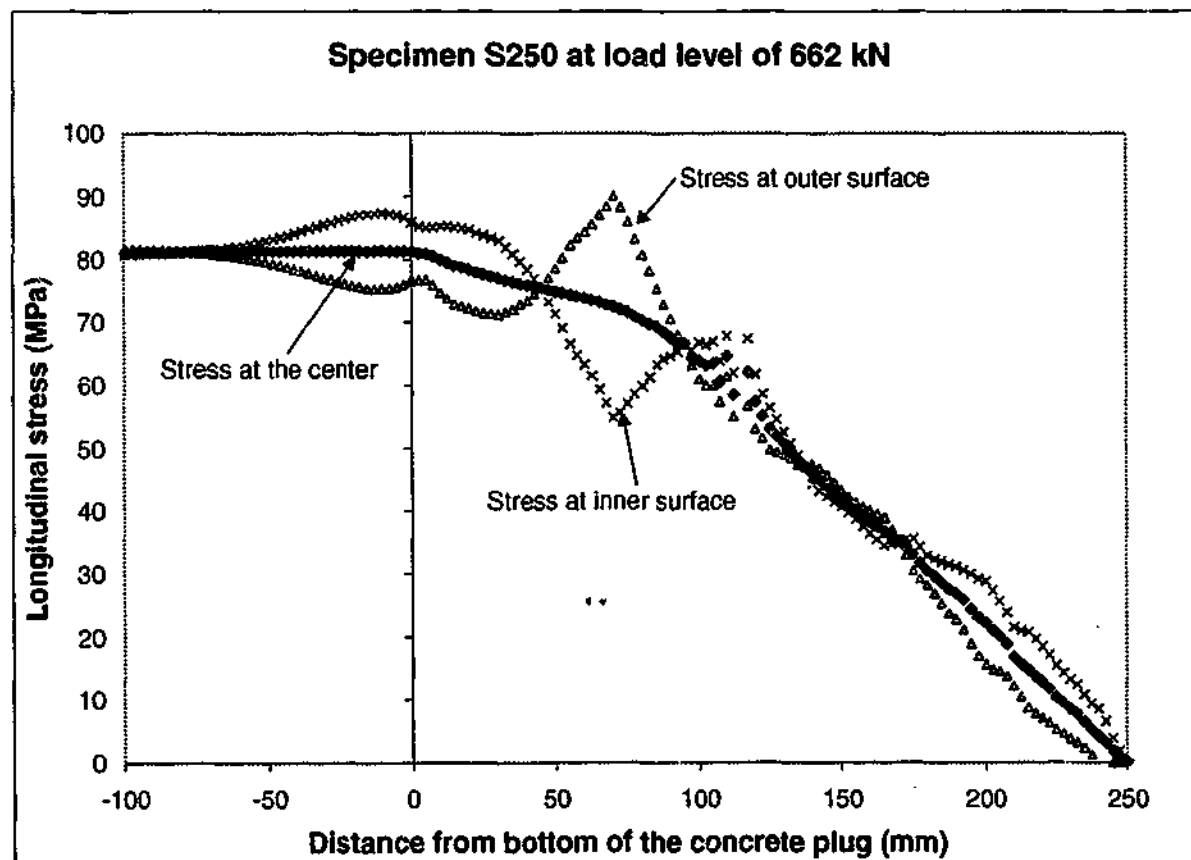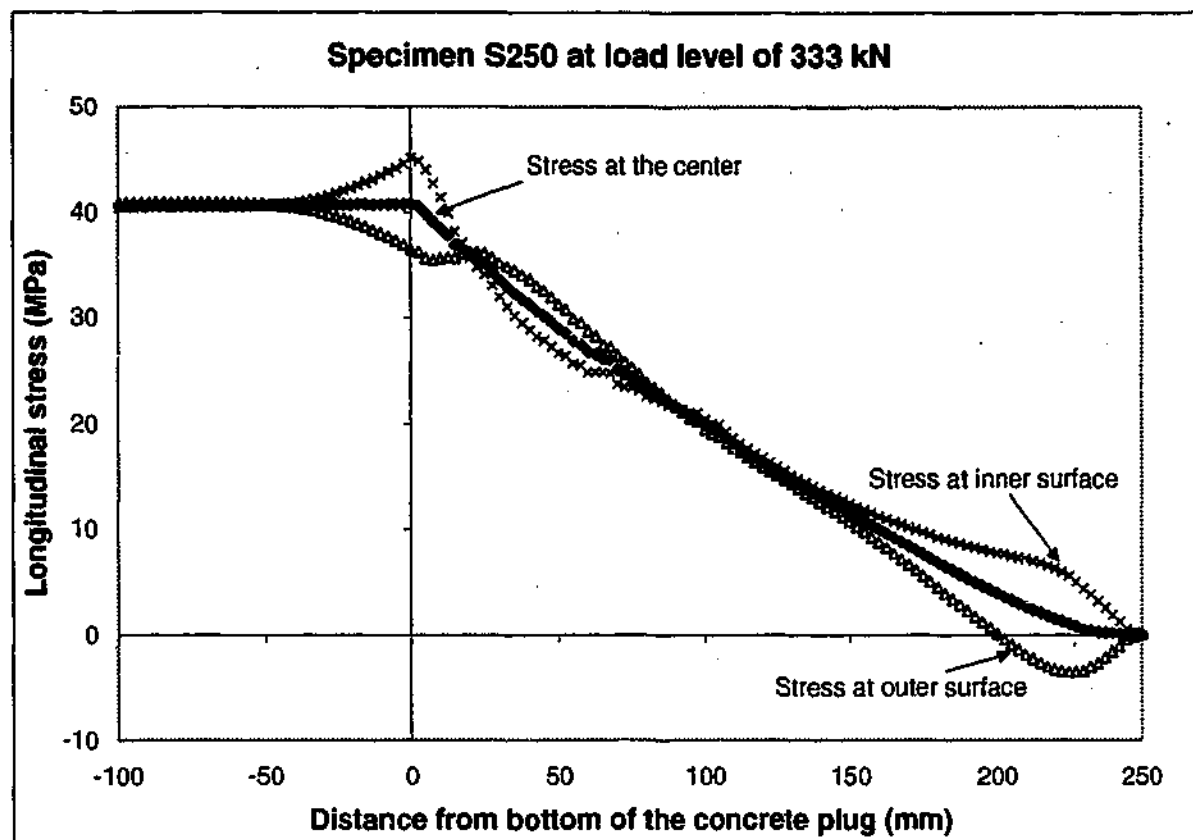X-axis: Distance from bottom of the concrete plug (mm)

Figure A3-1 Bending moment distribution along the steel tube for specimen S250 of the pull-out test
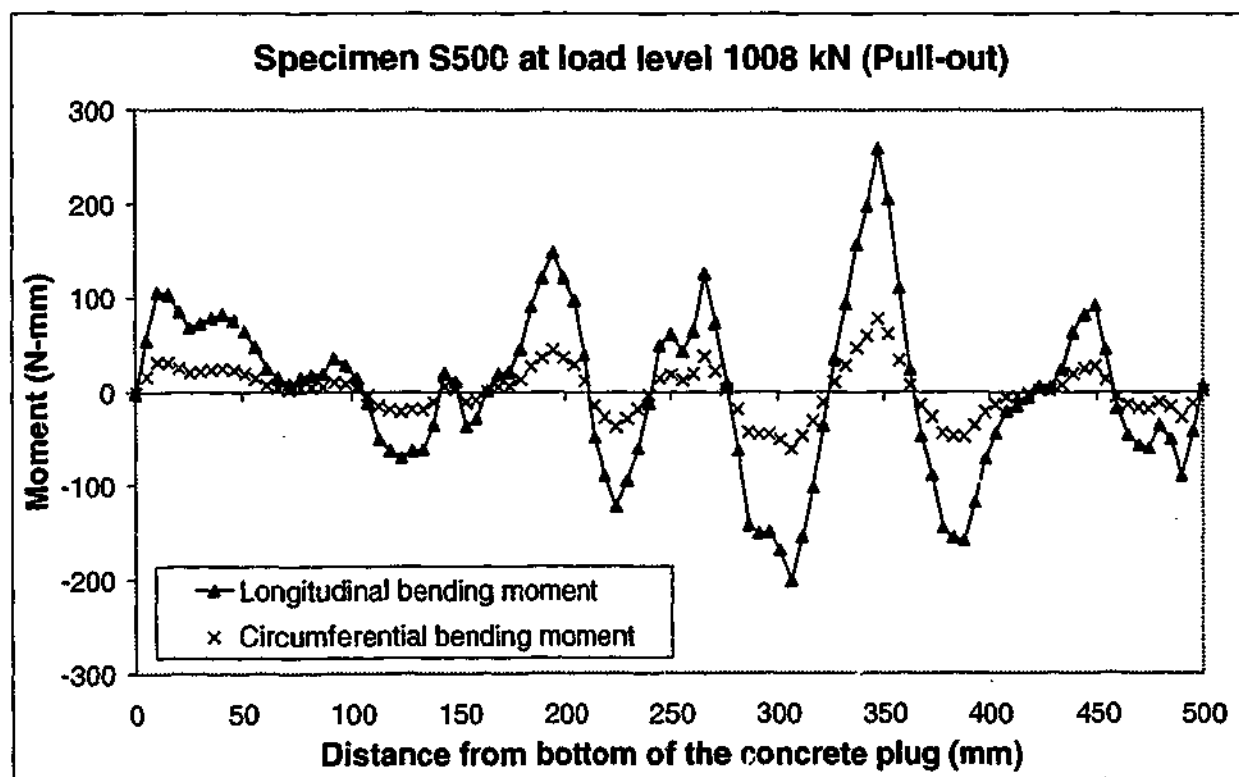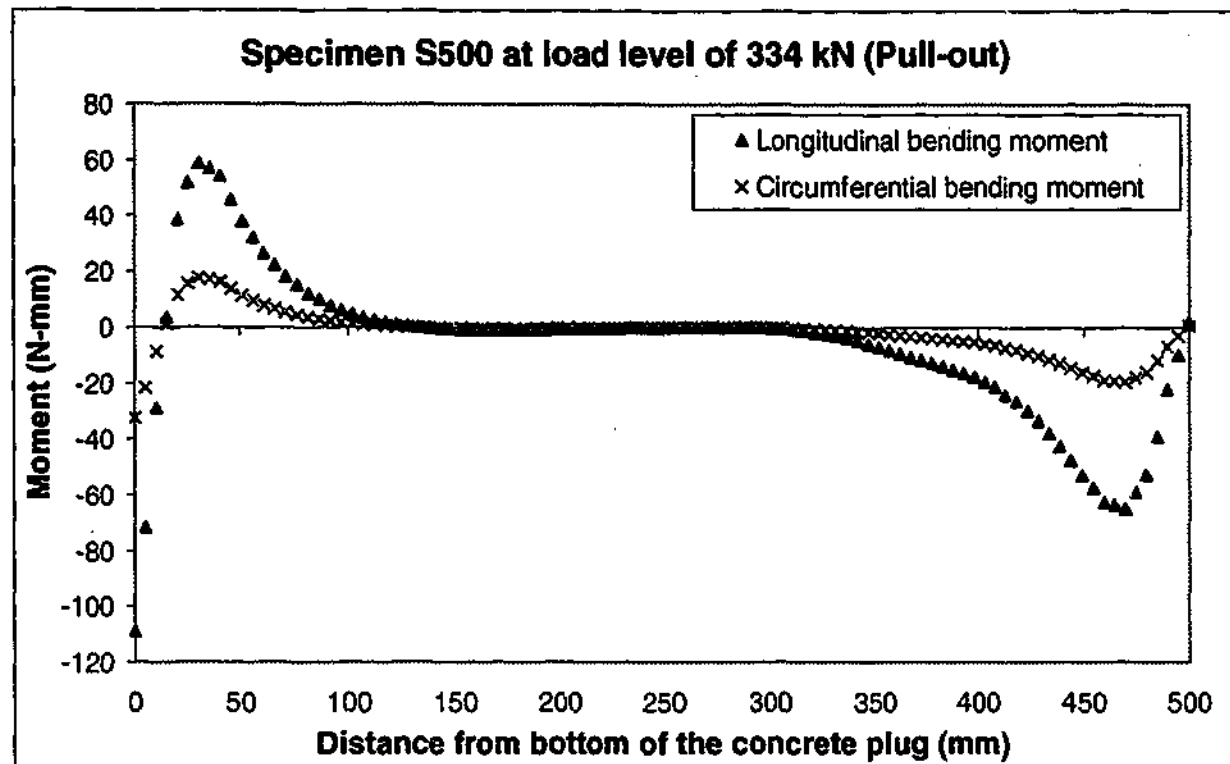
Figure A3-2 Bending moment distribution along the steel tube for specimen S500
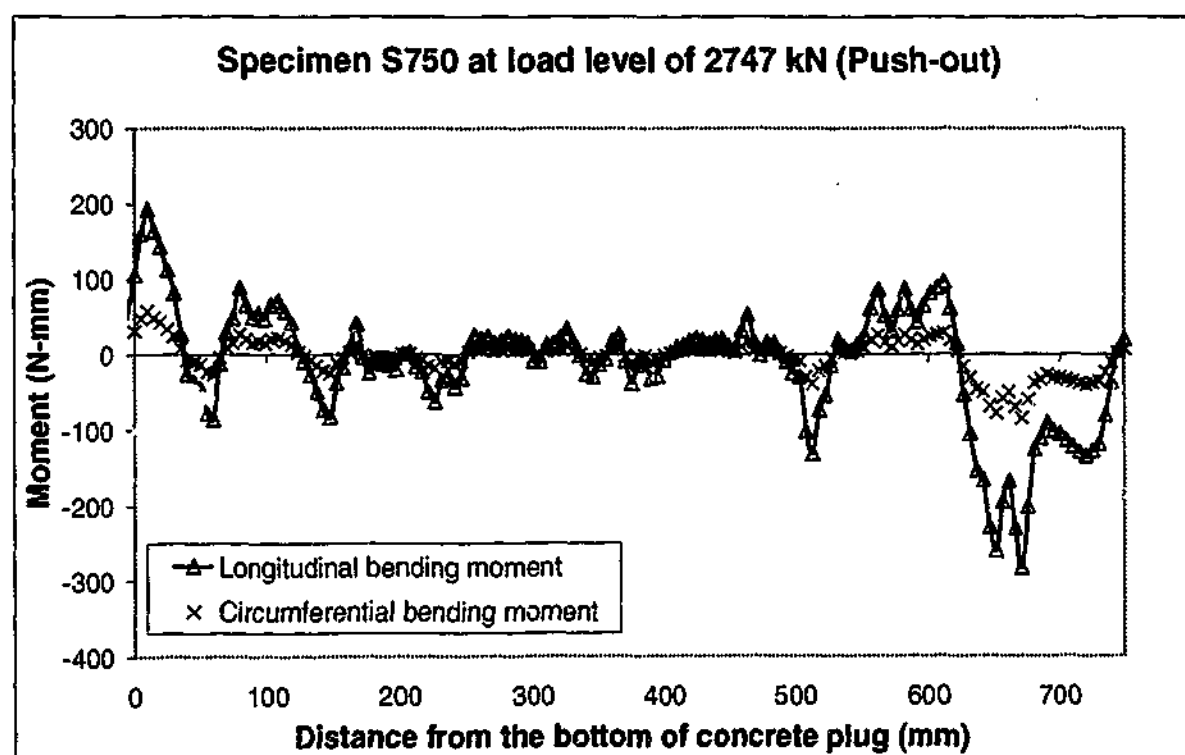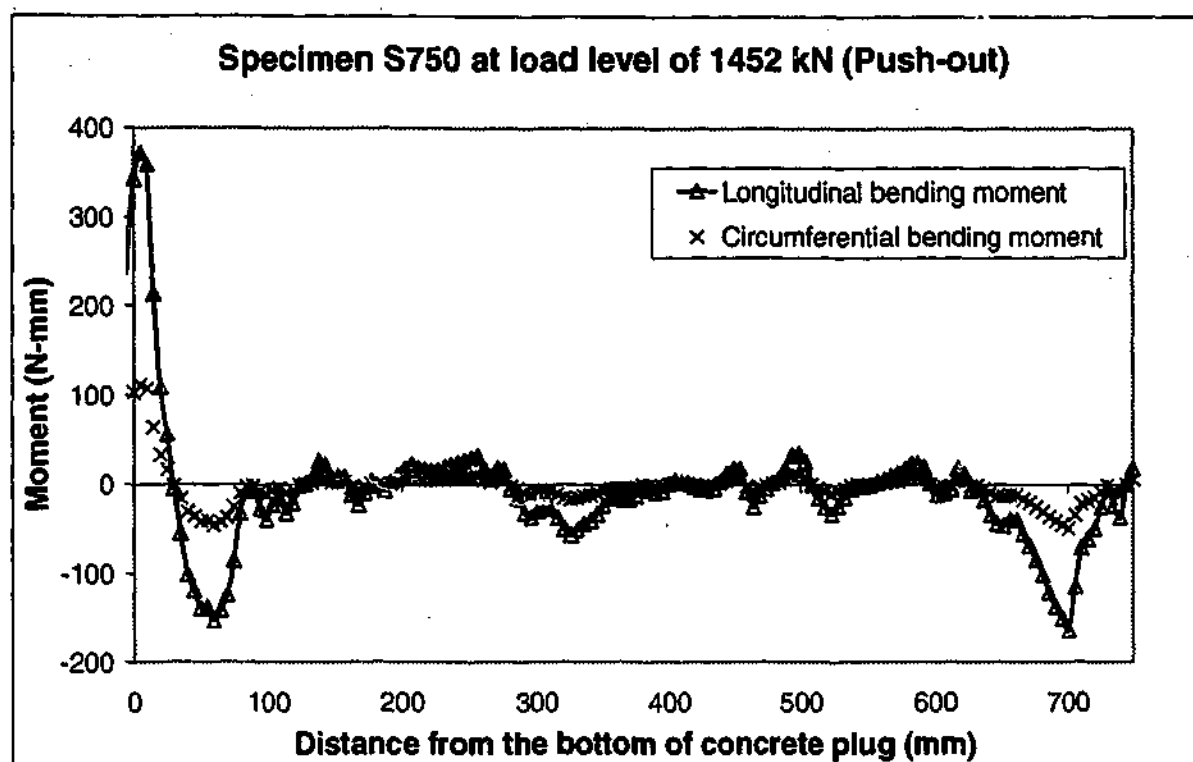
of the pull-out test

Figure A3-3 Bending moment distribution along the steel tube for specimen S750

of the push-out test

Specimen S1.0D at load level of 275 kN (Stage 1)

Legend:
- Longitudinal bending moment
- Circumferential bending moment

Y-axis: Moment (N-mm)
X-axis: Distance from bottom of the concrete plug (mm)

Specimen S1.0D at load level of 663 kN (Stage 1)

Legend:
- Longitudinal bending moment
- Circumferential bending moment

Y-axis: Moment (N-mm)
X-axis: Distance from bottom of the concrete plug (mm)
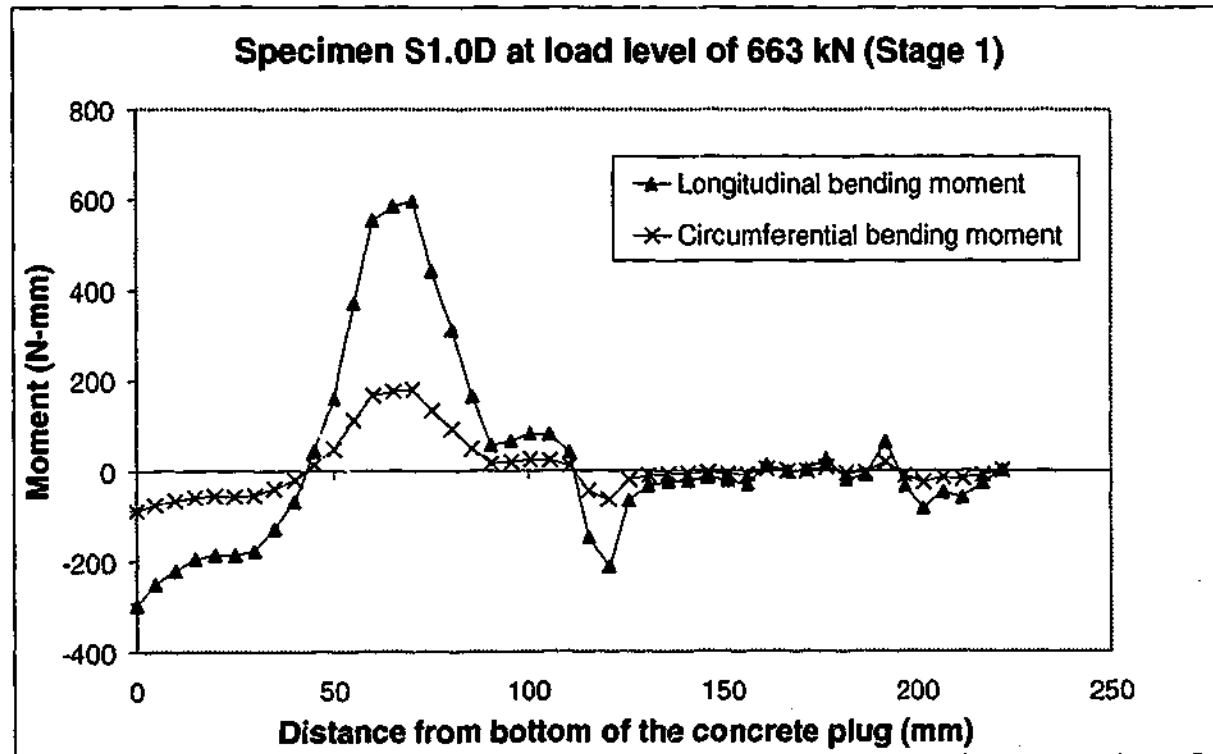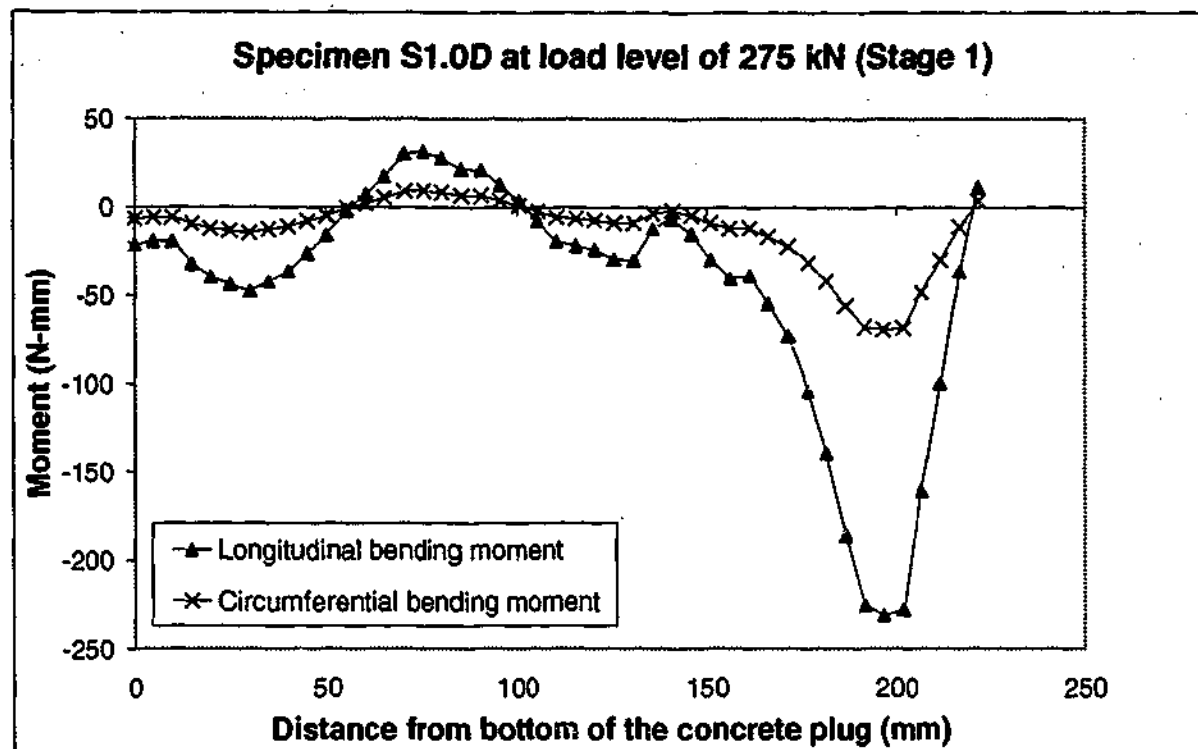
Figure A3-4 Bending moment distribution along the steel tube for specimen
S1.0D (Stage 1)

Specimen S1.5D at load level of 572 kN (Stage 1)

Legend:
- Longitudinal bending moment
- Circumferential bending moment

Y-axis: Moment (N-mm)
X-axis: Distance from bottom of the concrete plug (mm)

Specimen S1.5D at load level of 1000 kN (Stage 1)

Legend:
- Longitudinal bending moment
- Circumferential bending moment

Y-axis: Moment (N-mm)
X-axis: Distance from bottom of the concrete plug (mm)

Figure A3-5 Bending moment distribution along the steel tube for specimen

S1.5D (Stage 1)
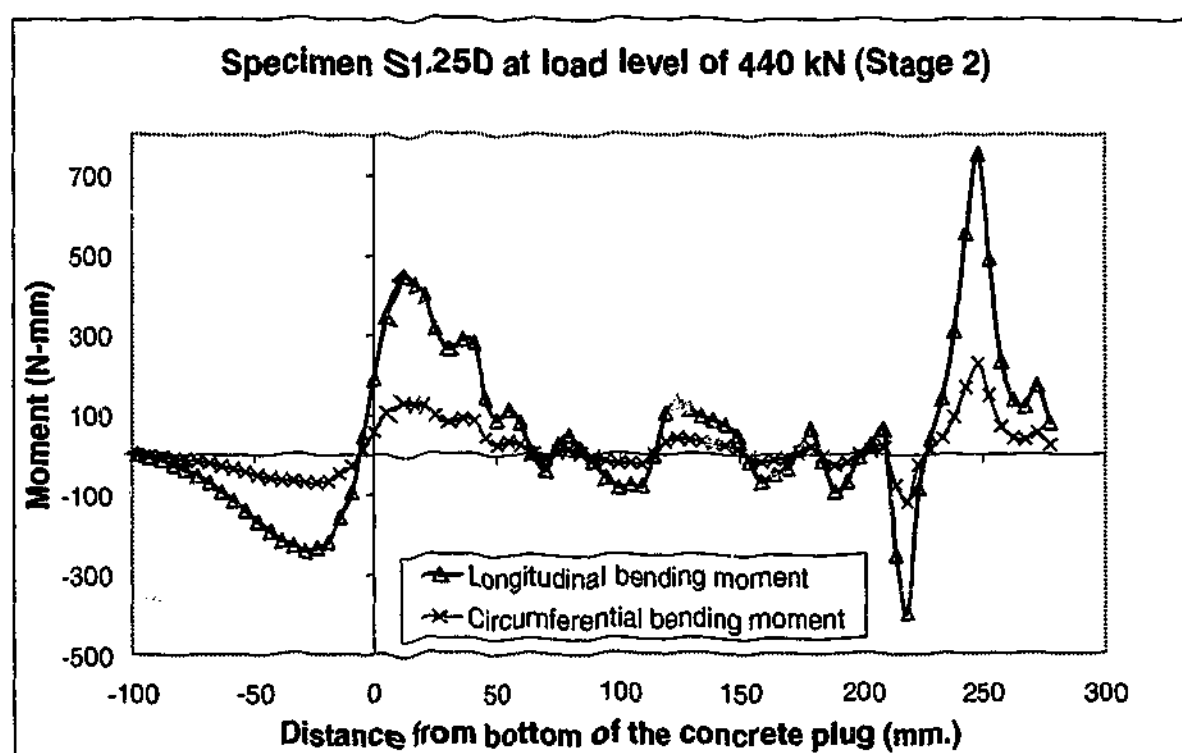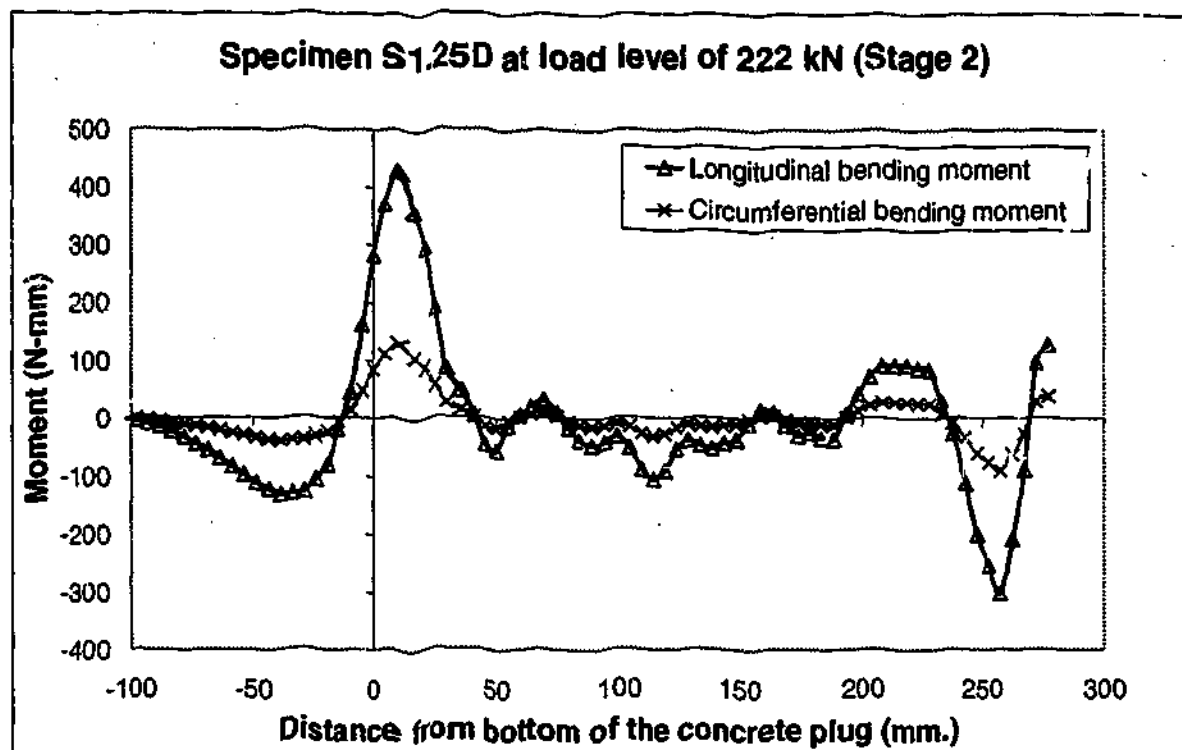
Figure A3-6 Bending moment distribution along the steel tube for specimen
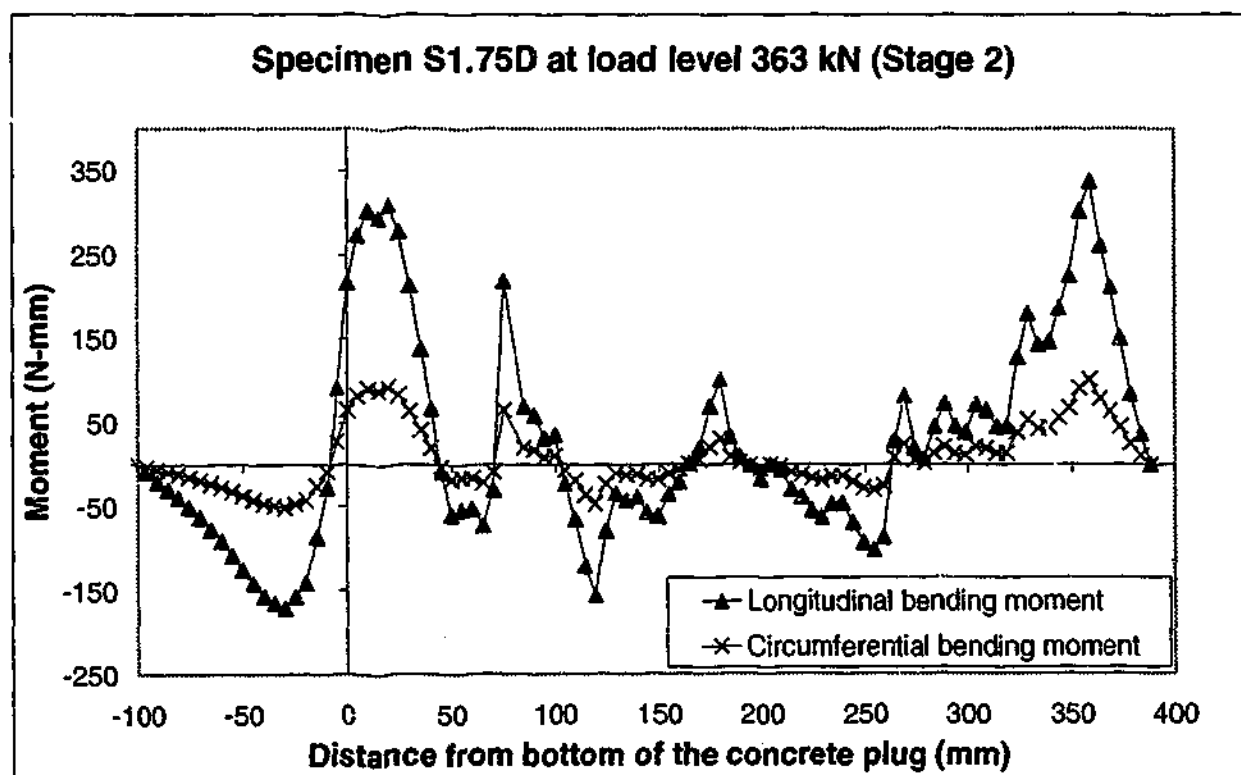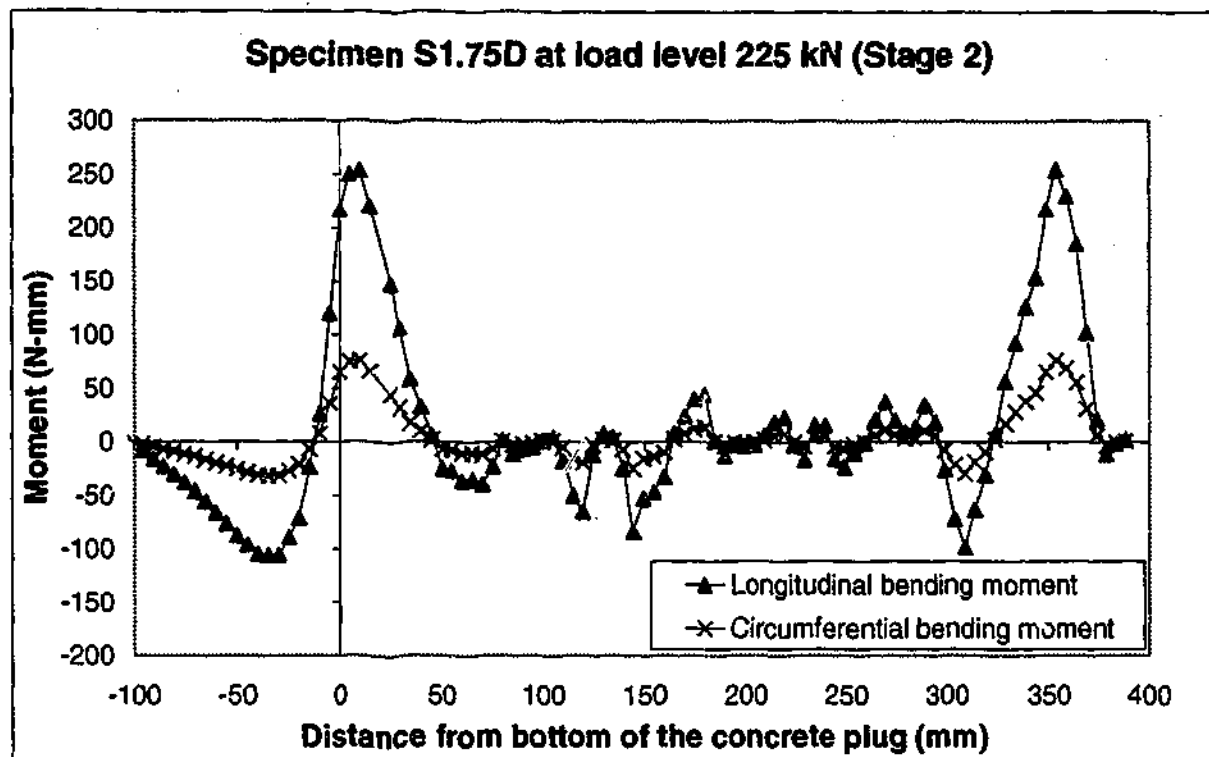
S1.25D (Stage 2)

Figure A3-7 Bending moment distribution along the steel tube for specimen

S1.75D (Stage 2)

Specimen S2.0D at load level of 418 kN (Stage 2)

Legend:
- Longitudinal bending moment
- Circumferential bending moment

X-axis: Distance from bottom of the concrete plug (mm.)
Y-axis: Moment (N-mm)

Specimen S2.0D at load level of 920 kN (Stage 2)

Legend:
- Bending moment distribution from NLFEA
- Circumferential bending moment

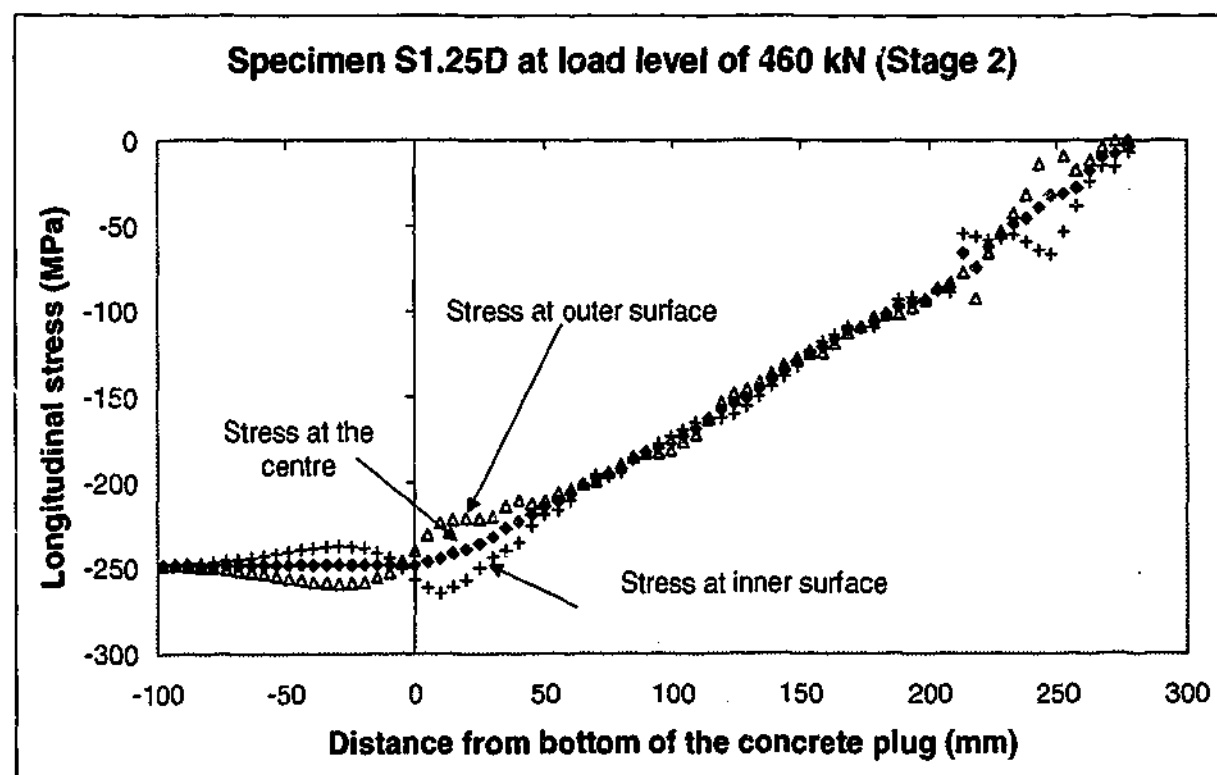X-axis: Distance from bottom of the concrete plug (mm.)
Y-axis: Moment (N-mm)
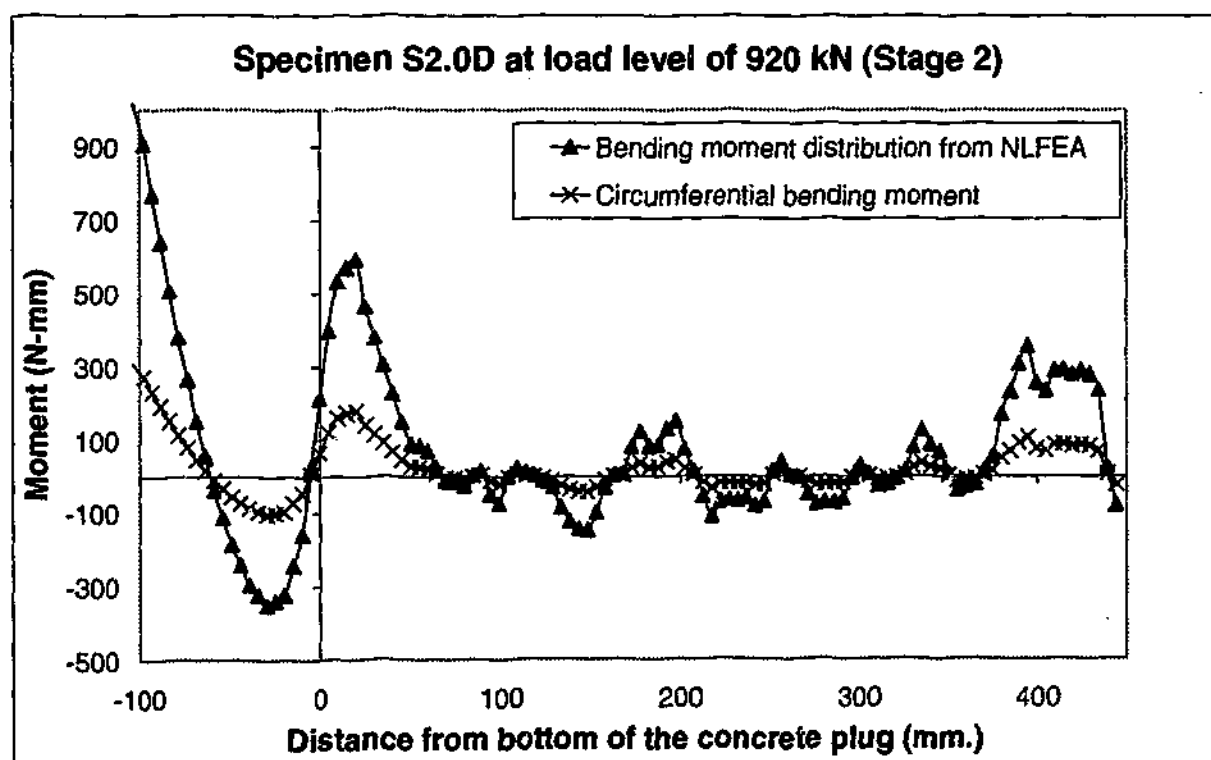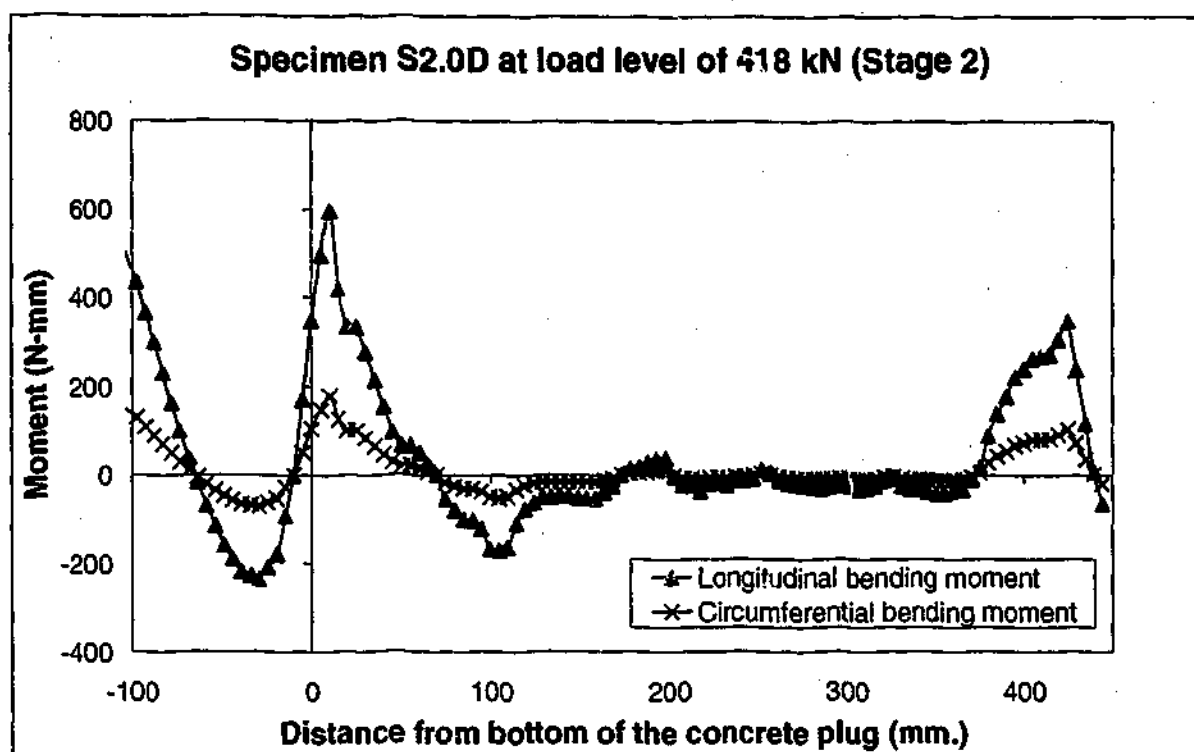
Figure A3-8 Bending moment distribution along the steel tube for specimen

S2.0D (Stage 2)

A4.   LONGITUDINAL STRESS DISTRIBUTIONS ALONG THE TUBE'S WALL

This appendix presents the longitudinal stress distributions for all specimens at ultimate load level and at load level of changing the slope of load-slip response. The longitudinal stress distributions are shown at the outer and inner surfaces and centre of the steel tube wall. The stress distribution at the centre of the steel tube wall is used to determine the shear/bond stress distribution along the interface. No discussion is provided in this appendix as the relevant discussion has been presented in Chapter 7.

Specimen S250 at load level of 333 kN

(Stress at the center, Stress at inner surface, Stress at outer surface)

Specimen S250 at load level of 662 kN

(Stress at outer surface, Stress at the center, Stress at inner surface)

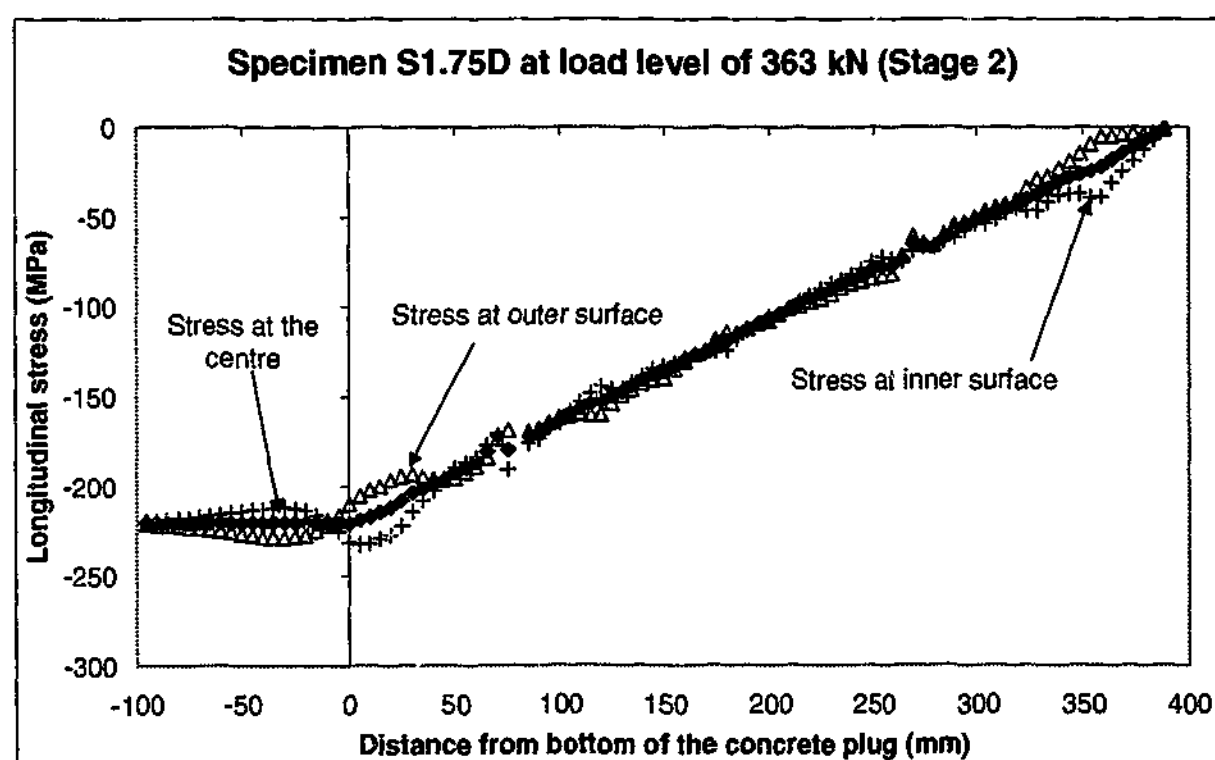Figure A4-1 Longitudinal stress distributions along the steel tube for specimen

S250 of pull-out test
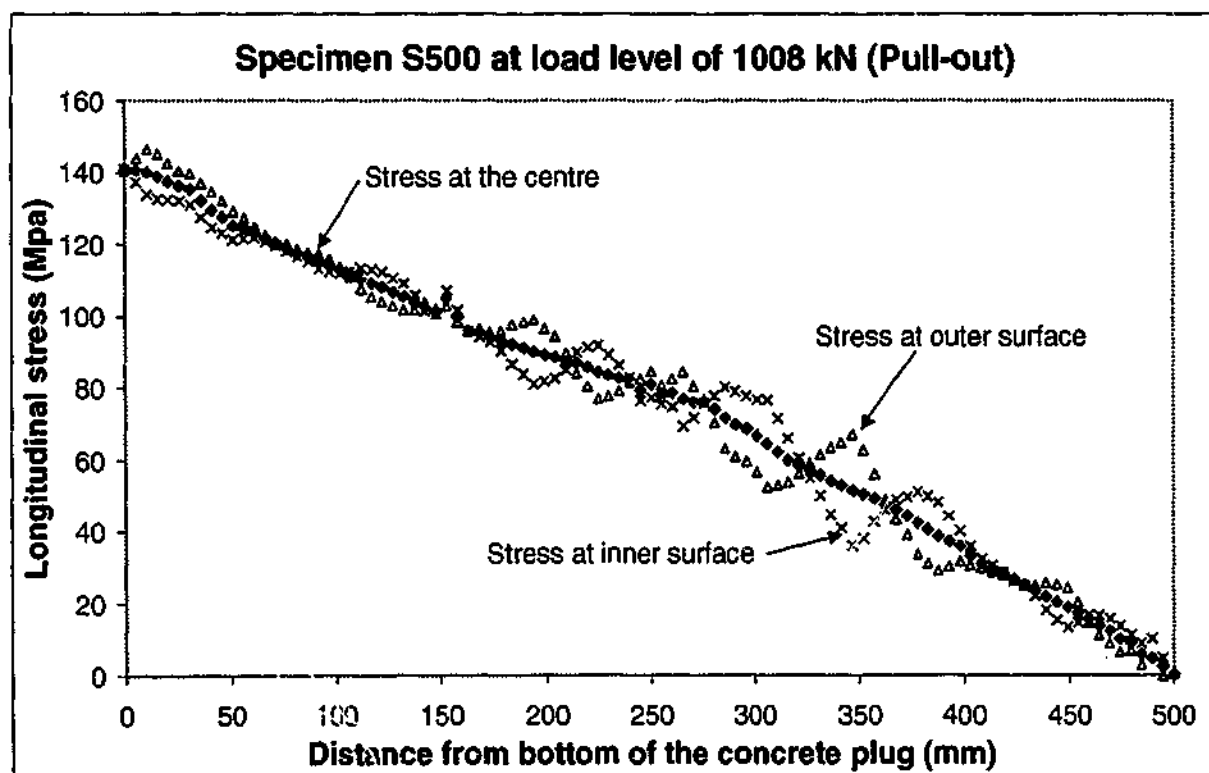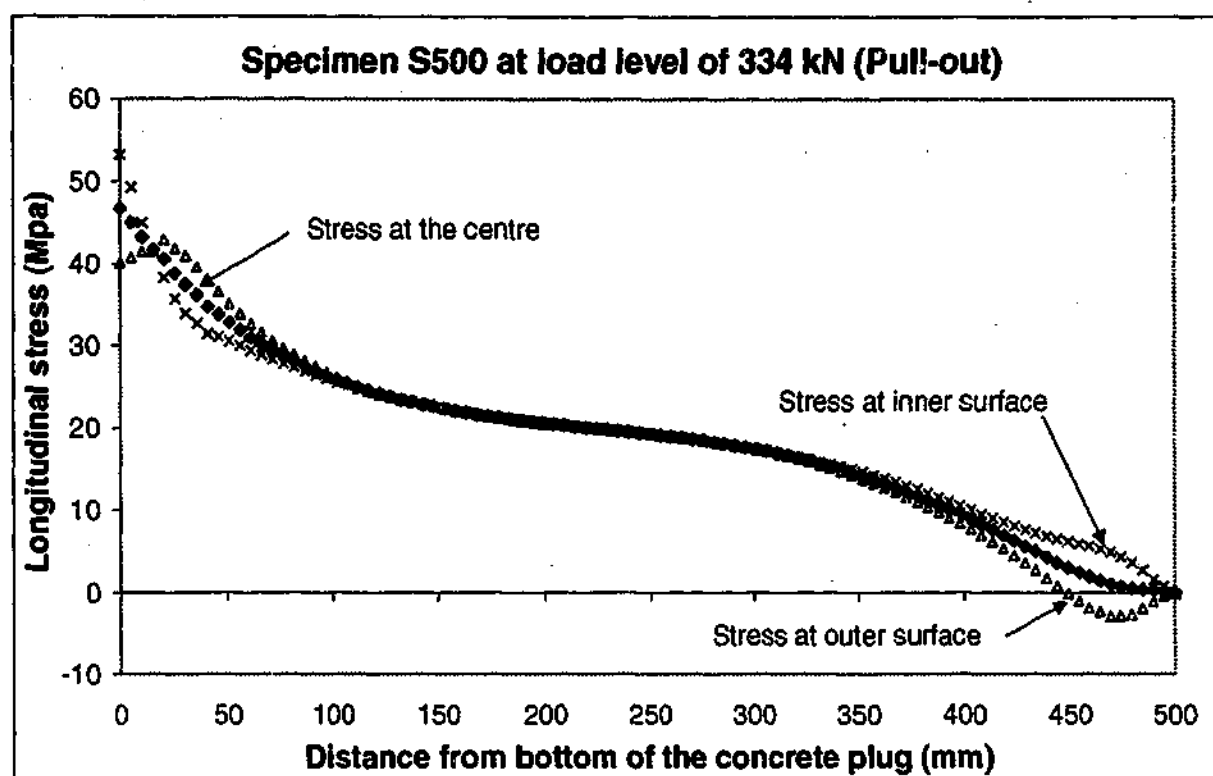
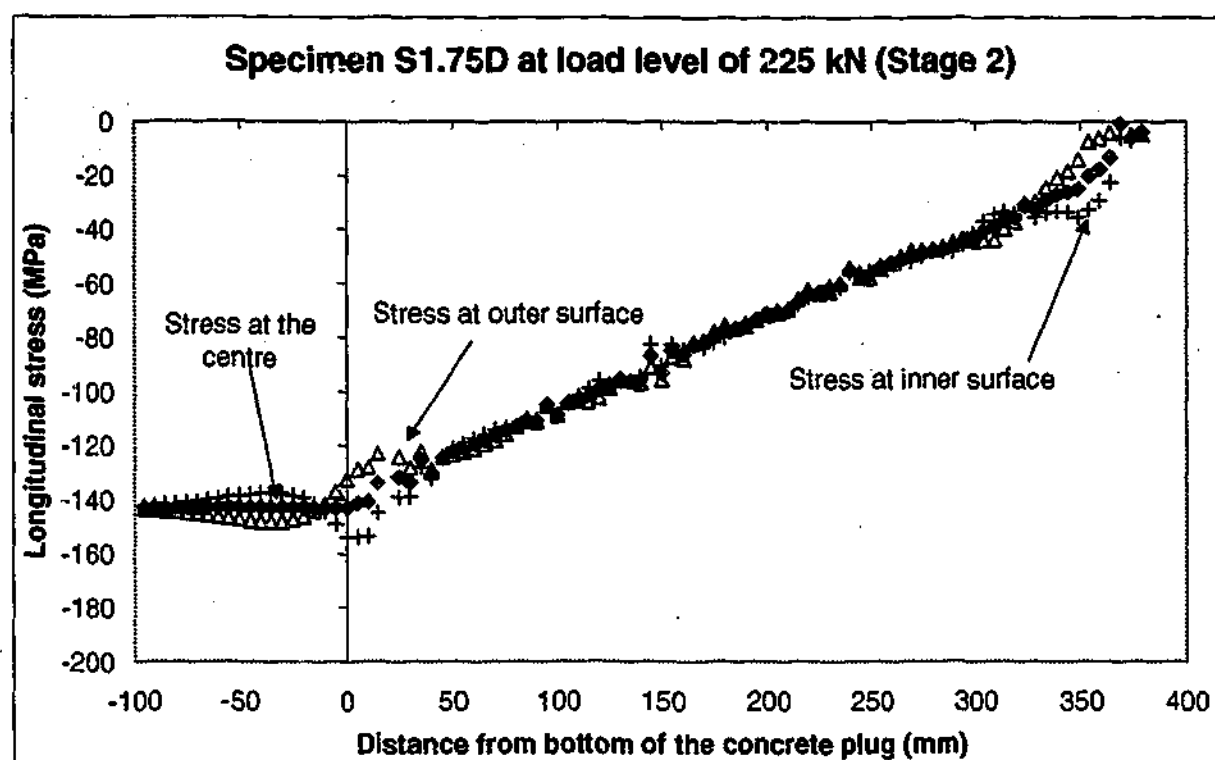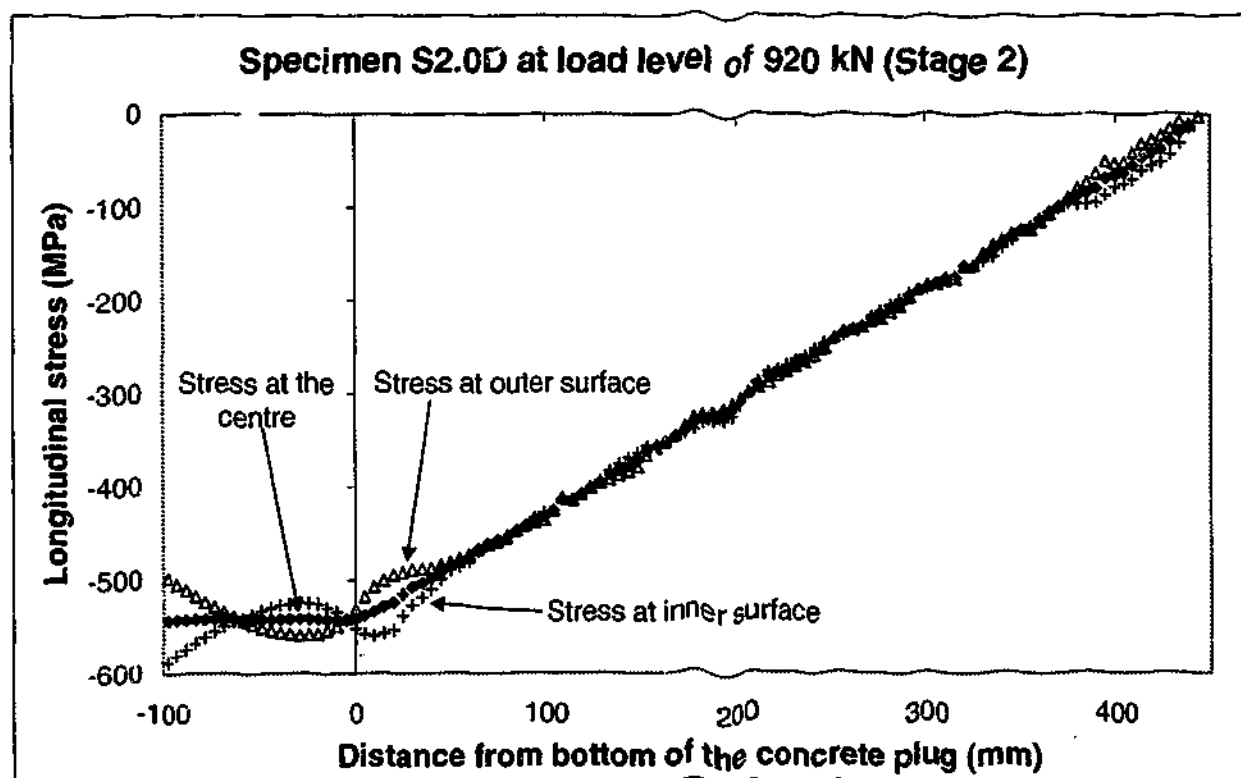Figure A4-2 Longitudinal stress distributions along the steel tube for specimen

S500 of pull-out test
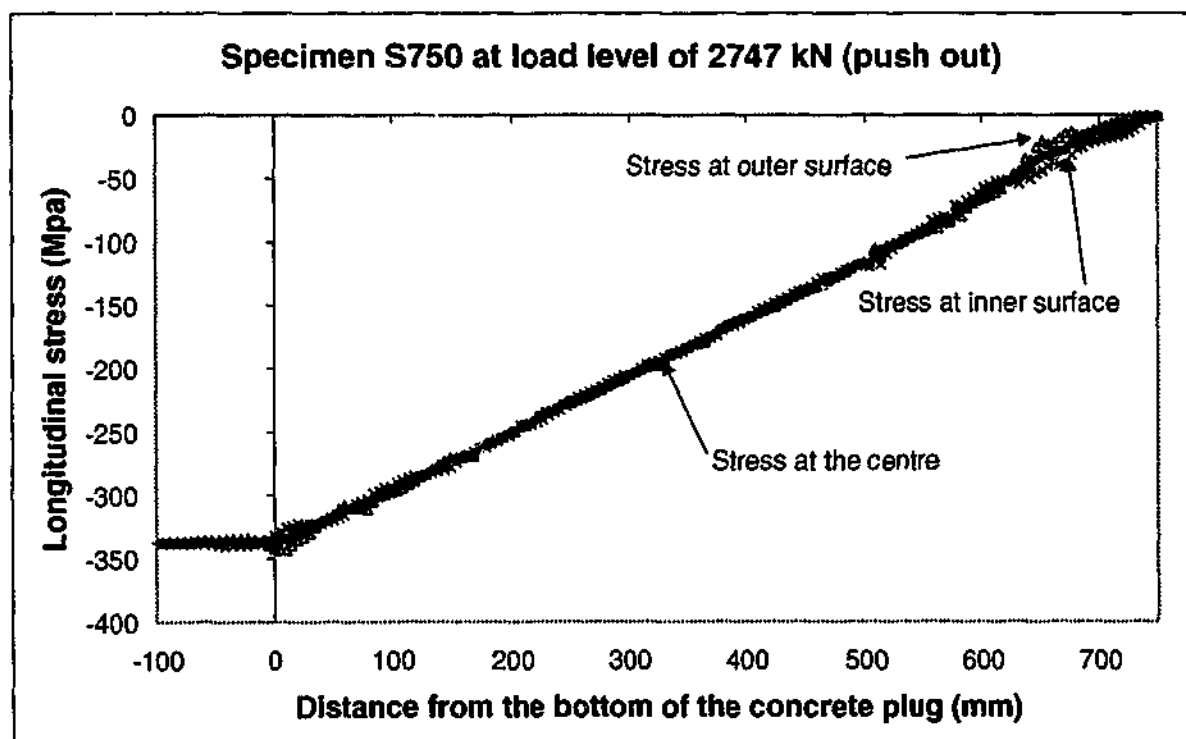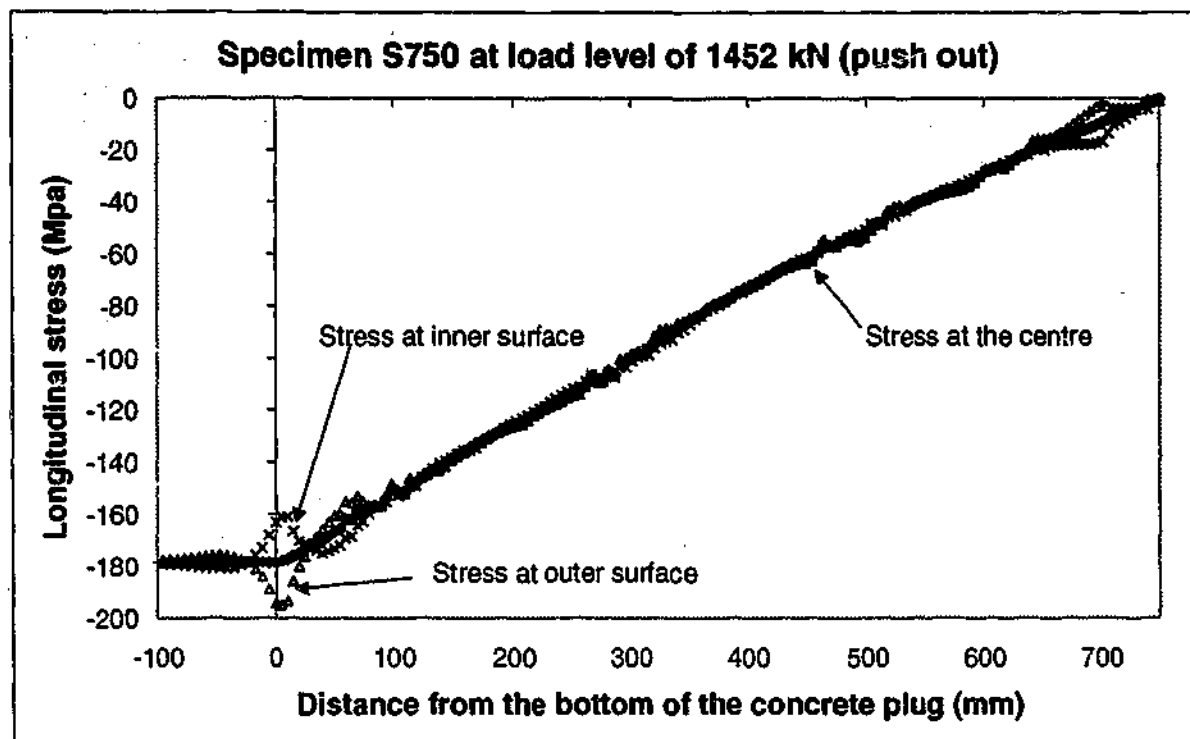
Figure A4-3 Longitudinal stress distributions along the steel tube for specimen
S750 of push-out test
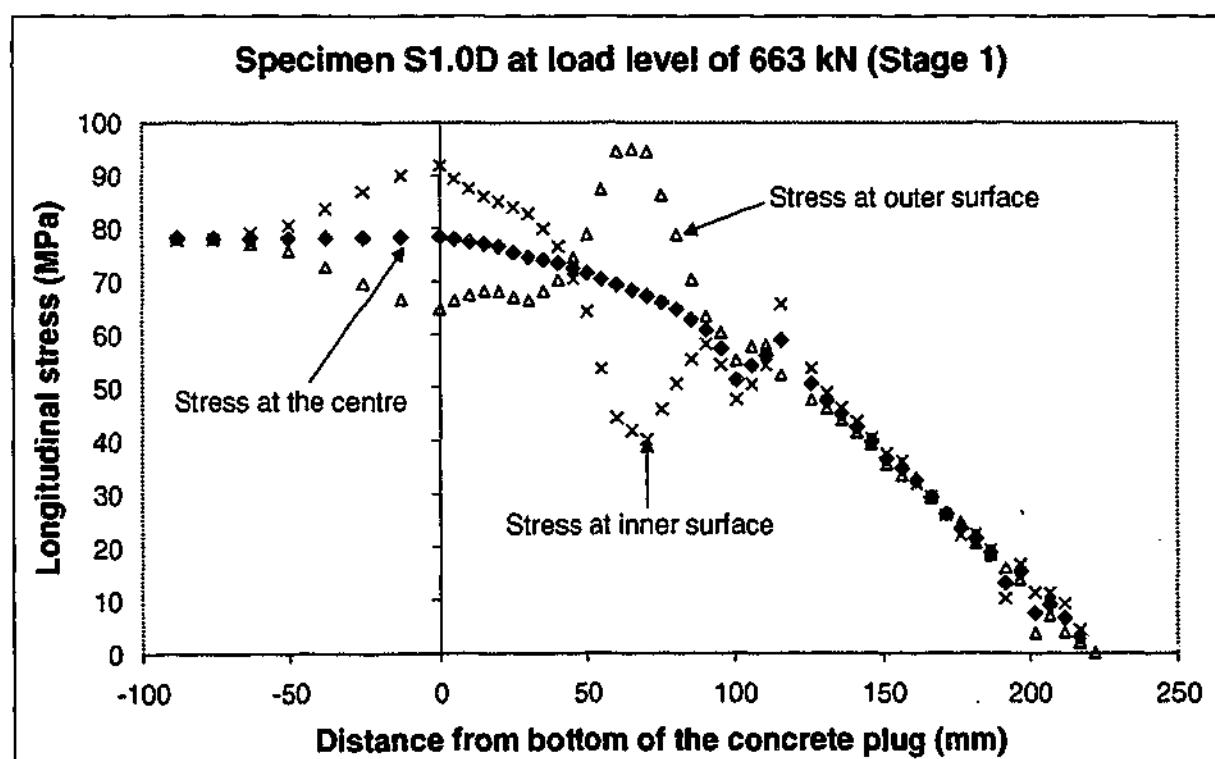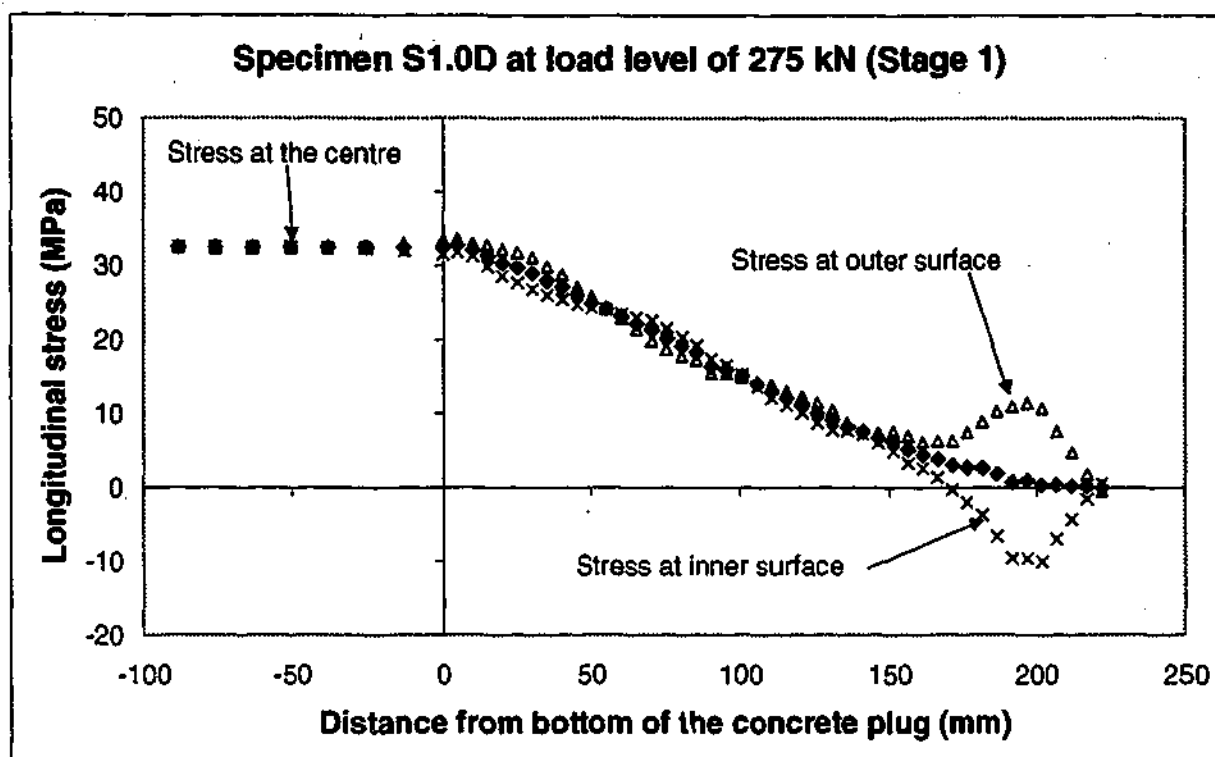
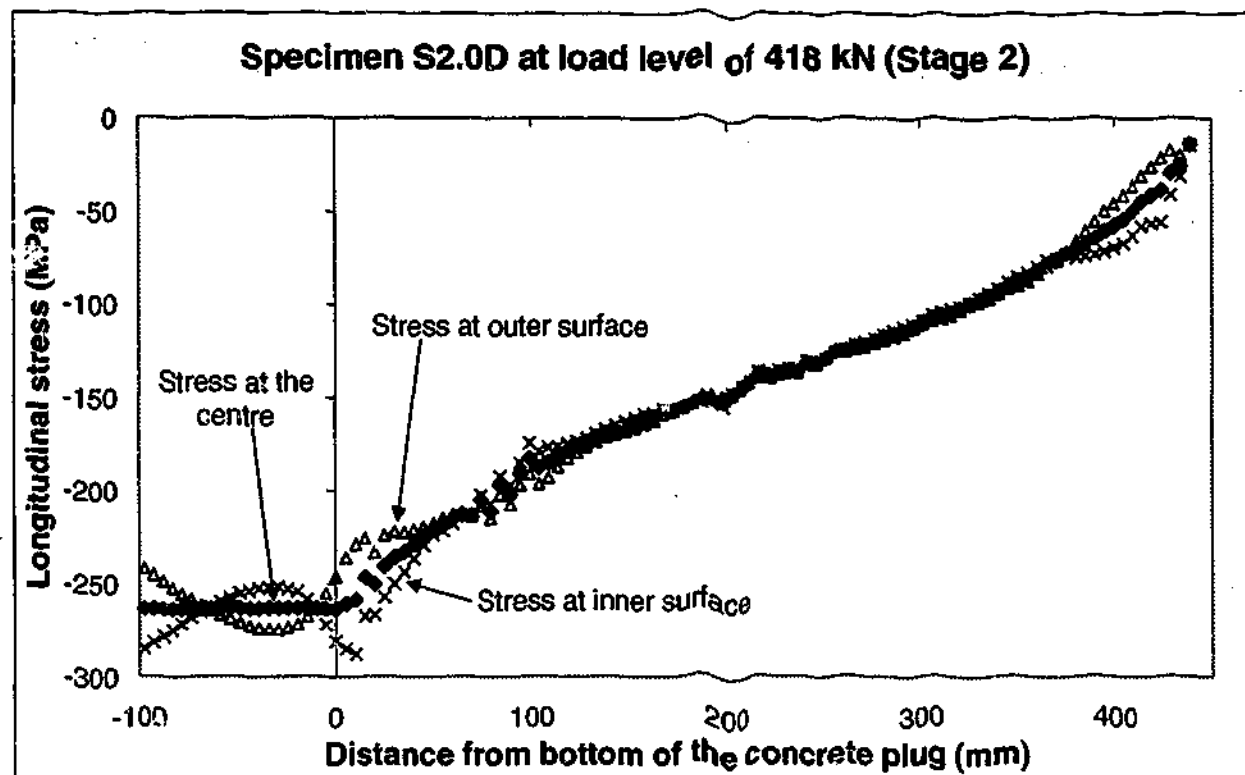Figure A4-4 Longitudinal stress distributions along the steel tube for specimen

S1.0D of Stage 1

Specimen S1.5D at load level of 572 kN (Stage 1)

Stress at the center

Stress at inner surface

Stress at outer surface

Specimen S1.5D at load level of 1000 kN (Stage 1)

Stress at outer surface

Stress at the center

Stress at inner surface
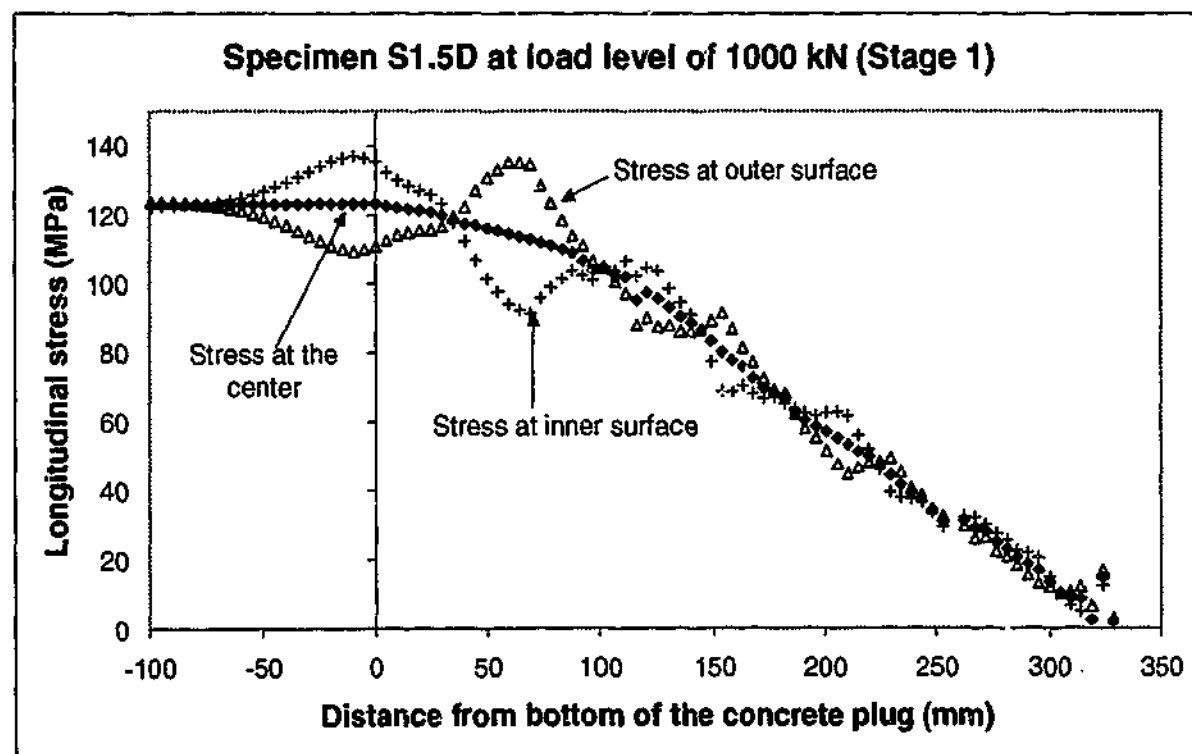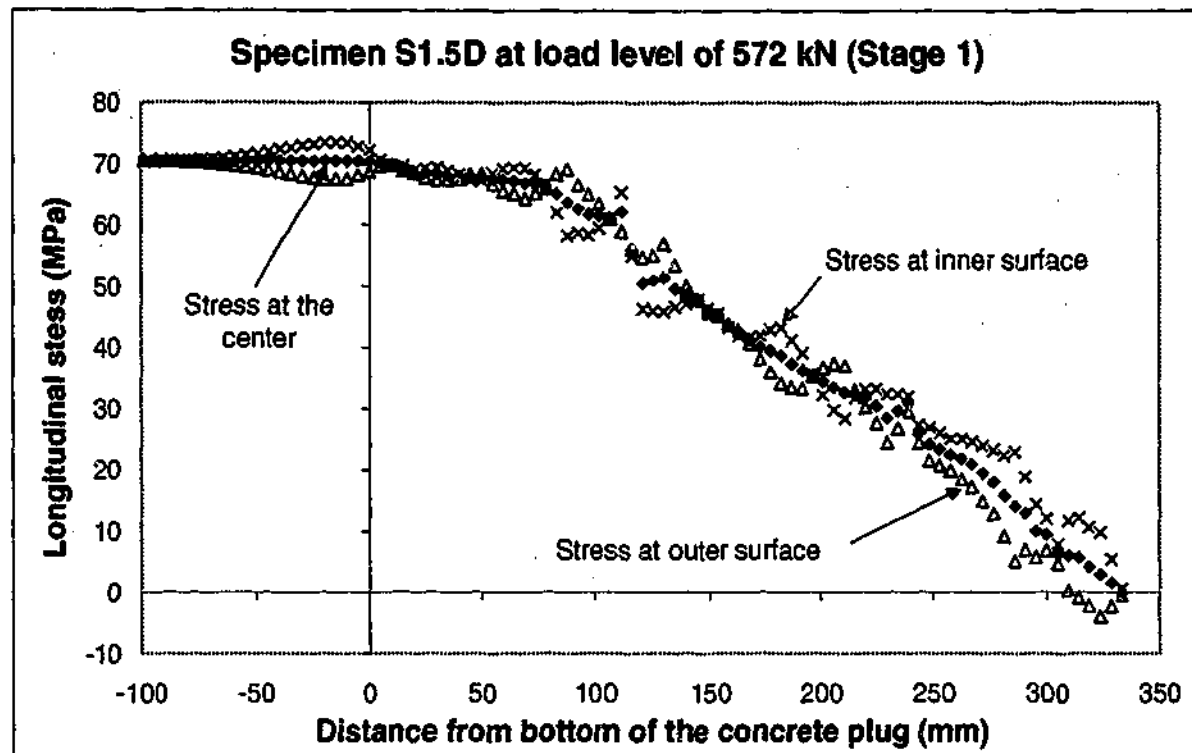
Figure A4-5 Longitudinal stress distributions along the steel tube for specimen
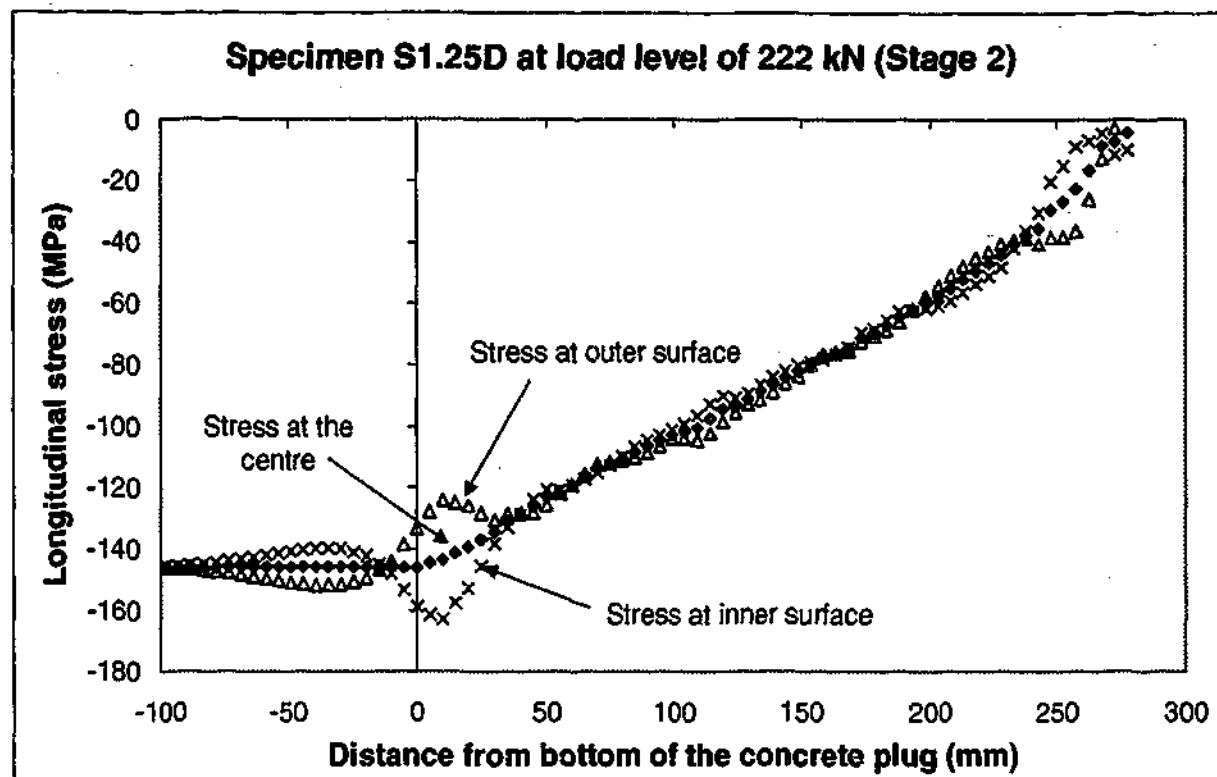
S1.5D of Stage 1

Figure A4-6 Longitudinal stress distributions along the steel tube for specimen

S1.25D of Stage 2

Figure A4-7 Longitudinal stress distributions along the steel tube for specimen

S1.75D of Stage 2

Specimen S2.0D at load level of 418 kN (Stage 2)

Specimen S2.0D at load level of 920 kN (Stage 2)

Figure A4-8 Longitudinal stress distributions along the steel tube for specimen

S2.0D of Stage 2

A5.   COMPARISON OF LOAD SLIP RESPONSE IN PARAMETRIC STUDY

The aim of this appendix is to give the reader a complete comparison of load-slip response of all specimens in aspect ratio parametric study using the NLFEA solution scheme. No discussion is provided in this appendix as the relevant discussion has been presented in Chapter 7.
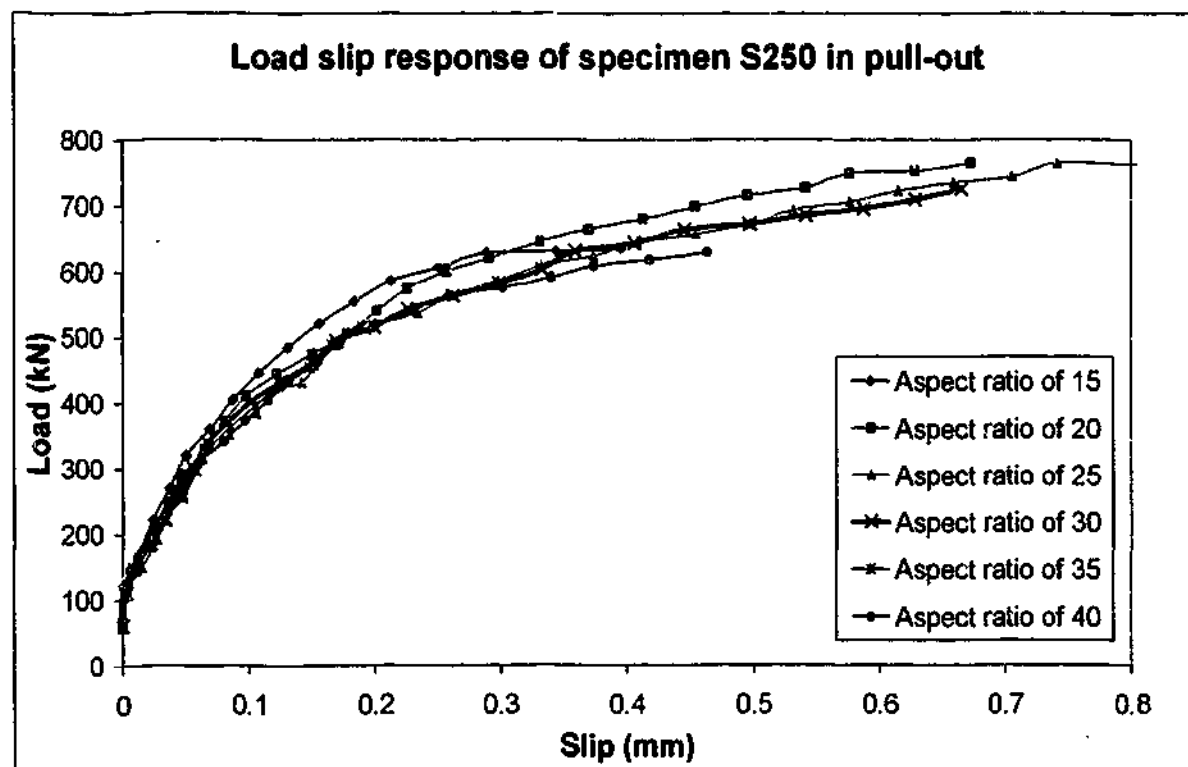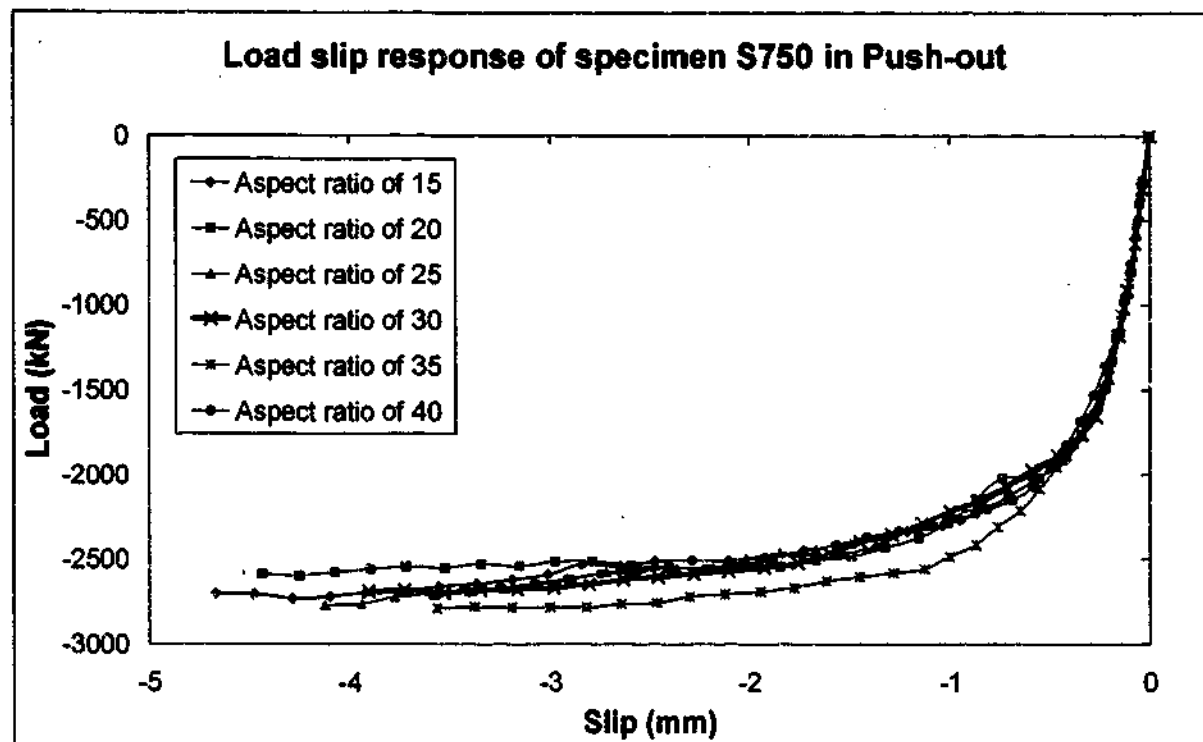

Figure A5-1: Load-slip behaviors of varying the aspect ratio of the steel tube for specimen S250 in pull-out test
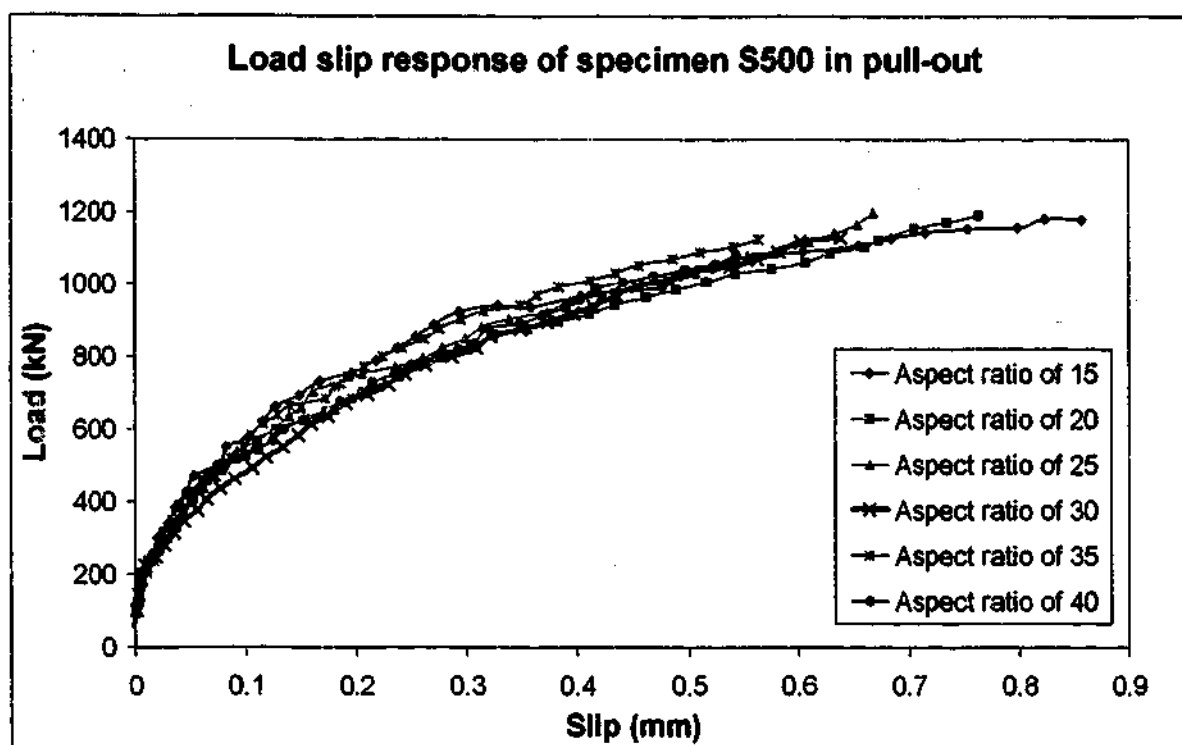
Figure A5-2: Load-slip behaviors of varying the aspect ratio of the steel tube for specimen S500 in pull-out test
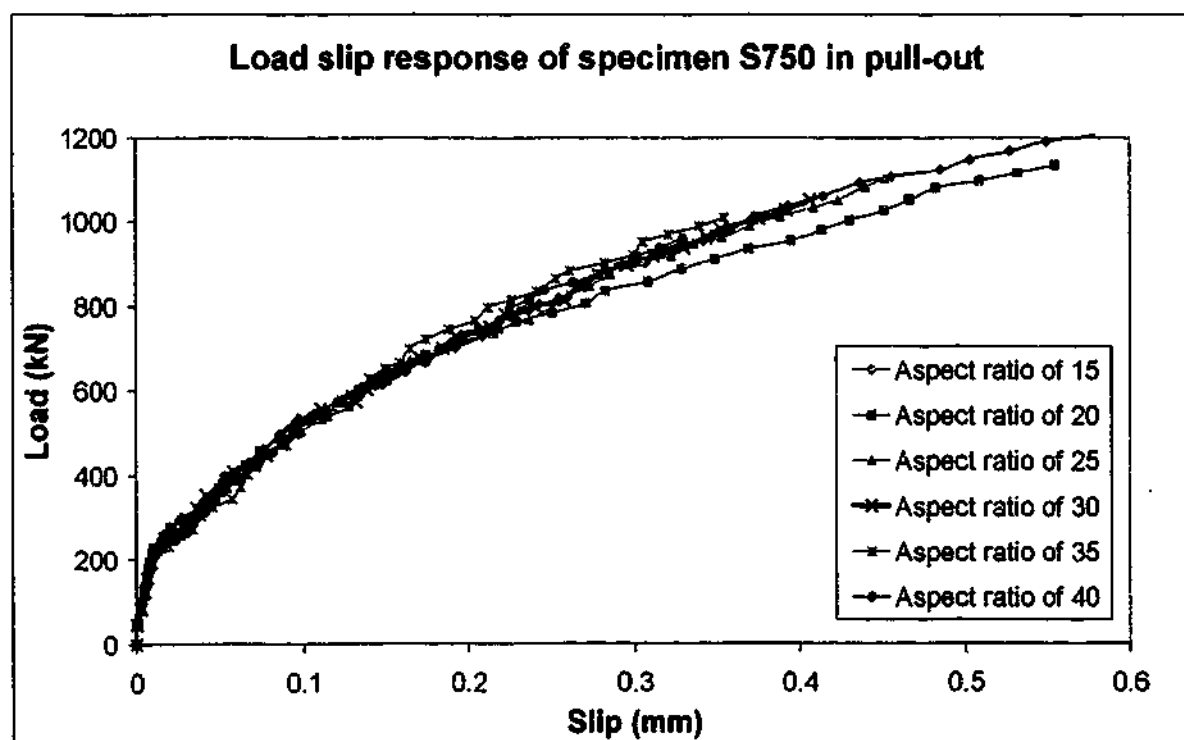
Figure A5-3: Load-slip behaviors of varying the aspect ratio of the steel tube for specimen S750 in pull-out test

Figure A5-4: Load-slip behaviors of varying the aspect ratio of the steel tube for specimen S750 in push-out test
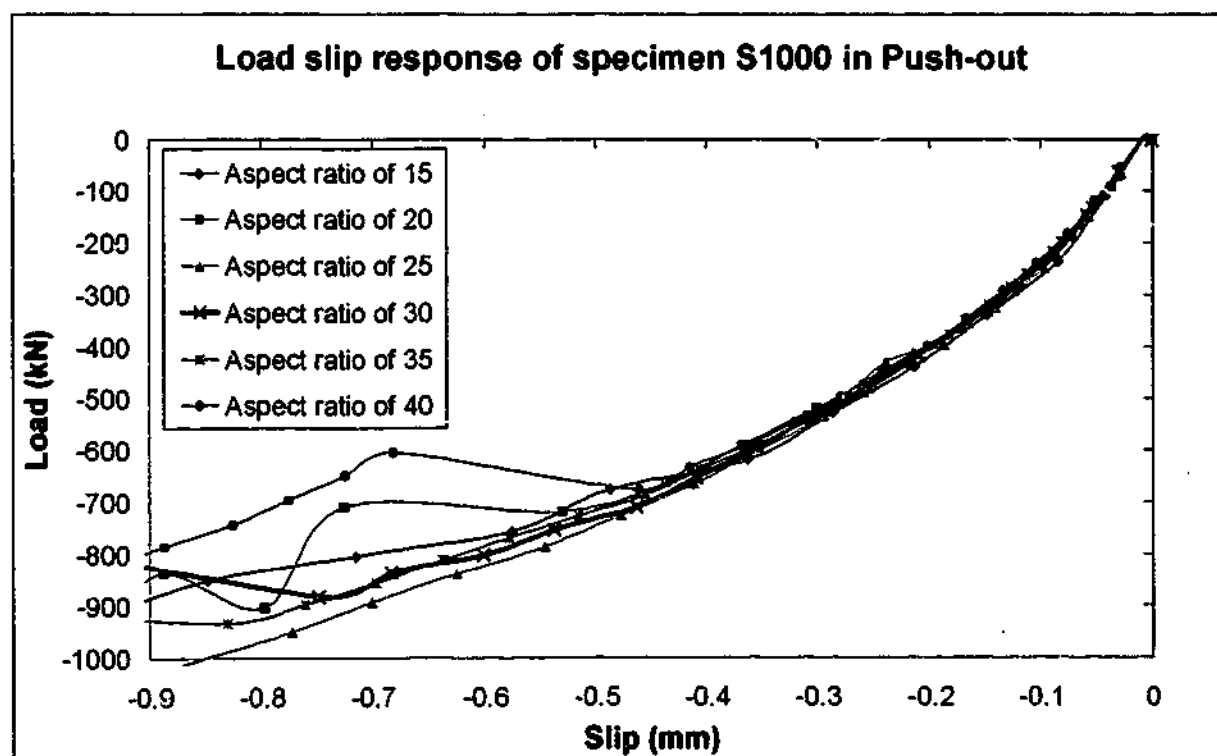

Figure A5-5: Load-slip behaviors of varying the aspect ratio of the steel tube for specimen S1000 in push-out test
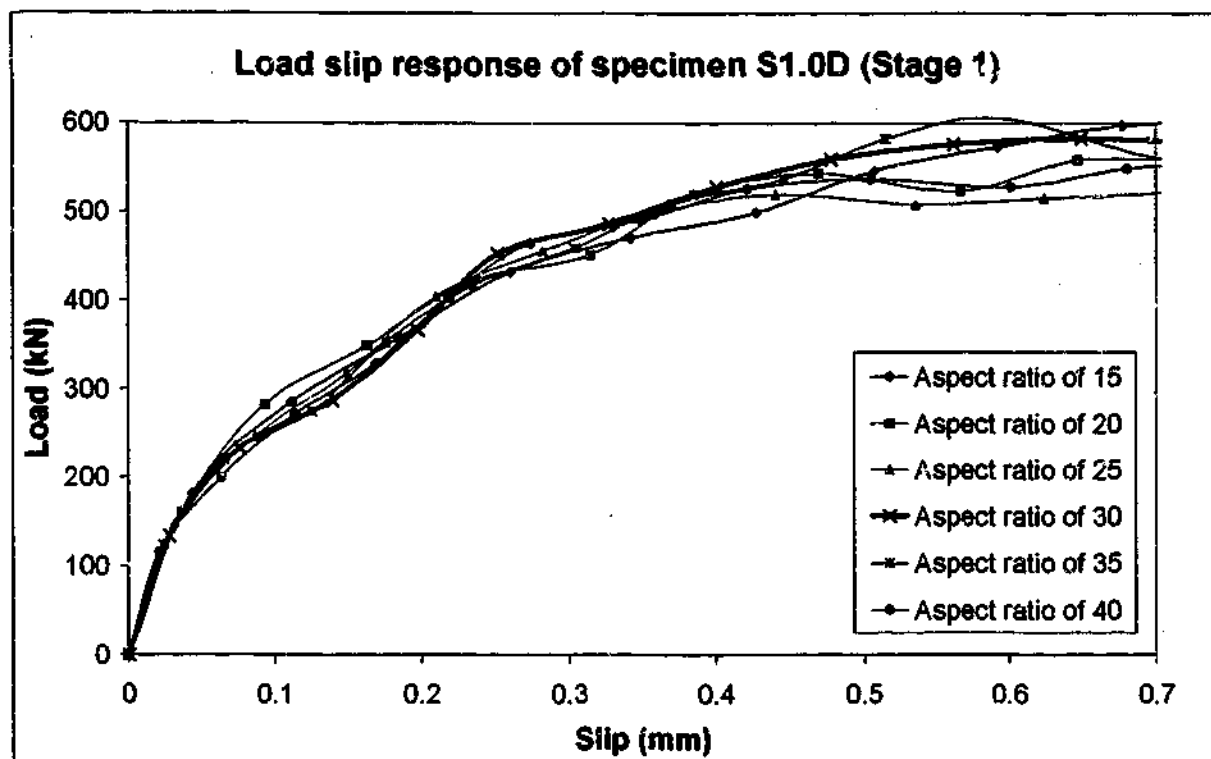
Figure A5-6: Load-slip behaviors of varying the aspect ratio of the steel tube for specimen S1.0D in pull-out test (Stage 1)
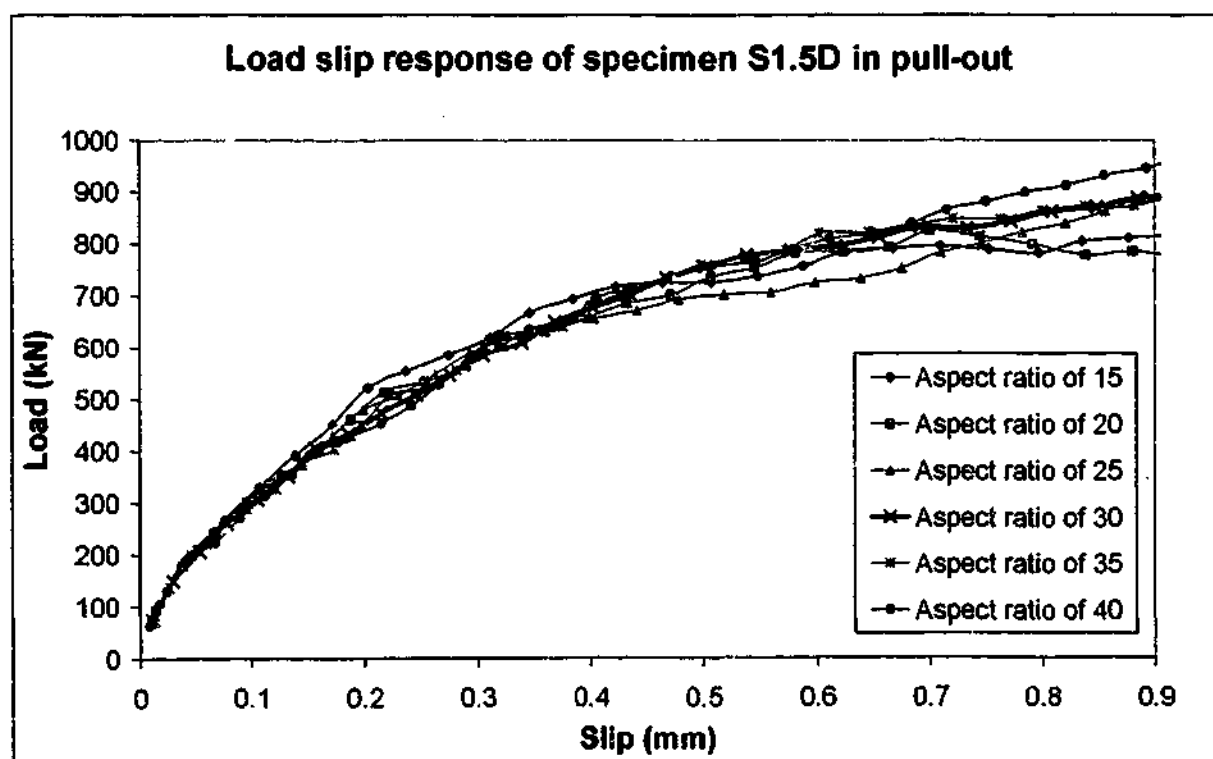

Figure A5-7: Load-slip behaviors of varying the aspect ratio of the steel tube for specimen S1.5D in pull-out test (Stage 1)
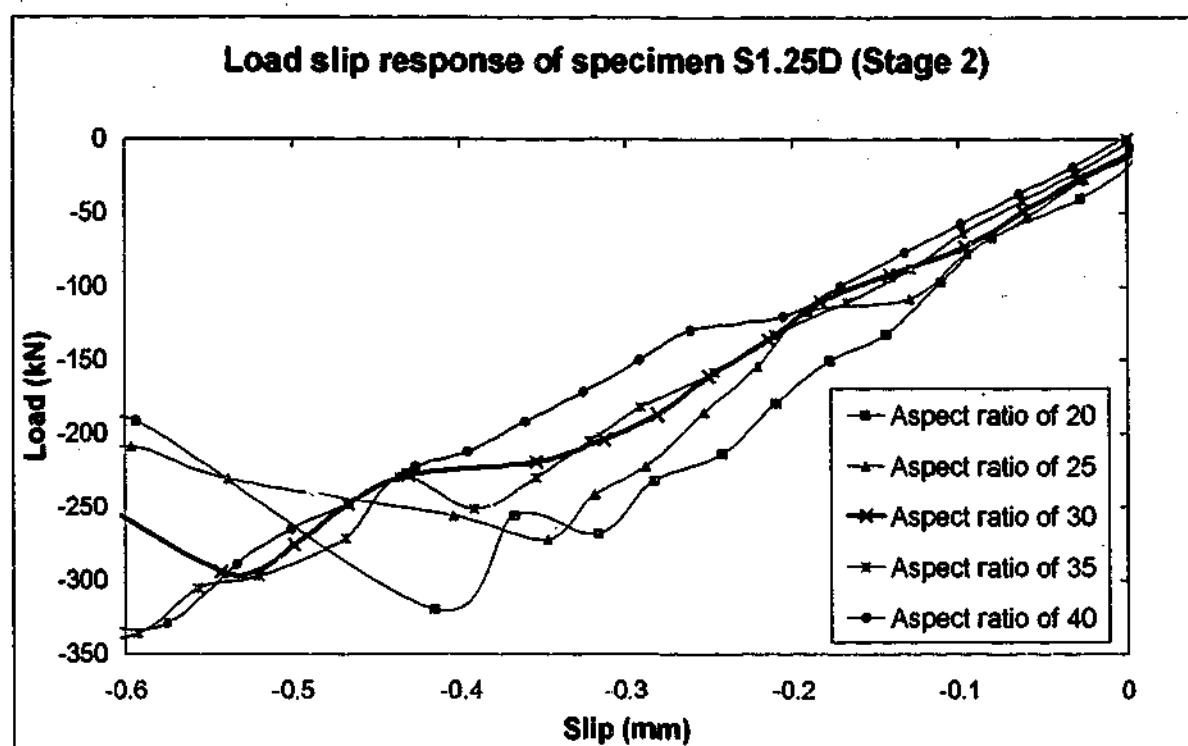
Figure A5-8: Load-slip behaviors of varying the aspect ratio of the steel tube for specimen S1.25D in push-out test (Stage 2)
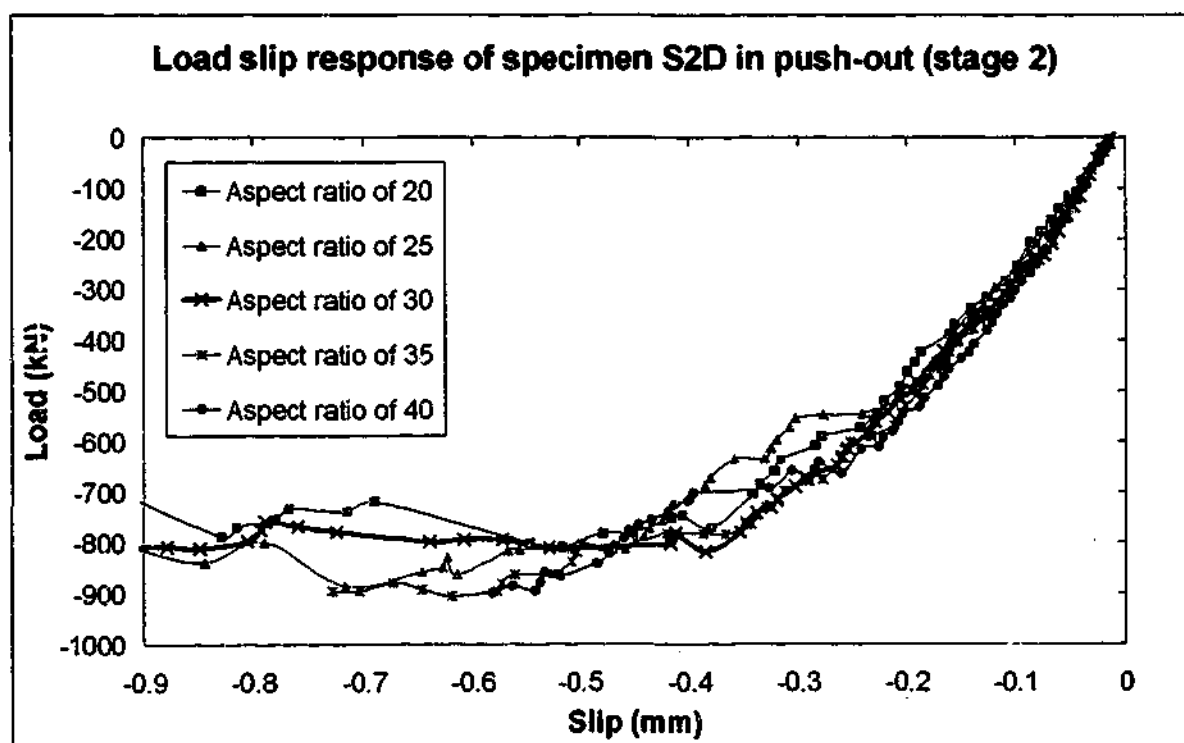

Figure A5-9: Load-slip behaviors of varying the aspect ratio of the steel tube for specimen S2.0D in push-out test (Stage 2)

A6.   LIST OF PUBLICATION

Nezamian, A., Al-Mahaidi, R. and Grundy, P., " Pull out strength of concrete plugs in tubular piles". 2nd International Conference On Mechanics of Structures, Materials and Systems, MSMS 2001, February 14 to 16, 2001, AUSTRALIA pp. 67-73

Nezamian, A., Al-Mahaidi, R. and Grundy, P.,_" Push out strength of concrete plugs in tubular piles". 12th International Offshore and polar Engineering Conference & Exhibition, May 26-31, 2002, Kitakyushu, JAPAN pp.60-65

Nezamian, A., Al-Mahaidi, R. and Grundy, P. " Effect of Cyclic Loading in Bond Strength of Concrete Plugs in Tubular Piles". Advanced in Structures, Steel, Concrete, Composite and Aluminium, ASSCCA 2003, June 23-27, 2003, Sydney, Australia